Accommodating a High Penetration of PHEVs and PV Electricity in Residential Distribution Systems

by

Mohamed Saad ElNozahy

A thesis
presented to the University of Waterloo
in fulfillment of the
thesis requirement for the degree of
Doctor of Philosophy
in
Electrical and Computer Engineering

Waterloo, Ontario, Canada, 2015

AUTHOR'S DECLARATION

I hereby declare that I am the sole author of this thesis. This is a true copy of the thesis, including any required final revisions, as accepted by my examiners.

I understand that my thesis may be made electronically available to the public.

Abstract

Global warming is threatening the world's delicate ecosystems to the point where the extinction of numerous species is becoming increasingly likely. Experts have determined that avoiding such a disaster requires an 80% reduction in the 1990 levels of global greenhouse gas emissions by 2050. The problem has been exacerbated by the booming demand for electrical energy. This situation creates a complex dilemma: on the one hand, energy sector emissions must be decreased; on the other, electrical energy production must be increased to meet the growing demand.

The use of renewable emission-free sources of electrical energy offers a feasible solution to this dilemma. Solar energy in particular, if properly utilized, would be an effective means of meeting worldwide electricity needs. Another viable component of the solution is to replace gasoline-powered vehicles with plug-in hybrid electric vehicles (PHEVs) because of their potential for significantly reducing greenhouse gas emissions from the transportation sector.

It was once believed that integrating solar electricity into distribution systems would be relatively straightforward; however, when the penetration level of photovoltaic (PV) systems began to increase, power utilities faced new and unexpected problems, which arose primarily due to the weak chronological coincidence between PV array production and the system peak demand. PV arrays produce their peak output at noon, during low demand periods, resulting in individual instances when the net PV production exceeds the system net demand. Power then flows from low voltage (LV) to medium voltage (MV) networks. Such reverse power flow results in significant over voltages along distribution feeders and excessive power losses. For PHEVs, the situation is the direct opposite because peak demand periods coincide closely with the hours during which the majority of vehicles are parked at residences and are thus probably being charged. This coincidence causes substantial distribution equipment overloading, hence requiring costly system upgrades.

Although extensive research has been conducted with respect to the individual impacts of PV electricity and PHEVs on distribution networks, far too little attention has been paid to studying the interaction between these two technologies or the resulting aggregated impacts when both operate in parallel. The goal of the research presented in this thesis is to fill this gap by developing a comprehensive benchmark that can be used to analyze the performance of the distribution system under a high penetration of both PV systems and PHEVs. However, the uncertainties associated with existing electrical loads, the PHEV charging demand, and the PV array output complicate the

achievement of this goal and necessitate the development of accurate probabilistic models to express them. The establishment of such models and their use in the development of the proposed benchmark represent core contributions of the research presented in this thesis.

Assessing the anticipated impacts of PHEVs and PV electricity on distribution systems is not the only challenge confronting the electricity sector. Another issue that has been tackled by numerous researchers is the formulation of solutions that will facilitate the integration of both technologies into existing networks. The work conducted for this thesis presents two different solutions that address this challenge: a traditional one involving the use of energy storage systems (ESSs), and an innovative one that hinges on a futuristic novel bilayer (AC-DC) distribution system architecture.

In the first solution, the author proposes using ESSs as a possible means of mitigating the aggregated impacts of both PV electricity and PHEVs. This goal can be achieved by storing PV electricity generated during low demand periods, when reverse power flow is most likely to occur, in small-scale dispersed ESSs located at secondary distribution transformers. Thereafter, this energy is then reused to meet part of the PHEV charging demand during peak periods when this demand is most likely to overload distribution equipment. While this solution would kill two birds with one stone, the uncertainties inherent in the system make its implementation difficult. In this respect, a significant contribution of the work presented in this thesis is the use of the previously developed probabilistic benchmark to determine the appropriate sizes, locations, and operating schedules of the proposed ESSs, taking into account the different sources of uncertainty in the system.

In the second solution, the author proposes a noocvel bilayer (AC-DC) architecture for residential distribution systems. With the proposed architecture, the distribution system becomes a bilayer system composed of the traditional AC layer for interfacing with existing system loads, plus an embedded DC layer for interfacing with PV arrays and PHEVs. A centralized bidirectional converter links the two layers and controls the power flow between them. The proposed solution offers a reasonable compromise that enables existing networks to benefit from both AC and DC electricity, thus metaphorically enjoying the best of both worlds. As with the first solution, the uncertainties that characterize the distribution system also create obstacles to the implementation of the proposed architecture. Another important contribution of the research presented in this thesis is the design and validation of the proposed bilayer system, with consideration of these different uncertainties.

Finally, the author compares the strengths and weaknesses of both solutions to determine the better alternative.

Acknowledgements

First and foremost, all praise and thanks are due to Allah Almighty, the Exalted, the Lord of the universe, for enlightening my path and aiding me to bring forth this thesis.

I would like first to express my deepest gratitude to my advisor, Professor Magdy Salama, for his guidance, support, and encouragement throughout the course of my research. His excellent guidance was crucial for the completeness of this thesis.

My appreciation is extended to my Ph.D. committee members: Professor Ziyad Salameh, Dr. Ramadan El-Shatshat, Dr. Tarek Abdel-Galil and Dr. Eihab Abdel-Rahman for their insightful comments and invaluable assistance.

I also offer my gratitude to my parents and my brother Ahmed for standing by me, not only during the course of this research, but throughout my entire life. I feel fortunate to have them always standing by my side.

A final word to my lovely wife Reham and my sweet daughter Mariam: without both of you, I would have never been able to finish this work. Your continued support and encouragement were, and always will be, a source of strength for me. Both of you are the light of my life.

Dedication

This work is dedicated to the memory of my late father, Saad Abdou ElNozahy.

He taught me to persevere and prepared me to face challenges with faith and confidence. He was a constant source of inspiration in my life. Although he is not here today to give me strength and support, I always feel his presence that used to urge me to strive to achieve my goals in life.

May Allah forgive him and bring him rest in eternal peace.

Table of Contents

List of Figures

List of Tables

Nomenclature

A_{BESS}	BESS annual replacement cost per kWh ($/kWh)
A_{Total}	PV array cross section area (m^2)
$ALL(i, j)$	Actual load level at the i^{th} hour in the j^{th} day (kW)
$AMRC_{Conv}$	Annual maintenance and replacement cost for centralized bidirectional converters ($)
$AMRC_{DCConv}$	Annual maintenance and replacement cost for DC/DC converters ($)
$AMRCS_{PHEV}$	Annual maintenance and replacement cost savings achieved by the elimination of PHEV battery chargers ($)
$AMRCS_{PV}$	Annual maintenance and replacement cost savings achieved by the elimination of PV array inverters ($)
$APTM_{PV\ clusters}$	Average Power/Time Mismatch index for the PV profiles clusters
$APTM_{Load\ clusters}$	Average Power Time Mismatch index for the resulting load profiles clusters
$AR(12)$	Autoregressive model of the 12^{th} order
ARC_{BESS}	BESS annual replacement cost ($)
B	Voltage Regulator's bandwidth
BCG	Boston Consulting Group
BESS	Battery Energy Storage System
BEV	Battery Electric Vehicle
BOP_{BESS}	Total cost of the BESS balance of plant ($)
$BOPU_{BESS}$	Unit cost for the BESS balance of plant ($/kWh)
C	PHEV battery capacity (kWh)
CAISO	California Independent System Operator
CC_{PV}	Capital cost for PV inverters ($)
cdf	Cumulative distribution function
cfd	Cumulative frequency distribution
$cos\theta(i)$	Distribution transformer power factor at hour i
$cos\varphi(i)$	Load power factor at hour i

CRF	Capital Recovery Factor
D	Annual operating days for the BESS (days)
d_{daily}	Daily distance travelled by the PHEV (miles)
d_f	Number of features in each data segment
DB	Davies Bouldin validity index
DC_{Penet}	Percentage of household electronic loads supplied by DC electricity
DG	Distributed Generation
DSM	Demand Side Management
E	PHEV specific energy (kWh/mile)
E(i -1)	Energy stored in the BESS at hour *(i- 1)* (kWh)
E(i)	Energy stored in the BESS at hour *i* (kWh)
E_1	BESS energy level at the end of the controlled charging/discharging period (kWh)
E_2	BESS energy level at the end of the forced charging period (kWh)
E_3	BESS energy level at the end of the forced discharging period (kWh)
$E_{BESS\ Rated}$	Energy rating of the BESS (kWh)
$E_{BESS\ Reserve}$	BESS minimum reserve level (kWh)
E_{Ch}	Daily charged energy into the BESS (kWh)
$E_{Ch}^{\max}$	BESS maximum daily charged energy (kWh)
$E_{Ch}^{\min}$	BESS minimum daily charged energy (kWh)
E_{Dis}	Daily discharged energy by the BESS (kWh)
$E_{Dis}^{\max}$	BESS maximum daily discharged energy(kWh)
$E_{Dis}^{\min}$	BESS minimum daily discharged energy(kWh)
EA(y)	Energy adequacy index for the y^{th} year
ELV	Extra low voltage
EPRI	Electric Power Research Institute
ESS	Energy Storage System

$ELS(i,x)$	Energy loss savings achieved by using DC electricity in household x at hour i (kW)
F_{BESS}	Future value of BESS replacement cost ($/kWh)
$FLL(i, j)$	Fictitious load level at the i^{th} hour in the j^{th} day (kW)
$F_{PV,AC}(i, j)$	PV fictitious power output in the i^{th} hour at the j^{th} day (kW)
FCM	Fuzzy C-means
HEV	Hybrid Electric Vehicle
i_r	Annual interest rate
ICE	Internal Combustion Engine
IEA	International Energy Agency
IEC	International Electrotechnical Commission
k_c	Number of clusters
K_T	Thermal derating coefficient of the PV module ($^oC^{-1}$)
KEPCO	Korean Electric Power Corporation
L_{DCSD}	Total length of DC service drops (MLF)
LA	Lead-acid batteries
LE_{Trans}	Distribution transformer fixed installation, labor, and equipment costs ($)
LLNs	Law of Large Numbers
$Loss_{Ch}(i)$	BESS charging losses at hour i (kW)
$Loss_{DCSD}(i)$	DC power losses in the DC service drops connected to the bidirectional converter DC bus at hour i (kW)
$Loss_{Dis}(i)$	BESS discharging losses at hour i (kW)
$Loss_{Idling}(i)$	BESS idling losses at hour i (kW)
$Loss_{Inv}(i)$	Bidirectional converter inversion losses at hour i (kW)
$Loss_{Rec}(i)$	Bidirectional converter rectification losses at hour i (kW)
LUT	Lappeenranta University of Technology
LV	Low Voltage

$M_{LE,\ Trans}$	The markup factor on the distribution transformer fixed installation, labor, and equipment costs
MC	Monte Carlo
MLF	Thousand linear feet
MP_{Trans}	Distribution transformer manufacturer's selling price ($)
MPP	Maximum Power Point
MPPT	Maximum Power Point Tracking
MV	Medium Voltage
N	Number of data segments in the cluster
n_a	Number of data segments in cluster a
n_b	Number of data segments in cluster b
$n_{Ch/Dis}$	Number of daily charge/discharge cycles for the BESS
$N_{Ch/Dis}$	Number of charge/discharge cycles in the life of the BESS
$N_{Households,\ System}$	Total number of households in the system
$N_{Households,Transformer}$	Number of households connected to the distribution transformer
N_{PHEVs}	Number of PHEVs in the test system
N_{PVs}	Number of PV arrays in the test system
N_{Reg}	Annual number of voltage regulator actions
NA/S	Sodium sulfur batteries
NERC	North American Electric Reliability Corporation
NHTS	National Household Travel Survey
$NOCT$	Nominal Operating Cell Temperature (^{o}C)
NREL	National Renewable Energy Laboratory
$OM_{f,\ BESS}$	Fixed operation and maintenance cost for the BESS ($/kVA.year)
OMC_{BESS}	Annual fixed maintenance and operation cost for the BESS ($)
OPA	Ontario Power Authority
$P_{Ch}(i)$	Theoretical active power charged into the BESS at hour i (kW)
$P_{Ch,Act}(i)$	Actual active power charged into the BESS at hour i (kW)

$P_{DC\ bus}(i)$	Aggregated DC power at the bidirectional converter bus at hour *i* (kW)
$P_{Dis}(i)$	Theoretical active power discharged by the BESS at hour *i* (kW)
$P_{Dis,Act}(i)$	Actual active power discharged by the BESS at hour *i* (kW)
$P_{Inv}(i)$	DC power inverted by the bidirectional converter at hour *i* (kW)
$P_{Loads,AC}(i)$	Active power consumed by AC loads connected to the secondary distribution transformer at hour *i* (kW)
$P_{Loads,AC}(i, x)$	AC active power demand of household *x* at hour *i* (kW)
$P_{Loads,DC}(i)$	DC power delivered by the bidirectional converter to DC-powered household electronic loads at hour *i* (kW)
$P_{Loads,DC}(i, x)$	DC power supplied to DC-powered household electronic loads in household *x* at hour *i* (kW)
$P_{PHEVs,DC}(i)$	DC power consumed by all PHEVs connected to the bidirectional converter DC bus at hour *i* (kW)
$P_{PV,AC}$	AC power output of a PV array (kW)
$P_{PV,AC}(i, j)$	PV array AC power output in the i^{th} hour at the j^{th} day (kW)
$P_{PV,DC}$	DC power output of the PV array (kW)
$P_{PVs,DC}(i)$	DC power generated by all PV arrays connected to the bidirectional converter DC bus at hour *i* (kW)
$P_{Rec}(i)$	DC power rectified by the bidirectional converter at hour *i* (kW)
$P_{Trans}(i)$	Active power supplied by the distribution transformer at hour *i* (kW)
PCA	Principle Component Analysis
PCS_{BESS}	Total cost for BESS power electronics ($)
$PCSU_{BESS}$	Unit cost for BESS power electronic ($/kVA)
$PCSU_{Conv}$	Unit cost for bidirectional converters ($/kVA)
$PCSU_{DCConv}$	Unit cost for DC/DC converters ($/kVA)
$PCSU_{PHEV}$	Unit cost for PHEV battery chargers ($/kVA)
PCU	Power Conditioning Unit
pdf	Probability density function
PHEV	Plug-in Hybrid Electric Vehicle

PLF	Probabilistic Load Flow
PU	Percentage unbalance in split phase distribution transformers
PV	Photovoltaic
$Q_{Dis}(i)$	Theoretical reactive power discharged by the BESS at hour i (kVAR)
$Q_{Dis,Act}(i)$	Actual reactive power discharged by the BESS at hour i (kVAR)
$Q_{Loads,AC}(i)$	Reactive power consumed by electrical loads connected to the secondary distribution transformer at hour i (kVAR)
$Q_{Trans}(i)$	Total reactive power supplied by the distribution transformer at hour i (kVAR)
r	BESS replacement period (years)
$RPI(a)$	Representative probability index for representative segment representing cluster a
RPS	Renewable Portfolio Standard
S	Total number of data segments within the data set
$S_{BESS\ Rated}$	Power rating of the BESS (kVA)
$S_{Ch}(i)$	BESS inverter charged power at hour i (kVA)
$S_{Ch}^{\max}$	BESS inverter maximum charging rating (kVA)
$S_{Conv\ Rated}$	Bidirectional converter rating (kVA)
$S_{Dis}(i)$	Apparent power discharged by the BESS at hour i (kVA)
$S_{Dis}^{\max}$	BESS inverter maximum discharging rating (kVA)
$S_{Feeder\ Rated}$	The kVA rating of the primary feeder (kVA)
S_{Global}	Global isolation (W/m^2)
$S_{Global,\ NOCT}$	Global isolation at PV cell nominal operating conditions (800 W/m^2)
$S_{Inv}(i)$	Bidirectional converter inverted power at hour i (kVA)
$S_{Inv}^{\max}$	Bidirectional converter maximum inversion rating (kVA)
$S_{Loads,AC}(i)$	Apparent power consumed by electrical loads connected to the secondary distribution transformer at hour i (kVA)
$S_{Main}(i, y)$	Apparent power flowing through the primary feeder main head-end at the i^{th} hour in the y^{th} year (kVA)

$S_{Phase\ A}$	Apparent power flowing through the first phase of the split phase distribution transformer (kVA)
$S_{Phase\ B}$	The apparent power flowing through the second phase of the split phase distribution transformer (kVA)
S_{PHEV}	PHEV battery chargers power rating (kVA)
$S_{Rec}(i)$	Bidirectional converter rectified power at hour *i* (kVA)
$S_{Rec}^{\max}$	Bidirectional converter maximum rectification rating (kVA)
$S_{Trans}(i)$	Total apparent power supplied by the distribution transformer at hour *i* (kVA)
$S_{Trans\ Rated}$	Distribution transformer rating (kVA)
SDPF	Smart Distribution Power Flow
SMB	Standardization Management Board
SMESS	Superconducting Magnetic Energy Storage System
SOC	State of Charge
STC	Standard Test Conditions
SUC_{BESS}	Total cost for storage units ($)
$SUCU_{BESS}$	Unit cost for storage units ($/kWh)
SUV	Sports Utility Vehicle
T_a	PV cell ambient temperature (^oC)
T_c	PV Cell internal temperature (^oC)
$T_{c,NOCT}$	PV cell internal temperature at nominal operating cell temperature (^oC)
T_{it}	Number of iterations
TAC_{BESS}	Total annual cost for BESSs ($/year)
TAC_{Conv}	Total annual cost for bidirectional converters ($/year)
TAC_{DCConv}	Total annual cost for DC/DC converters ($/year)
TAC_{DCSD}	Total annual cost for DC service drops ($/year)
$TACC_{BESS}$	Total annual capital cost for BESSs ($/year)
$TACC_{Conv}$	Total annual capital cost for bidirectional converters ($/year)
$TACC_{DCConv}$	Total annual capital cost for DC/DC converters ($/year)

$TACCS_{PHEV}$	Total annual capital cost savings achieved by the elimination of PHEV battery chargers ($/year)
$TACCS_{PV}$	Total annual capital cost savings achieved by the elimination of PV array inverters ($/year)
$TACS_{PHEV}$	Total annual cost savings achieved by the elimination of PHEV battery chargers ($/year)
$TACS_{PV}$	Total annual cost savings achieved by the elimination of PV array inverters ($/year)
$TACS_{Trans}$	Total annual cost savings achieved by avoiding distribution transformer upgrades ($/year)
TCC_{BESS}	Total capital cost for BESSs ($)
TCC_{Conv}	Total capital cost for bidirectional converters ($)
TCC_{DCConv}	Total capital cost for DC/DC converters ($)
TCC_{DCSD}	Total capital cost for DC service drops ($)
$TCCS_{PHEV}$	Total capital cost savings achieved by the elimination of PHEV battery chargers ($)
$TCCS_{PV}$	Total capital cost savings achieved by the elimination of PV array inverters ($)
$TCCS_{Trans}$	Total capital cost savings achieved by avoiding distribution transformer upgrades ($)
TCE	Total charging energy required to fully charge the PHEV battery (kWh)
THD	Total Harmonic Distortion
TOU	Time-of-use
UC_{DCSD}	Unit cost for DC service drops ($/MLF)
UNFCCC	United Nations Framework Convention on Climate Change
$V_m(i)$	System voltage being monitored at hour i
V_s	Voltage regulator's set voltage
V2G	Vehicle-to-Grid
VR	Vanadium redox batteries
VRLA	Valve-regulated lead-acid batteries
X_{penet}	PHEV percentage penetration level

XB	Xie-Beni index
z	Project lifetime (years)
ZEH	Zero Energy Housing
Zn/Br	Zinc bromine batteries
$\eta_{AC/DC}$	Efficiency of household AC/DC power supplies
η_{Ch}	BESS charging efficiency
$\eta_{DC/DC}$	Efficiency of DC/DC centralized buck converters installed at households
η_{Dis}	BESS discharging efficiency
η_{Inv}	Bidirectional converter inversion efficiency
η_{Module}	PV module efficiency
η_{MPP}	MPP tracker efficiency
$\eta_{Overall\ array}$	Overall efficiency of the PV array
$\eta_{PHEV\ charger}$	PHEV battery charger efficiency
$\eta_{PV\ inverter}$	PV inverter conversion efficiency
η_{Rec}	Bidirectional converter's rectification efficiency
η_{STC}	Efficiency of the PV module at standard test conditions
μ_v	Average number of vehicles per household

Chapter 1
Introduction

1.1 Motivation

Today, the production of energy is not sustainable; mankind is swiftly exhausting its fossil fuel resources like gas, oil and coal. Moreover, the global warming resulting from the burning of these fuels is threatening the world's delicate ecosystems to the point where the extinction of numerous species is becoming increasingly likely. To prevent such a disaster, The United Nations Framework Convention on Climate Change (UNFCCC) reached the conclusion that global warming should be limited to less than 2.0°C relative to pre-industrial temperatures [1]. For this target to become a reality, the global greenhouse gas emissions resulting from the burning of fossil fuels should be reduced by 80% from their 1990 levels by 2050 [2]. These ambitious targets of reducing dependency on fossil fuels – and hence, decreasing the resulting greenhouse gas emissions – cannot be achieved without active participation by the global energy sector, which is responsible for approximately two thirds the world's greenhouse gas emissions [3]. The situation has been exacerbated by the booming demand for electrical energy shown in Figure 1-1. The world's electrical energy consumption is expected to experience an annual growth rate of about 2.2% from 2010 to 2040, as compared with an average growth of 1.4% for all other delivered energy sources [4]. This forecast presents a complex dilemma: on the one hand, energy sector emissions must be reduced; on the other, electrical energy production must be increased to meet the growing demand.

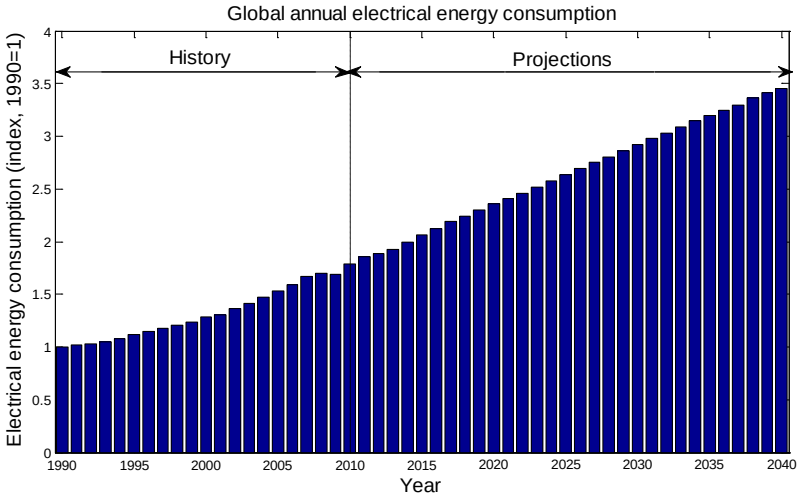

Figure 1-1: Global annual electrical energy consumption

The Smart grid futuristic vision for power systems, that is expected to prevail within the next few decades, provides two feasible solutions for this dilemma:

i) Utilizing renewable sources of energy such as wind and solar to generate electricity as these renewables are clean, emission-free sources of energy that can be used to generate electricity and at the same time protect our environment for future generations. Solar energy in particular, if properly utilized, would be an effective means of meeting worldwide electricity needs: a simple calculation reveals that the amount of solar energy received by the earth in one hour is equivalent to the world's annual energy consumption [5]. Another calculation shows that all the energy demand of the U.S. can be supplied by only 0.2% of the solar radiation it receives [6].

   In the residential energy sector, solar photovoltaic (PV) arrays are expected to be the most commonly used renewable generation technology. This expectation is based on the fact that PV arrays exemplify an emission-free renewable generation technology that can be easily installed on rooftops, without needing bureaucratic city land-use approvals, to generate electricity and at the same time protect the environment. Residential customers also prefer PV generation units due to the generous incentives offered by several government entities with the goal of promoting the adoption of solar electricity. For example, upon its launch in October 2009, the microFIT program (funded by the Ontario Power Authority) offered 80.2 CAD cents/kWh for PV-generated electricity, whereas the same program offered only 19 CAD cents/kWh for wind-generated electricity [7]. As a result, 1856 proposals out of the 1858 microFIT proposals received up to November 2013 are for rooftop PV systems [8]. For this reason, only the electricity generated by solar PV arrays is considered in this thesis.

ii) Replacing gasoline powered vehicles with plug-in hybrid electric vehicles (PHEVs) as this approach has the potential to significantly reduce greenhouse gas emissions from the transportation sector. A recent study in the United States [9, 10] showed that if 43% of the U.S. light-duty vehicle fleet is replaced by PHEVs, the nationwide greenhouse gas emissions would be reduced by 27%. Another study in New Zealand [11] concluded that a 50% PHEVs market share will reduce carbon dioxide emissions by 11.94 million tons over a 30-years period.

It was once believed that integrating these technologies into distribution systems would be relatively straightforward; however, when the penetration level of solar electricity and PHEVs began to increase, utilities faced new and unexpected problems, which arose primarily due to the chronological localization of their electrical profiles:

i) For PV arrays, there is a weak chronological coincidence between PV array production and the system peak demand. PV arrays produce their peak output at noon, during low demand periods, resulting in individual instances when the net PV production exceeds the net demand. Power then flows from low voltage (LV) to medium voltage (MV) networks. Such reverse power flow results in significant over voltages along distribution feeders and excessive power losses [12, 13]. Reverse power flow has also been reported to affect the operation of voltage regulators installed along distribution feeders because the settings of such devices must be modified to accommodate the shift in the load center [14]. For these reasons, local distribution utilities are currently imposing limitations on the maximum allowable penetration level of PV electricity in their systems. For example, Hydro One –the largest distribution utility in Ontario– requires that distributed generation "to be interconnected to a distribution system circuit line section, including the proposed generator, not to exceed 7% of the annual line section peak load" [15].

ii) For PHEVs, the situation is the direct opposite: the uncontrolled charging of PHEVs (depending only on customers' habits) is very likely to overload distribution networks because peak demand periods coincide closely with the hours during which the majority of vehicles are parked at residences and are thus probably being charged [16]. Overloading of the distribution network causes premature degradation of distribution equipment as the entire infrastructure is operated closer to its maximum capacity for longer periods, which increases the probability of components failure. Results from the literature indicate that distribution networks may become overloaded for PHEV penetration levels as low as 10% [17-21]. Accordingly, costly system upgrades are necessary to accommodate the anticipated growth in PHEV penetration levels.

Although extensive research has been conducted with respect to the individual impacts of PV electricity [22-31] and PHEVs [9, 10, 32-38] on distribution networks, far too little attention has been paid to studying the interaction between these two technologies or the resulting aggregated impacts when both operate in parallel. The goal of the research presented in this thesis is to fill this gap by developing a comprehensive benchmark that can be used to analyze the performance of the distribution system under a high penetration of both PV systems and PHEVs. This task, however, is difficult due to the uncertainties associated with the existing electrical loads, the PHEV charging demand, and the PV array output. Monte Carlo (MC) simulation is a computational technique based on the use of random numbers and probability theory to solve problems of a stochastic nature. This feature makes MC simulation a suitable tool to handle the uncertainties at hand, and was thus used in

this research in the development of the proposed benchmark. However, in order to generate the random variables required for the MC simulation, accurate probabilistic models must be developed to represent the previously mentioned uncertainties. The establishment of such probabilistic models and their use in the development of the proposed benchmark represent core contributions of this thesis.

Assessing the anticipated impacts of PHEVs and PV electricity on distribution networks is not the only challenge confronting the electricity sector. Another issue that has been tackled by numerous researchers is the formulation of solutions that will facilitate the synchronized integration of both technologies into existing distribution networks. The work conducted for this thesis presents two different solutions that address this challenge: a traditional one involving the use of energy storage systems (ESSs), and an innovative one that hinges on a futuristic novel bilayer (AC-DC) distribution system architecture.

In the first solution, the author proposes using ESSs as a possible means of mitigating the aggregated impacts of PV electricity and PHEVs. This goal can be achieved by increasing the synergy between PV electricity and PHEVs. PV electricity generated during low demand periods, when reverse power flow is most likely to occur, is stored in small-scale dispersed ESSs located at secondary distribution transformers. Thereafter, this energy is then reused to meet part of the PHEV charging demand during peak periods when this demand is most likely to overload distribution equipment. While this method would thus metaphorically kill two birds with one stone, its implementation is challenging due to the previously mentioned uncertainties. In this context, a significant contribution of the work presented in this thesis is the use of the previously developed benchmark to determine the appropriate sizes, locations, and operating schedules of the proposed ESSs, taking into account the different sources of uncertainty in the system.

In the second solution, the author proposes a novel bilayer (AC-DC) residential distribution system architecture. The inspiration for this solution is the fact that the main cause of the negative impacts of these two technologies on distribution networks is the architecture of the distribution system itself: distribution systems currently adopt the single layer architecture, with all loads and generation sources connected to the same layer. This single layer thus must meet all PHEV charging demands, resulting in substantial overloading of secondary distribution equipment during peak charging periods, and must also absorb any surplus PV generation, leading to excessive reverse power flow when PV arrays are generating their peak output. Another interesting fact is that both PV systems and PHEVs are inherently DC in nature: PV arrays produce DC power and PHEVs' batteries are

fundamentally charged by DC electricity. Providing a DC interface for these technologies would eliminate a power conversion stage and increase the conversion efficiency. These two factors led to the novel idea of the proposed solution which is modifying the distribution system architecture so that it becomes a bilayer system composed of the traditional AC layer for interfacing with existing system loads, plus an embedded DC layer for interfacing with DC technologies present in the distribution system and currently interfaced via power electronic converters (such as PV arrays and PHEVs). A centralized bidirectional converter links the two layers and controls the power flows between them. The proposed solution offers a reasonable compromise that enables existing networks to benefit from both AC and DC electricity, thus metaphorically enjoying the best of both worlds. As with the first solution, however, the uncertainties that characterize the distribution system also create obstacles to the implementation of the proposed architecture. Another important contribution of the research presented in this thesis is the design and validation of the proposed bilayer system, with consideration of these different uncertainties.

Finally, the author compares the strengths and weaknesses of both solutions to determine the better alternative.

1.2 Research Objectives

The proposed research investigates the anticipated impacts of PHEVs and PV systems on residential distribution systems and proposes solutions for facilitating their integration into existing networks.

The primary research objectives can be summarized as follows:

i) Developing probabilistic models to represent the uncertainties associated with the PV array output, the existing electrical loads and the PHEV charging demand.

ii) Utilizing the established probabilistic models for the development of a probabilistic benchmark that can be used to assess the aggregated impacts of PHEVs and PV systems on residential distribution networks, with consideration of different uncertainties inherent in the system.

iii) Developing a probabilistic sizing and scheduling methodology for ESSs to enable their use for facilitating the integration of PV arrays and PHEVs in residential distribution networks.

iv) Proposing a novel bilayer architecture for distribution systems as a means of mitigating the negative impacts of PHEVs and PV electricity on residential distribution networks.

v) Utilizing the developed probabilistic benchmark to size and schedule the operation of the components of the proposed bilayer system, with consideration of different uncertainties inherent in the system.

1.3 Thesis Outline

The remainder of the thesis is organized as shown in Figure 1-2.

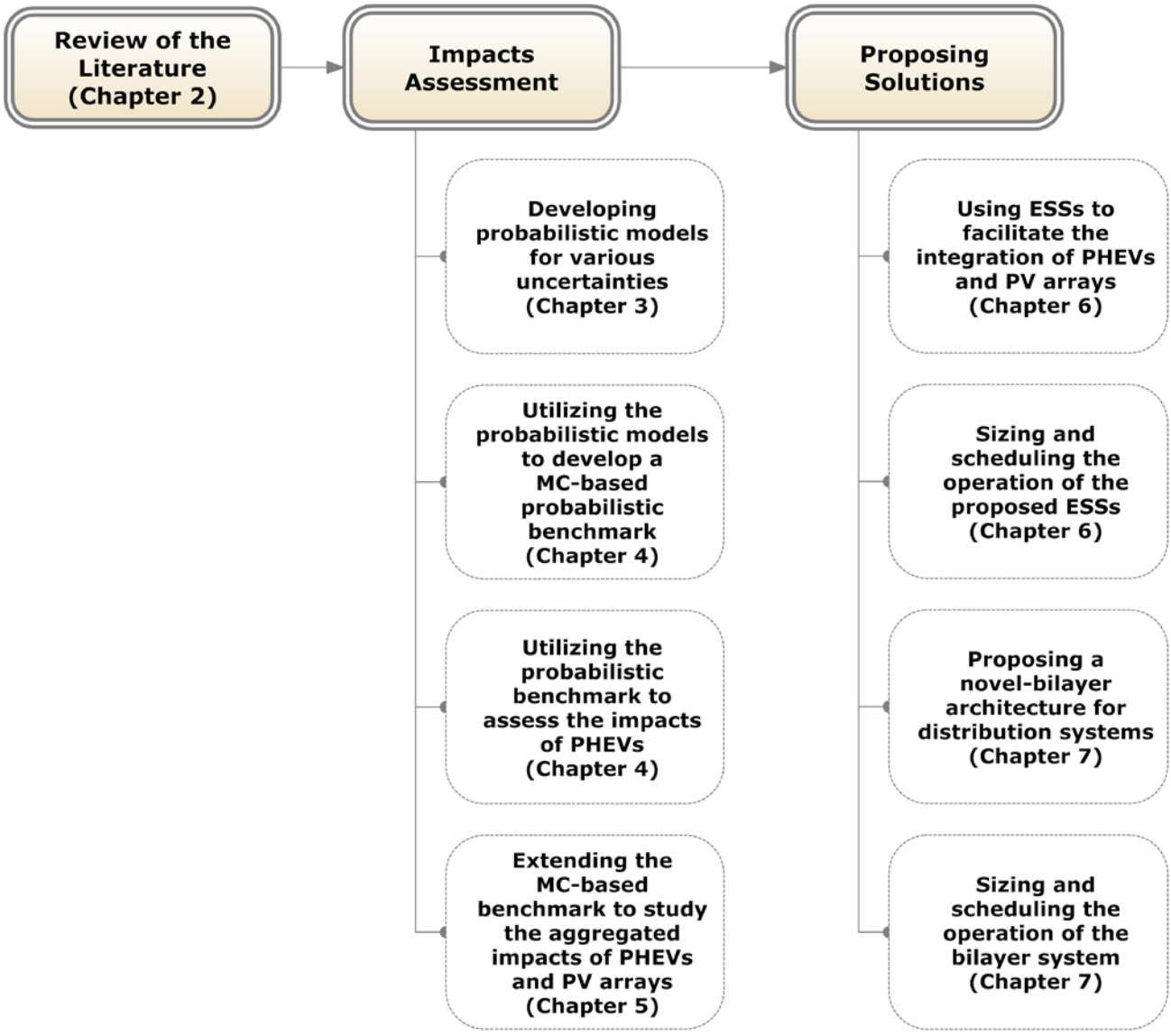

Figure 1-2: Thesis outline

The details of each chapter are as follows: Chapter 2 provides a brief review of two of the most important challenges facing power systems in the smart grid era, which are integrating PV systems and PHEVs in existing electrical networks. Chapter 3 describes the probabilistic models used in this research to represent the uncertainties associated with the PV array output, existing electrical loads and individuals' driving patterns that impact PHEV charging. In Chapter 4, the previously established probabilistic models are used to develop a MC-based probabilistic benchmark for assessing the impacts of the uncontrolled charging of PHEVs on residential distribution networks. In Chapter 5, the developed benchmark is extended to assess the aggregated impacts of both PHEVs and PV electricity on distribution networks. In Chapter 6, the author proposes a probabilistic sizing and scheduling methodology for ESSs to enable their use for facilitating the integration of PV arrays and PHEVs in residential distribution networks. In Chapter 7, a novel bilayer architecture for residential distribution systems is proposed as another means of facilitating the integration of PHEVs and PV electricity in existing residential distribution networks. The previously developed MC-based probabilistic benchmark is used to size and schedule the operation of different system components. In the last chapter, Chapter 8, the summary, conclusions and recommendations for future research areas are presented.

Chapter 2
Challenges Facing Power Systems in the Smart Grid Era

2.1 Introduction

As mentioned in the previous chapter, power systems in the smart grid era have to deal with a complex dilemma: on one hand, emissions from the energy sector must be reduced; on the other, the same sector must increase its production to meet the growing demand for electricity. This dilemma is made even more complex by the fact that mankind is swiftly exhausting its fossil fuel resources.

Utilizing renewable emission-free sources of energy (such as wind and solar) to generate electricity provides a feasible solution to this dilemma. Solar Energy in particular, if properly utilized, would be an effective means of meeting worldwide electricity needs. Section 2.2 introduces the different types of solar PV systems, discusses the benefits and drawbacks of installing grid-connected PV systems, and finally, presents some of the potential impacts associated with integrating PV systems into power networks.

EVs represent another feasible solution to the above dilemma. These vehicles are becoming an increasingly appealing alternative to gasoline fuelled cars due to global warming concerns, the consequent regulatory requirements, and the depletion of oil resources. Section 2.3 introduces the different types of EVs; their advantages and disadvantages are discussed. After that, some of the potential impacts associated with integrating PHEVs into distribution networks are presented.

Finally, the summary and conclusions of the chapter are presented in Section 2.4.

2.2 Integrating PV Systems into Power Networks

PV systems were first used as stand-alone systems to provide electricity to rural areas where no other sources of energy were available. The advances in the technology and the concerns about global warming are encouraging both governments and customers to use grid-connected PV systems, a trend discussed in the following sections.

2.2.1 Classification of PV Systems

According to the IEEE Std. 929-2000 [39], PV systems are classified based on their ratings into three distinct categories:

i) Small systems rated at 10 kW or less;

ii) Intermediate systems rated between 10 kW and 500 kW;

iii) Large systems rated above 500 kW.

The first two categories are usually installed at the distribution level, as opposed to the last category which is usually installed at the transmission/sub-transmission levels. The previous ranges are likely to be modified in the near future due to the huge power ratings of PV systems recently or soon to be installed.

Another classification for PV systems has been adopted by the International Energy Agency (IEA) and is based on the method of interconnection:

i) Off-grid domestic;

ii) Off-grid non-domestic;

iii) Grid-connected distributed;

iv) Grid-connected centralized.

The first two categories represent stand-alone PV systems, whereas the last two categories are grid-connected systems. The grid-connected centralized systems adopt the same philosophy as conventional centralized power plants, whereas the grid-connected distributed PV systems represent the new distributed generation (DG) philosophy. The study presented in this research is mainly concerned with small grid-connected distributed PV systems (rated at 10 kW or less) installed in residential distribution networks.

2.2.2 Components of PV Systems

The building blocks of a grid-connected PV system are shown in Figure 2-1. Different components of the system are discussed in the following sub-sections.

i) The sun: The instantaneous solar power received on a unit surface area is usually called the irradiance or insolation level and is measured in watts per square meter (W/m^2). Energy emitted by the sun travels around 150 million kilometers until it arrives at the terrestrial orbit of the earth. Of this energy, 17% is reflected back by clouds into space, 9% is scattered around by air molecules, and 7% is reflected off the earth's surface back into space. The luminous power reaching ground level is approximately 1000 W/m^2 [40].

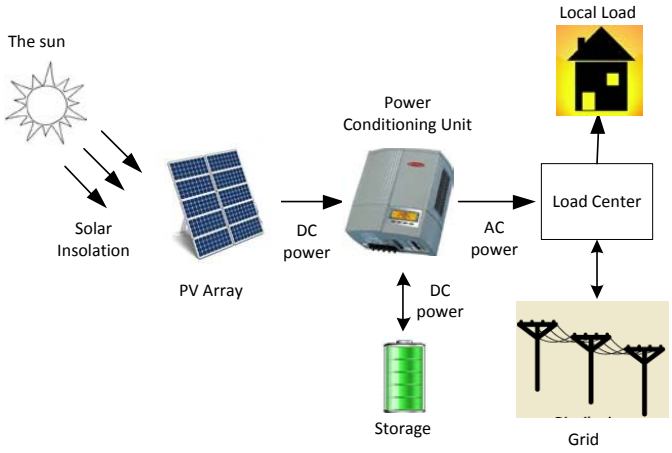

Figure 2-1: Main components of grid-connected PV systems

ii) PV array: The solar array is the most expensive component of the PV system. Solar cells are the electrical building blocks for solar arrays. The first silicon solar cell was developed at Bell Telephone Laboratories in 1954 by Chapin *et al*. [41]. Different types of materials can be used in manufacturing these cells. However, the most widely used cells are made of polycrystalline silicon (54.5% of the world's market share) and monocrystalline silicon (29.36% of the world's market share) [42]. Solar cells are usually connected in series to form a PV module, and modules are then connected in series to form a string. Finally, the strings are connected in parallel to form a PV array.

iii) Power conditioning unit (PCU): Grid-connected PV systems are interfaced to utility networks by means of PCUs. PCUs usually perform two basic functions:

- Control the output voltage or current of the PV array to extract the maximum power available at a certain temperature and irradiance. This algorithm is called maximum power point tracking (MPPT).
- Convert the DC output of PV arrays into AC power suitable to be fed into the utility grid.

Modern PCUs can perform additional functions such as output power quality assurance, various protection mechanisms (i.e., islanding detection) and reactive power control.

PCUs can be divided according to the number of power processing stages into single and double-stage systems. In single-stage systems, a DC/AC inverter is used to perform all the required control tasks, whereas in double-stage systems, a DC/DC converter is cascaded with the

DC/AC inverter, and the control tasks are divided among them. A major drawback of single-stage PCUs is that their MPPT algorithms are extremely slow compared to those of double-stage PCUs [43]. Accordingly, most PCUs for PV systems are of the double-stage type.

iv) Storage devices: PV systems depend on solar insolation to produce their electric output; thus, they become ineffective during night-time. For this reason, PV systems are usually equipped with storage devices to store energy during periods when generation exceeds the load demand, and then inject this energy back to the grid when the load demand is higher than the available generation. Moreover, these devices – if equipped with the proper control – can be used to reduce the power fluctuations of PV systems due to passing clouds [29]. Several types of storage technologies can be used with PV systems, such as battery energy storage systems (BESSs), superconducting magnetic energy storage systems (SMESSs) and super capacitors [5].

2.2.3 Benefits of PV Systems

Chapter 1 made clear that using emission-free sources of energy is no longer a luxury; it is a must if we are to protect our environment for future generations. The benefits of adopting solar electricity can be summarized as follows:

i) Solar energy is a free, universally available source of energy that can fulfill all of mankind's electricity needs. As mentioned earlier, the amount of solar energy received in one hour by the earth is equivalent to the world's annual energy consumption [5]. Another calculation reveals that the entire energy demand of the U.S. can be supplied by converting only 0.2% of the solar radiation it receives into usable energy [6].

ii) Solar energy is a secure source of energy; it imposes no military risks, unlike nuclear power, for example.

iii) Solar energy is dispersible and thus can be used to supply locations far from transmission and distribution networks.

iv) Solar PV arrays have no rotating parts and thus, are almost maintenance free.

v) Solar energy is not associated with any fuel transportation costs.

vi) PV arrays have a long lifetime due to the slow degradation of solar cells.

vii) PV modules can be flexibly assembled to obtain variable ratings from a few watts to megawatts.

2.2.4 Limitations of PV Systems

Despite all the previously mentioned benefits, PV systems have some limitations that constrain their widespread adoption:

i) The efficiency of PV systems is still too low; a maximum of only 15-16% conversion efficiency can be obtained using the expensive monocrystalline silicon arrays. This constraint results in limited power output for PV systems.

ii) Due to their limited power output, solar arrays require extensive land use if large amounts of power are to be generated (roughly estimated as 8 acres/MW [44]).

iii) PV systems are characterized by their low capacity factors. This is attributed to the fact that solar insolation is only available in the daytime. As a result, for a capacity factor of 20%, equipment rated up to 100 kW must be installed just to generate 20 kW of electricity, on the average.

iv) The cost of electricity generated by solar PV cells is still too high compared to other generating techniques (2800-5000 $/kW [45]). A recent study in Wisconsin [30] showed that the cost of electricity generated by PV arrays is much greater than its value: the levelized cost of PV electricity was calculated to be 0.614 $/kWh; however, the peak value of electricity using the time-of-use (TOU) rates in the same state was 0.138 $/kWh. Thus, production incentives totaling 0.476 $/kWh must be awarded to customers in order to make PV electricity economically viable.

However, when evaluating the economic aspects of solar electricity, it is important to consider the whole picture, as solar electricity also has several positive impacts on the national economy. For example, installing 3 GW of solar electricity in Ontario from 2011 to 2015 will create more than 72,429 person-years of employment, around 12 times the employment resulting from nuclear plants and 15 times the employment resulting from natural gas or coal power plants. This is associated with a less than 0.7% increase in the average electricity bill per year [31]. It was also noticed that the cost of jobs created by PV systems is 4-6 times less than the cost of jobs created by nuclear, natural gas or coal power plants. A million dollar investment in solar PV will create only 30-42% of the energy produced by other power plants, but 2.4-6.4 times more jobs [31].

Thus, when performing the financial assessment for a certain PV project, analysts should not only include the cost vs. energy criterion, but also other positive impacts on the economy as a whole.

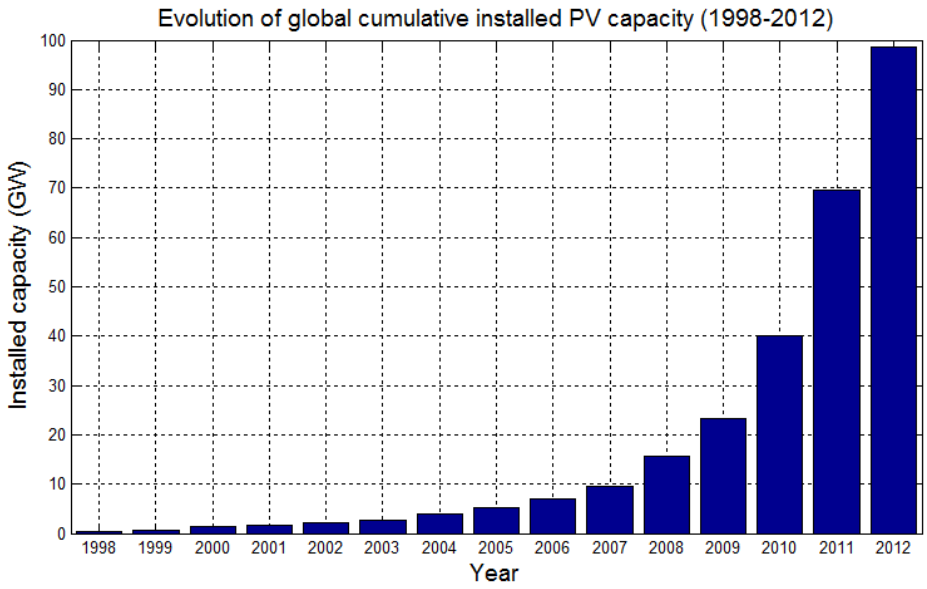

Figure 2-2: Evolution of global cumulative installed PV capacity (1998-2012) [46]

2.2.5 Growth in PV Installed Capacity

Despite the previous discouraging limitations, the global PV installed capacity has increased greatly over the past few decades. For example, during the past 15 years, global PV installed capacity has experienced an average annual growth rate of about 45% as shown in Figure 2-2 [46]. This is because the global energy sector realized that generating electricity from renewables will be the only available option to satisfy the growing demand for electricity once all available fossil fuel resources have been consumed.

Several countries have ambitious plans to increase their PV electricity production:

i) In Germany, the installation rate of solar PV systems increased from 800 MW/year in 2005 to 7.6 GW/year in 2012 [47-49]. This is basically attributed to the generous incentives offered by the German government to facilitate the widespread adoption of PV electricity [50].

ii) In Ontario, the FIT and the microFIT programs, funded by the Ontario Power Authority (OPA), were introduced to encourage the development of renewables in the province by offering competitive incentives. This initiative is conceptually important as 80% of the existing electric generation capacity in Ontario needs to be replaced within the next 20 years. Most of the microFIT proposals are rooftop PV systems. As a result, it is expected that there will be about 3 GW of solar energy in the Ontario electric system by 2015 [31].

iii) In California, the renewable portfolio standard (RPS) program launched by Governor Arnold Schwarzenegger mandates that the penetration level of renewables in the state reaches the 33% goal by 2020. Accordingly, more than 9500 MW of PV power projects are currently proposed for interconnection with the system [51].

iv) In China, the government has developed ambitious plans to install 10 GW of PV power by 2015. The Chinese government also targets 50 GW total PV installed capacity by 2020 [52].

v) In July 2009, the Indian government revealed a $19 billion plan to produce 20 GW of solar power by 2020 [53].

In addition to these future expansion plans, there are already several demonstration projects installed worldwide with high penetration levels of PV electricity. Most of these projects are being monitored in order to provide practical insight into the anticipated impacts of PV electricity if similar penetrations are to be installed in existing networks. Examples of such projects include:

i) The Gunma demonstration project in Japan (commissioned in 2002) comprises 550 houses equipped with rooftop grid-connected PV systems. The total PV installed capacity is estimated to be 2.2 MW in a 1 km^2 area [54, 55], which corresponds to a PV penetration level of approximately 85%.

ii) The PV settlement project in Freiburg, Germany, consists of 50 condominium apartments, with PV systems installed for each apartment. This amounts to approximately 300 kW of PV installed capacity [55, 56], which corresponds to 80% PV penetration.

iii) The Bronsbergen holiday park in the Netherlands consists of 210 cottages; 108 of them are equipped with solar rooftop PV systems yielding about 315 kW of PV power. This corresponds to approximately 80% PV penetration [57].

iv) The Nieuwland project in the Netherlands contains 500 houses equipped with rooftop grid-connected PV systems. The total PV installed capacity is 1.3 MW in a 12 km^2 area [55, 58], which corresponds to approximately 65% PV penetration.

v) In Porterville in the U.S., the 12.47 kV distribution feeder has 60% PV penetration [13].

vi) The SolarSmart project in Anatolia, California, consists of 795 homes; 600 of which are equipped with rooftop grid-connected PV systems. The total PV installed capacity is 1.2 MW, which corresponds to approximately 13% PV penetration [59].

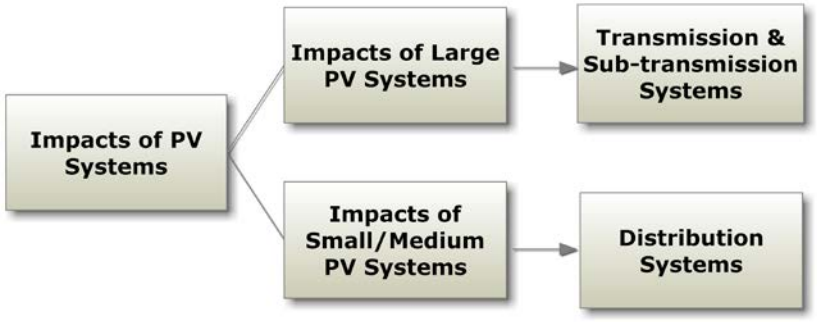

Figure 2-3: Impacts of PV systems on electrical networks

2.2.6 Technical Impacts of Grid-Connected PV Systems

Generally speaking, grid-connected PV systems are installed to enhance the performance of electrical networks. PV arrays (as well as other DG units) provide energy at the load side of the distribution network, thus reducing the feeder active power loading and improving the voltage profile. As a result, PV systems can reduce the operation time of shunt capacitors and voltage regulators, hence increasing their lifetime. PV systems can also reduce the losses in distribution feeders if optimally sized and allocated. The example given in [22] shows that for a distribution feeder supplying 10 MW of uniformly distributed load along its length, 4-6 MW of distributed PV generation will provide optimal minimum losses in the feeder. PV systems can also increase the load carrying capability, which is the amount of load a power system can handle while satisfying certain reliability criteria, of existing networks. To meet increased demand while satisfying the same reliability criteria, utilities have to increase their generation capacity. Nevertheless, in [60], it was shown that the load carrying capability of an electrical network can be doubled with a 10% PV penetration level. Thus, utilities can defer the addition of extra generating capacities to other areas.

However, PV systems can also impose several negative impacts on power networks. These impacts are dependent on the size and location of the PV system, as shown in Figure 2-3.

2.2.6.1 Impacts of Large PV Systems

This section reviews the literature regarding the anticipated negative impacts of large PV systems (above 500 kW) on transmission/sub-transmission networks.

i) Severe power, frequency and voltage fluctuations: The PV array output is unpredictable and is highly dependent on environmental conditions. Partial shading due to passing clouds, temperature

and insolation random variations are all factors that affect PV array production, resulting in rapid fluctuations in its output power [5]. In [22], the output power of a 2 MW solar power plant was measured and recorded every 5 minutes. Measurements showed sudden and severe fluctuations in the output power of the solar power plant, primarily due to passing clouds and morning fog. Active power fluctuations result in severe frequency variations in the power system, whereas reactive power fluctuations result in substantial voltage variations [61]. These voltage fluctuations may cause nuisance switching of capacitor banks. Moreover, in [62], it has been shown that voltage flickers occur more frequently in power systems with high penetration of PV electricity during clouds transients.

ii) Increased ancillary services requirements: The electrical grid acts as an energy buffer to compensate for any power fluctuations and firm up the output power of PV systems [55]; thus, generating stations' outputs need to be adjusted frequently to cope with the PV power fluctuations, i.e., to dance with the sun. For example, if a cloud blanked out a PV system supplying 1 MW of electricity in 10 seconds, then the electrical grid should be able to inject extra power at a rate of 1 MW/10 seconds or else severe voltage and frequency disturbances would occur in the system [40]. This situation results in a significant increase in the frequency regulation requirements of power systems with high PV penetration levels. For example, the current frequency regulation requirements at the California Independent System Operator (CAISO) are 1% of peak demand. It has been forecasted that 2% frequency regulation will be required for a penetration level of 20% PV electricity, and 4% to integrate 33% PV electricity [23]. A more conservative study performed in Japan [24] concluded that for 10% PV penetration, the frequency regulation requirements will increase 2.5% over the base no-PV case. At 30% PV penetration, the authors found that frequency regulation should increase by 10%. According to their conclusion, the cost of doing that will exceed any possible benefits from PV electricity. A similar study in Arizona [25] concluded that the maximum tolerable penetration level of PV systems – with the existing frequency regulation capacities – is approximately 5%. For the above mentioned reason, frequency regulation requirements play an important role in determining the maximum allowable penetration level of PV electricity in a given network.

Geographical distribution of PV arrays in a certain region also plays an important role in determining the maximum allowable PV penetration in that region. The closer these PV arrays are, the more correlated their output profiles are, the more power fluctuations are expected due to

moving clouds, and the more frequency regulation services are needed to balance out these power fluctuations. Jewell studied this phenomena in [63] and concluded that for existing frequency regulation capacities, the following penetration levels are acceptable:

- 1.3% if the PV system is located at a central station.
- 6.3% if the PV system is distributed over a 10 km^2 area.
- 18.1% if the PV system is distributed over a 100 km^2 area.
- 35.8% if the PV system is distributed over a 1000 km^2 area.

These results indicate that, due to their highly dispersed nature, small PV systems are not likely to impact the frequency regulation requirements and so, these requirements should be determined based on the penetration level of large, centralized PV stations only.

iii) Stability problems: As explained earlier, PV array output is unpredictable and is highly dependent on environmental conditions. This unpredictability greatly impacts the power system operation as they cannot provide a dispactable supply that is adjustable to the varying demand, and thus the power system has to deal with not only uncontrollable demand, but also uncontrollable generation [5]. As a result, greater load stability problems may occur, as explained below.

PV arrays do not have any rotating masses; thus, they do not have inertia and their dynamic behavior is completely controlled by the characteristics of the interfacing inverter. In [64], the effect of high penetration of PV generation on power system stability was addressed. Simulation results showed that PV systems have detrimental impact on power system stability. This is explained by the fact that the frequency change in the case of a sudden disturbance is larger for a system with low inertia (such as a system with high PV penetration) compared to a system with high inertia. Similarly, another study [65] showed that during fault conditions in a system with high PV penetration, rotors of some of the conventional generators swing at higher magnitudes.

The authors of [66] studied the impacts of large-scale PV systems on the voltage stability of sub-transmission systems. The study concluded that PV inverters operating in the constant power factor mode of operation would reduce the maximum loadability of the sub-transmission system being analyzed from 2.6855 p.u. to 1.5706 p.u.

2.2.6.2 Impacts of Small/Medium PV Systems

This section discusses the anticipated impacts of small/medium PV systems on distribution networks:

i) Excessive reverse power flow: In a traditional distribution system, the power flow is usually unidirectional from the MV system to the LV system. However, in distribution systems with a high penetration level of PV electricity, there are instances when the net production exceeds the net demand (especially at noon). As a result, the direction of power flow is reversed, and power flows from the LV side to the MV side. In a study [27] performed on a typical UK urban distribution network in the city of Leicester, 45% of the installed cables were shown to experience reverse power flow when 50% of the rooftops are equipped with 2 kW PV arrays.

   This reverse flow of power results in overloading of the distribution feeders and excessive power losses [13]. Reverse power flow has also been reported to affect the operation of automatic voltage regulators installed along distribution feeders as the settings of such devices need to be changed to accommodate the shift in load center [14]. Reverse power flow also has adverse effects on distribution transformers online tap changers, especially if they are from the single bridging resistor type [67].

ii) Over voltages along distribution feeders: Reverse power flow leads to over voltages along distribution feeders. Capacitor banks and voltage regulators, previously used to provide a slight voltage boost, can now push the voltage further, above acceptable limits [68]. Voltage rise on MV networks is often a constraining factor for the widespread adoption of wind turbines. Voltage rise in LV networks may impose a similar constraint on the installation of PV systems [27].

   The previous problem is more likely to occur in electrical networks with high penetration of PV power generation. In the SolarSmart project in Anatolia, California, it was noticed that at night the substation voltage was 0.4-0.7 V higher than the home voltage which is typical for a unidirectional power flow from the MV to the LV network. However, during daylight hours, this situation was reversed and the home voltage became 0.7 V higher than the substation voltage, which was still within the ANSI range-A limits [59]. Nevertheless, this situation took place at a 13% PV penetration level, and it was expected that if the PV penetration level increased to 40%, the over voltage might exceed the acceptable range-A limits. In the Gunma demonstration project in Japan, it was noticed that when the solar insolation was more than 5 kW/m^2, the voltages of individual inverters went up by 2%. Also, the difference between weekly household load demand and the weekend load demand could shift the voltage profile of the feeder by 1.5 to 2% above the

maximum limit [54]. In The PV settlement in Schlierberg, Germany, violations of the upper voltage limits have been noticed, especially during high solar insolation intervals [56]. A voltage analysis case study for a distribution feeder in Canada [55] showed that at high penetration levels of PV electricity, voltage at the point of interconnection may increase by 2-3% above the no-load voltage level of the feeder, especially when the PV cluster is located far from the distribution transformer. This voltage rise may exceed acceptable limits when the voltage along the feeder is already boosted by transformer tap changers to compensate for voltage drop along the line.

iii) Increased difficulty of voltage control: In a power system with embedded distributed generation, voltage control becomes a difficult task due to the existence of more than one supply point. All the voltage regulating devices, i.e., capacitor banks and voltage regulators, are designed to operate in a system with unidirectional power flow. The impacts of the backfeed of PV units on these devices still need to be studied thoroughly.

iv) Excessive system losses: DG units in general reduce power system losses as they bring generation closer to the load. This assumption is true until extreme reverse power flow starts to occur. A study [12] showed that distribution system losses reach a minimum value at a DG penetration of 5%, but as the penetration level increases, the losses also increase and exceed the no-DG case.

v) Phase unbalance: Inverters used in small residential PV installations are mostly single phase inverters. If these inverters are not distributed evenly among different phases, phase unbalance may take place shifting the neutral voltage to unsafe values and increasing the voltage unbalance. This problem was observed in the PV installation at Freiburg, Germany, where the power unbalance reached over 6% [57] (for 80% PV penetration).

vi) Power quality problems: Power quality issues are one of the major impacts of high PV penetration on distribution networks. Power inverters used to interface PV arrays with power networks are producing harmonic currents; thus, they may increase the total harmonic distortion (THD) of both voltage and currents at the point of common coupling. Previous research showed that voltage harmonics are usually within acceptable limits if the network is stiff enough with low equivalent series impedance [69]. Current harmonics, on the other hand, are produced by high pulse power electronic inverters and usually appear at high orders with small magnitudes [55]. An issue with higher order current harmonics is that they may trigger resonance in the system at high frequencies. This situation has occurred in the Bronsbergen holiday park in the Netherlands, where the 11^{th} and 15^{th} voltage harmonics exceeded permissible limits due to resonance between

the grid inductance and the inverter capacitance [57]. Diversity effect between different current harmonics can reduce the overall magnitude of these current harmonics; nevertheless, in [70] it is reported that the phase shift for single phase inverters is usually small, and thus these harmonic currents are added to each other, resulting in a total increase in the overall current THD. This condition was observed in the Nieuwland project in the Netherlands. Although each inverter complies with the Dutch power quality standards, measurements taken at the point of common coupling showed a high harmonic pollution level, which violates the Dutch power quality standards, due to interaction between the current harmonics of different inverters [58].

Another power quality concern is the inter-harmonics that appear at low harmonic range (below the 13^{th} harmonic). These inter-harmonics may interact with electronic loads in the vicinity of the inverter [71]. Even harmonics (especially the second harmonic) also adds to the unwanted negative sequence currents, resulting in overheating in three phase loads [40]. DC injections as well may accumulate and flow through distribution transformers, leading to a possible damage [40]. IEEE Std. 1547-2003 restricts DC injection from a PV system to 0.5%.

vii) Increased reactive power requirements: PV inverters normally operate at a unity power factor for two reasons:

- Current regulations do not allow PV inverters to operate in the voltage regulation mode. According to IEEE Std. 929-2000, PV inverters should operate at a power factor greater than 0.85 (leading or lagging) when the output is greater than 10% of its nominal rating.
- Owners of small residential PV systems in the incentive programs are revenued only for their active kilowatt-hour (kWh) production, not for their kilovolt-ampere hour (kVAh) production. Thus, they prefer to operate PV inverters at a unity power factor to maximize the active power generated, and accordingly, their return.

As a result, the active power requirements of existing loads are partially met by PV systems, reducing the active power supply from the utility. However, the reactive power requirements are still the same and have to be supplied completely by the utility.

A high rate of reactive power supply is not preferred by the utilities [55] because, in this case, distribution transformers will operate at very low power factor (as low as 0.6). Distribution transformers' efficiency decreases as their operating power factor decreases. As a result, the losses in distribution transformers increase, reducing the overall system efficiency.

viii) Electromagnetic interference issues: The high switching frequency of PV inverters may result in electromagnetic interference with neighboring circuits such as capacitor banks, protection devices, converters and DC-links [55] leading to malfunction of these devices.

ix) Difficulty of islanding detection: The North American Electric Reliability Corporation (NERC) requires PV systems to be disconnected once the connection with the utility supply is lost, as they can enlive the utility system and impose danger on personnel and equipment. Similarly, IEEE Std. 929-2000 recommends that PV inverters should be disconnected within six cycles if an islanding condition is detected.

Many techniques can be used to detect islanding, such as passive [72-80], active [81-87], hybrid [88-90] and communication-based techniques [91-94]. However, most of these techniques are characterized by the presence of non-detection zones defined as the loading conditions for which an islanding detection technique would fail to operate in a timely manner, and are thus prone to failure [95]. Moreover, the inclusion of islanding detection devices increases the overall cost of PV systems.

2.2.7 Maximum Recommended Penetration Levels for PV Systems

A considerable amount of the literature has focused on determining the maximum allowable penetration level of PV systems that will not violate any of the network's operational constraints. A summary of previous research findings is shown in Table 2-1 [68].

From these results, it can be concluded that there is no agreed-upon maximum allowable penetration limit for PV electricity. Results in the literature vary from 1.3% up to 40% depending on the limiting factor as well as the size, location and geographic distribution of PV arrays. Thus, a comprehensive techno-economic assessment should be performed for each individual network to determine the maximum allowable PV penetration in such a network. For example, Hydro One –the largest distribution utility in Ontario– requires that distributed generation "to be interconnected to a distribution system circuit line section, including the proposed generator, not to exceed 7% of the annual line section peak load" [15].

2.2.8 Measures to Increase the Penetration Limits of PV Systems

The literature contains several measures that can be adopted to Increase the maximum allowable penetration limits of PV electricity. Examples of these measures are included below:

Table 2-1 Summary of maximum allowable PV penetration limits reported in the literature [68]

Reference	Penetration Limit	Limiting Factor
[25]	5%	Ramping rates of generators during cloud transients (central station PV)
[61]	15%	Ramping rates of generators during cloud transients (distributed PV)
[63]	1.3%	Power fluctuations due to cloud transients for central station PV
[63]	6.3%	Power fluctuations due to cloud transients if the PV system is distributed in a 10 km^2 area.
[63]	18.1%	Power fluctuations due to cloud transients if the PV system is distributed in a 100 km^2 area.
[63]	35.8%	Power fluctuations due to cloud transients if the PV system is distributed in a 1000 km^2 area.
[24]	10%	Frequency regulation expansions vs. break-even costs.
[26]	Minimum feeder loading	Over voltages assuming no load tap changers (LTCs) exist in the MV/LV transformer.
[28, 96]	40%	Voltage regulation
[12]	5%	Minimum distribution system losses
[27]	33%	Over voltages

i) Utilizing fast-acting energy storage systems: Storage devices operating in parallel with PV systems can compensate for any rapid power fluctuations (due to partial shading and moving clouds) and firm up the output power of PV sources; thus, acting as a synthetic inertia [97]. This results in a reduction in voltage and frequency fluctuations in power networks, which improves the overall system stability.

However, currently available storage technologies have limited power densities and are relatively expensive. For these reasons, the storage capacity available worldwide is only 90 GW, which represents only 2.6% of the 3400 GW global electric production [98].

ii) To mitigate the negative impacts of PV electricity on power system stability, the authors of [64] suggested that critical synchronous generators should be always kept online to maintain sufficient inertia in the system. However, a drawback of this suggestion is that these generators might operate outside of their economical operating ranges.

iii) The authors of [26] suggested using controllable PV systems as a means to avoid over voltages along distribution feeders. This goal can be achieved by using automatic voltage-limiting inverters. In case of over voltages, the PV inverter reduces its output power using one of the following methods:

- Power factor control: Changing the operating power factor from unity to a lagging power factor to absorb reactive power and limit the over voltage in the network. However, this measure is prohibited under current standards (IEEE Std. 929-2000).
- Output current regulation [54]: Shifting the operating point of the PV array to a point above the maximum power point (MPP) on the array's I-V characteristics curve, such as to reduce the power extracted from the PV array during over voltage conditions. This method is currently adopted in the Gunma demonstration project in Japan. Field measurements showed that the output current regulation was not too frequent, but the associated energy losses were more than 50% in some cases; thus, this method is not preferred. Another disadvantage of this method is that it may interfere with the operation of active islanding detection techniques implemented in PV inverters [68].

Controllable PV systems require over voltage monitoring devices on all individual inverters. These monitoring devices increase the cost of PV systems significantly and make them more sensitive to short-term voltage fluctuations.

iv) Adjusting distribution transformer tap settings to avoid over voltages: This solution can be a suitable measure to increase the PV penetration in a given network with limited cost; however, it has the following drawbacks:

- It allows only for a limited increase in the PV penetration level.
- If the transformer tap setting is reduced to avoid over voltages during noontime, then after sunset, the voltage drop along the distribution feeder (during peak demand periods) may result in excessive under voltages at the far end customers.
- Due to variations between summer and winter load, the tap settings should be changed seasonally. Interruption of electricity supply will be required for the adjustment of offline tap changers.

v) Customer initiatives and demand side management (DSM): One of the efficient measures to accommodate higher PV penetration limits is to change the end customers' patterns of usage. Experience in Denmark [26] showed that when customers became themselves power producers, they became more aware of network problems, and were more willing to change their usage patterns either by:

- Moving their peak consumption to noon when PV systems are producing maximum power. This behavior can be encouraged by government or utility incentives, i.e., TOU rates.
- Implementing a smart load-shedding scheme for users at the far end of distribution feeders. These customers are the ones who are more likely to experience under voltages during heavy loading conditions. In the proposed load-shedding scheme [68], the distribution transformer tap setting is reduced, and when there are heavy loading conditions on the circuit, a low voltage threshold signal is sent to the non-critical loads at these customers so as to disconnect them and reduce the circuit loading, thus improving the system voltage. Reducing the sending end voltage gives more room for the utility to increase the PV penetration level; however, incentives should be given to customers to compensate for the frequent disconnection of loads.

vi) In [28], the authors suggested using dump loads at noon when PV arrays are generating their peak output. During the periods of over voltages, a dummy load is switched on to consume the excess power in the feeder, and limit over voltages. However, this method represents unjustified loss of energy.

It has to be noticed that integrating PV systems is not the only challenge facing power systems in the smart grid era; EVs represent another major challenge, which is discussed in the following section.

2.3 Integrating EVs into Power Networks

EVs are becoming an increasingly attractive alternative to vehicles powered by internal combustion engines (ICEs) because they produce considerably lower amounts of greenhouse gas emissions and achieve greater fuel economy. Types of electric vehicles, their benefits, limitations and potential impacts are discussed in the following sections.

2.3.1 Classification of EVs

EVs can be broadly classified into the three following categories:

i) Hybrid electric vehicles (HEVs): These vehicles combine an ICE, storage battery, electrical generator and electrical motor to optimize engine size and operation. HEVs use their ICE to generate electricity by spinning an electrical generator, to either recharge their batteries or to directly power the electrical motor. Thus, the operation of the electric motor complements that of the ICE. HEVs are equipped with different types of efficiency-improving technologies such as:

- Regenerative braking, which converts the vehicle's kinetic energy during braking into electric energy (that can be used to charge the battery), rather than wasting it as heat energy as conventional brakes do.
- Start-stop systems, which reduce idle emissions by shutting down the ICE at idle and restarting it when needed.

Since HEVs are powered only by gasoline or diesel fuels, some researchers do not classify them as EVs but as highly efficient conventional vehicles.

ii) Battery electric vehicles (BEVs): BEV is a type of EV powered only by an electrical motor supplied by a battery storage system. BEVs are mechanically simple, as the equipped electrical motor can deliver full torque from rest over a wide range of speeds; thus, this type of vehicle can be easily controlled without the need for multiple gears.

However, the substantial drawback of such vehicles is their limited range, resulting from the low energy density of the available battery technologies. This restriction represents a major constraint to their commercialization. Hence, they are used primarily in special applications for which low noise and emissions are important features such as small urban delivery vehicles.

iii) Plug-in hybrid electric vehicles (PHEVs): These are variants of HEVs but are equipped with a larger capacity battery that can be recharged from an external electricity supply, making them bi-fuel vehicles, i.e., fuelled by both gasoline and electricity. Batteries are thus rated based on the distance and speed the vehicle can be driven on electricity alone before the ICE is required to provide additional power for higher speeds and to recharge the battery. This represents a trade-off between the higher costs of larger capacity batteries and the distance the vehicle can operate using its battery only. Typically, this distance approximates average commuting distances; for example, the GM Volt is designed to operate for up to 40 miles on electricity only.

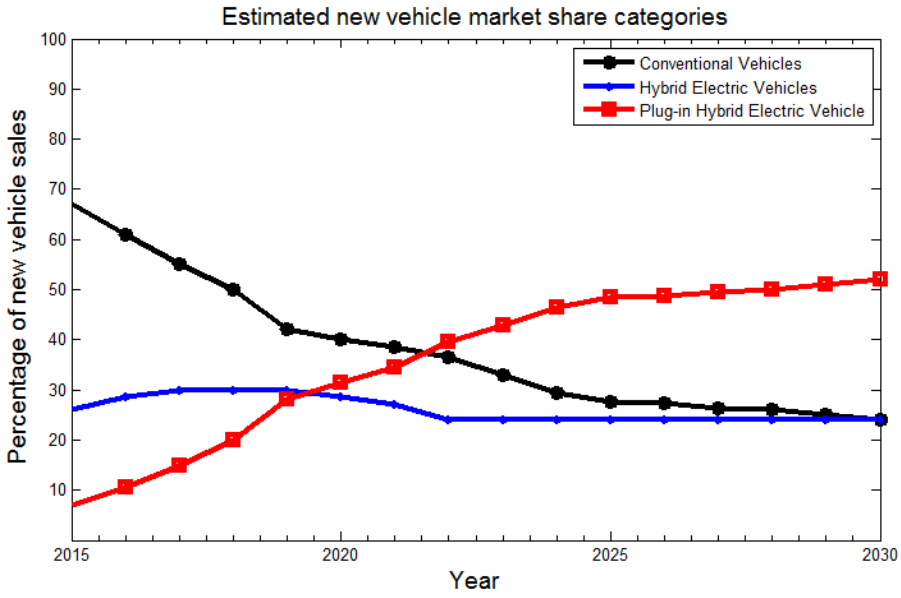

Figure 2-4 Projected new vehicle market share categories [99]

2.3.2 EV Market Forecast

In the medium-to-long term, PHEVs are expected to be the most commercially developed type of EVs [11]. This expectation is attributed to their greater fuel economy and lower price compared to other types of EVs. A study conducted by the Electric Power Research Institute (EPRI) [99] estimated that the sales of PHEVs in the U.S. are expected to become more than 50% of all new vehicle sales by 2030 as shown in Figure 2-4. Similar results have been reported in [100].

With regards to PHEV penetration levels, a study [101] conducted by the National Renewable Energy Laboratory (NREL) estimated that PHEVs will achieve a 50% total market penetration level by 2050. Similarly, the authors of [102] estimated the anticipated penetration level of PHEVs in the U.S. using a Bass forecasting model and concluded that PHEVs will reach approximately 32% total market penetration by 2030.

Based on the previous discussion, only PHEVs are considered in this research.

2.3.3 Benefits of PHEVs

Using PHEVs instead of conventional vehicles offers several potential benefits to both electric utilities and the environment. A summary of these benefits is provided below:

i) Greenhouse gas mitigation: One of the primary drivers for utilizing PHEVs is the associated reduction in greenhouse gas emissions. A study conducted by EPRI [32] revealed that, even when coal is used to generate the electricity, PHEVs emit 28% to 34% fewer well-to-wheel greenhouse gas emissions than their gasoline counterparts. Another study in the U.S. [9, 10] showed that if 43% of the U.S. light-duty vehicle fleet is replaced by PHEVs, the total greenhouse gas emissions would be reduced by 27%.

ii) High efficiency: PHEVs offer about 60% more mileage from the same amount of primary energy than conventional vehicles [33]. This extended mileage is attributed to the different types of efficiency-improving technologies associated with PHEVs, e.g., regenerative braking, start stop systems, etc.

iii) Energy security: The dependency on imported oil has been one of the national threats facing developed countries since the 2008 oil shock. This threat can be resolved by displacing petroleum with a less volatile and low marginal cost energy resource such as electricity [99]. In the U.S., the unutilized energy in the existing generation infrastructure can accommodate 74% of the light-duty vehicle fleet – a gasoline displacement potential of 6.5 million barrels of oil per day, which is equivalent to 52% of the U.S. oil imports [9]. This advantage was the main reason behind the allocation of $2.4 billion to transportation electrification projects in the U.S. 2009 economic stimulus package.

iv) Increased utilization of installed capacity: Using the unutilized generation capacity to charge PHEVs allows utilities to sell more electricity without installing additional power generation or transmission assets. This situation will be reflected as an increase in their gross revenue. In [9, 10] it was shown that there will be $1.04 billion additional revenue for U.S. utilities per 1% increase in the PHEV market share. This increased revenue can reduce the average cost of electricity generation by up to 20% [9, 10].

2.3.4 Limitations of PHEVs

Despite all the previously mentioned benefits, PHEVs have some serious limitations that constrain their commercialization. These limitations can be summarized as follows:

i) Cost: PHEVs nowadays are 50% to 100% more expensive than their conventional counterparts primarily due to the high cost of available battery storage technologies (approximately 500-1000 $/kWh) [103]. A study conducted in the U.S. [9, 10] calculated the life cycle cost (LCC) for a

PHEV and compared it with that for a conventional vehicle. The study concluded that at existing residential electricity rates and for a range of gasoline prices, prospective PHEV purchasers can afford to pay a premium of up to a few thousand dollars over the cost of a conventional vehicle and still break even on the LCC of purchasing and operating a PHEV. The lower the cost of electricity and the higher the price of gasoline, the more the premium is expected to be (can reach up to $7000). Nevertheless, the anticipated premium is not enough to cover the difference in price between a conventional vehicle and a PHEV. However, some studies expect that by the early 2020s, the cost of batteries could be reduced to 200 $/kWh [11]. Accordingly, the anticipated costs of PHEVs and conventional vehicles could converge, and the cost of PHEVs will align with that of gasoline engine vehicles by the mid-2020s [104].

ii) Charging infrastructure: Another limitation to the widespread adoption of PHEVs is the high initial cost of charging infrastructure. A report for Boston Consulting Group (BCG) [105] forecasts that $21 billion investments will be needed for charging infrastructure in Europe by 2020.

iii) Battery size and weight: As explained earlier, batteries are characterized by their low energy densities compared to petrol and diesel; thus, battery packs are usually heavy and take up considerable vehicle space. For example, the GM Volt has a battery weight of 197 kg for a battery capacity of 16 kWh.

iv) Range: The PHEV driving range is one of the most important drawbacks imposed by the low energy density of the available storage technologies. Today, the PHEV's electric-only operation is limited to only 40 miles. However, battery technologies are continually improving and with the advancements in lithium-ion and lithium-sulphur technologies, the limitations imposed by heavy weight and limited range are expected to erode with time. Energy density has already doubled between 1994 to 2004 [11]; thus, it is not too optimistic to predict that PHEVs' energy capacity may double, or even triple, over the next 20 years.

v) Extended charging duration: A major drawback for PHEVs is the long time required to recharge their batteries. These extended charging durations reduce the freedom to shift PHEV charging demands to off-peak periods. For example, a 16 kWh battery pack can take from 2 to 8 hours to recharge depending on how far the vehicle was last driven, and the charging method.

2.3.5 Technical Impacts of PHEVs

Despite their positive impacts on the environment and national economy, PHEVs have serious impacts on distribution systems:

i) Overloading of distribution equipment: Early PHEV integration studies focused mainly on determining whether the existing generation capacity would be sufficient for supplying PHEV charging demands. For example, a study conducted by EPRI [32] concluded that if PHEVs replace half of all vehicles in the U.S. by 2050, an increase of only 8% in the electric generation capacity will be required. Another study [10] concluded that 74% of the U.S. light-duty vehicle fleet can be supplied using the unutilized capacity within the existing generation infrastructure.

However, these optimistic predictions can be misleading for the following reasons:

- These studies assume that PHEV charging demands will simply fill the valley in the system load curve, an assumption that is not always true because of the natural coincidence between peak electricity demand and the hours during which the majority of vehicles are parked at residences and are thus probably being charged [34]. Moreover, as explained earlier, some battery packs require extended charging durations (up to 8 hours), which reduces the freedom to shift their charging demands to off-peak periods.
- They assume a homogenous distribution of PHEVs throughout distribution networks, which is not always the case: the PHEV charging loads are not likely to grow uniformly in a utility service area but are more likely to be spatially clustered in residential areas and less so in commercial or industrial centers [35, 106]. Such geographical clustering can result in significant overloads at secondary distribution levels where the anticipated diversity benefits are not as evident as at higher system levels, even though the utility system as a whole may have sufficient or excess generation capacity to supply the required charging demands.

Shafiee *et al.* [36] developed a comprehensive model to analyze the anticipated impacts of PHEVs on residential distribution systems. The study concluded that increased PHEV penetration increases the system peak demand. For example, at 35% PHEV penetration, the system peak demand increases by 22.7% from the corresponding no-PHEVs case. The authors of [18] analyzed the impacts of PHEVs on distribution networks in British Columbia. The study considered three types of networks, namely urban, sub-urban and rural. The authors concluded that even for only 5% PHEV penetration, the uncontrolled charging patterns would result in a

large increase in the existing peak demand for all the considered networks. If the penetration level increases to 25%, the resulting peak demand would exceed the system capacity (especially for rural networks), and so the existing distribution infrastructure should be upgraded. Putrus *et al.* [20] conducted a similar study in the UK and concluded that the uncontrolled charging of PHEVs would result in an increase of about 18% in the network peak demand per 10% increase in PHEV penetration. A study prepared by the Center for Entrepreneurship and Technology at the University of California, Berkley, [21] concluded that the uncontrolled charging of PHEVs tends to create secondary demand peaks greater in magnitude and duration than those of the existing system peaks. For example, at a 10% penetration level of PHEVs, the peak demand increases by 5% and lasts more than three-and-a-half hours.

Taken together, these results suggest that PHEVs will lead to significant overloading of the distribution system; however, there is inconsistency in the literature regarding the severity of the resulting overloads. This inconsistency is attributed to the several assumptions and approximations adopted by previous researchers while modeling different uncertainties characterizing PHEV charging, a point that is discussed in more detail in the later chapters.

Overloading of the distribution networks can cause premature degradation of the distribution equipment. It may also impact the overall system reliability as the entire infrastructure is operated closer to its maximum capacity for longer periods, which increases the probability of equipment failure. Overloading of the distribution feeders will result in excessive power losses and increased voltage drops that may exceed permissible limits.

ii) Power quality problems: The battery chargers associated with PHEVs are highly non-linear electronic circuits; thus, they produce negative effects on the utility distribution system. However, there is no general agreement on the THD levels generated by such chargers [33]. Some manufacturers claim to have designs that produce extremely low THD levels, but most researchers consider PHEV battery chargers to be highly contaminating loads, with average THD values of about 30%. A report prepared by the California Energy Commission [19] estimates the current THD at the beginning of charging to be between 2.36% and 5.26%, reaching up to 28% at the end of charging. Another study [107] concluded that the THD increases from 20% to 67% as the state of charge (SOC) varies from 0% to 88%, respectively. Practical measurements carried out on commercial chargers in [108, 109] showed THD values as high as 70%.

iii) Impacts on distribution equipment operation: Overloading of the distribution equipment as well as high levels of harmonic pollution impact the operation of different classes of distribution equipment:

- Transformers: PHEV charging loads cause overheating in distribution transformers. This overheating results from the additional power losses due to fundamental and harmonic components of the charging current. In addition to the previous losses, extra losses are caused by the non-uniform distribution of current in the transformer windings (skin and proximity effects). The net effect is a higher high-spot temperature which reduces the transformer useful life. Gomez *et al*. [33] investigated the effect of battery chargers on distribution transformer life expectancy and deduced that the uncontrolled charging of PHEV can be detrimental to transformer life. Calculations showed a quadratic relationship between the transformer life consumption and THD of the battery charger current. The study concluded that in order to have a reasonable transformer life expectancy, the charging current THD should be limited to only 25-30%.

- Cables: PHEV battery chargers draw highly distorted charging currents. These distorted currents have two direct impacts on electrical cables. The first is the non-uniform distribution of current in the conductors due to skin and proximity effects; these effects already exist at power frequency, but are more noticeable at higher harmonics. The second impact is the overloading of the neutral conductor due to the accumulation of triple-N harmonics. These impacts result in increased ohmic losses in cables and thus a reduction in their life expectancy. A study conducted in [33] concluded that these two impacts are more likely to occur in the case of single phase battery chargers. The authors recommend that neutral conductors should have a cross-section area at least double that of the phase conductors in distribution networks with high penetration levels of PHEVs.

- Circuit breakers: The harmonic distortion resulting from battery chargers strongly affects the interruption capability of circuit breakers. This is explained by the fact that distorted currents result in higher rates of change of current with respect to time (di/dt) at the natural zero current crossing, making the arc interruption more difficult, as it necessitates the control of higher arc energies [33]. Harmonic components also increase the root mean square value of the sensed current, shifting the overload thermal characteristics of circuit breakers.

- Fuses: Fuses are usually built with several parallel ribbons as fuse elements. Under a high penetration of PHEVs, these ribbons are susceptible to skin and proximity effects resulting from harmonic currents, which may shift the fuse operating characteristics [110].

2.3.6 Measures to Mitigate the Negative Impacts of PHEVs

In this section, some of the measures proposed in the literature to mitigate the negative impacts of PHEVs on distribution networks are presented:

i) Smart (coordinated) charging: In the previous section, it was shown that the uncontrolled charging of PHEVs (totally based on customer behavior) tends to create secondary demand peaks, greater in magnitude and duration than those of the existing system peaks. For this reason, the current research on the development of PHEVs' supply equipment emphasizes smart charging as a possible means to facilitate the integration of PHEVs within existing distribution networks.

Smart charging provides an interaction between PHEVs battery chargers and the electric utility, and thus, can shift PHEV charging demands to off-peak periods. This target can be achieved using several control strategies. Examples of such strategies include, but are not limited to:

- Adopting a real-time electricity tariff structure that aims to fill the valley in the system load profile. This strategy can be realized by offering real-time electricity rates that are proportional to the difference between the actual and the anticipated load demands. The battery charger should have an algorithm to determine whether to purchase electricity (and charge the vehicle) at the current electricity rate or not. This kind of control is complex and expensive, as it necessitates the installation of two-way communication infrastructure in distribution systems; however, it has the advantage of distributing the PHEV charging demand evenly throughout the whole off-peak period, resulting in a near-flat load profile.
- Adopting TOU electricity rates that divide the day into peak and off-peak periods. These rates provide economic incentives for customers to shift their PHEV charging to off-peak periods. However, this type of control may create high coincident charging load at the beginning of the off-peak period when all customers would tend to plug in their PHEVs simultaneously. A study performed by EPRI [16] found that this type of control can result in a PHEV peak charging demand three times higher than that resulting from the uncontrolled charging. The

study concluded that it is important to diversify the charging times throughout the whole off-peak period by installing proper communication and control capabilities.

The literature describes several smart charging schemes for PHEVs. For example, the authors of [111] proposed a smart charging scheme for PHEVs such as to minimize the power losses and to maximize the grid load factor. In [112], a smart distribution power flow (SDPF) framework was developed to determine the coordinated charging schedules for PHEVs such as to minimize the total feeder losses. Another study by Hilshey *et al.* [37] presented a smart charging scheme that manages EV charging based on estimated transformer temperatures. Similarly, reference [113] proposed a smart charging algorithm for PHEVs to reduce the loss of life in transformers.

Nevertheless, a March 2011 study by EPRI [114] reported that the full deployment of the two-way communication infrastructure necessary for the implementation of smart charging schemes is very unlikely to occur before 2030. Thus, smart charging is not considered in this research.

ii) Vehicle-to-grid (V2G) technology: The ability of PHEVs to store energy in their batteries has encouraged several manufacturers to design these batteries such that they are able to pump this energy back to the grid to provide voltage and frequency regulation, spinning reserve, and demand side management. This technology represents a potential alternative to increase the amount of distributed generation within the power system. A vehicle with this type of technology is defined as being vehicle-to-grid capable [115]. V2G vehicles can absorb excess electric energy produced by renewable resources when the grid is operating at light load conditions and the rate of electricity is low, and then sell this energy back to the utility at higher prices during peak demand periods, when other PHEVs are charging. Thus, V2G technology can provide some financial benefits to the owner of a PHEV to counteract its high initial cost.

However, V2G technology is not expected to be available in the near future for the following reasons [21]:

- The PHEV technology is still in its infancy; it is unlikely that either the manufacturers or the utilities will risk interconnecting at this early stage.
- Lack of two-way communication infrastructure in distribution systems [114].
- Economic justification for consumers is as yet unproven: PHEV batteries currently have only 2000-8000 charging cycles [116]; thus, the return received for selling electricity back to the utility should outweigh the cost of shortening the effective life span of the battery.

- Economic justification for utilities is also not yet proven: In order to support V2G technology, utilities will have to install two-way metering systems for each consumer, and make changes to their billing systems. It is not proven yet that the potential benefits of this technology would justify the extra cost.

Thus, for the previously mentioned reasons, V2G capability is not considered in this research.

2.4 Summary and Conclusions

In this chapter, two of the main challenges facing power systems in the smart grid era were discussed, which are integrating PV systems and PHEVs into existing networks.

In the first part of the chapter, the different components of solar PV systems were introduced; their benefits and limitations were highlighted; then the potential impacts of PV electricity on power networks were discussed. Finally, the literature findings regarding the maximum allowable PV penetration that can be safely integrated into existing networks were summarized. It was concluded that there is no agreed-upon maximum allowable penetration limit for PV electricity; results in the literature vary from 1.3% up to 40%.

In the second part of the chapter, the different types of EVs were presented; their benefits and limitations were reviewed; then the potential impacts of PHEVs on distribution networks were discussed. Finally, the measures proposed in the literature to facilitate the integration of PHEVs in distribution systems were highlighted. It was concluded that PHEV charging demands will cause substantial distribution equipment overloading, due to the natural coincidence between peak electricity demand and the hours during which most vehicles are parked at residences and are thus probably being charged.

An interesting observation made in this chapter is that, although researchers generally agree that high penetration levels of PV electricity and PHEVs will have significant impacts on distribution networks, there is inconsistency in the results reported in the literature regarding the severity of the anticipated impacts. This inconsistency is attributed to different sources of uncertainty inherent in distribution systems: uncertainties associated with the PV array output, the PHEV charging demand, and existing electrical loads are all contributing factors that make the assessment of such impacts a very difficult task. This, in turn, necessitates the development of accurate models to represent the previously mentioned uncertainties, a point that is discussed in the next chapter.

Chapter 3
Modeling Distribution System Uncertainties

3.1 Introduction

As explained earlier, assessing the anticipated impacts of PHEVs and PV electricity on residential distribution networks is a challenging task due to the uncertainties associated with existing electrical loads, the PHEV charging demand, and the PV array output. MC simulation is a computational technique based on the use of random numbers and probability theory to solve problems of a stochastic nature. During a MC simulation, the stochastic inputs of the system being analyzed are represented by probability distributions. By running the simulation over and over again, and each time using a different randomly selected set of inputs (generated from the predetermined probability distributions), it is possible to determine the range of probable outcomes that could occur and the likelihood of any of these outcomes occurring. This feature makes MC simulations a suitable tool to handle the uncertainties at hand, and was thus used in this research to analyze the performance of the distribution system under a high penetration levels of PV systems and PHEVs.

However, in order to generate the random variables required for the MC simulation, accurate probabilistic models must be developed for the previously mentioned stochastic quantities. This is explained by the fact that, according to MC simulation theory [117], if the inputs for a certain process are randomly sampled following their actual probability distributions, the output will be also random; however, the probability distribution for the random output will follow that of the true output with acceptable error, and according to the law of large numbers (LLNs) [118], both probability distributions will coincide after an infinite number of simulations. Conversely, if the simulation inputs are generated in a totally random fashion (without following their actual probability distributions), there is no guarantee that the estimated output will represent the true output [117].

In this chapter, the probabilistic models used in this research to represent the previously mentioned stochastic quantities are developed. Details of the proposed models are presented below.

3.2 Modeling PV Systems Electrical Output

Modeling PV systems electrical output is a very difficult task as the power output of PV array is highly dependent on the solar insolation and ambient temperature, as shown in Figures 3-1 and 3-2:

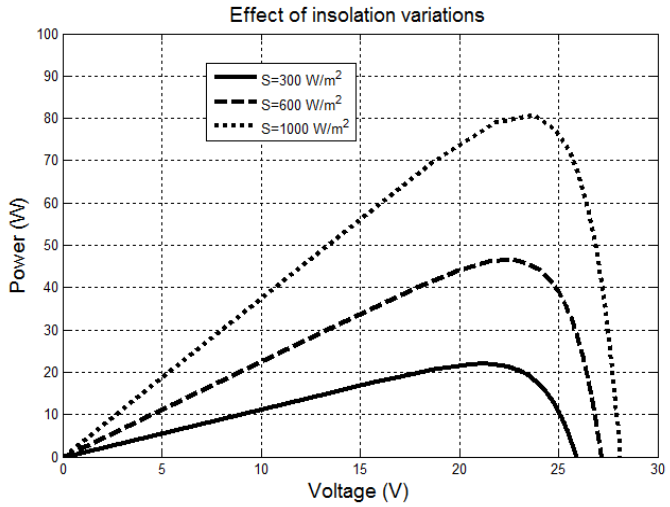

Figure 3-1: Effect of insolation variations on the power output of a 100 W PV module

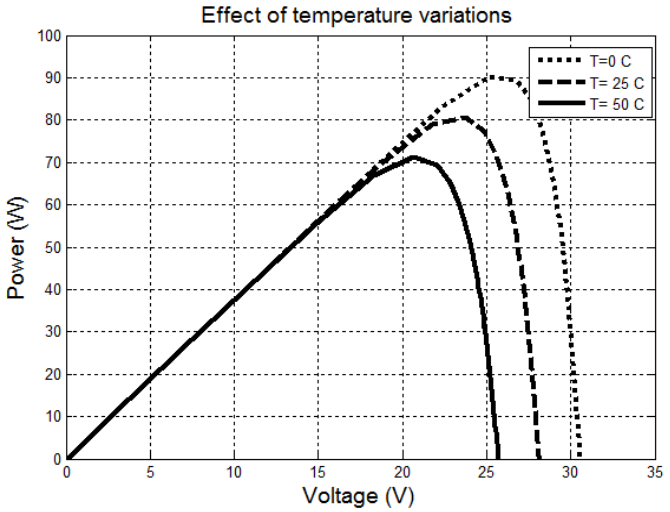

Figure 3-2: Effect of temperature variations on the power output of a 100 W PV module

To date, models used to represent PV systems electrical output can be broadly classified into two distinct categories [119]:

i) Deterministic models: In this modeling approach, PV systems are represented as constant power sources; this constant power can be either:

- The average power output calculated from the capacity factor for the PV system being analyzed. This modeling approach was used in [120] to assess the impacts of central PV stations on power system security.

- The worst-case scenario for the area under study, such as when the PV source is generating its maximum output and the load demand is minimal or vice versa. This modeling approach was used in [55] to study the impact of high penetration of PV generation on system voltages.

These models are straightforward and simple; however, they are not particularly suitable for assessing the long-term behaviour of PV systems, or to model the temporal variations in their electrical output. Accordingly, their results cannot be generalized to give an overall idea of the performance of PV systems. Another drawback of such models is that they only study predetermined situations, which may not be the ones leading to limits violations. These disadvantages make deterministic models unsuitable for use in MC simulations.

ii) Probabilistic models: In the probabilistic modeling approach, the PV system output is modeled as a random variable that follows a predetermined probability distribution (e.g. Weibull [121], beta [122] and normal [123] distributions). These models were used in [121] to design a PV station in a LV feeder, in [122] to assess the performance of utility-interactive PV systems and in [123] to determine the optimal configuration of energy storage systems operating in a distribution network with high penetration of PV generation.

The probabilistic modeling approach has several drawbacks. First, it does not consider the temporal variations in PV array output [119]. This is explained by the fact that the output of the PV array at the i^{th} hour is assumed to depend only on the value of the random variable generated at hour i and the predetermined probability density function (pdf). In PV systems, these temporal variations occur very frequently and cannot be neglected. This drawback can be eliminated by using a different pdf to represent the PV system electrical output in each hour of the day during each month of the year. However, the huge computational burden associated with using 288 different pdfs in the random variable generation during MC simulations makes this solution computationally expensive.

From the previous discussion, it becomes evident that a robust model for PV system output should satisfy the following criteria:

i) Assess the long-term behavior of the PV system under study;

ii) Consider the temporal variations in the PV system power output;

iii) Have a minimal computational burden.

These requirements were the motivation for the work by Omran *et al.* [119], in which the authors assembled the 24 data points representing the PV system electrical output for each day in a data segment. The resulting 365 data segments representing the whole year were then evaluated for similarities using principle component analysis (PCA), and similar segments were grouped together into the same cluster, using crisp clustering algorithms (K-means and hierarchical clustering). For each cluster, a representative segment was selected and used to model the behavior of all the days within the cluster. This approach reduces the computational burden to a minimum while keeping the temporal variations in the data set.

However, the described model has the following drawbacks:

i) All of the representative segments were assumed to have the same probability of occurrence, an assumption that ignores completely the probabilistic nature of the problem, making this model unsuitable for use in MC simulations.

ii) The authors used crisp clustering techniques to assign data segments to different clusters; however, in [124] it has been shown that fuzzy clustering techniques are more useful when clusters are not well separated and boundaries are ambiguous, which is the case with PV data sets.

In the subsequent sections, a model that avoids the previous drawbacks is developed. The flowchart of the proposed model is shown in Figure 3-3.

3.2.1 Data Collection Stage

The hourly insolation and temperature data used in this work was provided by the Solar Radiation Research Laboratory for a site with the following coordinates: Latitude: 39.742 North, Longitude: 105.18 West, for the period from March 20, 2010, to March 19, 2011. The total hemispheric solar irradiance on a south-facing surface tilted 40 degrees from horizontal was measured using two different Pyrometers, and the average of both readings was computed and used throughout the rest of this analysis. Ambient air temperature was measured with a Vaisala probe mounted in a naturally aspirated radiation shield, two meters above ground surface.

Based on the selected hourly resolution, the annual data set is represented by two vectors, each composed of 365 data segments (or days):

i) A (365 segments × 24 data point/segment) vector containing the global insolation data;

ii) A (365 segments × 24 data point/segment) vector containing the ambient temperature data.

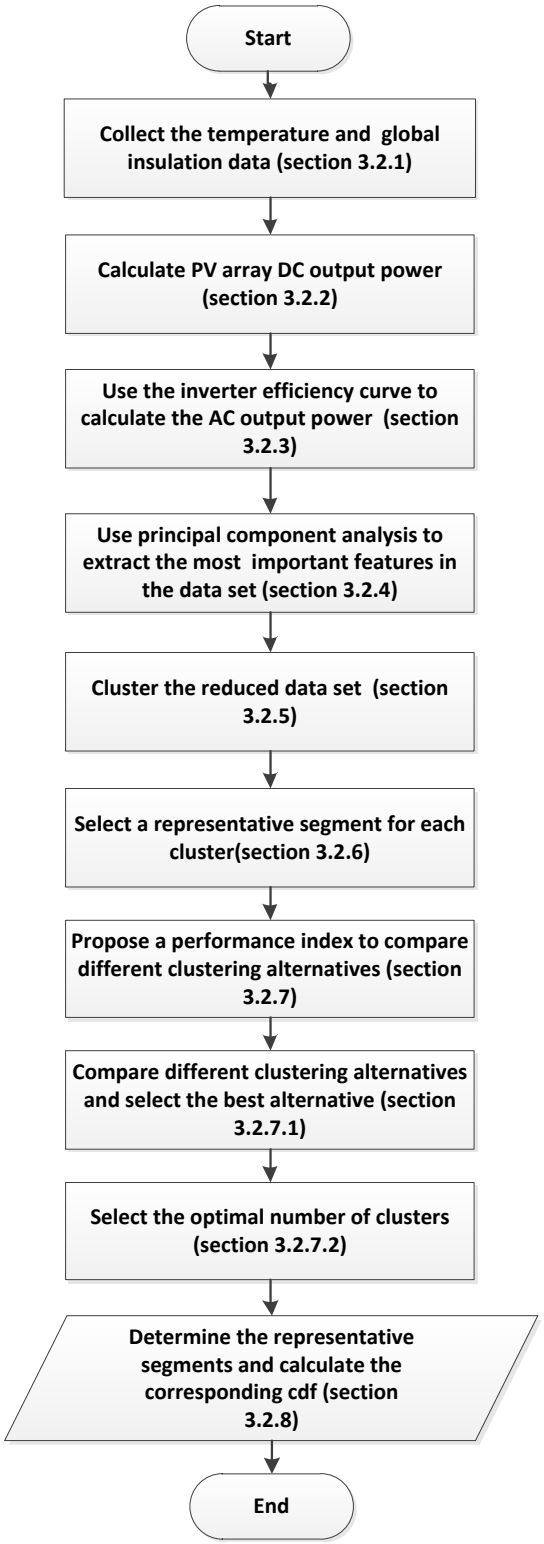

Figure 3-3: Flowchart of the proposed model

3.2.2 Calculating PV Array DC Power Output

The literature contains several methods that can be used to estimate PV array DC output. These methods can be broadly classified into the following two categories:

i) Detailed physical methods [125-129]: These methods accurately represent the physical behavior of PV cells using semiconductor device equations. This feature makes these methods suitable for applications that require detailed cell-level information (i.e. studying the effect of partial shading on PV cell behavior [130]). The only disadvantage of these methods is their complexity since the semiconductor device equations cannot be solved directly using analytical methods. Many dedicated software packages are available to solve these equations numerically, such as the PC1D software (developed by the University of New South Wales in Australia).

ii) Simplified methods [131-134]: These methods are based on empirical formulas that can estimate the power output of PV systems during different operating conditions. These methods are not as accurate as the detailed physical methods; however, they are simple, straightforward and their results are not too far from the exact results. For the above-mentioned reasons, these methods are favored when studying the impact of PV systems on the utility grid [12, 134], and so they will be used in this research.

The literature contains numerous simplified empirical methods that can be used to estimate PV system DC power output [131-134]. However, based on the results of [135], the simplified equations presented in [134] will be adopted in this research.

With the selected empirical method, the DC power output of a PV array ($P_{PV,DC}$) with total cross section area A_{Total}, receiving global isolation S_{Global} and with overall efficiency $\eta_{Overall\ array}$ is calculated as:

$$P_{PV\ ,DC} = A_{Total} * S_{Global} * \eta_{Overall\ array} \tag{3.1}$$

For this work, the total area is taken to be 80 m^2, which is typical for 10 kW PV array (56 modules × 180 watt/module).

The PV array overall efficiency ($\eta_{Overall\ array}$) is calculated as:

$$\eta_{Overall\ array} = \eta_{Dust} * \eta_{Mismatch} * \eta_{PV\ DC\ losses} * \eta_{MPP} * \eta_{\mathrm{Module}} \tag{3.2}$$

where

η_{Dust} = 1 - the fractional power loss due to dust on the PV array;

$\eta_{Mismatch}$ = 1 – the fractional power loss due to module parameter mismatch;

$\eta_{PV\ DC\ losses}$ = 1 – the fractional power loss in the DC side;

η_{MPP} = 1 – the fractional power loss due to MPPT algorithm error caused by the switching converter;

η_{Module} is the PV module efficiency.

Typical values for these efficiencies are given in Table 3-1:

Table 3-1: Typical percentage efficiencies of a PV module

Efficiency	η_{Dust}	$\eta_{Mismatch}$	$\eta_{PV\ DC\ losses}$	η_{MPP}
Percentage	96%	95%	98%	95%

η_{Dust} is verified experimentally in [133], η_{MPP} is given in [136], $\eta_{PV\ DC\ losses}$ and $\eta_{Mismatch}$ are suggestions of manufacturers [133].

The module efficiency (η_{Module}) is given by:

$$\eta_{\mathrm{Module}} = \eta_{STC}[1 + K_T(T_c - 25)] \tag{3.3}$$

where

η_{STC} is the efficiency of the PV module at STC (standard test conditions), which are the operating conditions when global irradiance equals 1000 watt/m^2 and ambient temperature equals 25^{o}C, and was calculated using the PC1D simulator to be equal to 13.62%;

K_T is the thermal derating coefficient of the PV module in $^oC^{-1}$ and was estimated experimentally in [136] to be equal to -0.0037 $^oC^{-1}$;

T_c is the cell internal temperature at ambient temperature (T_a) given by:

$$T_c = T_a + \frac{S_{Global}}{S_{Global,NOCT}}(T_{c,NOCT} - 20)(1 - \frac{\eta_{STC}}{0.9}) \tag{3.4}$$

where $T_{c,NOCT}$ is the cell internal temperature at nominal operating cell temperature, which are the operating conditions when global irradiance ($S_{Global,\ NOCT}$) equals 800 watt/m^2 and ambient temperature equals 20^{o}C, and was simulated using the PC1D simulator to be equal to 45 ^{o}C.

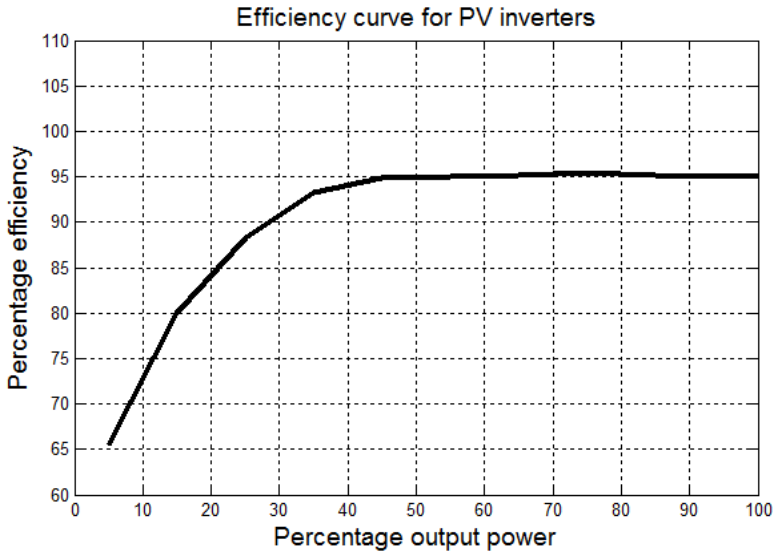

Figure 3-4: Efficiency curve for PV inverters

Thus, for each hour, the insolation and ambient temperature data for this specific hour are used to estimate the PV system DC power output using the previous equations.

3.2.3 Calculating PV Array AC Power Output

The DC output power of the PV system is converted into AC power through a DC/AC inverter. The AC power output of the array ($P_{PV,AC}$) is dependent on the inverter conversion efficiency ($\eta_{PV\ inverter}$):

$$P_{PV,AC} = P_{PV,DC} * \eta_{PV\ inverter} \tag{3.5}$$

The inverter conversion efficiency is not a constant value; nevertheless, it is usually a function of the ratio between the PV array actual and rated DC powers (percentage output power). A manufacturer's efficiency curve for a typical double-stage PV inverter is given in Figure 3-4 [137]. This curve is used to estimate the AC power vector from the corresponding DC one.

3.2.4 Data Pre-processing Stage

In this stage, the AC power vector is prepared for the clustering process. This preparation involves two steps:

i) Since PV arrays require a minimum level of insolation (called the insolation threshold) to generate electricity [138], all the insolation data below 50 W/m^2 are ignored. This reduces the daily data set from 24 data points/day to 13 data points/day (i.e. the PV system is delivering its output only from 6 am to 7 pm).

ii) The 365 AC power segments are analyzed using PCA to extract the most discriminative features of each segment (or day). PCA is a feature extraction tool used to compress a complex data set into a lower-dimension set while retaining, as much as possible, the variation within the data [139, 140]. This goal is achieved by means of an orthogonal linear transformation that re-expresses the original data set in terms of new, more-meaningful bases such that the components of the transformed data are uncorrelated [141]. The first coordinate in the new system coincides with the direction of the greatest variance of the original data and is defined as the first principal component. The second coordinate (which is orthogonal to the first coordinate) lies in the direction of the second greatest variation of the data, and so on. Dimensionality-reduction is achieved by neglecting the higher principle components with the least variance. Doing so filters out the noise and reveals the hidden structures within the data set [140, 142].

For this work, the number of principal components was selected so as to maintain at least 90% of the variance within the data set [119]. The results of the feature extraction stage show that the required variance can be maintained keeping only the first five principal components, as shown in Table 3-2.

Table 3-2: Percentage variance maintained after the application of PCA

Number of principal components	1	2	3	4	5
Percentage of variance kept within the data	64.1%	77.6%	85.3%	89.7%	93.1%

Reducing the dimensionality of the data set is highly important in clustering applications. For example, in K-means clustering, the time complexity is, at a minimum, in the order of $O(Sk_cd_fT_{it})$ [124], where S is the total number of data segments within the data set, k_c is the number of clusters, d_f is the number of features in each data segment, and T_{it} is the number of iterations. When PCA is applied, the total number of features drops from 13 to 5. This reduction corresponds to a 2.6 times decrease in the computation burden and time.

3.2.5 Data Clustering Stage

In this stage, days with similar principle components are grouped into the same cluster and treated as a single unit. Later on in the representative selection stage, only one representative segment will be chosen to represent all these different days.

Clustering algorithms can be broadly classified into exclusive and overlapping algorithms as shown in Figure 3-5. Exclusive clustering algorithms are those in which each data segment belongs to only one cluster, whereas in overlapping clustering (also known as fuzzy clustering), each data segment may belong to more than one cluster with different degrees of membership. Exclusive clustering can be further classified into hierarchical and partitional clustering. Partitional clustering directly divides data segments into predetermined number of clusters without building a hierarchical structure, whereas hierarchical clustering seeks to build a hierarchy of clusters with a sequence of nested partitions, either from singleton clusters to a cluster including all data segments or vice versa. The former is known as agglomerative hierarchical clustering, and the latter is called divisive hierarchical clustering. Divisive clustering algorithms need to compute $(2^n - 1)$ possible divisions for a cluster with n data segments, which is very computationally intensive [124]. Therefore, agglomerative methods are usually preferred, and only they are considered in this research.

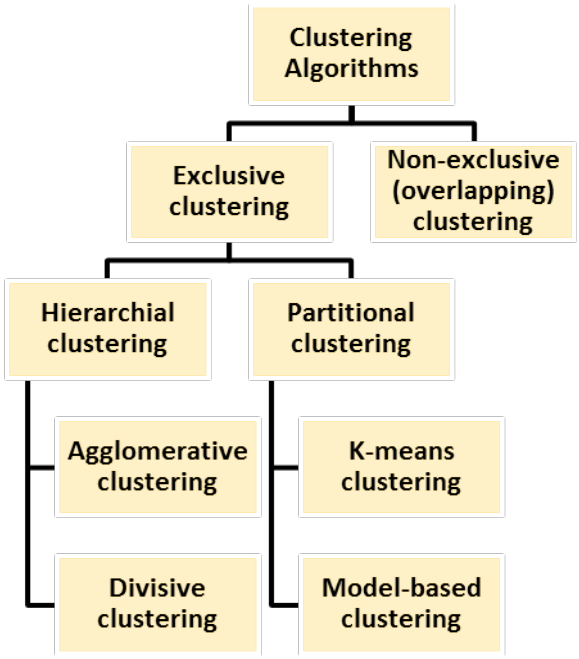

Figure 3-5: Classification of clustering techniques

Partitional clustering can be classified into the famous K-means clustering algorithm and the model-based clustering (also known as probabilistic clustering). In model-based clustering, each cluster is mathematically represented by a parametric distribution, like Gaussian (continuous) or Poisson (discrete). The entire data set is therefore modeled by a mixture of these distributions. The probabilistic clustering algorithm seeks to optimize the parameters of the mixture model so as to "cover" the data segments as much as possible. This is a very computationally intensive process. Therefore, model-based clustering is not considered in this research

For this research, the following clustering techniques are considered:

i) K-means clustering;

ii) Fuzzy C-means (FCM) clustering;

iii) Hierarchical clustering.

The following classes of hierarchical clustering are considered

- Single linkage hierarchical clustering;
- Complete linkage hierarchical clustering;
- Average linkage hierarchical clustering;
- Ward's linkage hierarchical clustering.

3.2.6 Representative Selection Stage

The goal of the representative selection stage is the selection of one segment (or day) from each cluster to represent all the days within the cluster, thus reducing the size of the data set.

For this research, representative segments can be selected in one of two ways:

i) The cluster mean: In this method, the representative segment is the one formed by the calculated mean (barycenter) of all segments included in the cluster.

ii) The cluster median: The representative data segment is the one that is originally included in the cluster and is the closest to the calculated mean.

3.2.7 Performance Evaluation Stage

In this stage, the performances of different clustering and representative selection alternatives are compared in order to select the best alternative. In clustering applications, this comparison is usually made by means of cluster validity indices.

Cluster validity indices are broadly classified into [143]:

i) External (supervised) validity indices, which assess the quality of clustering based on user-specific intuition. They thus require knowledge of external information about the data.

ii) Internal (unsupervised) validity indices, which are the most widely used indices. They assess the quality of clustering based on metrics within the resulting clustering schema itself. This task is usually achieved by measuring the cohesion within each cluster and the distances between different clusters [119]. Among such indices are the Dunn index [144], the Davies Bouldin (DB) index [145] and the Xie-Beni (XB) index [146].

iii) Relative validity indices, which use either internal or external indices to compare different clustering alternatives obtained from the application of different clustering algorithms or by applying the same algorithm but with different parameters [119]. The aim of the comparison is to choose the best clustering alternative for a given application.

In this research, since performances of different clustering and representative selection alternatives must be compared so as to select the best alternative, relative validity indices are the most suitable indices. An important decision when using relative validity indices is whether to use internal or external indices in the relative comparison. This question is answered below.

Internal validity indices measure the quality of clustering in terms of the compactness of each cluster and the separation between different clusters. The compactness of each cluster is mainly evaluated by calculating the distance between different data segments, or the distance between data segments and the centroid of the cluster. Consequently, these indices tend to prefer clustering algorithms that produce more singletons because, for these clusters, the compactness is zero. This preference does not serve the main purpose of this research, which is to reduce the size of the data set by grouping all days with similar PV output profiles together in one cluster, and using only one representative segment to represent all these days. Another disadvantage of internal validity indices is that there is no single index that can be used to compare all clustering algorithms. For example, the

famous XB index can be used only with fuzzy clustering algorithms. For these reasons, external validity indices will be used in this research for the relative comparison.

For this research, the author defined a novel external validity index, called the average power/time mismatch (*APTM*) index that measures the extent to which the resulting representative segments match the original data set. The proposed *APTM* index is computed as follows:

i) For the *n* data segments included in each cluster, calculate the cluster representative (either the cluster mean or median).

ii) Form a fictitious power vector *F* (365 segments × 24 data points/segment) by replacing each data segment with the representative segment of the cluster to which this data segment belongs.

iii) Calculate the *APTM* index as follows:

$$APTM_{PV\ clusters} = \frac{\sum_{i=1}^{24}\sum_{j=1}^{365}\left|\frac{P_{PV,AC}(i,j) - F_{PV,AC}(i,j)}{P_{PV,AC}(i,j)}\right|}{13\times 365}\times 100\% \qquad (3.6)$$

where

$APTM_{PV\ clusters}$ is the average power time mismatch index for the PV output profiles clusters;
$P_{PV,AC}(i, j)$ is the PV array AC power output in the i^{th} hour at the j^{th} day;
$F_{PV,AC}(i, j)$ is the fictitious PV array AC power output in the i^{th} hour at the j^{th} day.

The proposed *APTM* index is advantageous because it not only considers the power mismatch between the original data segments and their representatives, but also considers this power mismatch in a chronological manner, i.e., power/time mismatch. Accordingly, the set of representative segments that yields the lowest *APTM* error is the most truthful representative of the PV data set. In the following sections, the proposed index is used to select the best clustering alternative as well as the optimal number of clusters.

3.2.7.1 Selecting the Best Clustering Alternative

The performances of different clustering and representative selection alternatives are evaluated. For each clustering alternative, the *APTM* index is computed using both the cluster mean and median representatives:

i) K-means clustering: To overcome the famous initialization problem of the K-means algorithm, each case is repeated 100 times and the best run is taken.

ii) Fuzzy C-means clustering: In this technique, the data segment may belong to more than one cluster, with different degrees of membership. However, for the calculation of the *APTM* index, each data segment should be included in only one cluster. To overcome this problem, each data segment is assigned only to the cluster to which it belongs with the highest degree of membership (maximum membership rule [147]).

iii) Hierarchical clustering: The performances of four different classes of hierarchical clustering are compared.

Results of applying different clustering and representative selection techniques are depicted in Figure 3-6 and Table 3-3.

From the results, it is evident that all clustering and representative selection alternatives yield similar results. However, the *APTM* error curve for fuzzy C-means clustering using median representatives is slightly lower than the corresponding curves for the representative segments resulting from the application of other clustering alternatives. Thus, FCM clustering using median representatives is selected as the best clustering alternative. The previous conclusion agrees with the fact that fuzzy clustering techniques are the most suitable when the clusters are not well separated and the boundaries are ambiguous [124], which is the case with the problem at hand.

3.2.7.2 Selecting the Optimal Number of Clusters

Selecting the optimal number of clusters is a prominent dilemma in clustering applications. Choosing a large number of clusters ensures that only a small number of segments, which are really similar to one another, are grouped in the same cluster; however, data dimensionality is not greatly reduced. On the other hand, selecting a small number of clusters ensures that data dimensionality is reduced; however, data segments that are not really similar to one another are grouped together. Thus, the optimal number of clusters is never known a priori and is determined based on some kind of compromise between computational burden and accuracy.

Figure 3-6 shows that the *APTM* index for different clustering algorithms decreases rapidly as the number of clusters increases, and then it saturates around 10%. In other words: increasing the number of clusters does not reduce the error much beyond the 10% range.

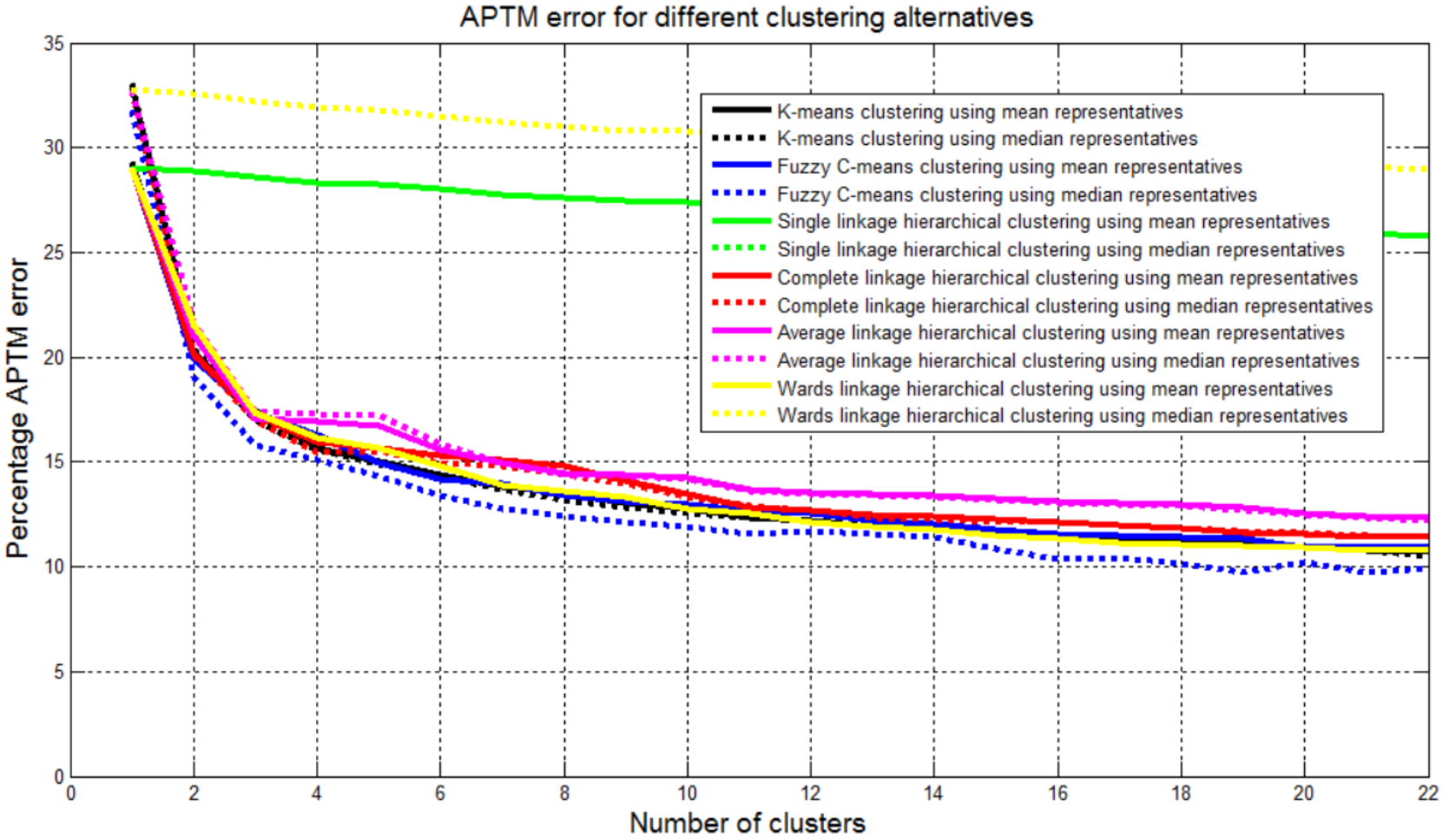

Figure 3-6: Results of applying different clustering alternatives

Table 3-3: Percentage APTM error for different clustering alternatives

Clustering Algorithm	K-means clustering		FCM clustering		Hierarchical clustering							
					Single		Complete		Average		Ward's	
Representatives	Mean	Median	Mean	Median	Mean	Median	Mean	Median	Mean	Median	Mean	Median
1 cluster	29.338	33.068	29.038	31.768	29.038	32.768	29.038	32.768	29.038	32.768	29.038	32.768
2 clusters	20.207	20.405	19.937	19.074	28.877	32.563	20.106	20.11	21.009	21.62	21.507	32.563
3 clusters	17.515	16.973	17.351	15.803	28.593	32.203	17.253	16.97	17.095	17.422	17.382	32.203
4 clusters	15.685	15.597	16.276	15.062	28.339	31.895	15.916	15.472	16.926	17.258	16.175	31.895
5 clusters	14.995	14.86	14.921	14.292	28.254	31.794	15.687	15.499	16.753	17.191	15.631	31.794
6 clusters	14.405	14.298	14.211	13.388	28.002	31.496	15.308	14.967	15.595	15.87	14.814	31.496
7 clusters	13.839	13.698	13.935	12.773	27.759	31.208	15.066	14.824	14.923	14.965	13.864	31.208
8 clusters	13.506	13.192	13.419	12.396	27.629	31.013	14.802	14.386	14.475	14.368	13.624	31.013
9 clusters	13.044	12.842	13.1	12.13	27.448	30.809	14.123	13.935	14.411	14.294	13.347	30.809
10 clusters	12.768	12.557	12.981	11.925	27.397	30.758	13.452	13.307	14.281	14.155	12.776	30.758
11 clusters	12.333	12.366	12.676	11.575	27.091	30.482	12.852	12.926	13.663	13.612	12.523	30.482
12 clusters	12.23	12.202	12.531	11.679	27.064	30.461	12.669	12.689	13.534	13.454	12.144	30.461
13 clusters	11.93	12.036	12.217	11.583	26.994	30.414	12.45	12.324	13.46	13.366	11.898	30.414
14 clusters	11.753	11.788	12.081	11.427	26.888	30.267	12.385	12.252	13.396	13.3	11.748	30.267
15 clusters	11.673	11.669	11.776	10.864	26.786	30.118	12.233	12.155	13.244	13.194	11.471	30.118
16 clusters	11.382	11.342	11.59	10.373	26.72	30.07	12.109	12.102	13.131	13.069	11.317	30.07
17 clusters	11.306	11.338	11.458	10.464	26.603	29.958	12.002	11.969	13.065	12.998	11.165	29.958
18 clusters	11.19	11.156	11.407	10.144	26.382	29.69	11.832	11.847	13.005	12.932	11.081	29.69
19 clusters	11.08	11.036	11.373	***9.709***	26.336	29.606	11.614	11.721	12.798	12.692	11.007	29.606
20 clusters	10.94	10.891	10.957	10.19	26.246	29.493	11.541	11.666	12.549	12.478	10.891	29.493

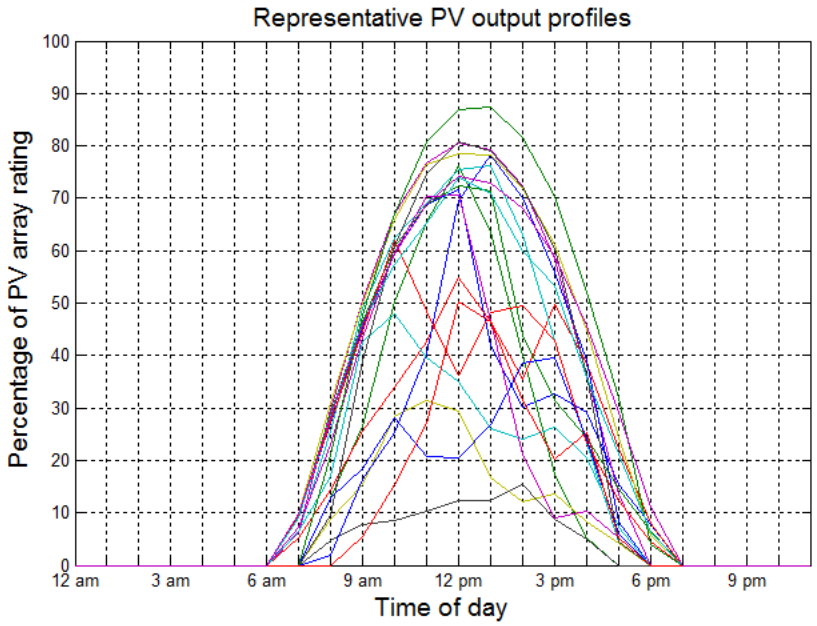

Figure 3-7: Selected representative segments for PV system output

Thus, for this research, the author defined the optimal number of clusters as the minimum number of clusters whose representative segments have an *APTM* error that is less than 10%. For the selected clustering and representative selection alternative (fuzzy C-means clustering using median representatives), it was found that the desired error can be obtained using only 19 clusters. The corresponding representative segments are depicted in Figure 3-7.

3.2.8 Probability Computation Stage

A question arises here: how can we reflect the different probabilities of occurrence of different representative segments during the random variable generation in MC simulations? To answer this question, we consider this example with two clusters, cluster *M* having *x* data segments, and cluster *P* having *2x* data segments. It is clear that the representative segment representing cluster *P* is twice as important as the one representing cluster *M*, as the former represents double the number of segments, and so should be repeated twice as much.

From the previous discussion, it is obvious that the probability of occurrence of each representative segment can be computed as the ratio of the number of data segments in the cluster to which this representative segment belongs, to the total number of data segments. This probability is computed using the representative probability index (*RPI*), given in Eq. (3.7):

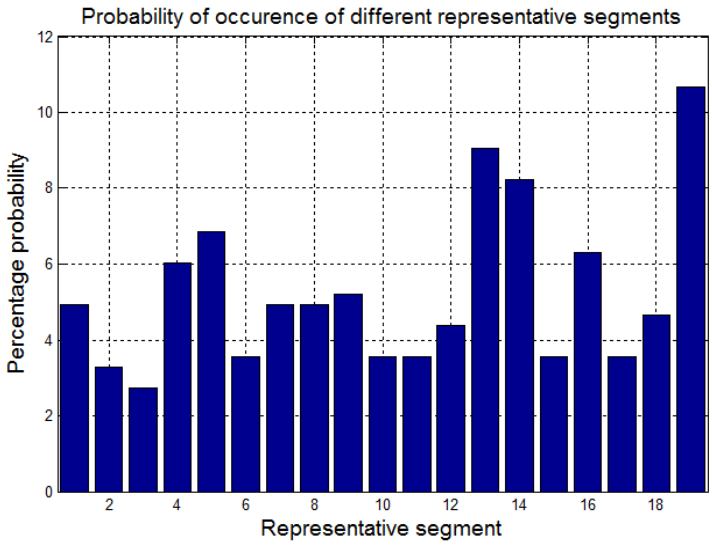

Figure 3-8: Discrete probability distribution for different representative segments

$$RPI\,(a) = \frac{n_a}{\sum_{j=1}^{k_c} n_b} \times 100\% \tag{3.7}$$

where

RPI(a) is the representative probability index for the representative segment representing cluster *a*;

n_a is the number of data segments within cluster *a*;

n_b is the number of data segments within cluster *b*;

k_c is the total number of clusters.

The *RPI* indices for the selected 19 representative segments are given in Figure 3-8 and Table 3-4. The corresponding cumulative distribution function (cdf) is depicted in Figure 3-9.

3.2.9 Comments on the Proposed Model

Previous sections presented the proposed probabilistic model used in this research to represent PV systems electrical output. In the following chapters, the resulting representative segments together with their probabilities of occurrence will be used to generate PV random output profiles during MC simulations.

Table 3-4: Percentage RPI indices for the chosen 19 representative segments

Representative segment	RPI index
1	4.93%
2	3.29%
3	2.74%
4	6.03%
5	6.85%
6	3.56%
7	4.93%
8	4.93%
9	5.21%
10	3.56%
11	3.56%
12	4.38%
13	9.04%
14	8.22%
15	3.56%
16	6.3%
17	3.56%
18	4.66%
19	10.69%

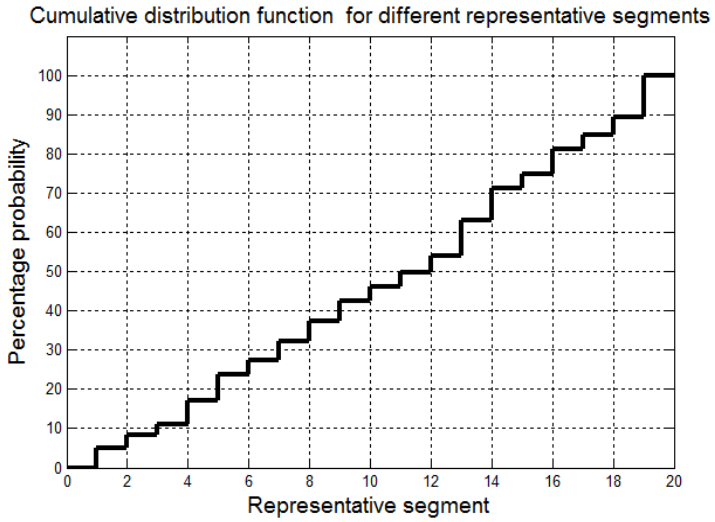

Figure 3-9: Cumulative distribution function for different PV representative segments

The proposed model has the following advantages:

i) It can model the long-term behavior of the PV array because the selected representative segments cover the whole year.

ii) The proposed model is also capable of modeling the temporal variations in PV array output, because the chosen 19 representative segments are themselves real-world PV output profiles.

iii) Unlike the model presented in [119], the proposed model uses a fuzzy clustering algorithm to group days with similar output power profiles together. Fuzzy clustering techniques have been proven to perform better when clusters are not well separated and boundaries are ambiguous [124], which is the case with PV data sets. This advantage was confirmed in the results evaluation stage.

iv) Unlike the model presented in [119], representative segments are assigned probability indices which correspond to the number of data segments present in the cluster they represent; thus preserving the probabilistic nature of the problem.

However, the uncertainty in the PV array output is not the only source of uncertainty present in the system; uncertainties in existing electrical loads should be modeled and addressed as well. This is discussed in the subsequent section.

3.3 Modeling Existing Electrical Loads

In power systems studies, electrical loads are usually modeled using one of the following methods:

i) Deterministic models: In this modeling approach, system loads are modeled as constant power sinks. This constant power can be either:

- The average demand obtained from historical data for the area under study. These average values can be daily, monthly or seasonal values. Such a modeling approach was used in [119] to analyze the impacts of grid-connected PV systems on electrical networks.
- The worst-case scenario for the system under study, such as when the load demand is minimal and a distributed energy resource, for example, is generating its maximum output. This approach was used in [64] to study the impacts of high penetration of solar PV generation on power system stability.

- Constant values that correspond to different loading conditions (peak, average and minimum demand). This modeling technique was used in [26, 30] to determine the maximum penetration of PV electricity that can be accommodated by existing networks.

A major drawback of deterministic models is that they represent only limited situations; thus, they are not suitable for assessing the long-term behavior of electrical loads or modeling their stochastic nature. Therefore, these models cannot be used to represent electrical loads in MC simulations.

ii) Probabilistic models: To address the above drawbacks, several attempts have been made to represent the stochastic nature of electrical loads using probabilistic models [148-155]. With the probabilistic modeling approach, electrical loads are usually modeled as random variables that follow predetermined pdfs, and hourly load levels are generated randomly according to these pdfs.

The analysis performed in [148-151] showed that the vast majority of electrical loads can be modeled using the normal distribution. The authors of [152] developed a probabilistic load model using a combination of uniform and normal probability distributions. Similarly, the authors of [153] used the joint-normal model and the autoregressive model of the 12^{th} order (*AR(12)*) to model electrical loads. Simulation results showed that the *AR(12)* model provides better results with limited measurement data, and that the joint-normal model is favored with a larger data set. In [154], electrical loads were modeled using the beta distribution, and the resulting cdf was discretized into equal steps. Finally, the probability of each step was computed and used in the random generation of load levels. In [155], the authors used K-means clustering to reduce the number of steps of the resulting cdf without sacrificing accuracy.

Previous probabilistic models have the disadvantage that the generation of hourly load levels takes place in a memoryless hourly fashion that does not account for the chronological nature of electrical loads. The value of the load level generated at the i^{th} hour is assumed to depend only on the value of the random variable generated at hour *i* and the predetermined pdf representing the load. As a result, peak load levels may be randomly generated during off-peak periods or vice versa. This situation also results in irregular daily load curves with load spikes, whereas in reality the load level at hour *i* has some correlation with the preceding load levels (*i-1, i-2*…, etc.). This correlation is justified by the fact that the aggregated demand at the transformer level, for example, does not experience any sudden spikes, but rather changes in a smooth manner. These

drawbacks make the use of probabilistic models suitable only for applications involving energy-based analyses (e.g., energy loss estimation), as these analyses are mainly dependent on the total energy consumed by electrical loads throughout the whole simulation period, rather than the chronological pattern by which these loads change. Thus, they are basically a function of the total area under the predetermined pdfs used in the random generation of load levels. However, these probabilistic models are not suitable for applications in which the chronological nature of electrical loads plays a significant role. Unfortunately, the application in hand (assessing the impacts of PV electricity and PHEVs on residential distribution network), is highly dependent on such chronological variations.

The proposed research aims to fill this gap by developing a probabilistic load model for electrical loads that satisfies the following requirements:

i) Model the long-term behavior of electrical loads;

ii) Capture the chronological nature of electrical loads;

iii) Have a minimal computational burden.

In this section, a probabilistic load modeling approach that fulfills all the previously mentioned requirements is developed. Similar to the modeling approach presented in Section 3.2, the proposed load modeling approach starts by grouping the 24 data points representing the hourly loading conditions of each day in a data segment. The resulting 365 data segments representing the whole year are evaluated for similarities using PCA, and segments with similar principal components are grouped into the same cluster. For each cluster, a representative segment is selected to represent all the days within the cluster, and its probability of occurrence is computed. The resulting representative segments can be used in the random variable generation during MC simulations.

Different stages of the proposed algorithm are introduced in the following sections.

3.3.1 Data Collection Stage

In this research, the load profiles being analyzed are adopted from the IEEE-RTS system [156]. This system provides the hourly peak load as a percentage of the daily peak load, the daily peak load as a percentage of the weekly peak load, and the weekly peak load as a percentage of the annual peak load. The provided data are assembled into 365 data segments, each consisting of 24 data points and representing a single day.

3.3.2 Data Pre-processing Stage

In this stage, the 365 data segments being studied are analyzed using PCA to extract the most discriminative features of each segment (or day). Similar to Section 3.2.4, the number of principal components was selected so as to maintain at least 90% of the variance within the data set [119]. Results of the feature extraction stage show that the required variance can be maintained, keeping only the first principal component as shown in Table 3-5.

Table 3-5: Percentage variance maintained after the application of PCA

Number of principal components	1	2	3	4	5
Percentage of variance kept within the data	93.1%	96.2%	98.5%	99.8%	99.9%

Accordingly, instead of each data segment (or day) being represented using 24 data points, it is represented using only the first principle component of these 24 data points. This reduction corresponds to a 24 times decrease in the computation burden (and time) of the data clustering stage.

3.3.3 Data Clustering and Representative Selection Stage

As in Sections 3.2.5 and 3.2.6, three clustering algorithms will be considered:

i) K-means clustering;

ii) Fuzzy C-means (FCM) clustering;

iii) Hierarchical clustering.

The following classes of hierarchical clustering are considered

- Single linkage hierarchical clustering;
- Complete linkage hierarchical clustering;
- Average linkage hierarchical clustering;
- Ward's linkage hierarchical clustering.

For each clustering algorithm, the cluster representative will be chosen in two different ways:

i) The cluster mean;

ii) The cluster median.

3.3.4 Performance Evaluation Stage

In this stage, the *APTM* index proposed in Section 3.2.7 is used to select the best clustering alternative as well as the optimal number of clusters. The *APTM* index for the resulting clusters is calculated as follows:

$$APTM_{\,Load\ clusters} = \frac{\sum_{i=1}^{24}\sum_{j=1}^{365}\left|\frac{ALL(i,j)-FLL(i,j)}{LL(i,j)}\right|}{24\times 365}\times 100\% \qquad (3.8)$$

where

$APTM_{Load\ clusters}$ is the average power time mismatch index for the resulting load profiles clusters;
$ALL(i, j)$ is the actual load level at the i^{th} hour in the j^{th} day;
$FLL(i, j)$ is the fictitious load level at the i^{th} hour in the j^{th} day.

Results of applying different clustering and representative selection techniques are depicted in Figure 3-10 and Table 3-6.

3.3.4.1 Selecting the Best Clustering Alternative

Previous results make it evident that all clustering and representative selection alternatives yield very similar results (especially the K-means and fuzzy C-means algorithms). However, the *APTM* error curve for K-means clusters' median representatives is slightly lower than the corresponding curves for the representative segments resulting from the application of other clustering alternatives.

Accordingly, K-means clustering using median representatives is selected as the best clustering alternative.

3.3.4.2 Selecting the Optimal Number of Clusters

Similar to Section 3.2.7.2, the optimal number of clusters is selected based on some kind of compromise between computational burden and accuracy. Figure 3-10 shows that the *APTM* index for different clustering algorithms decreases rapidly as the number of clusters increases, and then it saturates around 4%. Or, in other words: increasing the number of clusters does not reduce the error much beyond the 4% range. Thus, for this research, the author defined the optimal number of clusters as the minimum number of clusters whose representative segments have an *APTM* error that is less than 4%.

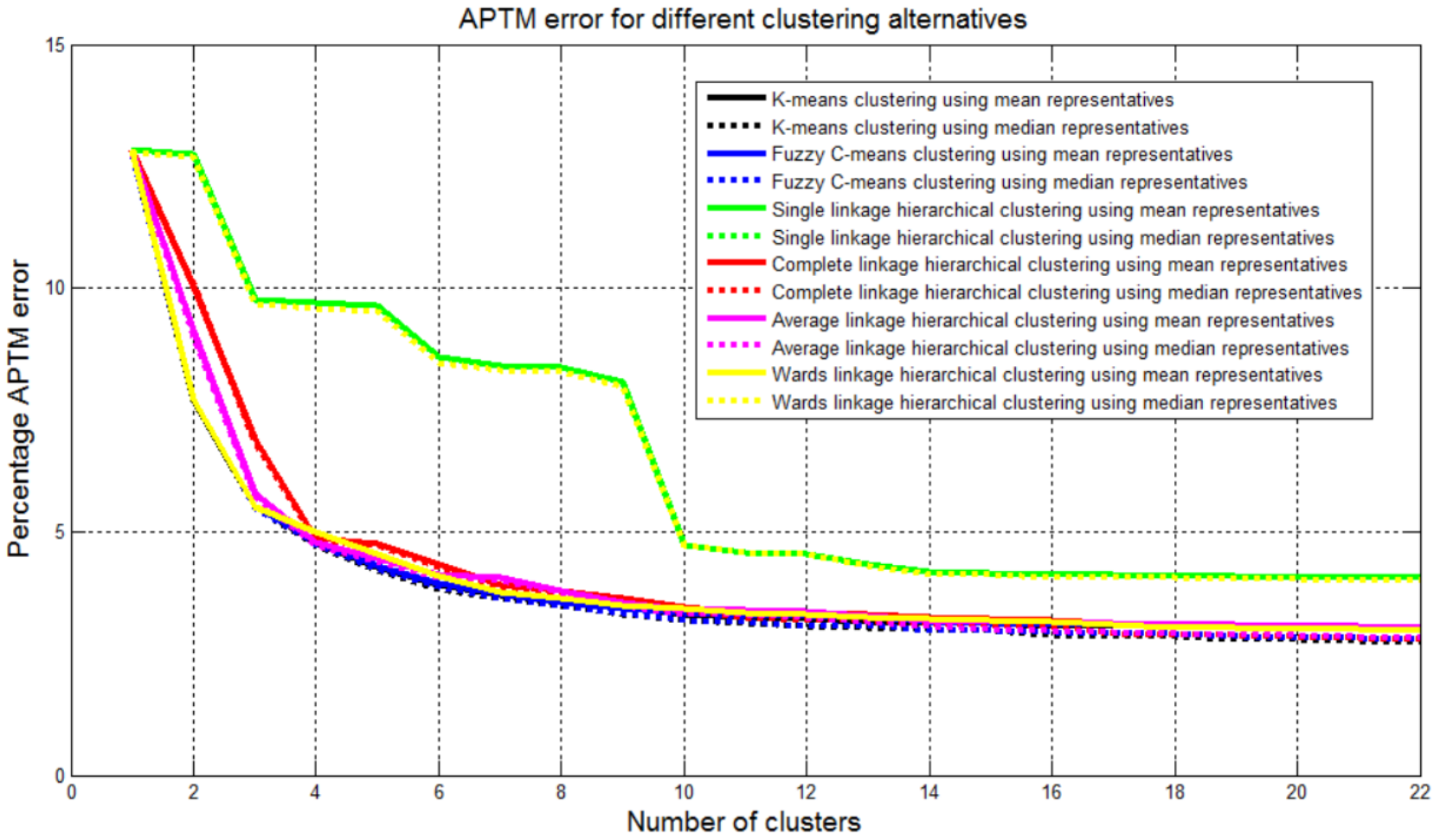

Figure 3-10: Results of applying different clustering alternatives

`  `

Table 3-6: Percentage APTM error for different clustering alternatives

Clustering Algorithm	K-means clustering		FCM clustering		Hierarchical clustering							
					Single		Complete		Average		Ward's	
Representatives	Mean	Median	Mean	Median	Mean	Median	Mean	Median	Mean	Median	Mean	Median
1 cluster	12.838	12.77	12.838	12.77	12.838	12.77	12.838	12.77	12.838	12.77	12.838	12.77
2 clusters	7.6817	7.6957	7.7006	7.7108	12.753	12.69	10.05	10.083	9.1204	8.9987	7.6996	12.69
3 clusters	5.5052	5.4642	5.512	5.4712	9.7717	9.6602	6.8916	6.8062	5.7799	5.7321	5.518	9.6602
4 clusters	4.7862	4.7318	4.7999	4.7454	9.6989	9.5923	4.8764	4.8277	4.7978	4.73	4.9962	9.5923
5 clusters	4.2767	4.2223	4.3037	4.239	9.6286	9.5263	4.764	4.7219	4.4473	4.3911	4.5361	9.5263
6 clusters	3.8985	**3.825**	3.9336	3.8748	8.5718	8.4751	4.3429	4.2656	4.1071	4.0637	4.0935	8.4751
7 clusters	3.7013	3.6278	3.7234	3.6451	8.4033	8.3128	3.894	3.8313	4.0539	4.0098	3.7631	8.3128
8 clusters	3.5525	3.485	3.5492	3.4721	8.3837	8.2931	3.8007	3.7308	3.8018	3.7475	3.6372	8.2931
9 clusters	3.4446	3.2937	3.4198	3.3234	8.0607	7.9755	3.6335	3.5457	3.5597	3.485	3.497	7.9755
10 clusters	3.2961	3.1959	3.3478	3.1972	4.7358	4.721	3.456	3.3555	3.4022	3.3028	3.4375	4.721
11 clusters	3.239	3.1331	3.2726	3.1527	4.5818	4.5588	3.3355	3.2354	3.3935	3.2929	3.3463	4.5588
12 clusters	3.2249	3.0773	3.2835	3.0572	4.5566	4.5281	3.2998	3.1884	3.3679	3.2573	3.3025	4.5281
13 clusters	3.1607	3.0307	3.2385	3.082	4.3431	4.3028	3.2912	3.1786	3.2855	3.1432	3.2325	4.3028
14 clusters	3.1226	2.9889	3.1548	2.9793	4.1679	4.1201	3.2556	3.1295	3.1989	3.0536	3.2098	4.1201
15 clusters	3.1144	2.9598	3.1199	2.9595	4.1637	4.1187	3.2175	3.0892	3.1639	3.0057	3.1845	4.1187
16 clusters	3.051	2.8942	3.0868	2.9528	4.111	4.0624	3.19	3.0485	3.1462	2.9743	3.1501	4.0624
17 clusters	3.0511	2.8651	3.0871	2.9229	4.105	4.0523	3.1153	2.9252	3.1162	2.9328	3.0909	4.0523
18 clusters	3.0645	2.8497	3.0534	2.918	4.1011	4.0482	3.0809	2.887	3.091	2.902	3.0305	4.0482
19 clusters	3.0633	2.797	3.0867	2.8389	4.075	4.0211	3.0711	2.8733	3.0862	2.8963	3.0198	4.0211
20 clusters	3.0273	2.8013	3.0252	2.812	4.0717	4.016	3.0584	2.8454	3.0758	2.8859	3.0099	4.016

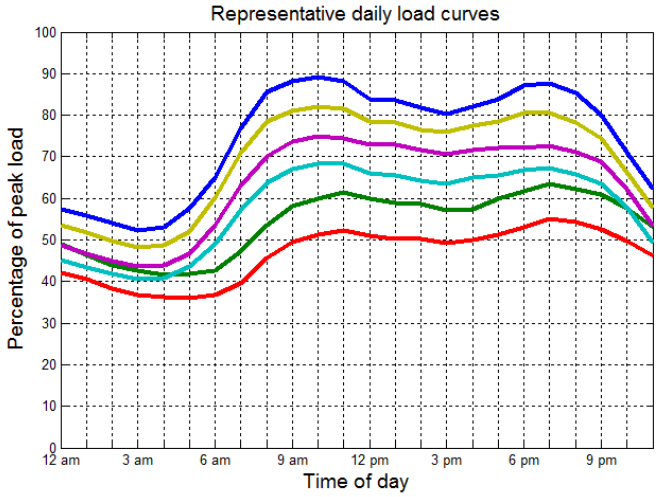

Figure 3-11: Selected representative segments for electrical loads

For the selected clustering and representative selection alternative (K-means clustering using median representatives), it was found that the desired error can be obtained using only six clusters. The corresponding representative segments are depicted in Figure 3-11

3.3.5 Probability Computation Stage

Similar to Section 3.2.8, the probability of occurrence of each representative segment is computed using the *RPI* index, given in Eq. (3.7). The resulting *RPI* indices for the chosen six representative segments are given in Figure 3-12 and Table 3-7. The corresponding cdf is depicted in Figure 3-13.

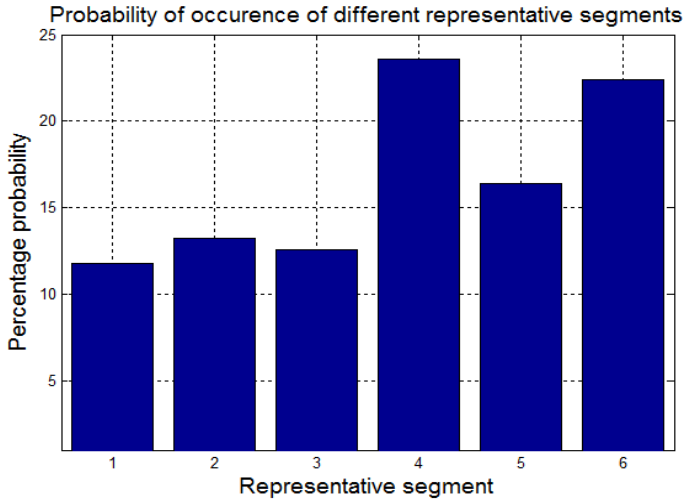

Figure 3-12: Discrete probability distribution for different representative segments

Table 3-7: Percentage RPI indices for the chosen six representative segments

Representative Segment	1	2	3	4	5	6
RPI index	11.8%	13.2%	12.6%	23.6%	16.4%	22.4%

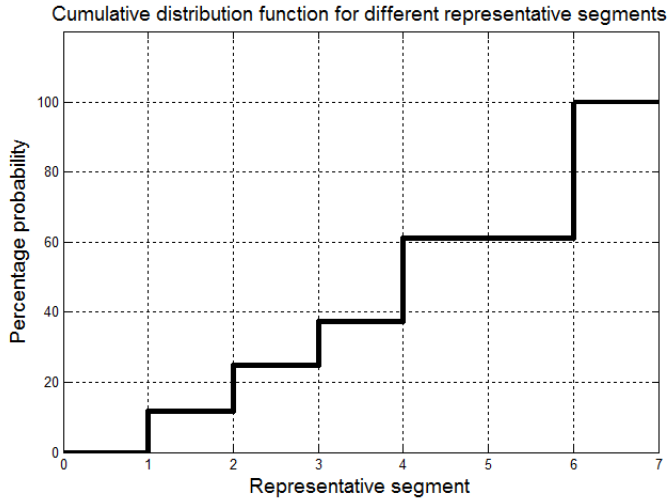

Figure 3-13: Cumulative distribution function for the six representative segments

3.3.6 Comments on the proposed model

Previous sections presented the probabilistic model used in this research to represent the stochastic nature of existing electrical loads. The resulting representative segments altogether with their probabilistic *RPI* indices will be used to generate random load profiles during MC simulations.

The performed analysis showed that it is possible to represent the stochastic nature of electrical loads using only six daily representatives instead of 365 different load profiles, with less than 4% error. Moreover, the proposed approach avoids many of the limitations of previous load models reported in the literature:

i) Unlike deterministic models, the proposed model can mimic the long-term behaviour of electrical loads because the chosen six segments are representative of the whole year.

ii) The proposed model is also capable of modeling the chronological nature of electrical loads, because the chosen six representative segments are themselves real-world daily load curves. This feature eliminates a significant drawback of the probabilistic models reported in the literature, which is that the generation of hourly load levels takes place in a memoryless hourly fashion,

resulting in irregular load curves with peak load levels being generated during off-peak periods, or vice versa. As a result, the proposed load model is capable of preserving the chronological synchronization between the electrical loading profiles and other power system parameters (e.g., PV array output profiles).

3.4 Modeling Individuals' Driving Patterns Impacting PHEV charging

Assessing the impacts of PHEVs on distribution systems requires an accurate determination of their chronological charging profiles. Researchers find estimating such profiles tedious due to the uncertainties related to individual' driving habits that may impact the charging process, such as variable home arrival times and daily distances travelled. For this research, the author utilized an approach similar to that outlined in [157] as a means of deriving cdfs for describing these uncertainties during MC simulations. Details of the proposed modeling approach are presented in the following sections.

3.4.1 Data Collection Stage

Data for 1,048,576 people and 309,164 vehicles were taken from the 2009 national household travel survey (NHTS) [158] conducted by the U.S. Department of Transportation. The survey was carried out by telephone interviews with a random dialing list that excluded hotels, motels and group quarters. Extracted data included reported annual mileage and home arrival times for each vehicle. However, the required data were distributed among several excel files. Thus, the author had to compile different files together using common fields (house ID, vehicle ID and vehicle type), which required an extensive search and indexing process.

3.4.2 Data Pre-processing Stage

The compiled common file contained the following data: house ID, vehicle type, home arrival time (rounded to the nearest hour), and distance travelled. Vehicles whose owners refused to report their annual mileage were excluded from the data set. The data were filtered so that only three types of vehicles were considered: automobiles, vans, and sports utility vehicles (SUVs). The resulting data set is representative of a total of 129,274 vehicles: 63.08% automobiles, 10.48% vans, and 26.44% SUVs [158].

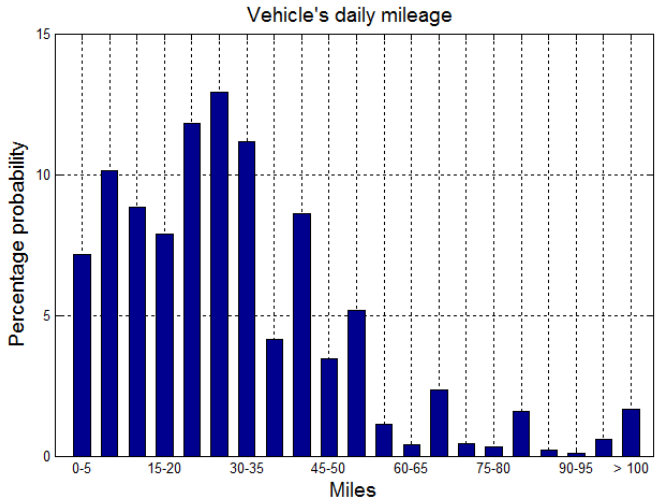

Figure 3-14: Discrete probability distribution for daily distance travelled by each vehicle

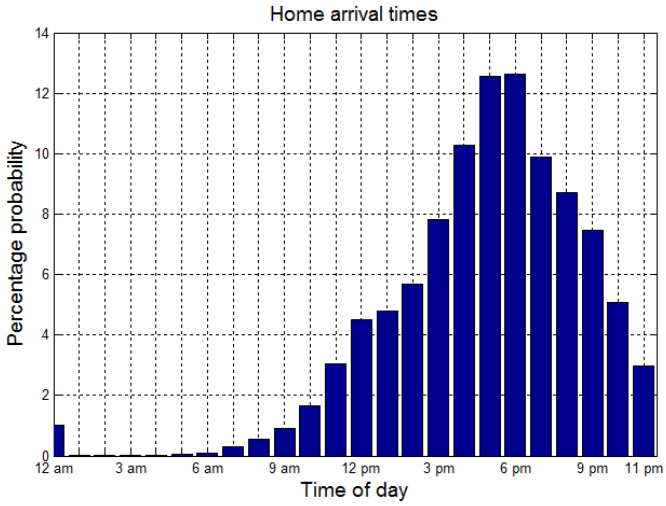

Figure 3-15: Discrete probability distribution for home arrival times

3.4.3 Probability Computation Stage

The resulting data set is processed to extract probability functions that describe daily mileage and home arrival times. The resulting discrete probability distributions are depicted in Figures 3-14 and 3-15, respectively.

Previous figures were used to construct the corresponding cdfs. Results are depicted in Figures 3-16 and 3-17, respectively. These cdfs will be used in the random generation of PHEV charging profiles during MC simulations.

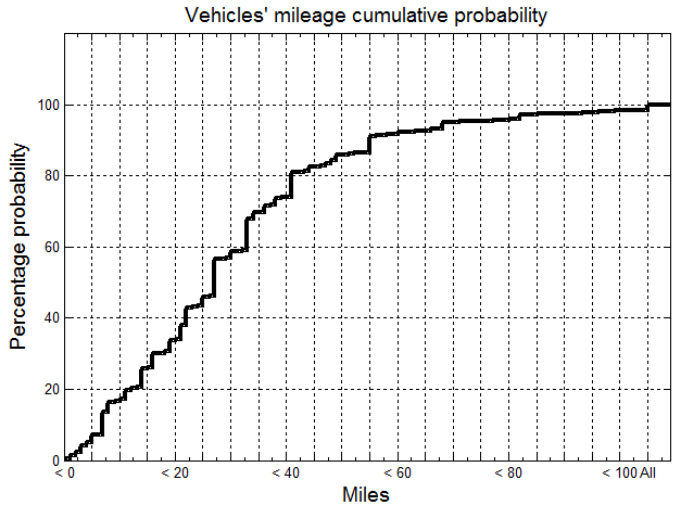

Figure 3-16: Cumulative distribution function for daily vehicle mileage

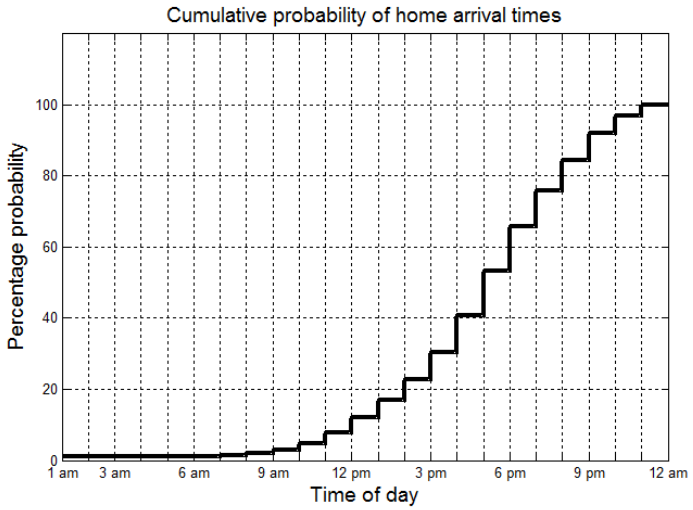

Figure 3-17: Cumulative distribution function for home arrival times

The results reveal that the peak arrival time is between 3 pm and 7 pm and that the majority of vehicles are driven between 25–30 miles daily. These findings agree closely with the findings of [157]. Figure 3-16 indicates the percentage of vehicles that are driven less than a specified daily mileage. For example, 56.7% of vehicles are driven 30 miles or less daily. This result agrees with the estimations provided in [157, 159, 160] (55%, 61%, and 63%, respectively).

Finally, the correlation coefficient between home arrival times and vehicles' daily mileage was evaluated and was found to be equal to 3.95%, a weak correlation that permits these two quantities to be generated independently in MC simulations.

`  `

3.5 Summary and Conclusions

In this chapter, the probabilistic models required to represent the uncertainties associated with existing electrical loads, the PHEV charging demand, and the PV array output during MC simulations are developed.

Hourly insolation and temperature data provided by the Solar Radiation Research Laboratory are used to estimate the PV array DC power output using the empirical method described in Section 3.2.2. The equivalent AC output power is then computed using the inverter's efficiency curve. The 24 data points representing the PV array electrical output for each day are assembled in a data segment. The resulting 365 data segments representing the whole year are evaluated for similarities using PCA, and similar segments are grouped into the same cluster. For each cluster, a representative segment is selected, and its probability of occurrence is computed and used to construct the cdf in Figure 3-9. The same approach is repeated for the data segments containing the loading profiles for existing electrical loads (abstracted from the IEEE RTS system). The resulting representative segments altogether with the resulting cdfs will be used in the random variable generation during MC simulations.

To model individuals' driving habits that impact PHEV charging, data for 1,048,576 people and 309,164 vehicles provided by the 2009 U.S. NHTS were analyzed for the extraction of cdfs representing daily mileage and home arrival times. Similarly, these cdfs will be used in subsequent chapters in the random generation of PHEV charging profiles during MC simulations.

Chapter 4

Studying the Impacts of the Uncontrolled Charging of PHEVs on Residential Distribution Systems

4.1 Introduction

After having introduced appropriate probabilistic models for different uncertainties inherent in the distribution system in Chapter 3, the author will use these models to develop a MC-based probabilistic benchmark for assessing the impacts of the uncontrolled charging of PHEVs on residential distribution networks.

Section 4.2 reviews the weaknesses of previous approaches employed to assess the impacts of PHEVs on distribution networks; Section 4.3 describes the probabilistic models used in this research to represent different uncertainties inherent in the distribution system; Section 4.4 outlines different stages of the proposed MC-based probabilistic benchmark; Section 4.5 presents the simulation results; and finally, Section 4.6 concludes the chapter.

4.2 Weaknesses of Previous Approaches

A large and growing body of literature has investigated the potential impacts of the uncontrolled charging of PHEVs on electric grids. However, as explained earlier, early integration studies focused mainly on determining whether the existing generation capacity would be sufficient for supplying the PHEV charging demands. For example, a study conducted by EPRI [32] forecast that if PHEVs replace half of all vehicles in the U.S. by 2050, only an 8% increase in generation capacity will be required. Another study [9, 10] concluded that 74% of the light-duty vehicle fleet in the U.S. can be supported by the unutilized capacity within the existing generation infrastructure. However, as indicated earlier, these optimistic predictions can be misleading as these studies assumed that the PHEV charging load will simply fill the valley in the utility load curve, an assumption that is not always true due to the natural coincidence between peak demand and the hours during which most vehicles are parked at residences and are thus probably being charged [34]. These studies also assumed a homogenous distribution of PHEVs throughout the whole electrical network, which is not always the case: the PHEV charging load is more likely to be spatially clustered in residential areas than in commercial or industrial centers [35, 106]. Such clustering can result in significant overloads at secondary distribution levels where the diversity benefits are not as marked as at primary levels.

The previous discussion makes it evident that it is more important to assess the impacts of PHEVs on localized distribution networks rather than on the system's overall generation capacity, which is the motivation for the research presented in this chapter.

Analyzing recorded data for PHEVs can give an insight into their anticipated impacts on distribution networks. For instance, by determining a battery's SOC at the onset of charging, the charging profile for its PHEV can be accurately determined, and the resulting impacts on the electric grid can be estimated. The main drawback of this approach is that such data are not always available due to the current low penetration of PHEVs and the need for expensive GPS-based monitoring devices. For example, the authors of [161] used a database of field-recorded commutating cycles for 76 PHEVs to predict the overall increase in Manitoba's electric grid load profile due to PHEV charging. Similarly, the authors of [162] used the recorded data for ten PHEVs to analyze drivers' usage patterns and behaviours affecting PHEV charging. However, the samples used in these studies are not large enough to reflect the wide variations in individuals' driving habits impacting the charging process.

Due to the lack of such data, several researchers have rightfully used statistical modeling to estimate PHEV charging profiles. For example, EPRI [99, 163, 164] used transportation data provided by the 2001 NHTS to develop a methodology for assessing the anticipated impacts of PHEVs on distribution networks. However, the developed methodology studied only predefined deterministic scenarios, and so does not provide a reliable estimate for these impacts. For example, assuming that all PHEVs are charged at 5 pm during the peak demand period using 7.2 kW level-2 rapid chargers will result in overestimation of the anticipated impacts of PHEVs on distribution networks, and vice versa.

In light of the previous discussion, it becomes clear that an accurate assessment of the impacts of PHEVs on distribution systems necessitates precise determination of their stochastic charging profiles. This task, however, is challenging due to the uncertainties related to individuals' driving habits affecting the charging process, such as variable home arrival times and daily distances travelled by each vehicle.

The literature describes a number of models that have been proposed as a means of handling these uncertainties. DeForest *et al.* [21] proposed a model for assessing the impacts of PHEVs on system demand peaks. However, several factors were ignored in the development of the model: it was based on the assumption that all PHEVs are driven 33 miles/day, which is the U.S. average. Another study

[165] examined the impacts of the PHEV charging load through a comparison of the utility load duration curve with and without the charging load. However, the model was based on the assumption that the overall PHEV fleet derives 40% of its miles from electricity, neglecting the arbitrariness of the daily distance travelled by each vehicle. The authors of [166] used a large-scale distribution planning model to study the impacts of PHEVs on investment cost and incremental energy losses in the distribution network. However, the model again did not include consideration of the dissimilarities in individuals' driving habits; instead, the assumption was that 85% of the vehicles are charged during valley hours and the remaining 15% are charged during peak hours, irrespective of their arrival times. Another paper [18] proposed a probabilistic approach based on MC simulations as a means of investigating the impacts of the uncontrolled charging of PHEVs on distribution networks. However, the authors simplified the problem by assuming that each vehicle starts charging with a battery SOC that is uniformly distributed between empty and half of its capacity. The impacts of PHEVs on the distribution grid in terms of power losses and voltage deviations were studied in [111]; however, the model developed in these papers assumed that the batteries would begin charging from a fully discharged state irrespective of the individual distance travelled and that all PHEVs are equipped with 11 kWh batteries charged by 4 kW chargers. The authors of [167] studied the impacts of PHEVs on distribution transformers for a variety of charging scenarios. However, they assumed that all PHEVs start charging at 6 pm, with an initial SOC of 30%, contrary to the findings reported in [157], which showed that a considerable number of vehicles begin charging at other times of the day. The authors of [168] attempted to determine the percentage of conventional vehicles that could be replaced by PHEVs without violating the system's technical constraints in terms of voltage profiles, branches' congestion levels and unbalances between phases. However, the model was based on the assumption that all PHEVs are charged for four hours daily irrespective of the daily distance travelled by each vehicle. The aggregated impacts of DG units and PHEVs on distribution networks was evaluated in [169]. However, the authors based their analysis on the generation of a totally random charging duration for each vehicle owner irrespective of the distinct distance travelled by each vehicle. The authors also assumed that the uncontrolled charging of PHEVs occurs at "the time when residential peak load occurs", which is not always true [30] and results in overestimation of the anticipated impacts.

The several biased assumptions used in the previous models may affect the accuracy and validity of their results; assessing the impacts of PHEVs on distribution networks is basically a probabilistic load flow (PLF) problem solved by most researchers using MC simulation. As explained earlier in

Chapter 3, according to MC simulation theory [117], if the inputs for a certain process are randomly sampled following their actual probability distributions, the output will be also random. However, the probability distribution for the random output will follow that of the true output with acceptable error, and both probability distributions will coincide after an infinite number of simulations (according to the Law of Large Numbers [118]). Conversely, if the simulation inputs are generated in a totally random fashion, there is no guarantee that the estimated output will represent the true output. Previous researchers adopted several unrealistic assumptions in their models; thus, random numbers were generated in a totally random fashion without following their actual probability distributions. Accordingly, the obtained results are not necessarily accurate.

Providing a more realistic modeling of different uncertainties present in the PLF problem is the core contribution of this research; instead of relying on unbacked assumptions, the author used the previously developed probabilistic models (described in Chapter 3) to represent these uncertainties as precisely as possible; hence obtaining more-accurate results. This is explained in the following section.

4.3 Representing Distribution System Uncertainties in the MC Simulation

In this research, MC simulations are used to assess the anticipated impacts of PHEVs on distribution networks. The first stage of the MC simulation is the development of proper probabilistic models to represent different uncertainties inherent in the system. This is explained in the following sections.

4.3.1 Modeling Uncertainties Related to Existing Loads

Two different approaches are used in this work to represent the stochastic nature of existing electrical loads based on the nature of the load, whether residential or commercial.

4.3.1.1 Modeling Existing Residential Loads

Previous research represented residential loads either using a single load curve (that denotes average demand) [170] or using a randomly selected load curve from a set of recorded measurements that are assumed to occur with the same probability [111, 168]. This assumption is not necessarily true, as profiles representing weekdays, for example, are more likely to occur than profiles representing weekends.

To avoid this drawback, the load modeling approach presented in Section 3.3 is used here to model the stochastic nature of existing residential loads. As explained earlier, the proposed load modeling approach starts by grouping the 24 data points representing the loading conditions during a given day in a data segment. The resulting 365 data segments representing the whole year are processed using PCA, and segments that are found to have a similar first principle component are grouped into the same cluster. Finally, for each cluster, a representative segment is selected to represent the whole cluster, and its probability of occurrence is computed.

The utilized approach has the advantage that it allows for the representation of the stochastic nature of electrical loads using only six daily representatives instead of 365 different profiles, with less than 4% error. The selected representative and the corresponding cdf are depicted in Figures 3-11 and 3-13, respectively.

4.3.1.2 Modeling Existing Commercial Loads

Commercial loads are characterized by low variability in their demands [171] and thus can be represented using only one load curve. The load curve used in this research for representing commercial loads is depicted in Figure 4-1 based on the data provided in [172]. This curve will be used during MC simulations to generate random loading profiles for commercial loads present in the system.

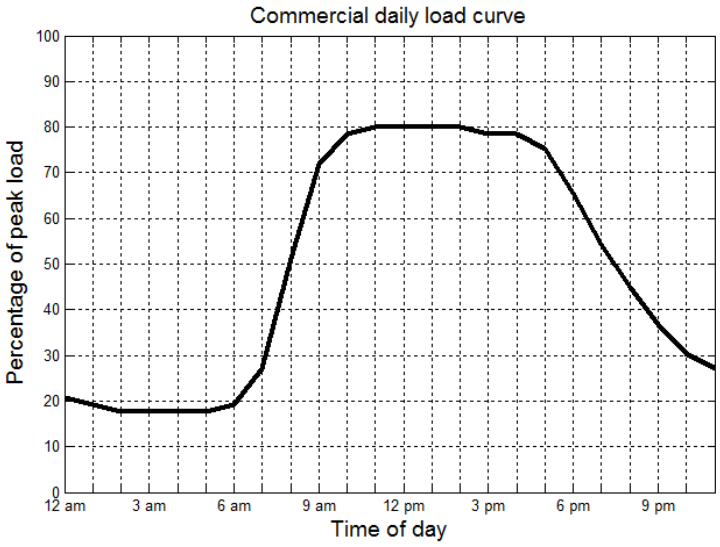

Figure 4-1: Representative daily load curve for commercial loads

`  `

4.3.2 Modeling Uncertainties Related to Individuals' Driving Patterns

This research uses the approach outlined in Section 3.4 as a means of deriving cdfs modeling individuals' driving habits impacting the charging process. Data for 1,048,576 people and 309,164 vehicles were taken from the 2009 NHTS. The data were filtered so that only three types of vehicles were considered: automobiles, vans, and SUVs. The data set is representative of a total of 129,274 vehicles: 63.08% automobiles, 10.48% vans, and 26.44% SUVs. Finally, the resulting data set was processed to extract probability functions that represent daily mileage and home arrival times. Figures 3-16 and 3-17 depict the resulting cdfs.

4.3.3 Study Assumptions and Scenarios

This section outlines the different assumptions made in this research with regards to the types, penetration levels and charging levels of PHEVs.

4.3.3.1 Types of PHEVs

Previous research either considered a single type of PHEVs [111, 167, 169] in the analysis, or used several types with assumed market share percentages and battery capacities [168].

The author improved on these assumptions by dividing PHEVs into three different types (automobiles, vans and SUVs), and choosing a representative vehicle for each type to exemplify the whole type. To date, no data are available on the market share of different types of PHEVs. To reflect real-life as accurately as possible, it is assumed that the three types have the same market share as that reported in the 2009 NHTS for their gasoline counterparts as shown in Table 4-1.

Table 4-1: Data for PHEVs

Vehicle Type	Automobiles	Vans	SUVs
Percentage	63.08%	10.48%	26.44%
Representative PHEV	Chevrolet Volt	Volvo V70	Ford Escape
Range	40 miles	30 miles	30 miles
Battery Capacity (C)	16 kWh	11.3 kWh	10 kWh
Specific Energy (e)	0.4 kwh/mile	0.377 kwh/mile	0.333 kwh/mile

`  `

4.3.3.2 PHEV Penetration Levels

For this work, the author studies all possible market penetration scenarios for PHEVs: 11 different penetration levels are considered, from 10% penetration up to 100%, in addition to the no-PHEVs case.

4.3.3.3 PHEV Charging Levels

SAE J1772 standard defines two residential single phase charging levels for PHEVs [173]. These two levels have been used in numerous studies [157, 164] and are shown in Table 4-2.

Table 4-2: AC Charging levels according to SAE J1772

Level	Voltage	Current	Power
Level-1 (Normal Charging)	120 V	12 A	1.44 kW
Level-2 (Rapid Charging)	240 V	30 A	7.2 kW

To study the impact of different charging schemes on distribution systems' infrastructure, the analysis considers three different charging scenarios, given in Table 4-3.

Table 4-3: PHEV Charging scenarios

Scenario	Percentage of level-1 chargers	Percentage of level-2 chargers
Scenario 1-Ch4	100%	0%
Scenario 2-Ch4	50%	50%
Scenario 3-Ch4	0%	100%

Accordingly, the performed analysis studies 31 different scenarios: three charging scenarios for each of the 10 penetration levels, in addition to the no-PHEVs case.

4.4 MC-Based Probabilistic Benchmark

This section describes how MC analysis is used to assess the impacts of PHEVs on a representative test system, with consideration of the uncertainties mentioned above. The following sections explain different stages of the proposed benchmark.

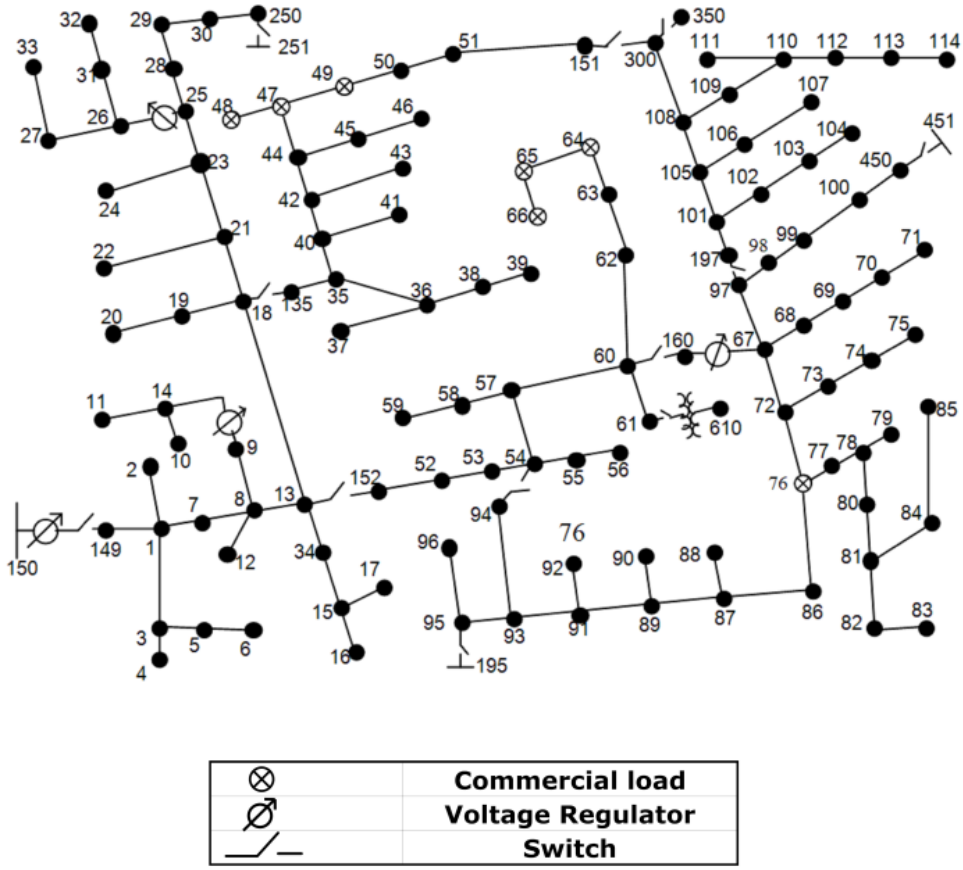

Figure 4-2: IEEE 123 node test feeder

4.4.1 Description of the Test System

The test system used in this research is an expanded version of the IEEE 123 node test feeder [174] shown in Figure 4-2. The original system has 91 spot loads, 47 and 31 of which are single phase loads rated 44.72 kVA and 22.36 kVA, respectively, at a 0.894 lagging power factor. Each of the 44.72 kVA spot loads was expanded into a 50 kVA distribution transformer feeding 10 households, and each of the 22.36 kVA spot loads was expanded into a 25 kVA distribution transformer supplying 5 households. Thus, a total of 625 residential customers are present in the system.

Secondary distribution circuits were appropriately modeled based on practical data provided by a power utility in Ontario. Each transformer has a secondary circuit composed of NS90 1/0 AWG triplex service drops with random lengths between 50 and 75 feet. A sample secondary distribution circuit is depicted in Figure 4-3. The remaining 13 spot loads are assumed to be commercial loads

serving the residential area. The system was modeled using OpenDSS software from the substation down to the customer meter, resulting in a system with 1684 nodes. This detailed representation of the system allows an enhanced estimation of the system losses and of the voltages observed at the meter [18]. Based on the same practical data, each household peak demand was taken to be 6.2 kVA which is close to the results obtained in [175]. The peak demands of commercial loads are taken as per the test feeder data [174].

4.4.2 Generating Random Loading Profiles for Existing Loads

The load modeling approaches explained in Section 4.3.1 are used to generate random loading profiles for different loads existing in the system. For each residential load, random loading profiles (from the six representative segments depicted in Figure 3-11) are sampled based on the cdf given in Figure 3-13. The selected percentage loading profiles are then multiplied by the household peak demand (6.2 kVA at a 0.894 lagging power factor). For commercial loads, the load curve shown in Figure 4-1 is multiplied by the peak demands provided in the test feeder data to generate loading profiles for these loads. This procedure is repeated 365 times every year for each load in the system.

In North America, a single phase three-wire split-phase distribution system like the one depicted in Figure 4-4 is commonly used for distributing power among residential customers. In this system, light loads (e.g., lighting loads) are supplied power at 120 V (connected between a live conductor and the neutral) whereas heavy loads (e.g., electric heaters) are connected between two live conductors and receive 240 V.

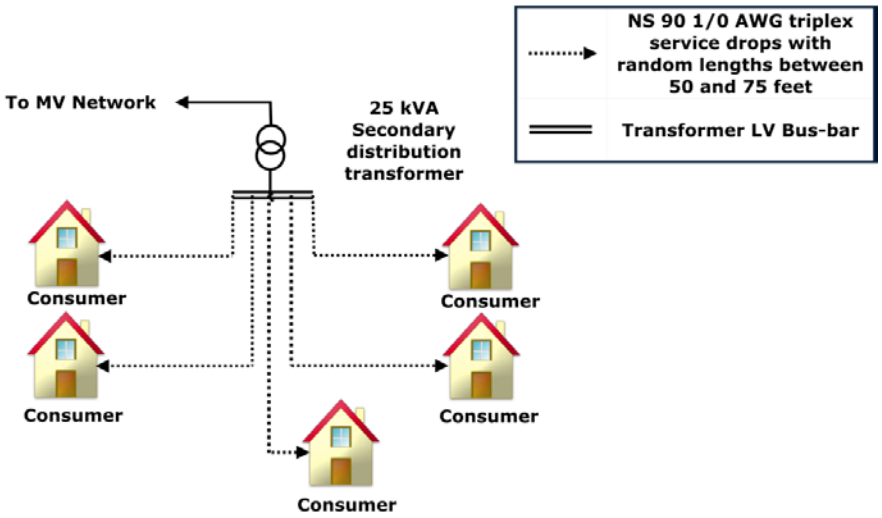

Figure 4-3: Sample secondary distribution circuit

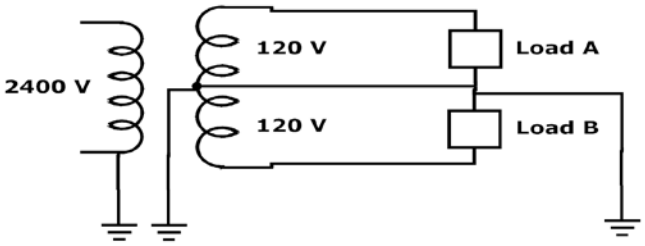

Figure 4-4: Split-phase distribution system

Unbalanced distribution of 120 V loads between the two circuits results in one of two split phases of the center-tapped transformer being loaded more than the other, making it more likely to be overloaded even though the transformer as a whole may have enough capacity to supply existing loads.

For this study, the author investigated the unbalance occurring in secondary distribution transformers due solely to the charging demand of the PHEVs. The existing system loads are thus assumed to be equally distributed between the two split phases.

4.4.3 Generating Random Charging Profiles for PHEVs

Previous research estimated PHEV charging profiles by adopting several assumptions. For example, some studies simply assumed that that all PHEVs are driven the same distance daily and hence have the same SOC at the onset of charging [21, 165, 167]. Other studies assumed that PHEVs start charging either at fully discharged state [111, 176] or at a totally random SOC [18, 169]. In [111, 166, 167, 169, 176], it was assumed that PHEVs will start charging at specific hours with no statistical support for these assumptions.

In this analysis, the author rectified these assumptions by using the cdfs derived in Section 3.4 to provide a more realistic estimation for PHEV charging profiles, as explained below.

4.4.3.1 PHEV Adoption Rates

The number of PHEVs existing in the system at different penetration levels is given by:

$$N_{PHEVs}(\mu) = X_{penet} \times N_{Households,System} \times \mu_v \quad (4.1)$$

where

$N_{PHEVs}(\mu)$ is the number of PHEVs at a given penetration level μ;
X_{penet} is the PHEV percentage penetration level (PHEV/vehicle);
$N_{Households,\ System}$ is the total number of households in the system (625);
μ_v is the average number of vehicles per household, estimated in the 2009 NHTS to be 1.9 vehicles/household.

Thus, for each penetration limit, the number of PHEVs in the system is calculated as per Eq. (4.1). PHEVs are then randomly assigned to the end customers, maintaining the percentages of each vehicle type as given in Table 4-1. Finally, battery chargers are allocated for PHEVs according to the charging scenarios depicted in Table 4-3.

4.4.3.2 Determining the Daily Energy Requirements for PHEVs

For this research, it is assumed that PHEV charging occurs solely at owners' residences. This assumption is based on the results of the EV research project [177] funded by the U.S. Department of Energy. The study concluded that the vast majority of consumers (80%) tend to charge their PHEVs at home. Similar results were obtained in another study prepared for the VDE 2010 E-mobility congress [178]. The German study reported that consumers prefer to charge their PHEVs in their own garage. Charging in the parking lots of shops and on company grounds is expected to represent less than 6% and 4%, respectively.

Determining the daily energy requirement for each vehicle entails the generation of two random variables (representing the home arrival time and the daily mileage for this PHEV) based on the cdfs shown in Figures 3-16 and 3-17. The *SOC* of the battery when the PHEV arrives home depends on the daily distance travelled and is given as:

$$SOC = Max(1 - \frac{d_{daily} \times e}{C} \times 100\% \ , 30\%) \tag{4.2}$$

where

SOC is the percentage state of charge of the battery;
d_{daily} is the daily distance travelled by the PHEV in miles;
e is the specific energy consumption of the vehicle in kWh/mile;
C is the PHEV battery capacity in kWh.

` `

The vehicle is initially powered by its battery system, and when the battery *SOC* drops to 30% [167, 179], the vehicle is powered by the ICE. This procedure is designed to reduce wear on the battery and increase its life. The *SOC* for the battery can therefore not drop below 30%, as shown in Eq. (4.2).

The total charging energy (*TCE*) required for the battery to be fully charged is given by:

$$TCE = \frac{(1-SOC)\times C}{\eta_{PHEV\ charger}} \tag{4.3}$$

where *TCE* is the total charging energy required to charge the battery in kWh and $\eta_{PHEV\ charger}$ is the battery charger efficiency, taken as 90% [99, 163, 164].

4.4.3.3 Determining Chronological Charging Profiles for PHEVs

The charging profile of a PHEV is determined based on three quantities: the time the charging starts, the power rating of the charger, and the duration required to charge the battery.

In this research, only the impact of the uncontrolled charging of PHEVs is assessed, and the resulting charging profiles are thus dependent mainly on consumer habits. Drivers are most likely to plug in their vehicles as soon as they arrive home from work. Home arrival time is therefore taken to be the start time for the charging. This assumption was also adopted in [157, 167, 180]. The *TCE* and charging level are the two key factors that determine the duration and power rating of the charging. The author adopted the approximation utilized in [157, 181], based on which the *TCE* is broken down into a series of 1.44 kWh for level-1 battery chargers (or 7.2 kWh for level-2 chargers). For example, given a battery with a *TCE* equal to 8.4 kWh and charged by a level-1 battery charger, the battery will be charged at a rate of 1.44 kW for the first 5 hours. At the 6th hour, the battery charger operates at a derated charging mode and charges the battery with the remaining energy (1.2 kWh).

If the time the charging starts, the power rating of the charger, and the duration required for the battery to be charged are all established, the chronological charging profile for each PHEV can be determined with an adequate degree of accuracy. This procedure is then repeated for each PHEV existing in the system.

The charging demand supplied by level-2 battery chargers (240 V) does not cause an unbalance in the distribution transformer because this demand is shared evenly by the two split phases. However,

this is not the case for level-1 battery charger, for which the charging demand is assigned randomly to one of the two split phases.

4.4.4 Running the Load Flow Analysis

The aggregated demand for each customer is obtained through the addition of the existing household demand and the charging profile(s) of the PHEV(s) owned by the customer. These aggregated demands form the input to the OpenDSS software that is used to perform the load flow analysis. The resulting electrical quantities (power flows, voltages, losses, etc.) for different scenarios are stored for future processing.

4.4.5 Stopping Criterion

Choosing an appropriate stopping criterion is crucial for the accuracy and robustness of MC simulations. In this research, an energy adequacy (*EA*) index is proposed as a determinant for stopping the simulation. The proposed index is analogous to the expected energy not supplied (EENS) index commonly used in risk assessment studies. The *EA* index for the y^{th} year is given as:

$$EA(y) = \begin{cases} \sum_{i=1}^{8760} S_{Feeder\ Rated} - S_{Main}(i,y), & \forall\ Max(S_{Main}(i,y)) < S_{Feeder\ Rated} \\ Max(\sum_{i=1}^{8760} S_{Main}(i,y) - S_{Feeder\ Rated}, 0), & \forall\ Max(S_{Main}(i,y)) > S_{Feeder\ Rated} \end{cases} \quad (4.4)$$

where

$EA(y)$ is the energy adequacy index for the y^{th} year;
$S_{Feeder\ Rated}$ is the kVA rating of the primary feeder;
$S_{Main}(i, y)$ is the apparent power flowing through the feeder head-end at the i^{th} hour in the y^{th} year.

The first part of the equation represents the annual energy that can still be supplied by the three phases of the primary feeder without exceeding its rated capacity, whereas the second part represents the annual energy supplied that results in violation of the feeder capacity limits.

The *EA* index is calculated for every year, and the mean value for the *EA* indices up to and including the current year is then evaluated. Finally, the coefficient of variation is computed for these mean values. The simulation is said to have converged when the coefficient of variation is less than 5%.

`  `

4.4.6 Reiterating the Analysis for Different Scenarios

The previous analysis is repeated three different times (according to the charging scenarios depicted in Table 4-3) for each penetration level, in addition to the no-PHEVs base scenario.

4.5 Results and Discussion

This section presents the simulation results abstracted from the developed benchmark. MC simulations do not produce definitive indices; however, the resulting outcomes they do provide are probabilistic in nature, i.e., come with probability distributions. The proposed research utilized this feature to eliminate one of the major drawbacks of the models described in the literature, most of which [166, 170, 180-182] addressed only the impacts of PHEVs without consideration of the probabilities of such impacts occurring. A comprehensive impact analysis, however, should represent a combination of both impact and likelihood, as explained in the following sections.

4.5.1 Probability of Overloading Distribution Equipment

The probabilistic analysis began by computing the frequencies of occurrence of different kVA loadings in each equipment class (primary feeder, secondary distribution transformers, single phase laterals and service drops) throughout the total simulation interval (several thousand years). The resulting frequency distributions are then utilized to develop the cumulative frequency distribution curves (cfd) for the resulting kVA loadings. The resulting cfd specifies the probability that this equipment class will supply a demand that is equal to or less than a specific kVA loading. However, in distribution planning studies, determining the probability by which a component's loading will exceed a certain kVA provides more important information. The last probability is represented by the complement of the cfd (1-cfd). To simplify the analysis, these (1-cfd) curves are normalized with respect to the equipment's nominal capacity to give the percentage loading.

Figure 4-5 shows a sample normalized (1-cfd) curve for 50 kVA distribution transformers at 70% PHEV penetration, during the worst-case charging scenario (charging scenario 3-Ch4). Similar curves can be derived for different scenarios. The probability of exceeding a certain class of equipment rating can be determined directly from the normalized (1-cfd) curves as the probability corresponding to 100% loading. This probability gives the percentage of time this class of equipment will supply a demand above its rated capacity. For example, this probability equals 28% for the curve depicted in Figure 4-5.

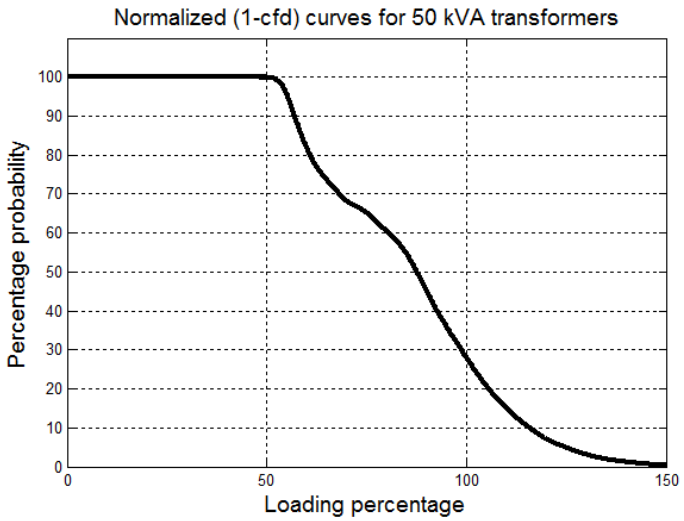

Figure 4-5: Probability of exceeding a specific loading for 50 kVA transformers

The probabilities of overloading 50 kVA transformers for different study scenarios are depicted in Figure 4-6. The figure reveals that 50 kVA transformers are susceptible to significant overloads at PHEV penetrations as low as 10%. Similar results are obtained for 25 kVA transformers. The susceptibility of secondary distribution transformers to significant overloads is attributed to their reduced diversity. However, the same concept does not apply to laterals and service drops, as North American utilities usually oversize such equipment for mechanical considerations. Hence, their loading does not exceed 70% and 50% of their rated capacity, respectively, as shown in their normalized (1-cfd) curves. Thus, laterals and service drops are excluded from the rest of the analysis.

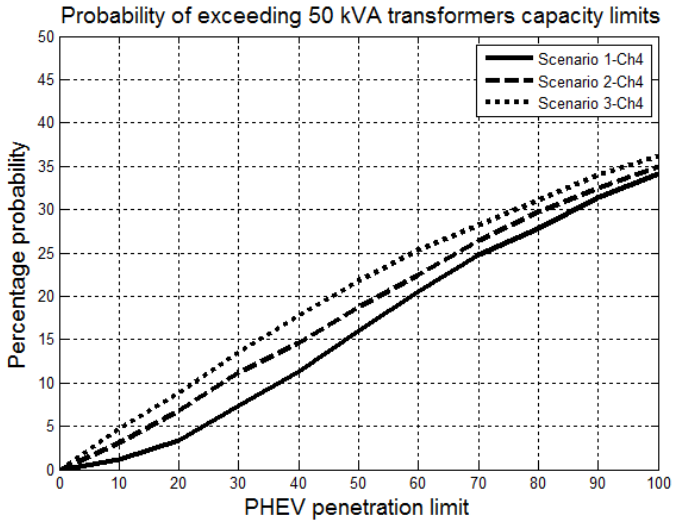

Figure 4-6: Probability of overloading 50 kVA transformers

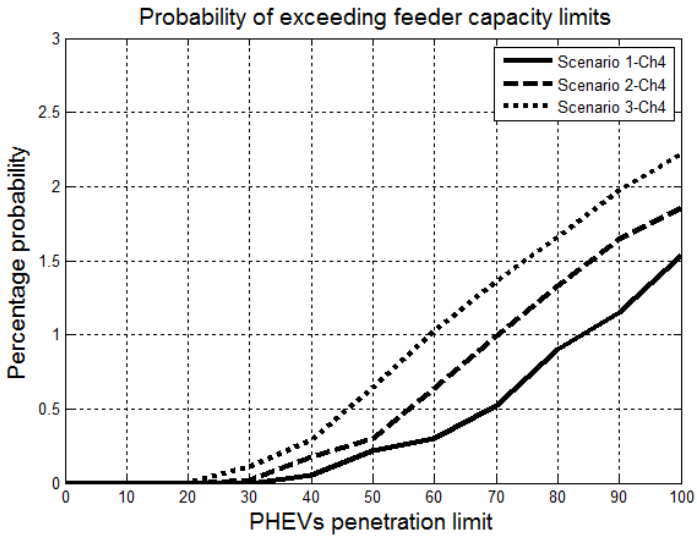

Figure 4-7: Probability of overloading the primary feeder

Figure 4-7 depicts the probability of overloading different sections of the primary feeder. The impact of diversity is quite significant: the feeder exhibits an overload with only a very small probability (less than 2.3% in the worst-case scenario).

4.5.2 Upgrade Requirements

One problem with MC simulations is that the peak demand supplied by specific piece of equipment cannot be determined accurately due to the presence of peak spikes that occur with very small probabilities. For this work, the author has defined peak demand as the demand with less than 5% probability of being exceeded. This peak demand is the percentage loading on the normalized (1-cfd) curves that corresponds to a probability of 5%. This definition implies that the designated demand is the maximum demand with a 95% confidence level.

Thus, the peak demand occurring in each piece of equipment is computed for different scenarios and the equipment is flagged as overloaded and in need of upgrading if the designated peak demand exceeds its rated capacity.

Figure 4-8 depicts, for the three charging scenarios, the percentage of 50 kVA transformers that require upgrading. The figure indicates that the overloading of 50 kVA transformers depends on the charging scheme: level-2 chargers cause a greater overload than level-1 chargers do.

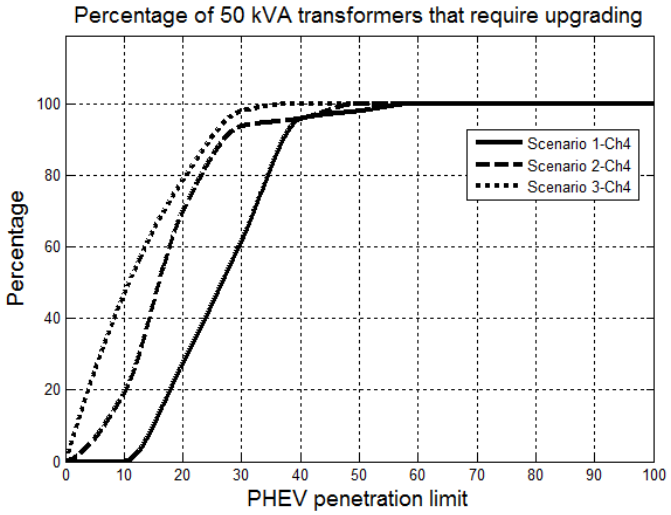

Figure 4-8: Percentage of 50 kVA transformers that require upgrading

The obtained results are quite alarming: even for level-1 chargers, 27% of the 50 kVA transformers need to be replaced at 20% PHEV penetration. The situation is even worse for level-2 chargers: 46% of 50 kVA transformers need to be upgraded at 10% PHEV penetration, and all 50 kVA transformers should be replaced at 40% PHEV penetration. Similar results are obtained for 25 kVA transformers.

Due to its increased diversity, the situation is much better for the primary feeder, as shown in Figure 4-9. The feeder requires upgrades starting from 40% PHEV penetration for scenario 1-Ch4 and from 30% for scenarios 2-Ch4 and 3-Ch4.

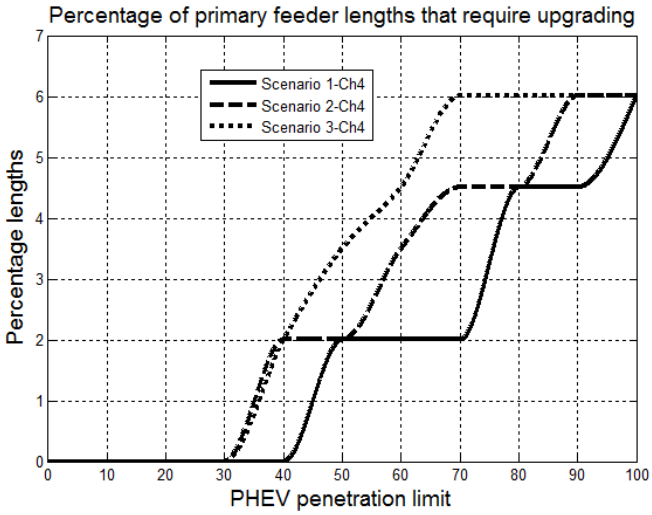

Figure 4-9: Percentage of primary feeder lengths that require upgrading

` `

The feeder sections that require upgrading with the worst-case scenario are the first four main head-ends. This problem is common with radial feeders: the first head-ends carry the entire circuit load, so their loads are greater than those of the rest of the sections.

4.5.3 Unbalanced Loading of Distribution Transformers

This section presents an evaluation of the unbalance in secondary distribution transformers due to the 120 V level-1 chargers. As mentioned earlier, this unbalance may cause one of two split phases of the center-tapped distribution transformer to become overloaded even though the capacity of the transformer as a whole may be sufficient for supplying existing loads. Unfortunately, the literature contains so little work related to such unbalances that additional research is apparently required in order to address the possible associated impact.

For this research, the percentage unbalance (*PU*) in the transformer was calculated as follows:

$$PU(i) = \frac{\left| S_{Phase\ A}(i) - S_{Phase\ B}(i) \right|}{S_{Phase\ A}(i) + S_{Phase\ B}(i)} \times 100 \tag{4.5}$$

where

PU(i) is the percentage unbalance in the split phase secondary distribution transformer at hour *i*;
$S_{Phase\ A}(i)$ is the kVA flow in the first split phase at hour *i;*
$S_{Phase\ B}(i)$ is the kVA flow in the second split phase at hour *i*.

Figure 4-10 depicts the average daily unbalance in the 25 kVA transformers for charging scenario 1-Ch4. Based on the results shown in the figures, it is evident that the unbalance increases during the hours of peak charging demand (5 pm–1 am).

Following the same procedure outlined in the previous section, the peak unbalance with a 95% confidence can be estimated. Figure 4-11 depicts the results for 25 kVA transformers during scenario 1-Ch4. Results indicate that charging scenario 1-Ch4 exhibits greater unbalance than charging scenario 2-Ch4. This observation can be easily explained by the fact that transformer unbalance occurs solely due to 120 V level-1 chargers. Scenario 3-Ch4 shows no unbalanced loading. Similar results are obtained for 50 kVA transformers.

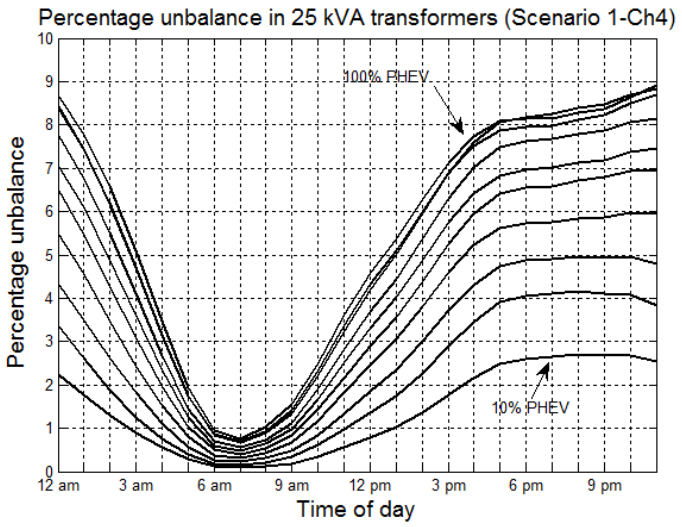

Figure 4-10: Average daily unbalance in 25 kVA transformers (scenario 1-Ch4)

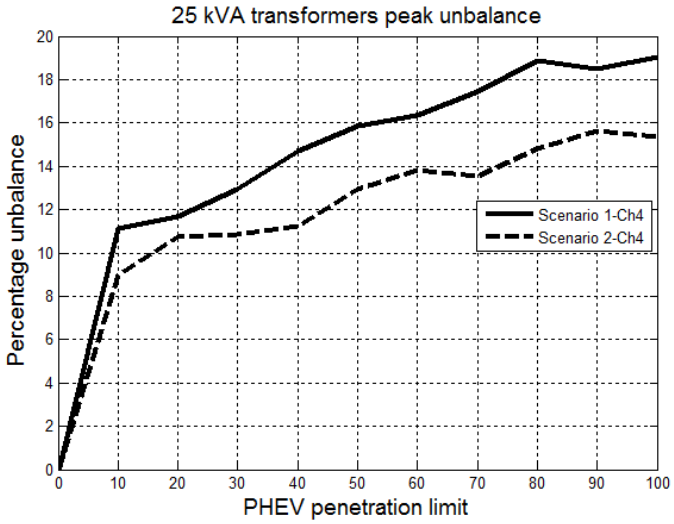

Figure 4-11: Peak unbalance in 25 kVA transformers

4.5.4 Number of Voltage Regulators Operations

Voltage regulators are special autotransformers with automatic tap-changing equipment and are inserted along the primary feeder or at the substation bus as a means of maintaining within acceptable limits the voltages at the end customers. The IEEE 123 Node Test Feeder has 4 voltage regulators.

The annual number of regulator actions (N_{Reg}) is given by:

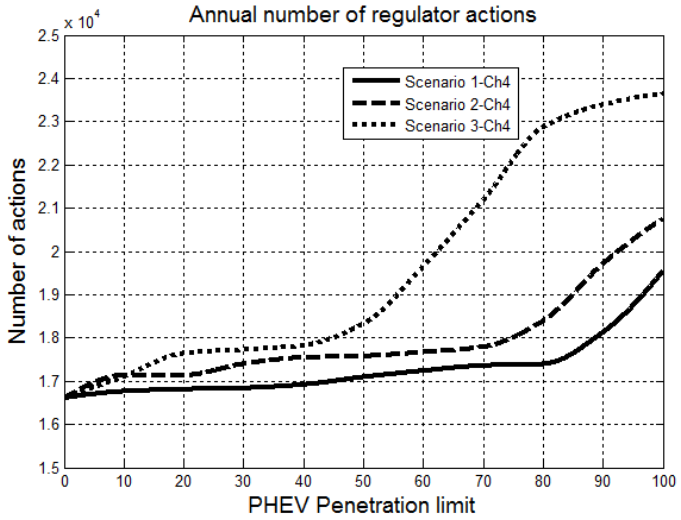

Figure 4-12: Annual voltage regulators control actions

$$N_{Reg} = \sum_{i=1}^{8760} x(i) \tag{4.6}$$

where *x(i)* is a binary integer whose value equals 1 when the voltage being monitored (V_m) deviates from the voltage regulator's set voltage (V_s) by more than the predetermined bandwidth (B), and equals zero otherwise:

$$x(i) = \begin{cases} 1, & \forall \left| V_m(i) - V_s \right| > B \\ 0, & otherwise \end{cases} \tag{4.7}$$

The annual numbers of regulators actions for different penetration levels and different charging scenarios are depicted in Figure 4-12.

Based on the results shown in Figure 4-12, it can be concluded that the number of operations of voltage regulators depends on two factors:

i) PHEV penetration level: the number of regulators actions increases as PHEV penetration increases;

ii) Charging level: level-2 chargers increase the number of operations of voltage regulators more than level-1 chargers do.

Any increase in the number of control actions reduces the life expectancy of the voltage regulators.

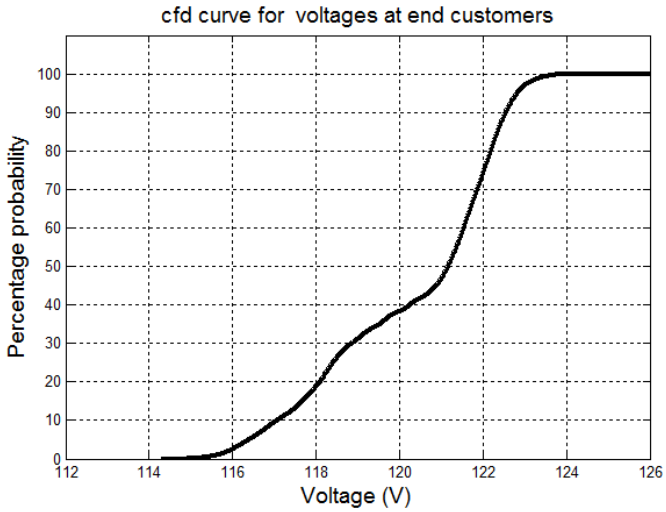

Figure 4-13: Probability of voltages being below a specific value at the end customers

4.5.5 System Voltages

A major concern about PHEVs is the resulting under voltages at the end customers (120 V) during the heavy loading conditions that coincide with the peak charging times for PHEVs. The proposed benchmark enables an accurate computation of these voltages because it models the secondary distribution networks in detail.

Since under voltages are the quantities of concern, it is more convenient to obtain the probability of voltages being lower than a specific value. Thus, cfd curves are used in this stage rather than (1-cfd) curves. The cfd curve representing the voltages at the end customers at 100% PHEV penetration during the worst-case charging scenario (charging scenario 3-Ch4), is depicted in Figure 4-13.

Similar curves can be derived for voltages along the main feeder, and across secondary distribution transformers for diverse PHEV penetrations and charging scenarios. From these curves, two important quantities can be derived, as explained in the following sections.

4.5.5.1 Minimum System Voltages

For this research, the minimum voltage is defined as the voltage that corresponds to the 5% probability on the cfd curve. This definition means that the designated voltage is the minimum voltage with a 95% confidence level. The minimum voltages at different locations in the distribution system are depicted in Figures 4-14, 4-15, and 4-16.

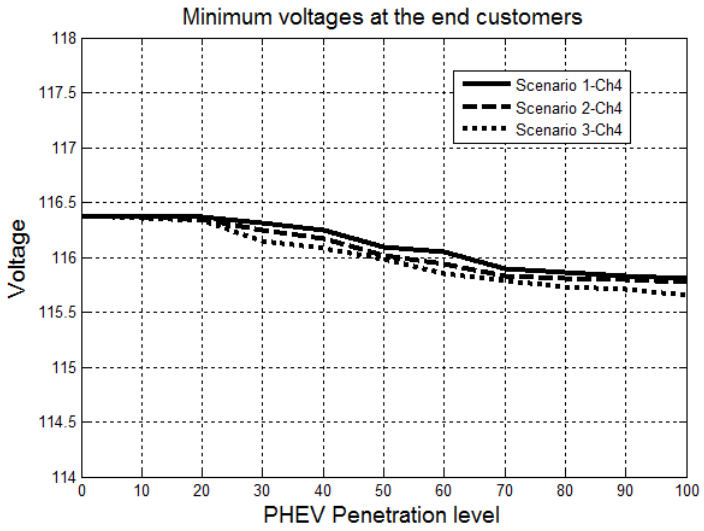

Figure 4-14: Minimum voltages at the end customers

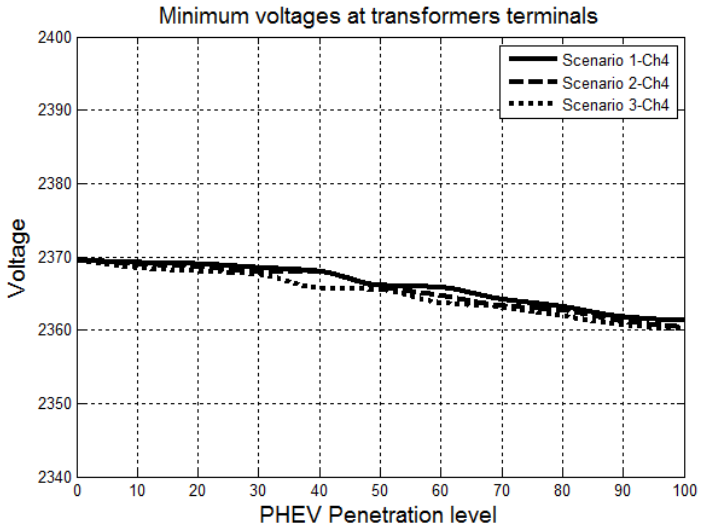

Figure 4-15: Minimum voltages at transformers terminals

Figures 4-14, 4-15 and 4-16 reveal that PHEVs are unlikely to affect system voltages even during the heaviest loading conditions as voltage regulators installed in the system are capable of maintaining system voltages within acceptable limits. However, this is achieved on the expense of additional control actions (as shown in Figure 4-12). For example, as PHEV penetration increases from 0% to 100%, voltages at the end customers are reduced by less than 1%; nevertheless, this is accompanied by 40% increase in the number of annual regulators actions.

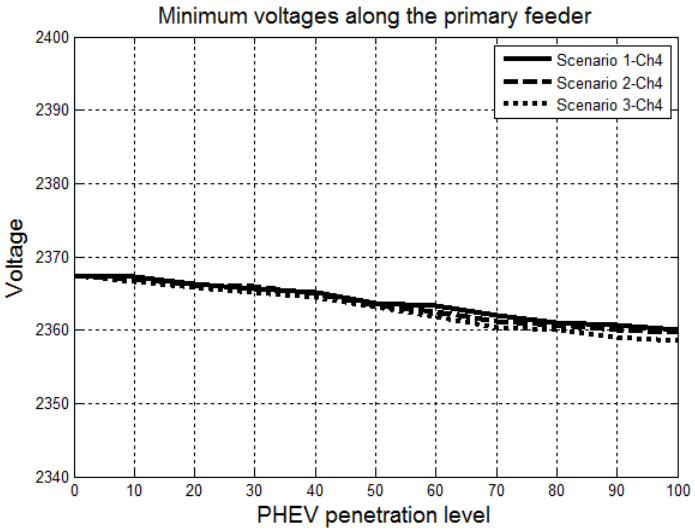

Figure 4-16: Minimum voltages along the primary feeder

4.5.5.2 Probability of Violating Range-A Voltage Limits

ANSI C84.1-1995 defines range-A voltage limits for 120 V and 2400 V systems to be 114 V–126 V and 2340 V–2520 V, respectively. The probabilities of violating these limits for different PHEV scenarios at different locations in the distribution system are shown in Figures 4-17, 4-18, and 4-19.

Results indicate that the probability of violating these limits is less than 0.8% in the worst-case scenario. However, this ability is achieved at the expense of additional regulators actions, as explained earlier.

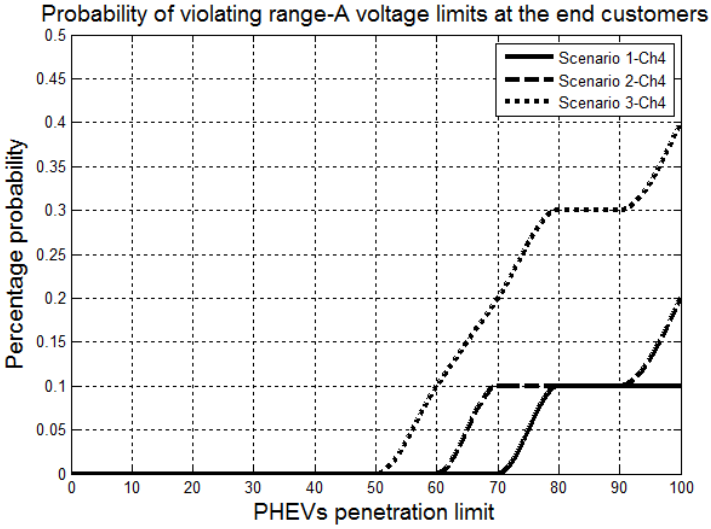

Figure 4-17: Probability of violating range-A voltage limits at the end customers

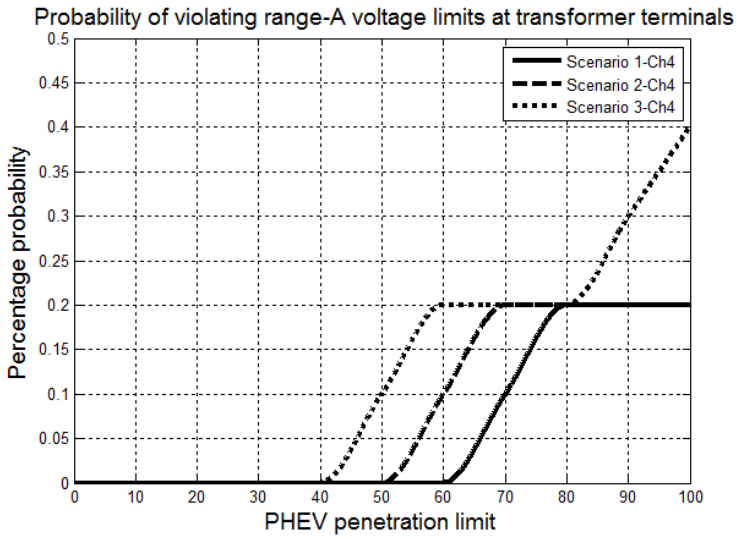

Figure 4-18: Probability of violating range-A voltage limits at transformer terminals

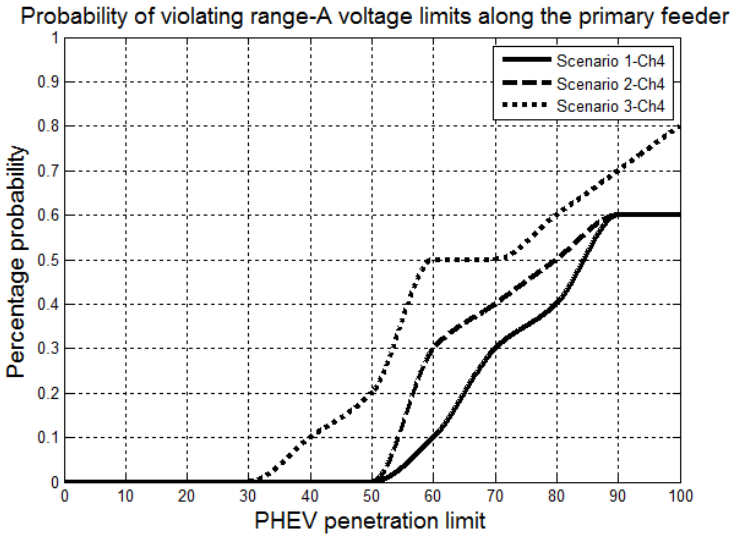

Figure 4-19: Probability of violating range-A voltage limits along the primary feeder

4.5.6 Total System Losses

The total annual active and reactive energy losses for different PHEV penetrations are depicted in Figures 4-20 and 4-21 respectively.

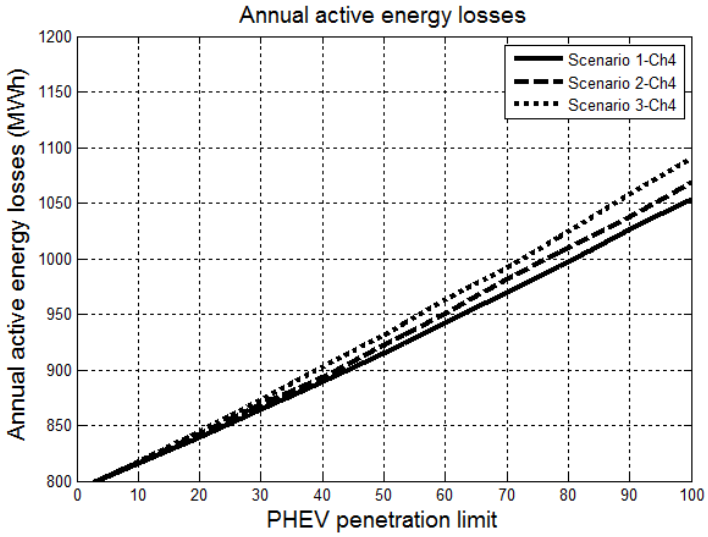

Figure 4-20: Annual active energy losses

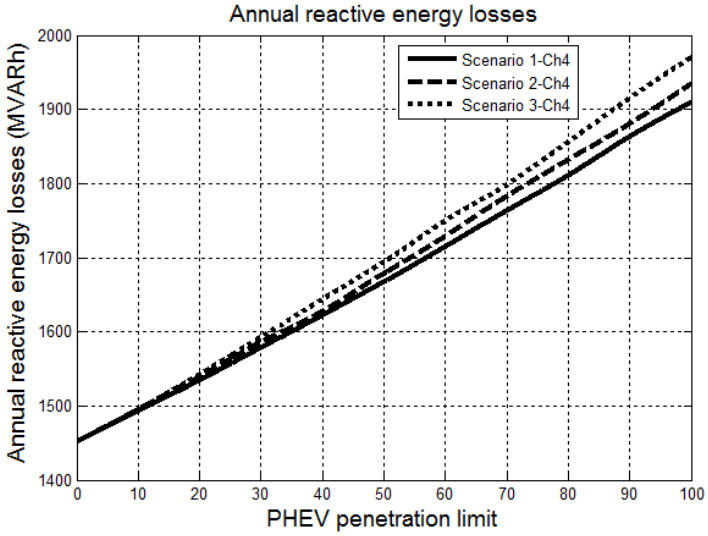

Figure 4-21: Annual reactive energy losses

The results imply that the annual system losses are dependent on PHEV penetration as well as on the charging scenario. Level-2 chargers incur more energy losses than level-1 chargers. The system active energy losses increase linearly with increased PHEV penetration, by about 3.3%, 3.5% and 3.75% per 10% PHEV penetration for scenarios 1-Ch4, 2-Ch4, and 3-Ch4, respectively. Similar figures are obtained for the reactive energy losses. These additional energy losses increase the cost of integrating PHEVs within existing systems.

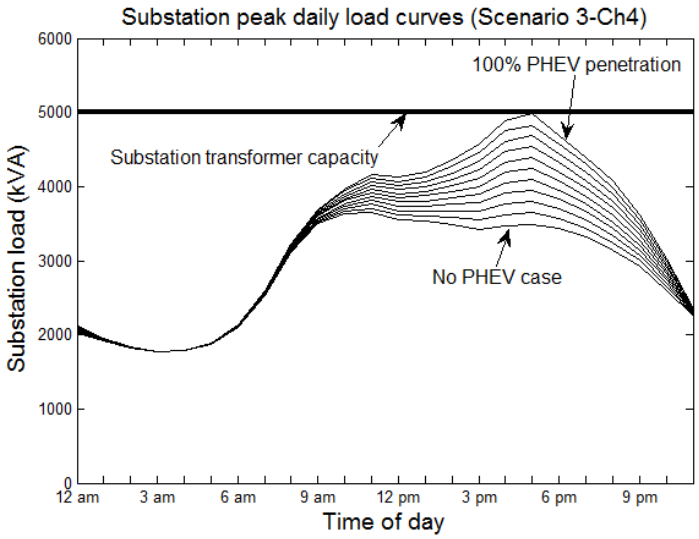

Figure 4-22: Distribution substation peak daily load curves

4.5.7 Substation Transformer Capacity Limits

Utility engineers are mostly concerned about how much load the distribution substation has to supply and at what time horizon. Figure 4-22 depicts the peak daily load curves (with 95% confidence) supplied by the substation transformer for different PHEVs penetrations during the worst-case scenario (charging scenario 3-Ch4). Similar curves can be derived for other charging scenarios. From the figure, it is evident that PHEVs increase the system peak demand and shift it to the early evening period (which is the peak charging period).

Due to its high diversity, the substation transformer is not likely to be overloaded during any of the scenarios. Figure 4-23 depicts the increase in the peak demand (with 95% confidence) of the substation transformer for different charging scenarios. Results reveal that the substation transformer peak demand increases linearly with increased PHEV penetration by only 2.2%, 2.5% and 3.2% per 10% PHEVs penetration for charging scenarios 1-Ch4, 2-Ch4, and 3-Ch4, respectively.

4.6 Summary and Conclusions

This chapter introduced a MC-based probabilistic benchmark for assessing the impacts of the uncontrolled charging of PHEVs on residential distribution networks. The proposed benchmark uses the probabilistic models, previously explained in Chapter 3, to represent uncertainties associated with existing electrical loads and individuals' driving patterns that may impact the charging process.

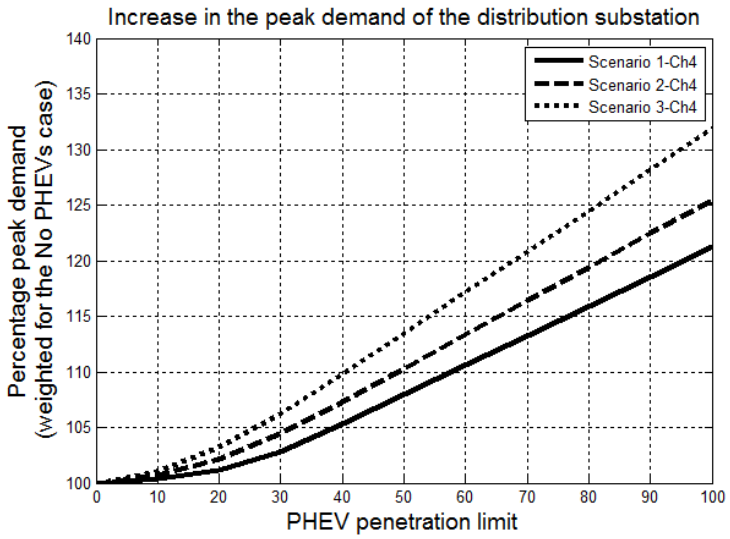

Figure 4-23: Increase in the peak demand for the distribution substation

The chapter started by reviewing the weaknesses of previous approaches used to assess the impacts of PHEVs on distribution networks; then the probabilistic models used in this research to represent different uncertainties inherent in the distribution system were described. After that, the different stages of the MC-based probabilistic benchmark were outlined; and finally, the simulation results were presented.

The performed analysis showed that secondary distribution transformer overloading is the bottleneck blocking the widespread adoption of PHEVs. The uncontrolled charging of PHEVs can be detrimental to these transformers, for which the diversity effect is not as clear as it is at primary system levels. For example, 46% of 50 kVA transformers must be upgraded at a 10% PHEV penetration with level-2 chargers. This conclusion is consistent with the author's postulate that it is more important to assess the impacts of PHEVs on localized distribution networks rather than on the system's overall generation capacity (as previous researchers did).

However, as explained earlier, PHEVs are not the only challenge facing distribution systems in the smart grid era; integrating PV electricity in existing distribution networks represents another major challenge. An important question that arises here is: how would these two technologies (PHEVs and PV electricity) interact with each other? Or, in other words, what are the resulting aggregated impacts when the distribution system is under a high penetration of both PHEVs and PV electricity? This question is covered in the next chapter.

Chapter 5
Studying the Aggregated Impacts of PHEVs and PV Arrays on Residential Distribution Systems

5.1 Introduction

In the previous chapter, the author analyzed the impacts of the uncontrolled charging of PHEVs on residential distribution networks. The performed analysis showed that secondary distribution transformer overloading is the bottleneck blocking the widespread adoption of PHEVs. The uncontrolled charging of PHEVs can be detrimental to these transformers, for which the diversity effect is not as clear as it is at primary system levels.

However, as mentioned earlier, PHEVs are not the only challenge facing distribution systems in the smart grid era. Integrating PV electricity in existing distribution networks represents another major challenge. The important question that arises here is: how would these two technologies (PHEVs and PV electricity) interact with each other? Or, in other words, what are the resulting aggregated impacts when the distribution system is under a high penetration of both PHEVs and PV electricity?

Although extensive research has been conducted with respect to the individual impacts of PHEVs [9, 10, 32-37] and PV electricity [22-31] on distribution networks, far too little attention has been paid to studying the interaction between these two technologies or the resulting aggregated impacts when both operate in parallel. Moreover, previous researchers who have conducted research on the same topic failed to provide adequate models for different uncertainties present in the system. For example, the authors of [183] studied the aggregated impact of PV arrays and PHEVs on distribution system performance in terms of network voltages and power losses. However, the performed analysis has several drawbacks. PV intermittency was not considered in the analysis, and individuals' driving patterns impacting the charging process were not modeled properly: PHEV home arrival times were simply assumed to follow a normal distribution centered at 6 pm, with a 2-hour variance. Also the stochastic nature of electrical loads was completely ignored; only one load shape was used in the analysis. As explained earlier, these unbacked assumptions may affect the accuracy and validity of the obtained results.

The research presented in this chapter aims to avoid the previous drawbacks by using the MC-based probabilistic benchmark, previously developed in Chapter 4, to analyze the aggregated impacts

of both PV electricity and PHEVs on distribution system performance, with consideration of different uncertainties inherent in the system. The remainder of the chapter is organized as follows: Section 5.2 describes the MC-based probabilistic benchmark; Section 5.3 presents the simulation results for different study scenarios; and finally, Section 5.4 concludes the chapter.

5.2 MC-Based Probabilistic Benchmark

This section provides an overview of the MC-based probabilistic benchmark used in this research to analyze the performance of the distribution system under a high penetration of PHEVs and PV electricity.

5.2.1 Representing Distribution System Uncertainties in the MC Simulation

The first step in implementing the proposed benchmark is the development of appropriate probabilistic models to represent different uncertainties present in the distribution system.

5.2.1.1 Modeling Uncertainties Related to PV Array Output

For this work, the author uses the approach described in Section 3.2 to model the stochastic nature of PV array output. Hourly insolation and temperature data provided by the Solar Radiation Research Laboratory are used to estimate PV arrays' DC power output using the empirical model described in [134]. The equivalent AC output power is computed using a typical inverter efficiency curve [137]. The 24 data points representing the PV array daily output are assembled in a data segment. The resulting 365 data segments representing the whole year are evaluated for similarities using PCA, and then similar segments are grouped into one cluster. For each cluster, a representative segment is selected to represent all the segments (or days) within the cluster, and its probability of occurrence is computed. The results of the clustering process reveal that the complete data set can be represented using only 19 representative segments (instead of 365) while retaining temporal variations within the data, thus reducing the computational burden to a minimum. The resulting representative data segments and the corresponding cdf are depicted in Figures 3-7 and 3-9 respectively.

5.2.1.2 Modeling Uncertainties Related to Existing Loads

To model the stochastic nature of residential loads, the author uses the load modeling approach presented in Section 3.3. As explained earlier, the utilized load modeling approach starts by grouping

the 24 data points representing the loading conditions during a given day in a data segment. The resulting 365 data segments representing the whole year are processed using PCA, and segments that are found to have a similar first principle component are grouped into the same cluster. Finally, for each cluster, a representative segment is selected to represent the whole cluster, and its probability of occurrence is computed. This approach makes it possible to represent the stochastic nature of residential loads using only six daily representatives instead of 365 different profiles. The selected representative segments and the corresponding cdf are depicted in Figures 3-11 and 3-13, respectively.

Commercial loads, on the other hand, are characterized by low variability in their demands [171] and thus can be represented using only one load curve. The load curve used in this research for representing commercial loads is depicted in Figure 4-1.

5.2.1.3 Modeling Uncertainties Related to Individuals' Driving Patterns

For this work, the author uses the approach outlined in Section 3.4 as a means of deriving cdfs modeling individuals' driving habits impacting the charging process. Data for 1,048,576 people and 309,164 vehicles were taken from the 2009 NHTS. The data were filtered so that only three types of vehicles were considered: automobiles, vans, and SUVs. Finally, the resulting data set was processed to extract probability functions that represent daily mileage and home arrival times. Figures 3-16 and 3-17 depict the resulting cdfs.

5.2.2 Description of the Test System

For this work, the author uses the same test system previously described in Section 4.4.1. As explained earlier, this system is an expanded version of the IEEE 123 node test feeder [174] shown in Figure 4-2, in which each existing 22.36 kVA spot load has been expanded into a 25 kVA distribution transformer that supplies 5 households, and each 44.72 kVA spot load has been expanded into a 50 kVA distribution transformer that feeds 10 households. The system thus has a total of 625 residential households. Secondary distribution networks are modeled based on practical data provided by a power utility in Ontario. Based on the same practical data, each household peak demand was taken as 6.2 kVA. The remaining 13 spot loads are assumed to be commercial loads serving the residential area. The network was modeled using OpenDSS from the substation down to the customer meter, resulting in a system with 1684 nodes.

5.2.3 Study Assumptions and Scenarios

This section outlines the different assumptions made in this research with regards to the types, penetration levels and charging levels of PHEVs, as well as PV array ratings.

5.2.3.1 Types of PHEVs

Similar to Section 4.3.3.1, the author divided PHEVs into three different types (automobiles, vans and SUVs), and chose a representative vehicle for each type to exemplify the whole type. To date, no data are available with respect to the market share of different types of PHEVs. It was therefore assumed that the types included in the study have the same current market share as that reported in the 2009 NHTS for their gasoline counterparts, as shown in Table 4-1.

5.2.3.2 PHEV Adoption Rates

To limit the number of studied scenarios, the author assumed only two penetration levels for PHEVs, based on the results of [101, 184]:

i) Medium-term projection (2031 case): 28% PHEV penetration.

ii) Long-term projection (2052 case): 52% PHEV penetration.

Given that the average number of vehicles per household is estimated in the 2009 U.S. NHTS to be 1.9 vehicles/household, then the total number of PHEVs present in the system in both scenarios is calculated to be 333 and 618 PHEVs, respectively. PHEVs are randomly assigned to the end customers, preserving the percentage of each vehicle type, as given in Table 4-1.

5.2.3.3 PV Arrays Ratings

Many published studies have investigated the maximum PV array size that can be seamlessly accommodated by existing distribution networks without altering their performance. In [134], the authors found no negative impacts with PV arrays of 1 kW installed at all households; however, over voltages occurred at a PV size of 2 kW per household. Another study [185] found that LV networks can handle PV arrays of up to 5 kW per household; however, the benefits of PV arrays were most significant at 1 kW per household. In Ontario, it was observed that most of the participants in the microFIT program prefer to install larger PV arrays [173] as they provide greater return on investment [186]. Thus, in this study the worst-case scenario is assumed, in which each household with a PHEV is equipped with a 10 kW PV array (which is the maximum allowable DG size in the

microFIT program). This last assumption is made in accordance with the current environmental directives encouraging the adoption of net zero energy housing (ZEH). Such green houses are expected to receive generous financial incentives from several government entities [187]. Similar assumption has been adopted in [183, 188-191].

5.2.3.4 PHEV Charging Levels

As mentioned earlier, SAE J1772 standard defines two residential AC single phase charging levels for PHEVs (given in Table 4-2). The analysis performed in Chapter 4 demonstrated that level-2 chargers impact distribution networks more severely than level-1 chargers. Therefore, in this analysis, the author is assuming the worst-case scenario, whereby all PHEVs are charged by level-2 chargers.

5.2.3.5 Study Scenarios

The main focus of this chapter is to analyze the aggregated impacts of PHEVs and PV arrays on residential distribution networks. To achieve this target, the author evaluated the resulting aggregated impacts when the distribution system is under a high penetration of both PHEVs and PV electricity and then compared these impacts to the ones resulting when only PHEVs are existent in the system. The author chose five study scenarios that would reflect these different situations for both medium and long-term projections. The proposed scenarios are given in Table 5-1

Table 5-1: Study scenarios

	Time frame	PHEV penetration	PV arrays
Scenario 1-Ch5	Base-case	0%	N/A
Scenario 2-Ch5	2031	28%	N/A
Scenario 3-Ch5	2031	28%	10 kW/PHEV
Scenario 4-Ch5	2052	52%	N/A
Scenario 5-Ch5	2052	52%	10 kW/PHEV

5.2.4 Generating Random Profiles for Stochastic Electrical Quantities

In this section, the probabilistic models derived earlier are used to generate random profiles for different stochastic quantities inherent in the distribution system.

`  `

5.2.4.1 Generating Random Output Profiles for PV Arrays

For this research, the cdfs derived earlier in Section 3.2 are used to generate random output profiles for PV arrays present in the system. For each day, a random number between 0 and 1 is generated. This random number is applied to the cdf in Figure 3-9 to select a random output profile from the 19 profiles given in Figure 3-7. Since all PV arrays are within the same residential area, they are all assumed to experience the same environmental conditions and are all assigned the same output profile. All PV inverters are assumed to operate at a unity power factor, as per IEEE Std. 929-2000.

5.2.4.2 Generating Random Loading Profiles for Existing Loads

In this stage, the load modeling approaches explained earlier are used to generate random loading profiles for electrical loads existing in the system. For residential loads, a random number between 0 and 1 is generated. This random number is applied to the cdf given in Figure 3-13 so that a loading profile can be selected from the six representative segments depicted in Figure 3-11. The selected percentage loading profile is then multiplied by the household peak demand (6.2 kVA at a 0.894 lagging power factor). For commercial loads, the load curve depicted in Figure 4-1 is simply multiplied by the load peak demand provided in the test feeder data. This procedure is repeated 365 times per year for each load in the system.

5.2.4.3 Generating Random Charging Profiles for PHEVs

As in Section 4.4.3, the generation of random charging profiles for PHEVs entails the generation of two random numbers between 0 and 1. These two numbers are used to generate random home arrival time and daily mileage for this PHEV using the cdfs shown in Figures 3-16 and 3-17, respectively. The *SOC* of the battery when the PHEV arrives home depends on the random daily distance travelled and is calculated by Eq. (4.2). After that, the *TCE* required for the battery to be fully charged is estimated using the expression given in Eq. (4.3).

The charging profile for each PHEV is determined based on the time the charging starts and the duration required for the battery to be fully charged. Similar to Section 4.4.3.3, the random home arrival time is taken to be the charging start time [157, 167, 180]. To estimate the charging duration, the author adopted the approximation utilized in [157, 181], based on which the *TCE* is broken down into a series of 7.2 kWh for level-2 chargers. For example, given a battery that requires *TCE* of 8.4 kWh, the battery will be charged at a rate of 7.2 kW in the first hour. In the second hour, the charger

operates at a derated charging mode and charges the battery with the remaining 1.2 kWh. By determining the time the charging starts and the required duration to charge the battery, the charging profile for each vehicle can be determined with sufficient accuracy. This procedure is then repeated 365 times per year for each PHEV in the system.

5.2.5 Running the Load Flow Analysis

The three electrical quantities obtained using the previous models (PHEV charging demands, PV array output and existing load demands) are aggregated to form the inputs to the OpenDSS software that is used in this research to perform the load flow analysis. This process is repeated until the designated stopping criterion is fulfilled.

5.2.6 Stopping Criterion

As in Section 4.4.5, the *EA* index given in Eq. (4.4) is used as a stopping criterion. The *EA* index is calculated for every year, and the mean value for the *EA* indices up to and including the current year is evaluated. Finally, the coefficient of variation for these mean values is computed. The MC simulation is said to have converged when the coefficient of variation is less than 5%.

5.2.7 Reiterating the Analysis for Different Scenarios

The previous analysis is repeated for the five study scenarios. The resulting electrical quantities (power flows, voltages, losses, etc.) for different scenarios are stored for future processing.

5.3 Results and Discussion

This section presents the results of running the MC simulation procedure for the system under study.

5.3.1 Substation Average Daily Demand

The average daily demand for the distribution substation during different study scenarios is depicted in Figure 5-1. The negative values in the Figure indicate the occurrence of reverse power flow.

From Figure 5-1, it is observed that PHEVs increase the system peak demand and shift it from morning to the early evening. Figure 5-1 also signifies the natural coincidence between peak electricity demand and the hours during which the majority of vehicles are charged. As mentioned before, this natural coincidence results in significant overloads at secondary distribution levels.

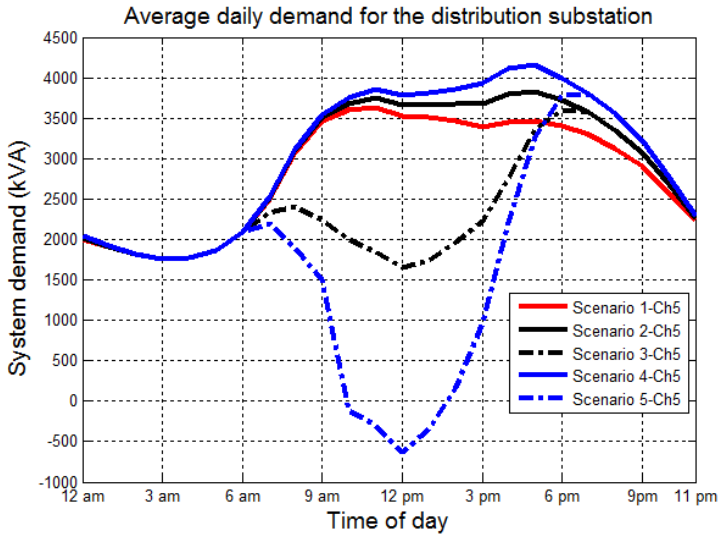

Figure 5-1: Average daily demand for the distribution substation

PV arrays shave the resulting peak demand in scenarios 3-Ch5 and 5-Ch5. However, they can only shave it slightly due to the weak chronological coincidence between PV array production and PHEV charging demands. PV arrays produce their maximum output at noon, whereas PHEV charging occurs mainly in the evening. This weak coincidence also results in reverse power flow occurring in the distribution network in scenario 5-Ch5 at noontime, when PV arrays are generating their peak output.

A drawback of the previous average curve is that it does not provide an insight into the likelihood of the anticipated impacts, thus disregarding one of the main strengths of MC simulations. MC simulations do not produce definitive indices; however, the resulting outcomes they do provide are probabilistic in nature, i.e., come with probability distributions. This feature will be used in the following sections to derive valuable probabilistic indices.

5.3.2 Probability of Overloading Distribution Equipment

As in Section 4.5.1, the probabilistic analysis begins by computing the probabilities of occurrence of different kVA loadings in each equipment class (primary feeder, 25 kVA transformers, 50 kVA transformers, single phase laterals and service drops) throughout the total simulation interval. The resulting frequency distributions are then utilized to develop the cfd curves for the kVA loadings. The resulting cfd specifies the probability that this equipment class will supply a demand that is equal to or less than a specific kVA loading. However, as explained earlier, determining the probability by which a component's loading will exceed a certain kVA provides more important information. The

last probability is represented by the complement of the cfd (1-cfd). For this reason, the (1-cfd) curves are used in this research rather than the cfd curves. To simplify the analysis, these (1-cfd) curves are normalized with respect to the equipment's nominal capacity to give the percentage loading. Figure 5-2 shows the normalized (1-cfd) curves for 25 kVA distribution transformers during different scenarios.

The probability of exceeding a certain class of equipment rating can be determined directly from the normalized (1-cfd) curves as the probability corresponding to 100% loading. This probability represents the percentage of time this class of equipment will be supplying a demand above its rated capacity. Table 5-2 shows the results.

Table 5-2: Probability of exceeding equipment ratings

Scenario	1-Ch5	2-Ch5	3-Ch5	4-Ch5	5-Ch5
Primary Feeder	0%	0.08%	0.01%	0.73%	0.11%
50 kVA transformers	0%	13.10%	5.31%	21.01%	9.18%
25 kVA transformers	0%	13.60%	6.07%	22.5%	9.33%
Single phase laterals	0%	0%	0%	0%	0%
Service drops	0%	0%	0%	0%	0%

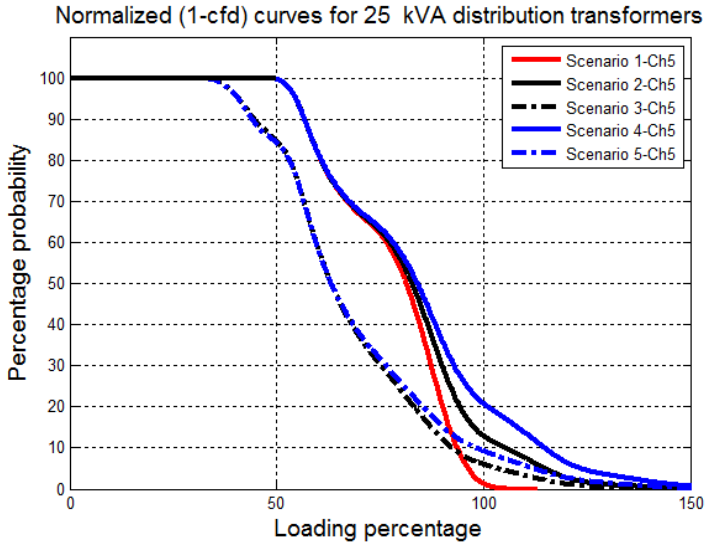

Figure 5-2: Probability of exceeding a specific percentage loading for 25 kVA distribution transformers

Impacts of diversity are quite significant as seen in Table 5-2. The primary feeder is not likely to be overloaded during any of the analyzed scenarios; the overload probability does not exceed 0.73% at worst (scenario 4-Ch5). Results also reveal that secondary distribution transformers are susceptible to significant overloads due to their reduced diversity. However, the same concept does not apply to laterals and service drops as utilities usually oversize such equipment for mechanical considerations. Hence, their loading does not exceed 65% and 32% of their rated capacity, respectively, as indicated in their normalized (1-cfd) curves shown in Figures 5-3 and 5-4, respectively. Thus, they are excluded from the rest of the analysis.

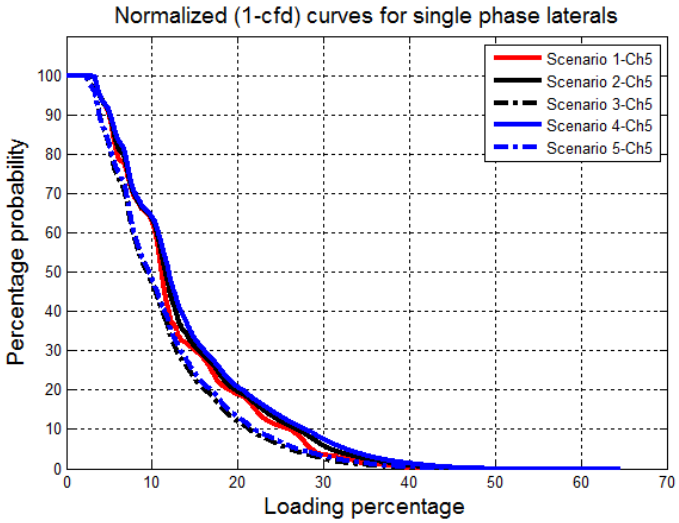

Figure 5-3: Probability of exceeding a specific percentage loading for single phase laterals

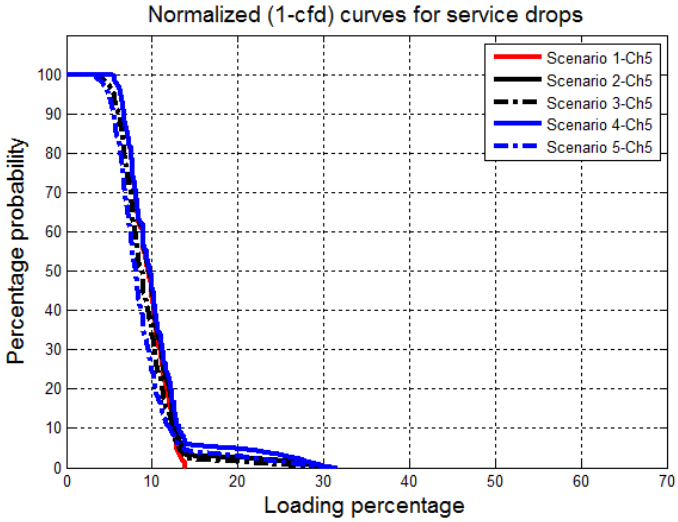

Figure 5-4: Probability of exceeding a specific percentage loading for service drops

` `

Generally speaking, the presence of PV arrays in scenarios 3-Ch5 and 5-Ch5 reduces the overloading of different distribution equipment for both medium and long-term projections. This is explained by the fact that PV arrays meet a portion of PHEV charging demands locally, and so reduce the overloading probability. However, this reduction is only minor, due to the weak chronological coincidence between PV supply and PHEV charging demands. The inclusion of PV arrays in the system reduces 25 kVA distribution transformers' overloading probability from 13.6% in scenario 2-Ch5 to 6.07% in scenario 3-Ch5 and from 22.5% in scenario 4-Ch5 to 9.33% in scenario 5-Ch5. Similar results are obtained for 50 kVA distribution transformers. The previous findings are also evident in Figure 5-2, where the normalized (1-cfd) curves for scenarios 3-Ch5 and 5-Ch5 are shifted to the left, indicating a reduction in the loading of the 25 kVA distribution transformers.

5.3.3 Upgrade Requirements

As in Section 4.5.2, the author defines the peak demand for a specific piece of equipment as the demand for which the probability that it will be exceeded is less than 5%. This peak demand is the percentage loading on the normalized (1-cfd) curve of this specific piece of equipment that corresponds to a probability of 5%. This definition means that the designated demand is the maximum demand with a 95% confidence level. Thus, the peak demand occurring in each piece of equipment is computed for different scenarios. This equipment is flagged as overloaded and in need of upgrading if the designated peak demand exceeds its rated capacity. Table 5-3 shows the results for the test system under study.

Table 5-3: Percentage of equipment requiring upgrades

Scenario	1-Ch5	2-Ch5	3-Ch5	4-Ch5	5-Ch5
Primary Feeder	0%	0%	0%	3.5%	0%
50 kVA transformers	0%	100%	57.45%	100%	100%
25 kVA transformers	0%	100%	67.74%	100%	100%

From Table 5-3, it is evident that the primary feeder can accommodate the increased demands of the medium-term scenarios without exceeding its rated capacity. However, in scenario 4-Ch5, PHEVs caused the first two main head-ends to exceed their nominal kVA ratings, and thus should be upgraded. As explained earlier, this problem is common in radial feeders; the feeder's first head-ends carry the entire circuit load and are overloaded more than remaining sections. In scenario 5-Ch5, PV

electricity comes into play and meets a portion of the demand locally, thus reducing the dependency on the main substation and alleviating the overloading of the first two main head-ends.

Due to their reduced diversity, secondary distribution transformers are found to be the components most influenced by increased PHEV penetration: all secondary distribution transformers are overloaded and should be upgraded during scenarios 2-Ch5 and 4-Ch5. However, in scenario 3-Ch5, PV arrays are able to alleviate the overloading of many of the impacted transformers in scenario 2-Ch5, thus reducing the number of transformers that require upgrading by 38%. This is not the case for the long-term projection (scenarios 4-Ch5 and 5-Ch5), as all secondary distribution transformers should be upgraded whether PV arrays are present in the system or not. These interesting findings can be explained by means of Table 5-4, which shows the peak demand of different distribution transformer classes during the different study scenarios.

Table 5-4: Peak demand of different distribution transformers (as a percentage of the transformer rating)

Scenario	1-Ch5	2-Ch5	3-Ch5	4-Ch5	5-Ch5
50 kVA transformers	94.4%	109.6%	103.2%	120.6%	109.8%
25 kVA transformers	96.8%	112.2%	104.7%	124.0%	112.5%

According to Table 5-4, PHEV charging demands cause the 50 kVA transformer class to exceed its rated capacity by approximately 9.6% and 20.6% (of the nominal rating) in scenarios 2-Ch5 and 4-Ch5. PV electricity, on the other hand, meets a portion of the demand locally and shaves the peak demand of the 50 kVA distribution transformers in scenarios 3-Ch5 and 5-Ch5 by 6.4% and 10.8% (of the nominal rating), respectively.

During the medium-term projection, although this peak-shaving is only minor (6.4%), it is still sufficient to alleviate the overloading of many of the impacted 50 kVA transformers, as PHEV charging demands caused these transformers to exceed their rated capacity by only a small percentage (9.6%). Nevertheless, this is not the case in the long-term projection, as the peak-shaving achieved by PV electricity (10.8%) is not able to meet the much larger increase in peak demand (20.6%) resulting from higher PHEV penetration. Similar results are obtained for 25 kVA distribution transformers.

5.3.4 Reverse Power Flow

Due to the weak chronological coincidence between the PV supply and PHEV charging demands, PV production may exceed the local demand at noontime, when PV arrays are generating their peak output. As a result, the direction of power flow is reversed, and power flows from the LV side to the MV side. Reverse power flow has several negative impacts on distribution networks [13, 14]. Thus, local distribution utilities usually impose limitations on the maximum allowable reverse flow of power in their networks. In Ontario, reverse power flow is limited to 60% of the transformer nominal rating [192].

The probabilistic indices for the reverse power flow are extracted using the same procedure outlined in previous sections. Table 5-5 shows the probability of occurrence of reverse power flow in different transformers, whereas Table 5-6 provides the corresponding maximum magnitude for this reverse flow of power as a percentage of the transformer rating (for the test system under study).

Table 5-5: Probability of the occurrence of reverse power flow

Scenario	1-Ch5	2-Ch5	3-Ch5	4-Ch5	5-Ch5
Substation transformer	0%	0%	0%	0%	14.88%
50 kVA transformers	0%	0%	5.6%	0%	20.49%
25 kVA transformers	0%	0%	6.17%	0%	20.59%

Table 5-6: Peak reverse power flow as a percentage of the transformer rating

Scenario	1-Ch5	2-Ch5	3-Ch5	4-Ch5	5-Ch5
Substation transformer	0%	0%	0%	0%	30%
50 kVA transformers	0%	0%	37.90%	0%	80.48%
25 kVA transformers	0%	0%	57.84%	0%	82.92%

Due to the presence of commercial loads in the system, the substation transformer does not experience high rates of reverse power flow. In scenario 3-Ch5, no reverse power flow is expected, whereas in scenario 5-Ch5, reverse power is restricted to only 30% of the substation transformer rating, which is within the acceptable limits. Secondary distribution transformers, on the other hand, experience higher rates of reverse power flow. In scenario 3-Ch5, the reverse flow of power through 25 kVA transformers may reach 57.84% of the transformer rating, which is still within the acceptable limits. However, this is not the case in scenario 5-Ch5, where the reverse flow of power may reach 82.92% of the transformer rating, thus violating the designated permissible limits.

`  `

5.3.5 System Voltages

As mentioned earlier, a major concern about PHEVs is the resulting under voltages at the end customers (120 V) during the heavy loading conditions occurring at peak charging periods. Utilities are also concerned about the over voltages occurring due to reverse power flow when PV arrays are generating their peak output. The probabilities of violating range-A voltage limits (114 V–126 V and 2340 V–2520 V for 120 V and 2400 V systems, respectively) at a variety of locations in the test system during different study scenarios was estimated using the probabilistic benchmark. The results are listed in Table 5-7.

Table 5-7: Probabilities of violating range-A voltage limits

Scenario	1-Ch5	2-Ch5	3-Ch5	4-Ch5	5-Ch5
At the end customer	0%	0%	0%	0.1%	0.1%
At the distribution transformers	0%	0%	0%	0.1%	0.1%
Along the primary feeder	0%	0%	0%	0.25%	0.3%

Results show that voltage regulators installed in the test network are capable of keeping voltages within range-A limits; the probability of violating these limits is 0.3% at worst (in scenario 5-Ch5). However, this is achieved at the expense of additional control actions, as will be seen in the next section. PV arrays have minimal impact on system voltages.

5.3.6 Number of Voltage Regulators Operations

The annual number of regulators actions in different scenarios is given in Table 5-8.

Table 5-8: Annual number of regulators actions

Scenario	1-Ch5	2-Ch5	3-Ch5	4-Ch5	5-Ch5
Regulators actions	16595	17725	19948	18515	28755

Results reveal that the total number of regulators actions depends on both PHEVs and PV electricity penetrations. In scenarios 2-Ch5 and 4-Ch5, PHEVs cause under voltages in the system during the peak charging period (early evening), thus increasing the number of regulators actions by 6.8% and 11.57% respectively. In scenarios 3-Ch5 and 5-Ch5, PV arrays cause over voltages during the peak production period (at noon), which necessitates a further increase in the number of regulators actions by 13.4% and 61.71%, respectively, to keep voltages within acceptable limits.

`  `

5.3.7 Total System Losses

The total annual active and reactive energy losses in the test system during different scenarios are depicted in Table 5-9.

Table 5-9: Total system losses

Scenario	1-Ch5	2-Ch5	3-Ch5	4-Ch5	5-Ch5
Annual active energy losses (MWh)	791.9	867.9	612.9	937.4	608.4
Annual reactive energy losses (MVARh)	1451.7	1583.9	1114.3	1704.8	1100.2

Results show that PHEVs increase the losses in the system due to the additional energy required to meet their charging demands. The active energy losses increase by 9.6% and 18.3% in scenarios 2-Ch5 and 4-Ch5, respectively, from the corresponding value in the base-case scenario. PV arrays, on the other hand, reduce the network losses as they bring power generation closer to load centers. The active losses in scenarios 2-Ch5 and 4-Ch5 are reduced by 29.3% and 35.1%, respectively, when PV arrays are added in scenarios 3-Ch5 and 5-Ch5. Similar results are obtained for the reactive energy losses.

5.4 Summary and Conclusions

In this chapter, the MC-based probabilistic benchmark previously developed in Chapter 4 is used to assess the aggregated impacts of PHEVs and PV electricity on residential distribution systems. The performed analysis confirmed the conclusion obtained in Chapter 4: secondary distribution transformer overloading is the bottleneck blocking the widespread adoption of PHEVs in the system under study. PV arrays, on the other hand, have the potential to meet a portion of PHEV charging demands and thus reduce the loading of different distribution system equipment. This reduction leads to a decrease in the number of distribution transformers that require upgrading in the medium-term projection. However, this is not the case for the long-term projection, as PV electricity is not able to meet the much increased demand resulting from higher PHEV penetrations. Thus, all secondary transformers should still be upgraded whether PV arrays are present in the system or not. Moreover, the obtained results showed that the negative impacts of PV electricity, such as reverse power flow that exceeds permissible limits, are substantial in the long-term projection. These findings are attributed to the weak chronological coincidence between PV array production and PHEV charging demands.

Another important conclusion made in this chapter is that the negative impacts of PHEVs and PV electricity on distribution networks are restricted to secondary networks only, with an insignificant impact on the primary system.

The challenge now for the electricity sector is to come up with solutions to facilitate the integration of PHEVs and PV electricity into the existing distribution infrastructure. In this thesis, the author is proposing two possible solutions: a traditional solution using ESSs, and a futuristic solution using a bilayer (AC-DC) distribution system architecture. These solutions are discussed in detail in the next two chapters.

` `

Chapter 6
Uncertainty-Based ESS Sizing and Scheduling for Improved Integration of PHEVs and PV Electricity in Residential Distribution Systems

6.1 Introduction

In the previous chapter, the author analyzed the aggregated impacts of PHEVs and PV electricity on residential distribution networks. The performed analysis showed that these technologies have adverse impacts on distribution networks in terms of secondary distribution transformer overloading (during PHEV peak charging periods) and increased reverse power flow (during PV peak production periods). Nevertheless, the obtained results showed that these impacts are restricted to secondary distribution networks only, with an insignificant impact on the primary system.

ESSs are thought to be an effective tool for mitigating these negative effects. The primary challenge in implementing ESS technology in distribution networks lies in the difficulty of determining appropriate sizes and operating schedules for these units, given the uncertainties inherent in the PV array production, existing electrical loads and the PHEV charging demand.

This chapter presents a probabilistic sizing and scheduling methodology for ESSs taking into account the different sources of uncertainty in the system. The technical and economic feasibility of the proposed design methodology is validated using the previously developed MC-based probabilistic benchmark.

The remainder of the chapter is organized as follows: Section 6.2 presents the main idea underlying the research presented in this chapter; Section 6.3 outlines the proposed operation of the ESS; Section 6.4 describes different stages of the probabilistic methodology used to size and schedule the operation of the proposed ESS; Section 6.5 presents the case study used to validate the proposed design methodology; Section 6.6 presents the simulation results for a range of scenarios; and finally, Section 6.7 summarizes the conclusions.

6.2 Using ESSs to Mitigate the Impacts of PHEVs and PV Electricity on Distribution Systems

A large and growing body of literature has investigated the possible use of ESSs to reduce the adverse impacts of PV generation on distribution systems. For example, the authors of [193] suggested using BESSs in public LV networks as a means of deferring the upgrades needed in order to increase the penetration of PV electricity. In another paper [194], a methodology was proposed in order to determine the appropriate size of a BESS used in a grid-connected PV system for the purpose of power arbitrage and peak shaving. Reference [195] describes a number of operation and control strategies for a grid-connected BESS designed to reduce the negative impacts of PV generation on distribution networks and to improve overall system efficiency. Similarly, the use of ESSs to facilitate PHEV integration has also been addressed in several investigations: the findings reported in [196] shows that integrating ESSs into distribution networks can mitigate the negative impacts of the uncertainties associated with PHEV charging, thus increasing PHEV aggregators' revenue by up to 7.8%. Another study [197] suggested using PHEV battery switch stations as a countermeasure to offset the surplus electricity produced by centralized PV plants. The results confirmed the economic feasibility of the proposed charging methodology; however, a significant limitation is that it can be applied only to centralized PV stations.

The main concept underlying the research presented in this chapter is to use ESSs to mitigate the aggregated impacts of both PV electricity and PHEVs when these two technologies operate in conjunction. This goal can be achieved by increasing the synergy between PV electricity and PHEVs. PV electricity generated during low demand periods, when reverse power flow is most likely to occur, is stored in small-scale dispersed ESSs located at secondary distribution transformers. Thereafter, this energy is then reused to meet part of the PHEV charging demand during peak demand periods when this demand is likely to overload distribution transformers, thus metaphorically killing two birds with one stone. However, determining the appropriate sizes and operating schedules of the proposed ESS such as to continuously have sufficient energy and power capacities to accommodate the surplus PV electricity (during peak production periods), and to supply the deficit in power (during PHEVs peak charging periods) is a very difficult task due to the uncertainties associated with the PV array output, existing electrical loads and the PHEV charging demand.

In this context, it is worth mentioning that the ESS sizing problem has been addressed in several investigations [198-201] for different power systems applications through the use of a variety of

optimization techniques (such as dynamic programming, genetic algorithms, etc). The primary drawback of these techniques, however, is that they fail to include consideration of the stochastic nature of supply and demand. These techniques are also predicated on prior knowledge of load and generation levels, which is usually infeasible. In this respect, a significant contribution of the work presented in this chapter is the development of a MC-based probabilistic method that can determine the appropriate sizes and operating schedules of the proposed ESSs, taking into account the above uncertainties.

6.3 Proposed Operation of the ESS

This section provides a brief description of the proposed operation of the ESS.

6.3.1 Proposed ESS Technology

Several types of ESSs are currently commercially available, including BESSs, SMESSs, super capacitors, and flywheels. Storage technologies such as SMESSs, super capacitors, and flywheels are characterized by their high energy cost ($/kWh) and so are used primarily for high power, short duration applications [5, 202]. Storage technologies that are best suited for distribution system applications are long-term storage technologies such as BESSs [192, 202]. The author therefore selected BESSs for the application at hand. The following variants of BESSs were considered: lead-acid (LA), valve-regulated lead-acid (VRLA), sodium sulfur (NA/S), zinc bromine (Zn/Br), and vanadium redox (VB) batteries. In a subsequent section, the author will estimate the cost of integrating different variants of BESSs to select the most economical option.

6.3.2 Location of the Proposed BESS

In the research presented in this chapter, BESSs are used to alleviate secondary distribution transformer overloading during PHEV peak charging periods and to limit the reverse flow of power when PV arrays are generating their peak output. These requisites suggest that the BESS should be able to supply part of the demand connected to the secondary distribution transformer locally (i.e., from the LV network) and also to absorb excess PV generation and prevent its escalation to the MV network. These two considerations make it clear that the storage device must be placed downstream from the secondary distribution transformer (i.e., at the transformer LV bus), as shown in Figure 6-1.

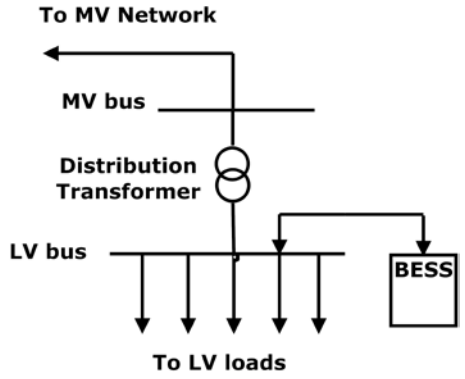

Figure 6-1: Location of the proposed BESSs

6.3.3 BESS Operating States

A BESS is basically a device that can be programmed to either discharge or charge active/reactive power within its energy (kWh) and power (kVA) ratings. The integrated bidirectional inverter controls these charging/discharging operations. A BESS can discharge active power as long as its stored energy level is greater than a minimum threshold called the basic reserve level; it can be charged with active power as long as the stored energy level is less than the device's kWh rating. A BESS can also generate or consume reactive power within its inverter's kVA capacity [203, 204]; however, the stored energy level is impacted only by the active power flow in/out of the device. BESSs can thus operate in one of three states: charging, discharging, or idling, which are associated with charging, discharging, and idling losses, respectively. Charging and discharging losses are dependent on the efficiency of the device, while idling losses correspond to the power consumed in ancillary components and internal controls and are usually represented as a percentage of the inverter's kVA rating. In this research, these losses are taken as 1% of the inverter rating as per [203, 204]. The following sections explain the proposed operation of the BESS during these different states:

6.3.3.1 Charging state

In this research, a BESS operates in the charging state when PV arrays generate their peak output and surplus production is in effect. Reverse power is thus flowing through the secondary distribution transformer. The BESS stores the excess active power so that the reverse flow of power through the transformer is limited to a predefined threshold determined by utility regulations. For example, in Ontario, reverse power flow is restricted to 60% of the transformer rating [192]. The excess theoretical active power that should be charged into the BESS in this case equals:

`  `

$$P_{Ch}(i) = Max\,(-60\% S_{Trans\ Rated} - P_{Loads,AC}(i)\ ,\ 0) \tag{6.1}$$

where $P_{Ch}(i)$ is the theoretical active power charged into the BESS at hour i, $S_{Trans\ Rated}$ is the transformer kVA rating, and $P_{Loads,AC}(i)$ is the active power consumed by electrical loads connected to the secondary distribution transformer at hour i. The negative sign in Eq. (6.1) denotes that the active power is flowing in the reverse direction (from the LV to the MV network).

However, the actual power that can be charged into the BESS in one hour is constrained by its power and energy ratings; thus, the previous expression is modified to:

$$P_{Ch,Act}(i) = Min\,(P_{Ch}(i), S_{BESS\ Rated}, \frac{E_{BESS\ Rated} - E(i-1)}{\eta_{Ch}}) \tag{6.2}$$

where $P_{Ch,Act}(i)$ is the actual power charged into the BESS at hour i, $S_{BESS\ Rated}$ is the power rating of the BESS in kVA, $E_{BESS\ Rated}$ is the energy rating of the BESS in kWh, $E(i\ -1)$ is the energy level stored in the BESS at hour (i- *1*) in kWh, and η_{Ch} is the BESS charging efficiency.

The charging losses ($Loss_{Ch}(i)$) in kW are given by:

$$Loss_{Ch}(i) = P_{Ch,Act}(i) \times (1 - \eta_{Ch}) \tag{6.3}$$

The stored energy level in the BESS after operating in this state for one hour ($E(i)$) is given by:

$$E(i) = E(i-1) + (P_{Ch,Act}(i) \times \eta_{Ch} \times 1h) \tag{6.4}$$

The reactive power flow for this state is zero.

6.3.3.2 Discharging State

In this research, a BESS operates in the discharging state when the secondary distribution transformer becomes overloaded due to PHEV charging demands. The BESS thus injects both active and reactive power in order to alleviate transformer overloading. However, infinite combinations of the active and reactive power can be injected to achieve this goal. For this work, the author derived expressions for these combinations that consume minimum power (kVA) or minimum energy (kWh) from the BESS,

resulting in two possible discharging states, namely power and energy-saving states. The cost of BESSs operating in both states will be evaluated and compared in a subsequent section.

6.3.3.2.1 Power-Saving State

In this state, the BESS operates to alleviate transformer overloading using minimum power (kVA).

Assume that at a given hour *i*, the distribution transformer AC loads are drawing $P_{Load,ACs}(i)$ (kW), $Q_{Loads,AC}(i)$ (kVAR), and $S_{Load,ACs}(i)$ (kVA) at a power factor of $cos\varphi(i)$. The distribution transformer is supplying $P_{Trans}(i)$ (kW), $Q_{Trans}(i)$ (kVAR), and $S_{Trans}(i)$ (kVA) at a power factor of $cos\theta(i)$. The BESS must supply the deficit $P_{Dis}(i)$ (kW), $Q_{Dis}(i)$ (kVAR), and $S_{Dis}(i)$ (kVA), as follows:

$$S_{Dis}^2(i) = P_{Dis}^2(i) + Q_{Dis}^2(i) = (P_{Loads,AC}(i) - P_{Trans}(i))^2 + (Q_{Loads,AC}(i) - Q_{Trans}(i))^2 \quad (6.5)$$

The previous expression can be rewritten as:

$$\begin{aligned} S_{Dis}^2(i) = {} & (S_{Loads,AC}(i)\cos\phi(i) - S_{Trans}(i)\cos\theta(i))^2 \\ & + (S_{Loads,AC}(i)\sin\phi(i) - S_{Trans}(i)\sin\theta(i))^2 \end{aligned} \quad (6.6)$$

Eq. (6.6) can be further expanded into:

$$\begin{aligned} S_{Dis}^2(i) = {} & S_{Loads,AC}^2(i) - 2S_{Loads,AC}(i)S_{Trans}(i)\cos\phi(i)\cos\theta(i) \\ & - 2S_{Loads,AC}(i)S_{Trans}(i)\sin\phi(i)\sin\theta(i) + S_{Trans}^2(i) \end{aligned} \quad (6.7)$$

To find the theoretical $P_{Dis}(i)$ and $Q_{Dis}(i)$ combination that will mitigate transformer overloading while consuming the minimum $S_{Dis}(i)$, the expression in Eq. (6.7) is differentiated with respect to the controlled variable ($\theta(i)$), and the derivative is equated to zero:

$$\begin{aligned} 2S_{Dis}(i) \times \frac{\partial S_{Dis}(i)}{\partial\theta} = {} & 2S_{Loads,AC}(i)\, S_{Trans}(i)\, \cos\phi(i)\, \sin\theta(i) \\ & - 2S_{Loads,AC}(i)\, S_{Trans}(i)\, \sin\phi(i)\, \cos\theta(i) \end{aligned} \quad (6.8)$$

Solving the previous equation yields:

$$\tan\phi(i) = \tan\theta(i) \quad (6.9)$$

` `

In other words, the transformer must operate at the same power factor as the load. Thus, $P_{Dis}(i)$ and $Q_{Dis}(i)$ equal:

$$P_{Dis}(i) = Max(P_{Loads,AC}(i) - S_{Trans\,Rated} \times \cos\phi(i), 0) \quad (6.10)$$

$$Q_{Dis}(i) = Max(Q_{Loads,AC}(i) - S_{Trans\,Rated} \times \sin\phi(i), 0) \quad (6.11)$$

However, the actual active and reactive powers that can be discharged by the BESS at hour *i* are limited by its power and energy ratings as well as by the minimum reserve level ($E_{BESS\ Reserve}$), as follows:

$$P_{Dis,Act}(i) = Min(P_{Dis}(i), S_{BESS\,Rated} \times \eta_{Dis}, (E(i-1) - E_{BESS\,Reserve}) \times \eta_{Dis}) \quad (6.12)$$

$$Q_{Dis,Act}(i) = Min(Q_{Dis}(i), \sqrt{S^2_{BESS\,Rated} - \frac{P^2_{Dis,Act}(i)}{\eta_{Dis}^{\,2}}}) \quad (6.13)$$

where η_{Dis} is the BESS discharging efficiency, $P_{Dis,Act}(i)$ and $Q_{Dis,Act}(i)$ are the actual active and reactive power discharged by the BESS at hour *i*, respectively.

The discharging losses ($Loss_{Dis}(i)$) in kW are given by:

$$Loss_{Dis}(i) = P_{Dis,Act}(i) \times (\frac{1-\eta_{Dis}}{\eta_{Dis}}) \quad (6.14)$$

The level of stored energy in the BESS after operation in this state for one hour ($E(i)$) is given by:

$$E(i) = E(i-1) - (\frac{P_{Dis,Act}(i)}{\eta_{Dis}} \times 1h) \quad (6.15)$$

6.3.3.2.2 Energy-Saving State

In the energy-saving state, the BESS operates to alleviate transformer overloading using minimum energy (kWh). It is intuitively clear that the transformer must supply as much active power as possible. Two scenarios are possible:

i) The load active power is less than the transformer rating ($P_{Loads,\,Ac}(i) < S_{Trans\,Rated}$): In this case, the transformer will supply all of the active power requirements, and therefore:

$$P_{Dis}(i) = 0 \tag{6.16}$$

The remaining transformer capacity will be used to supply the reactive power, as follows:

$$Q_{Trans}(i) = \sqrt{S^2_{Trans\ Rated} - P^2_{Loads,AC}(i)} \tag{6.17}$$

The reactive power deficit is then supplied by the BESS:

$$Q_{Dis}(i) = Max\,(Q_{Loads,AC}(i) - Q_{Trans}(i), 0) \tag{6.18}$$

However, the actual reactive power that can be supplied by the BESS is limited by its inverter kVA capacity; thus, the previous equation is modified to:

$$Q_{Dis,Actual}(i) = Min(Q_{Dis}(i), S_{BESS\ Rated}) \tag{6.19}$$

The discharging losses in the BESS in this state are equal to the idling losses (taken as 1% of the BESS inverter rating [203, 204]) given by:

$$Loss_{Dis}(i) = 1\% \times S_{BESS\ Rated} \tag{6.20}$$

The level of kWh energy in the BESS after operation in this state for one hour (*E(i)*) equals:

$$E(i) = E(i-1) - (1\% \times S_{BESS\ Rated} \times 1h) \tag{6.21}$$

ii) The load active power is greater than the transformer rating ($P_{Loads,\ Ac}(i) > S_{Trans\ Rated}$): In this case, the transformer capacity will be fully utilized to supply the active power requirements (unity power factor operation), and the BESS supplies the active power deficit together with all the reactive power requirements:

$$P_{Dis}(i) = Max\,(P_{Loads,AC}(i) - S_{Trans\ Rated}) \tag{6.22}$$

$$Q_{Dis}(i) = Q_{Loads,AC}(i) \tag{6.23}$$

To account for energy and power rating constraints, the expressions in (6.22) and (6.23) are modified to (6.12) and (6.13), respectively. For this state of operation, the discharging losses

($Loss_{Dis}(i)$) are given by Eq. (6.14), and the level of kWh energy in the BESS after operation in this state for one hour ($E(i)$) is given by Eq. (6.15).

6.3.3.3 Idling State

In the idling state of operation, the BESS neither consumes nor produces any active power. The only losses incurred in the device are the idling losses ($Loss_{Idling}(i)$), given by:

$$Loss_{Idling}(i) = 1\% \times S_{BESS\ Rated} \tag{6.24}$$

The level of kWh energy in the BESS after operation in this state for one hour ($E(i)$) is given by:

$$E(i) = E(i-1) - (Loss_{Idling}(i) \times 1h) \tag{6.25}$$

However, as explained earlier, determining the appropriate sizes and operating schedules of the proposed ESS such as to continuously have sufficient energy and power capacities to accommodate the surplus PV electricity (during peak production periods), and to supply the deficit in power (during PHEVs peak charging periods) is a very difficult task due to the different uncertainties inherent in the system. In the following section, the author is proposing a probabilistic method that can determine the appropriate sizes and operating schedules of the proposed ESSs, taking into account these different uncertainties.

6.4 Probabilistic Sizing and Scheduling Methodology for the Proposed BESS

This section describes the probabilistic methodology used for sizing and scheduling the operation of the proposed BESS.

6.4.1 Modeling Uncertainties Present in the System

To account for the stochastic nature of the problem at hand, it is first necessary to develop appropriate probabilistic models for the various uncertainties inherent in the system. To model the stochastic nature of PV array output, hourly insolation and temperature data provided by the Solar Radiation Research Laboratory are processed using the PV modeling approach presented in Section 3.2. This approach uses PCA and data clustering to produce 19 daily output profiles (depicted in Figure 3-7) that represent the stochastic nature of the variable PV supply while retaining the temporal variations

within the data. The probabilities of occurrence of different output profiles are then computed and used to develop the cdf depicted in Figure 3-9. The resulting cdf is used later in the random generation of PV output profiles.

To model the stochastic nature of existing residential loads, the daily load profiles provided in [156] are processed using the load modeling approach described in Section 3.3, which represents the stochastic nature of residential loads using only six daily profiles (depicted in Figure 3-11) rather than 365. The probabilities of the occurrence of different profiles are computed and used to develop the cdf depicted in Figure 3-13. The resulting cdf is subsequently used for the generation of random loading profiles in the MC simulation. Because commercial loads are characterized by low variability in electrical demand [171], they are represented using only one load curve (depicted in Figure 4-1).

To model individual driving habits that impact PHEV charging, the author adopted the approach described in Section 3.4. Data for 1,048,576 people and 309,164 vehicles provided by the 2009 U.S. NHTS are processed in order to extract cdfs representing daily mileage and home arrival times. These cdfs (given in Figures 3-16 and 3-17) are then employed in the random generation of PHEV charging profiles.

To model uncertainties related to PHEV type, three types of vehicles were considered: automobiles, vans, and SUVs. To date, no data are available with respect to the market share of different types of PHEVs. These types were thus assumed to have the same current market share as that reported in the 2009 NHTS for their gasoline counterparts. For each type, a representative PHEV was selected: the Chevrolet Volt for automobiles, Volvo V70 for vans, and Ford Escape for SUVs.

6.4.2 Running the MC Simulation

The MC simulation procedure starts with the generation of random output profiles for different stochastic quantities present in the system. Random PV output profiles (from the predetermined 19 representative segments) are sampled based on the previously developed cdf. Since all PV arrays are within the same residential area, all are subject to the same environmental conditions, and all are assigned the same daily output profile. The load modeling approaches explained previously are then used to generate random loading profiles for different system loads (residential and commercial). The final step is to use the cdfs derived earlier for the modeling of individual driving habits in order to generate random PHEV charging profiles. The *SOC* of the battery when the PHEV arrives home, and hence the energy required to charge the battery, depends on the random daily distance travelled.

Because drivers are most likely to plug in their vehicles as soon as they arrive home, the random home arrival time is taken to be the charging start time [157, 167, 180]. The duration required to charge the battery is dependent on the charging level. As mentioned earlier, SAE J1772 standard defines two residential AC single phase charging levels for PHEVs: level-1 and level-2 chargers (described in Table 4-2). The analysis performed in Chapter 4 demonstrated that level-2 chargers have a more severe impact on distribution networks than do level-1 chargers. For this reason, the author has assumed the worst case scenario, in which all PHEVs are charged by level-2 chargers. Establishing the charging start time, the power rating of the charger, and the required charging duration enables a sufficiently accurate determination of the charging profile for each PHEV using the methodology explained in Section 4.4.3.

The three electrical quantities obtained using the previous models (PHEV charging demands, PV array supplied power, and existing load demands) are aggregated for each household to form the inputs to the OpenDSS software used in this research to perform the load flow calculations. This procedure is executed 365 times every year and is repeated for several thousands of years until the stopping criterion given in Eq. (4.4) is fulfilled. The resulting electrical quantities (power flows, voltages, losses, etc.) for each year are calculated using OpenDSS and stored for future processing.

6.4.3 BESS Sizing

In this section, the author is presenting different stages of the proposed sizing methodology. A flowchart of the proposed methodology is depicted in Figure 6-2.

6.4.3.1 Determining Daily Charging/Discharging Periods

The initial task of the proposed methodology is the running of the MC simulation for the test system without the inclusion of any BESSs until the convergence criterion is fulfilled. Based on the MC results, each day is divided into three periods:

i) The controlled charging/discharging period: In this period (usually around late night) , the probability of overloading the distribution transformer as well as the probability of the occurrence of excessive reverse power flow through it (in excess of 60% of its rating) is less that 5% (corresponding to a 95% confidence level). The BESS can thus operate in any of the three operating states in order to regulate the BESS energy level to a specific pre-designated level. The energy level at the end of this period is denoted by E_1.

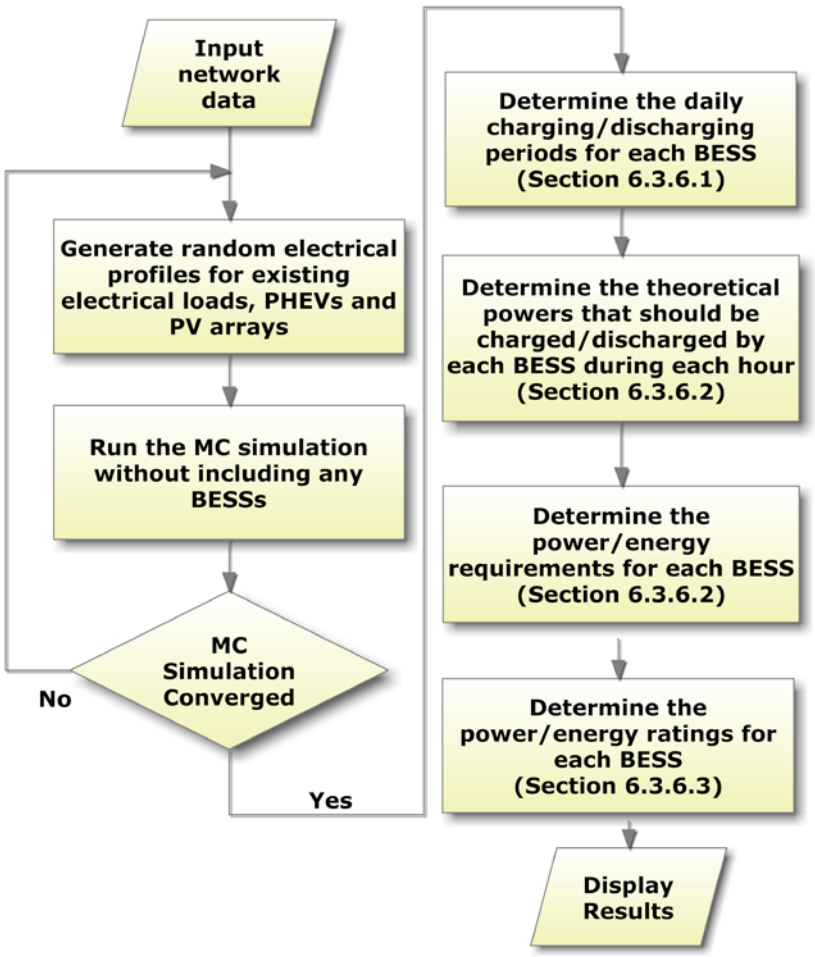

Figure 6-2: BESS probabilistic sizing methodology

ii) The forced charging period: In this period: In this period (usually around noontime), the probability of the occurrence of reverse power flow (in excess of 60% of the transformer rating) is more than 5%, and the probability of overloading the secondary distribution transformer is less than 5%; thus, the distribution transformer is likely to be subject to reverse power flow (with a 95% confidence level). The energy level at the end of this period is denoted by E_2.

iii) The forced discharging period: This period (usually around evening) is characterized by conditions that are the exact opposite of those that occur during the previous period: the probability of overloading the secondary distribution transformer is more than 5%, and the probability of the occurrence of reverse power flow in excess of 60% of its rating is less than 5%. The distribution transformer is thus highly likely to become overloaded (with a 95% confidence level). The energy level at the end of this period is denoted by E_3.

`  `

6.4.3.2 Determining Energy and Power Requirements

After the definition of these three periods, equations (6.1), (6.10), (6.11), (6.16), (6.18), (6.22), and (6.23) are applied in order to determine the theoretical active and reactive powers that should be charged/discharged by the BESS during each hour of the day throughout the whole simulation period to mitigate distribution transformer overloading and limit the reverse flow of power through the transformer so that it is kept within permissible limits. In this stage, the kWh and kVA rating constraints of the BESS are not considered. After the charging/discharging powers have been established, four important quantities are estimated:

i) Theoretical daily charged energy (E_{Ch}): The summation of the amounts of active power charged into the BESS throughout the day.

ii) Theoretical daily discharged energy (E_{Dis}): The summation of the amounts of active power discharged by the BESS throughout the day. This quantity is calculated for each of the two discharging states.

iii) Theoretical hourly inverter charging rating ($S_{Ch}(i)$): This quantity is calculated for the hours during which the BESS operates in the charging state. Since the reactive power flow in this state is zero, the designated charging rating for a given hour equals the active power charged into the BESS during this hour.

iv) Theoretical hourly inverter discharging rating ($S_{Dis}(i)$): This quantity is calculated twice (once for each of the two discharging states) for the hours during which the BESS operates in the discharging state:

$$S_{Dis}(i) = \sqrt{(\frac{P_{Dis}(i)}{\eta_{Dis}})^2 + Q_{Dis}^2(i)} \tag{6.26}$$

The probabilistic analysis then continues with the calculation of the cfd curves for the previous four quantities. Figure 6-3 depicts a sample cfd. The developed cfds are used to estimate the following:

i) Maximum daily charged energy with 95% confidence ($E_{Ch}^{\max}$): This quantity is defined as the energy corresponding to a 95% probability on the daily charged energy cfd curve for the BESS. This definition implies that there is only a 5% probability of charging an amount of daily energy that exceeds this value, or in other words, the designated energy is the maximum daily charged energy with 95% confidence.

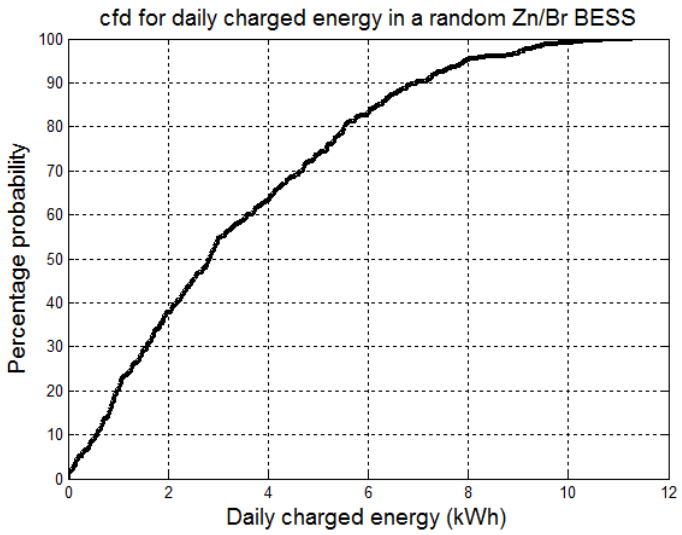

Figure 6-3: cfd for daily charged energy in a Zn/Br BESS connected to the first 25 kVA distribution transformer

For the BESS whose cfd is depicted in Figure 6-3, this quantity equals 8.04 kWh.

ii) Minimum daily charged energy with 95% confidence ($E_{Ch}^{\min}$): This quantity is the energy corresponding to a 5% probability on the daily charged energy cfd curve, implying that the designated energy is the minimum daily charged energy with 95% confidence.

iii) Maximum charging kVA with 95% confidence ($S_{Ch}^{\max}$): This quantity is the kVA corresponding to a 95% probability on the hourly inverter charging rating cfd curve and is used for determining the inverter rating required during the charging process.

iv) Maximum daily discharged energy with 95% confidence ($E_{Dis}^{\max}$): This quantity is the energy corresponding to a 95% probability on the daily discharged energy cfd curve and is calculated for each of the two discharging states.

v) Minimum daily discharged energy with 95% confidence ($E_{Dis}^{\min}$): This quantity is the energy corresponding to a 5% probability on the daily discharged energy cfd curve, implying that the designated energy is the minimum daily discharged energy with 95% confidence.

` `

vi) Maximum discharging kVA with 95% confidence ($S_{Dis}^{\max}$): This quantity is the kVA corresponding to a 95% probability level on the hourly inverter discharging rating cfd curve and is used to determine the inverter kVA rating required during the discharging process.

6.4.3.3 Determining the BESS Energy and Power Ratings

The previous six quantities are then used for estimating the energy and power ratings of the BESS such as to accommodate the surplus electricity generated by PV arrays during peak production periods, and to supply the deficit in power required to meet PHEV uncontrolled charging demands during peak charging periods.

To meet these objectives, two scenarios are possible:

i) Minimum daily charged energy is less than the maximum daily discharged energy ($E_{Ch}^{\min} < E_{Dis}^{\max}$): In order to cover all possibilities within this scenario, the two most extreme cases are analyzed:

- The BESS is charged by $E_{Ch}^{\min}$ and discharges $E_{Dis}^{\max}$: This situation enables a determination of the energy to be charged/discharged during the controlled charging/discharging period. In this case, the BESS should have sufficient energy at the beginning of the day to allow it to discharge $E_{Dis}^{\max}$ (in the forced discharging period) after being charged only by $E_{Ch}^{\min}$ (in the forced charging period) while keeping the level of stored energy above the minimum allowable reserve level ($E_{BESS\ Reserve}$). This requisite necessitates that the charging/discharging process during the controlled charging/discharging period is controlled such that the energy level at the end of this period (E_1) is at least:

$$E_1 = E_{BESS\,\mathrm{Re}serve} + E_{Dis}^{\max} - E_{Ch}^{\min} \tag{6.27}$$

- The BESS is charged by $E_{Ch}^{\max}$ and discharges $E_{Dis}^{\min}$: This situation enables the energy rating of the BESS to be established. In this case, the maximum energy level in the BESS occurs at the end of the forced charging period (E_2). The BESS energy rating is therefore selected so that it can be charged by $E_{Ch}^{\max}$ (in the forced charging period) without exceeding its energy rating. This criterion is met if the BESS has an energy rating of:

$$E_{BESS\ Rated} = E_1 + E_{Ch}^{\max} \tag{6.28}$$

Substituting E_1 from Eq. (6.27) into the previous equation yields:

$$E_{BESS\ Rated} = E_{Ch}^{\max} + E_{BESS\,\mathrm{Re}serve} + E_{Dis}^{\max} - E_{Ch}^{\min} \tag{6.29}$$

ii) Minimum daily charged energy is greater than the maximum daily discharged energy ($E_{Ch}^{\min} > E_{Dis}^{\max}$): As with the previous scenario, the two most extreme cases are examined:

- The BESS is charged by $E_{Ch}^{\min}$ and discharges $E_{Dis}^{\max}$: The amount of energy to be charged/discharged in the controlled charging/discharging period should be regulated such that the BESS can supply $E_{Dis}^{\max}$ after being charged only by $E_{Ch}^{\min}$ while keeping the level of stored energy above the minimum allowable reserve. To reach that target, the energy level at the end of this period (E_1) should be at least:

$$E_1 = E_{BESS\,\mathrm{Re}serve} \tag{6.30}$$

- The BESS is charged by $E_{Ch}^{\max}$ and discharges $E_{Dis}^{\min}$: This situation enables the determination of the energy rating of the BESS. In this case, the maximum energy level in the BESS occurs at the end of the forced charging period (E_2).

  Accordingly, the energy rating of the BESS should be at least:

$$E_{BESS\,Rated} = E_1 + E_{Ch}^{\max} \tag{6.31}$$

  Substituting E_1 from Eq. (6.30) into the previous equation yields:

$$E_{BESS\,Rated} = E_{BESS\,\mathrm{Re}serve} + E_{Ch}^{\max} \tag{6.32}$$

The sizing algorithm presented above ensures that the energy stored in the BESS throughout the day satisfies the following:

$$E_{BESS\,\mathrm{Re}serve} \le E(i) \le E_{BESS\,Rated} \tag{6.33}$$

` `

The kVA power rating of the BESS for all previous scenarios is determined based on $S_{Ch}^{\max}$ and $S_{Dis}^{\max}$, as follows:

$$S_{BESS\,Rated} = Max(S_{Ch}^{\max}, S_{Dis}^{\max}) \tag{6.34}$$

A final factor is that the BESSs are assumed to have power and energy ratings that are multiples of 5 kVA and 5 kWh, respectively. The ratings obtained are thus rounded to the next available rating.

6.4.4 BESS Scheduling

Based on the previous section, the operation of the BESS during the three charging/discharging periods is scheduled according to Figure 6-4:

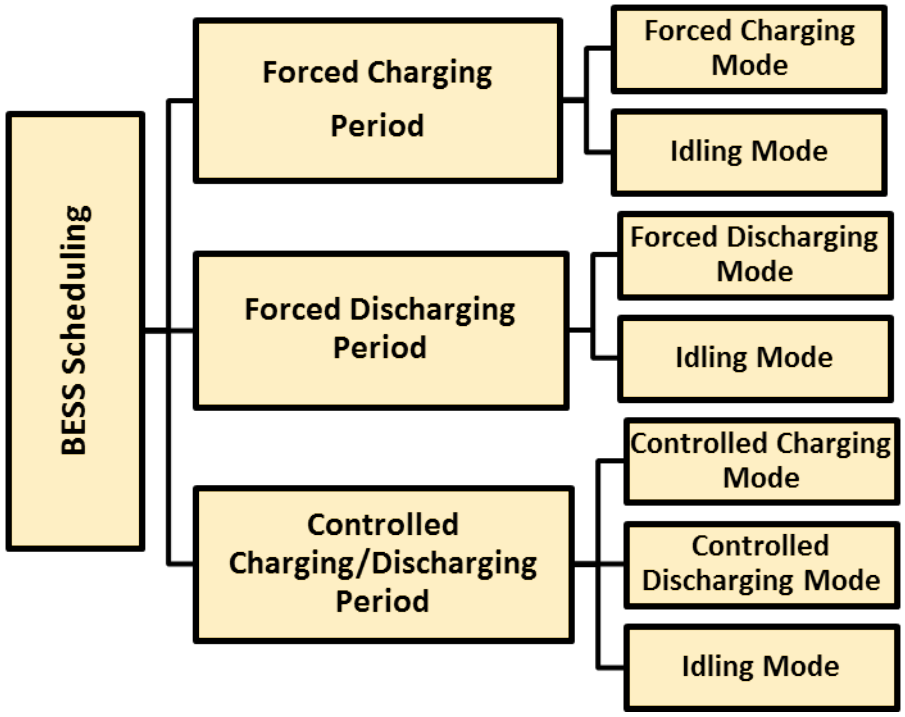

Figure 6-4: BESS Scheduling

`  `

6.4.4.1 Forced Charging Mode

This mode of operation occurs in the forced charging period when the reverse flow of power exceeds 60% of the transformer rating. Equations (6.2), (6.3), and (6.4) describe this mode of operation.

6.4.4.2 Forced Discharging Mode

This mode of operation occurs in the forced discharging period when the power supplied by the transformer exceeds its kVA rating. In this case, the BESS aims to limit transformer overloading by injecting the optimum combination of active and reactive power. The BESS operation during such a period is given by equations (6.12), (6.13), (6.14), and (6.15) for the power-saving state and by (6.16) plus (6.19) to (6.23) for the energy-saving state.

6.4.4.3 Controlled Charging/Discharging Mode

This mode of operation occurs in the controlled charging/discharging period. In this case, the charging controller operates so that the energy stored in the BESS is regulated at the previously determined E_1 levels. To achieve this target quickly, the entire inverter rating is utilized to charge/discharge active power only, and accordingly, the reactive power flow in this mode of operation is zero. The following two cases are considered:

i) Energy level in the BESS is less than E_1: In this case, the BESS operates in the controlled charging mode, storing active power so that the stored energy reaches the desired E_1 level:

$$P_{Ch,Act}(i) = Min\left(\frac{E_1 - E(i)}{\eta_{Ch}}, S_{BESS\ Rated}, \sqrt{S^2_{Trans\ Rated} - Q^2_{Loads,AC}(i)} - P_{Loads,AC}(i)\right) \quad (6.35)$$

The charging losses ($Loss_{Ch}(i)$) and the kWh energy level after operation in this mode for one hour ($E(i)$) are given by equations (6.3) and (6.4), respectively.

ii) Energy stored in the BESS is greater than E_1: In this case, the BESS operates in the controlled discharging mode, injecting active power so that stored energy reaches the desired E_1 level. However, the power injected by the BESS must not result in a reverse flow of power through the distribution transformer in excess of 60% of its rating. The active power discharged by the BESS in this mode of operation is given as:

$$P_{Dis,Actual}(i) = Min\left((E(i) - E_1) \times \eta_{Dis}, S_{BESS\ Rated} \times \eta_{Dis}, P_{Loads,AC}(i) + 60\% S_{Trans\ Rated}\right) \quad (6.36)$$

` `

The discharging losses ($Loss_{Dis}(i)$) and the kWh energy level after operation in this mode for one hour ($E(i)$) are given by equations (6.14) and (6.15), respectively.

6.4.4.4 Idling Mode

If the conditions for any of the previous modes of operation have not been met, the BESS operates in the idling mode. Equations (6.24) and (6.25) describe this mode of operation.

6.5 Case Study

This section outlines the case study used to validate the proposed design methodology.

6.5.1 Description of the Test System

For this chapter, the author adopts the same test system previously described in Sections 4.4.1 and 5.2.2. As explained earlier, this system is an expanded version of the IEEE 123 node test, in which each existing 22.36 kVA spot load has been expanded into a 25 kVA distribution transformer that supplies 5 households, and each 44.72 kVA spot load has been expanded into a 50 kVA distribution transformer that feeds 10 households. The system thus has a total of 625 residential customers. As explained earlier, each secondary distribution transformer should be equipped with a BESS that is connected to the transformer LV bus. Accordingly, the test system will have a total of 78 BESSs. Secondary distribution circuits were modeled based on practical data provided by a power utility in Ontario, Canada. Based on the same practical data, each household peak demand was taken to be 6.2 kVA, which is close to the findings reported in [175]. The remaining 13 spot loads are assumed to be commercial loads serving the residential area. The system was modeled using OpenDSS from the substation down to the customer meter, resulting in a system with 1684 nodes.

6.5.2 Study Assumptions and Scenarios

In this chapter, and similar to the assumptions adopted in Section 5.2.3, two penetration levels are assumed for PHEVs, based on the results presented in [101, 184]: short-term projection (2031 case) with 28% penetration and long-term projection (2052 case) with 52% penetration. PHEVs are assigned randomly to the end customers maintaining the percentage of each vehicle type. A further assumption is that each household with a PHEV is equipped with a 10 kW PV array (maximum allowable size for small-scale generation in Ontario). The rationales behind these assumptions are

explained in detail in Section 5.2.3.2 and 5.2.3.3. Finally, the basic reserve level ($E_{BESS\ Reserve}$) for BESS is taken as 30% of their rated kWh [201].

The aim of this chapter is to use BESSs to mitigate the aggregated impact of PV electricity and PHEVs. The author chose five study scenarios that would reflect different operational situations for both short- and long-term projections. The scenarios studied are shown in Table 6-1.

Table 6-1: Study scenarios

	Time frame	PHEV penetration	PV arrays	BESS Included
Scenario 1-Ch6	Base-case	0%	N/A	No
Scenario 2-Ch6	2031	28%	10 kW/PHEV	No
Scenario 3-Ch6	2031	28%	10 kW/PHEV	Yes
Scenario 4-Ch6	2052	52%	10 kW/PHEV	No
Scenario 5-Ch6	2052	52%	10 kW/PHEV	Yes

In comparing Tables 6-1 and 5-1, it becomes evident that scenarios 1-Ch5, 3-Ch5 and 5-Ch5 are the same as scenarios 1-Ch6, 2-Ch6 and 4-Ch6, respectively.

The MC simulation procedure (described in Section 6.4.2) is executed initially for scenarios 2-Ch6 and 4-Ch6. Based on the MC simulation results, the probabilistic sizing methodology (explained in Section 6.4.3) is used to determine the energy and power ratings for each of the 78 BESSs present in the system in scenarios 3-Ch6 and 5-Ch6. The same MC simulation is then executed again for the test system after the inclusion of the proposed 78 BESSs.

6.6 Results and Discussion

In this section, the costs of integrating different types of BESSs technologies are evaluated such as to select the most economical option. After that, the author analyzes the technical merit of the proposed BESS design methodology.

6.6.1 Selecting the Most Economical BESS Technology

The previously explained BESS sizing methodology is used to determine the energy and power ratings for each anticipated BESS, for scenarios 3-Ch6 and 5-Ch6. Using the approach described in [192, 205], the resulting ratings are then applied in the calculation of the annual cost of integrating different BESS technologies (LA, VRLA, NA/S, Zn/Br, and VB batteries) into the test system. In this

approach, the total annual cost of the BESS is the sum of three terms: the total annual capital cost, the annual replacement cost, and the annual maintenance and operation cost.

The total capital cost itself is composed of three items: the total cost for power electronics (power cost), total cost for storage units (energy cost), and cost of the balance of plant:

$$TCC_{BESS} = PCS_{BESS} + SUC_{BESS} + BOP_{BESS} \tag{6.37}$$

where TCC_{BESS} is the total capital cost of the BESS, PCS_{BESS} is the total cost for power electronics, SUC_{BESS} is the total cost for storage units and BOP_{BESS} is the total cost of the balance of plant.

The total cost of for the power electronics (PCS_{BESS}) is given by:

$$PCS_{BESS} = PCSU_{BESS} \times S_{BESS\ Rated} \tag{6.38}$$

where $PCSU_{BESS}$ is the unit cost for power electronics ($/kVA).

The total cost for the storage units (SUC_{BESS}) is given by:

$$SUC_{BESS} = SUCU_{BESS} \times E_{BESS\ Rated} \tag{6.39}$$

where $SUCU_{BESS}$ is the unit cost for storage units ($/kWh).

The total cost for the balance of the plant (BOP_{BESS}) is given by:

$$BOP_{BESS} = BOPU_{BESS} \times E_{BESS\ Rated} \tag{6.40}$$

where $BOPU_{BESS}$ is the unit cost for balance of plant ($/kWh).

The total annual capital cost ($TACC_{BESS}$) can be computed by multiplying the total capital cost (TCC_{BESS}) by the capital recovery factor (CRF):

$$TACC_{BESS} = TCC_{BESS} \times CRF \tag{6.41}$$

The capital recovery factor is given by:

$$CRF = \frac{i_r(1+i_r)^z}{(1+i_r)^z - 1} \tag{6.42}$$

where

i_r is the annual interest rate and is taken as 7.7% [205, 206];
z is the project lifetime and is taken as 40 years [205, 206].

BESSs used in a given project may have to be replaced one or more times during the lifetime of the project. The annual replacement cost per kWh is calculated as follows:

$$A_{BESS} = F_{BESS} \times [(1+i_r)^{-r} + (1+i_r)^{-2r} + ...] \times CRF \tag{6.43}$$

where

A_{BESS} is the annual replacement cost per kWh ($/kWh);
F_{BESS} is the future value of replacement cost ($/kWh);
r is the replacement period, which depends on the battery life, as given below:

$$r = \frac{N_{Ch/Dis}}{n_{Ch/Dis} \times D} \tag{6.44}$$

where $N_{Ch/Dis}$ is the number of charge/discharge cycles in life of BESS, $n_{Ch/Dis}$ is the number of daily charge/discharge cycles for the BESS, and D is the number of operating days for the BESS per year (days/year).

For this work, and based on the previous discussion, it is obvious that each BESS will experience only one charge/discharge cycle per day ($n_{Ch/Dis}$=1), throughout the whole year (D=365 days/year).

The annual replacement cost (ARC_{BESS}) is calculated by:

$$ARC_{BESS} = A_{BESS} \times E_{BESS\ Rated} \tag{6.45}$$

The annual fixed maintenance and operation cost (OMC_{BESS}) is given by:

$$OMC_{BESS} = OM_{f,BESS} \times S_{BESS\ Rated} \tag{6.46}$$

where $OM_{f, BESS}$ is the fixed operation and maintenance cost ($/kVA.year).

` `

Finally, the total annual cost (TAC_{BESS}) is the sum of the following three quantities:

$$TAC_{BESS} = TACC_{BESS} + ARC_{BESS} + OMC_{BESS} \quad (6.47)$$

Data provided in [205] (and shown in Table 6-2) are used for the calculation of the annual cost of integrating each type of BESS technology in the system (for different modes of operation).

The results for scenarios 3-Ch6 and 5-Ch6 are shown in Tables 6-3 and 6-4, respectively.

Table 6-2: Cost components for different BESS technologies [205]

	LA	VRLA	NA/S	Zn/Br	VB
Unit cost for storage units ($/kWh)	305	360	500	225	740
Efficiency of storage device	75%	75%	77%	70%	70%
Unit cost for balance of plant ($/kWh)	50	50	0	0	30
Future value of replacement cost ($/kWh)	305	360	500	225	740
Number of charge/discharge cycles	3200	1000	2500	10000	10000
Unit cost for power electronic ($/kVA)	175	175	1000	175	*
Fixed operation and maintenance cost ($/kVA.year)	15	5	20	20	20

*Unit cost for power electronic of VB is included in unit cost for storage units

Table 6-3: Annual cost of integrating different BESS technologies for scenario 3-Ch6 ($/year)

	LA	VRLA	NA/S	Zn/Br	VB
Power-saving state	161177	394067	340295	**89449**	196590
Energy-saving state	148635	320403	343640	96933	168026

Table 6-4: Annual cost of integrating different BESS technologies for scenario 5-Ch6 ($/year)

	LA	VRLA	NA/S	Zn/Br	VB
Power-saving state	346256	908278	689519	**167031**	432885
Energy-saving state	316580	782536	668282	169337	380887

The results reveal that Zn/Br batteries operating in the power-saving discharge state offer the most economical option, and will thus be used in the proposed design. In the subsequent sections, only Zn/Br batteries operating in the power saving state will be considered for detailed technical analysis.

6.6.2 BESSs Energy and Power Ratings

Figures 6-5 and 6-6 depict the average energy and power ratings of the 78 Zn/Br BESSs installed in the test system (in scenarios 3-Ch6 and 5-Ch6) as a function of the number of PHEV/PV array sets connected to the distribution transformer. For example, given a 25 kVA distribution transformer having only one PHEV/PV array set connected to its secondary terminals, a BESS with average energy and power ratings of 15 kWh and 10 kVA, respectively, should be installed at the distribution transformer LV bus, such as to mitigate transformer overloading and limit the reverse flow of power through the transformer so that it is kept within permissible limits (30% to 100% of the BESS energy rating). Tables 6-5 and 6-6 give the corresponding minimum and maximum energy/power ratings of the installed BESSs.

From the results, it becomes evident that due to the non-coincident nature of PHEV charging demands, the normalized BESS energy and power ratings (rating per PHEV/PV array set) decrease as the number of PHEV/PV array sets connected to the transformer increases: for a 25 kVA distribution transformer having 5 PHEV/PV array sets connected to its secondary terminals, the installed BESS would have average energy and power ratings of only 60 kWh and 15 kVA, respectively, rather than 75 kWh and 50 kVA. This corresponds to energy and power diversity factors of 1.25 and 3.33, respectively.

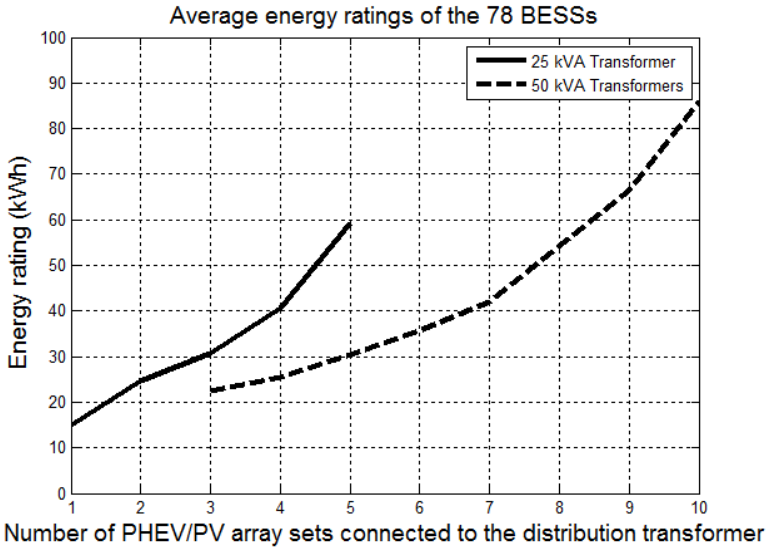

Figure 6-5: Average energy ratings of the selected 78 Zn/Br BESSs

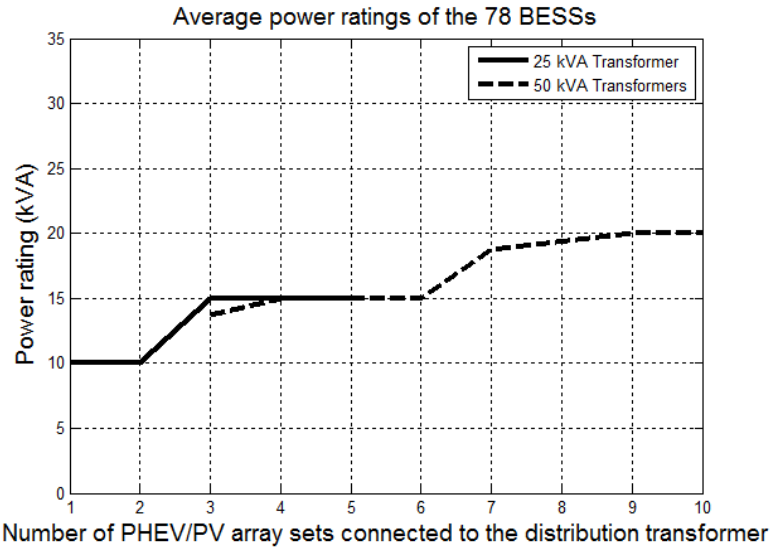

Figure 6-6: Average power ratings of the selected 78 Zn/Br BESSs

Table 6-5: Minimum and maximum energy/power ratings of the selected Zn/Br BESSs (50 kVA transformers)

Number of PHEV/PV array sets	Energy Rating (kWh)		Power rating (kVA)	
	Minimum	Maximum	Minimum	Maximum
1	N/A	N/A	N/A	N/A
2	N/A	N/A	N/A	N/A
3	20	25	10	15
4	25	30	15	15
5	30	35	15	15
6	35	40	15	15
7	40	45	15	20
8	N/A	N/A	N/A	N/A
9	65	70	20	20
10	80	90	20	25

Table 6-6: Minimum and maximum energy/power ratings of the selected Zn/Br BESSs (25 kVA transformers)

Number of PHEV/PV array sets	Energy Rating (kWh)		Power rating (kVA)	
	Minimum	Maximum	Minimum	Maximum
1	15	15	10	10
2	20	25	10	10
3	25	35	15	15
4	35	45	15	15
5	55	65	15	15

6.6.3 BESSs Stored Energy Levels

As indicated earlier by Eq. (6.33), the level of the energy stored in the proposed BESSs should always be restricted between $E_{BESS\ Rated}$ and $E_{BESS\ Reserve}$ (taken as 30% of the rated kWh). To verify this condition, the author used the MC simulation results for scenarios 3-Ch6 and 5-Ch6, abstracted from the previously developed probabilistic benchmark, in order to calculate the frequency distribution of the energy stored in the 78 proposed BESSs throughout the entire simulation period. The results for the worst-case high-penetration scenario (scenario 5-Ch6) are depicted in Figure 6-7.

Figure 6-7 indicates that the energy stored in the proposed BESSs is always maintained within the designated limits (30% to 100% of the rated kWh), thus satisfying the design criteria. These results confirm the effectiveness of the proposed BESS sizing methodology presented in Section 6.4.3 Similar results are obtained for scenario 3-Ch6.

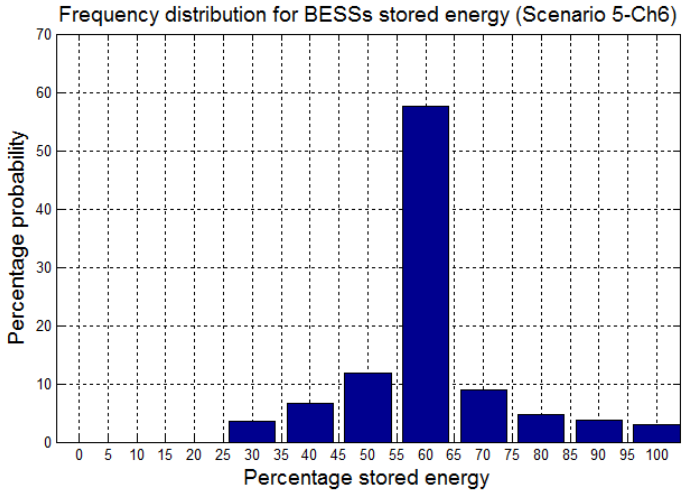

Figure 6-7: Frequency distribution for BESSs stored energy (Scenario 5-Ch6)

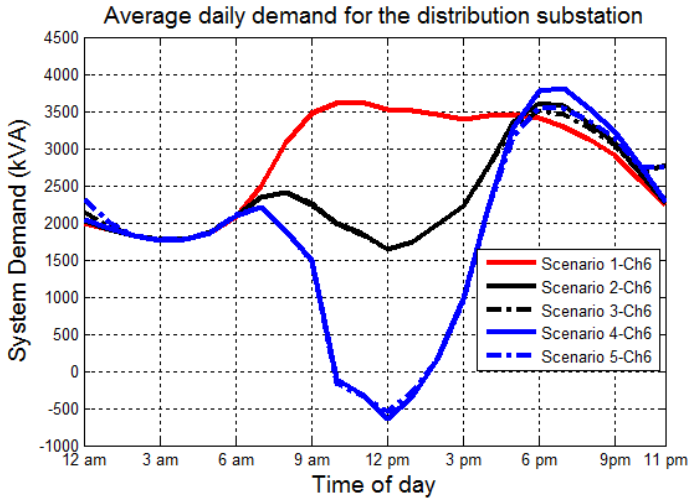

Figure 6-8: Average daily demand for the distribution substation

6.6.4 Evaluating the Performance of the System after the Inclusion of the Proposed BESSs

In this section, the author uses the MC simulation results in order to evaluate the performance of the system after the inclusion of the previously designed BESSs. The evaluation criteria are discussed in the following subsections.

6.6.4.1 Substation Average Daily Demand

The average daily demand for the distribution substation during the study scenarios is depicted in Figure 6-8. The negative values indicate the occurrence of reverse power flow.

From Figure 6-8, it can be observed that, for scenarios 2-Ch6 and 4-Ch6, PHEV charging demands increase the peak substation demand over the base-case value (scenario 1-Ch6), and shift it from morning to the early evening. PV arrays, on the other hand, produce their maximum output at noon, which, for scenario 4-Ch6, results in reverse power flow through the substation transformer at noon.

As indicated in Figure 6-8, the positive impact of the installed BESSs is quite significant: at noon, excess PV production is stored in BESSs to limit the reverse power flow through the secondary distribution transformers so that it remains within acceptable thresholds (60% of the transformer rating). As a result, for scenario 5-Ch6, the reverse power flow evident at the substation transformer is slightly less than that for scenario 4-Ch6. However, the amount of the previous reduction is only minor (approximately 1.3%) because BESSs start to charge only after the reverse power flow exceeds

the predetermined threshold. This stored energy is then reused in order to meet a portion of the PHEV charging demand to avoid distribution transformers overloading. The peak substation demands with scenarios 3-Ch6 and 5-Ch6 are therefore significantly less than the corresponding values for scenarios 2-Ch6 and 4-Ch6, respectively. As states earlier, the drawback of using average data is that it provides no insight with respect to the likelihood of realizing the anticipated benefits of the proposed BESSs, thus negating one of the primary strengths of MC simulations: MC output includes a probability distribution that can be used for deriving valuable probabilistic indices, as explained below.

6.6.4.2 Probability of Overloading Distribution Equipment

The probabilistic analysis starts with the computation of the frequencies of occurrence of different kVA loadings in each equipment class during the entire simulation interval. The resulting frequency distributions are then utilized for the development of normalized (1-cfd) curves for each equipment class. As explained earlier, the probability of exceeding a certain class of distribution equipment rating is determined directly from the corresponding normalized (1–cfd) curve as the probability corresponding to 100% loading. Table 6-7 shows the probability of exceeding the ratings for a variety of equipment classes for the system under study.

The impact of diversity revealed in Table 6-7 is rather significant: the primary feeder is unlikely to be overloaded during any of the scenarios studied, with the worst probability at only 0.11% for scenario 4-Ch6. Table 6-7 also indicates that, for scenarios 2-Ch6 and 4-Ch6, increased PHEV charging demands render the secondary distribution transformers susceptible to significant overloads.

However, with the proposed BESSs (scenarios 3-Ch6 and 5-Ch6), during peak demand periods, energy stored in the BESSs is used for meeting a portion of the demand locally, thus mitigating the overloading of the distribution transformers. This effect is illustrated by the bend occurring at 100% loading in the (1-cfd) curve depicted in Figure 6-9. As a result, the probability of overloading the distribution transformers is substantially reduced with scenarios 3-Ch6 and 5-Ch6: the overloading probability of 25 kVA transformers, for example, decreases from 6.07% in scenario 2-Ch6 to 0.37% in scenario 3-Ch6 and from 9.33% in scenario 4-Ch6 to 0.61% in scenario 5-Ch6. These promising results can be improved further by increasing the confidence level adopted in Section 6.4.3 during the BESS sizing process. Increasing the confidence level, however, will increase the required BESSs ratings, and hence, their overall cost.

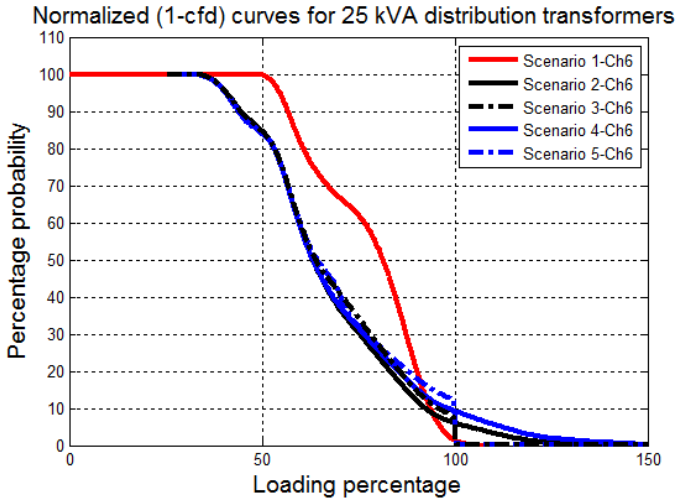

Figure 6-9: Probability of exceeding a specific percentage loading for 25 kVA distribution transformers

Table 6-7: Probability of exceeding equipment ratings

Scenario	1-Ch6	2-Ch6	3-Ch6	4-Ch6	5-Ch6
Primary Feeder	0%	0.01%	0%	0.11%	0%
50 kVA transformers	0%	5.31%	0.22%	9.18%	0.44%
25 kVA transformers	0%	6.07%	0.37%	9.33%	0.61%
Single phase laterals	0%	0%	0%	0%	0%
Service drops	0%	0%	0%	0%	0%

As mentioned earlier, for mechanical reasons, North American utilities usually oversize overhead laterals and service drops. As a result, their loading does not exceed 60% and 30% of their rated capacity, respectively, during study scenarios 2-Ch6 and 4-Ch6, as indicated by their normalized (1-cfd) curves. Laterals and service drops are therefore unlikely to be overloaded during any of the scenarios, as shown in Table 6-7, and thus have not been included in the remainder of the analysis.

6.6.4.3 Upgrade Requirements

As explained earlier, the peak demand (with a 95% confidence level) for a specific piece of equipment is the demand whose probability of being exceeded is less than 5%.The peak demand for each piece of equipment in the system is computed accordingly for each scenario. This piece of equipment is flagged as overloaded and requiring upgrading if the peak demand calculated exceeds its rated capacity. The results for the system under study are shown in Table 6-8.

Table 6-8: Percentage of equipment requiring upgrades

Scenario	1-Ch6	2-Ch6	3-Ch6	4-Ch6	5-Ch6
Primary Feeder	0%	0%	0%	0%	0%
50 kVA transformers	0%	57.45%	0%	100%	0%
25 kVA transformers	0%	67.74%	0%	100%	0%

As stated earlier, the components most influenced by increased PHEV penetration are the secondary distribution transformers. For the system under study, with scenario 2-Ch6, 57.45% and 67.74% of 50 kVA and 25 kVA secondary distribution transformers, respectively, are overloaded and require upgrading, and with scenario 4-Ch6, all secondary distribution transformers must be upgraded. The installed BESSs, on the other hand, can provide a means of eliminating this problem completely because its application ensures that the power flowing through each distribution transformer never exceeds its rated capacity. As a result, with scenarios 3-Ch6 and 5-Ch6, no transformers must be upgraded and costly system upgrades can be avoided.

6.6.4.4 Reverse Power Flow

Figure 6-8 emphasizes the weak chronological coincidence between PV array production and system peak demand, which results in excessive reverse power flows at noon, when PV arrays are generating their peak output. This reverse power flow has adverse impacts on distribution networks [13, 14].

To study the impact of the proposed BESSs on such reverse power flows, the author employed the MC-based probabilistic benchmark for two calculations: the probability of the occurrence of reverse power flow in the different classes of distribution transformers, and the corresponding maximum magnitude for that reverse power flow (as a percentage of the transformer rating), during different study scenarios. The results for the system under study are shown in Tables 6-9 and 6-10, respectively.

Table 6-9: Probability of the occurrence of reverse power flow

Scenario	1-Ch6	2-Ch6	3-Ch6	4-Ch6	5-Ch6
Substation transformer	0%	0%	0%	14.88%	14.43%
50 kVA transformers	0%	5.6%	5.58%	20.49%	20.42%
25 kVA transformers	0%	6.17%	6.11%	20.59%	20.53%

Table 6-10: Peak reverse power flow as a percentage of the transformer rating

Scenario	1-Ch6	2-Ch6	3-Ch6	4-Ch6	5-Ch6
Substation transformer	0%	0%	0%	30%	21%
50 kVA transformers	0%	37.90%	37.74%	80.48%	59.78%
25 kVA transformers	0%	57.84%	57.82%	82.92%	59.93%

Due to the presence of commercial loads in the system, the substation transformer is not subjected to high rates of reverse power flow. However, this is not the case for the secondary distribution transformers, where higher rates of reverse power flow can occur in scenarios 2-Ch6 and 4-Ch6. For example, with scenario 2-Ch6, the reverse power flow through the 25 kVA transformers may reach 57.84% of the transformer rating, which is still within the acceptable Ontario limits (60% of the transformer rating). However, this is not the case with scenario 4-Ch6, in which the reverse power flow may reach 82.92% of the transformer rating, thus violating acceptable limits. Similar results were obtained for 50 kVA transformers. Table 6-9 indicates that the proposed BESSs have a minor impact on the probability of the occurrence of reverse power flow in the distribution transformers. This result is attributable to the fact that BESSs begin to charge only after the reverse power flow exceeds the pre-designated design threshold (60% of the transformer rating). However, as shown in Table 6-10, the proposed BESSs are capable of limiting the maximum reverse power flow through the distribution transformers so that it remains within the acceptable 60% threshold. For scenarios 3-Ch6 and 5-Ch6, this effect is exemplified by the bend at the point corresponding to 60% reverse power in the (1-cfd) curve for the susceptible 25 kVA transformers, as depicted in Figure 6-10.

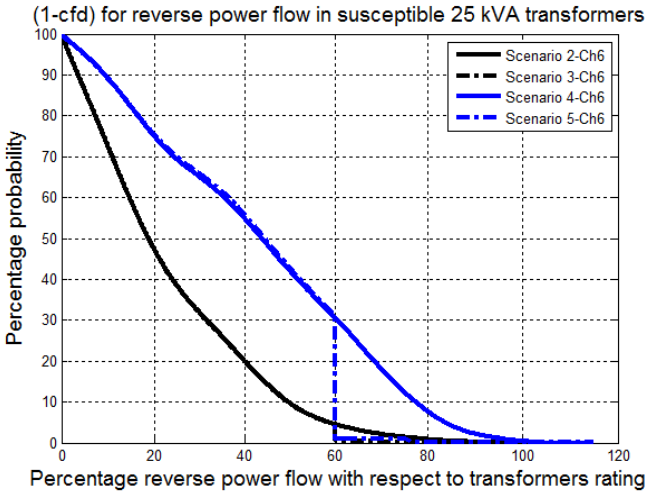

Figure 6-10: Probability of exceeding a specific reverse power flow for 25 kVA transformers

`  `

6.6.4.5 AC System Voltages

As explained earlier, a major challenge associated with PHEVs is the resulting under voltages at the end customers (120 V) during the heavy loading conditions that occur during peak charging periods. Utilities are also concerned about the over voltages that occur due to reverse power flows when PV arrays are generating their peak output. The probability of violating range-A voltage limits at a variety of locations in the system during different study scenarios was estimated using the probabilistic benchmark. The results are listed in Table 6-11.

Table 6-11: Probability of violating range-A voltage limits

Scenario	1-Ch6	2-Ch6	3-Ch6	4-Ch6	5-Ch6
At the end customer	0%	0%	0%	0.1%	0%
At the distribution transformers	0%	0%	0%	0.1%	0%
Along the primary feeder	0%	0%	0%	0.3%	0%

Table 6-11 reveals that, for scenario 4-Ch6, increased PV and PHEV penetration leads to only a minor violation of range-A voltage limits. The proposed BESSs, however, have a positive impact on system voltages because it eliminates completely the probability of violating range-A voltage limits, as indicated for scenario 5-Ch6. This effect can be attributed to the fact that, in scenarios 3-Ch6 and 5-Ch6, BESSs operate to alleviate secondary distribution transformer overloading during PHEV peak charging periods, and to limit the reverse power flow when PV arrays are at peak output. The under voltages that accompany PHEV peak charging periods as well as the over voltages that occur due to excessive reverse power flows are thus significantly reduced.

6.6.4.6 Number of Voltage Regulators Operations

Table 6-12 gives the average number of annual regulators actions during the study scenarios, abstracted from the probabilistic benchmark.

Table 6-12: Annual number of regulators actions

Scenario	1-Ch6	2-Ch6	3-Ch6	4-Ch6	5-Ch6
Regulators actions	16595	19948	17567	28755	24717

Table 6-12 indicates that, in scenarios 2-Ch6 and 4-Ch6, the presence of PV arrays and PHEVs increases the number of regulators actions by 20% and 73%, respectively, compared to the base-case scenario (scenario 1-Ch6). The installed BESSs, however, reduce the number of regulators actions for

scenarios 3-Ch6 and 5-Ch6 by 11.94% and 14.04% relative to their values in scenarios 2-Ch6 and 4-Ch6. Overall, these results, together with those presented in the previous section, indicate that BESSs have a positive impact on system voltages. The net effect is a reduction in the total number of regulators actions, which increases their longevity.

6.6.4.7 Total System Losses

The annual active and reactive energy losses in the test system during different scenarios are given in Table 6-13, and depicted in Figures 6-11 and 6-12.

Table 6-13: Total system losses

Scenario	Active energy losses (MWh)			Reactive energy losses (MVARh)
	AC Network losses	BESSs losses	Overall system losses	
1-Ch6	791.87	0	791.87	1451.71
2-Ch6	612.99	0	612.99	1114.27
3-Ch6	611.28	132.72	744.00	1111.38
4-Ch6	608.41	0	608.41	1100.17
5-Ch6	590.22	223.85	814.07	1067.68

As explained earlier in Section 5.3.7, PHEVs increase the network losses due to the additional energy required to meet their charging demands. PV arrays, on the other hand, reduce the network losses as they bring power generation closer to load centers. Another important observation is that the positive impact of PV electricity on network losses is more significant than the negative impact of PHEVs. As a result, the network active energy losses in scenarios 2-Ch6 and 4-Ch6 are reduced by 22.59% and 23.17% from the corresponding value in the base-case scenario (1-Ch6). Similar figures are obtained for the reactive energy losses (23.24% and 24.22%).

Figures 6-11 and 6-12 make it evident that the inclusion of BESSs has a positive impact on the network losses. This observation is explained by the fact that BESSs meet a portion of the network demand locally (i.e., from the LV network) during PHEV peak charging periods, thus lessening the dependency on the primary distribution network and reducing the total incurred network losses. As a result, the network active energy losses for scenarios 3-Ch6 and 5-Ch6 are reduced by 0.3% and 3% from the corresponding values for scenarios 2-Ch6 and 4-Ch6, respectively. Similar figures are obtained for reactive energy losses (0.26% and 2.95%).

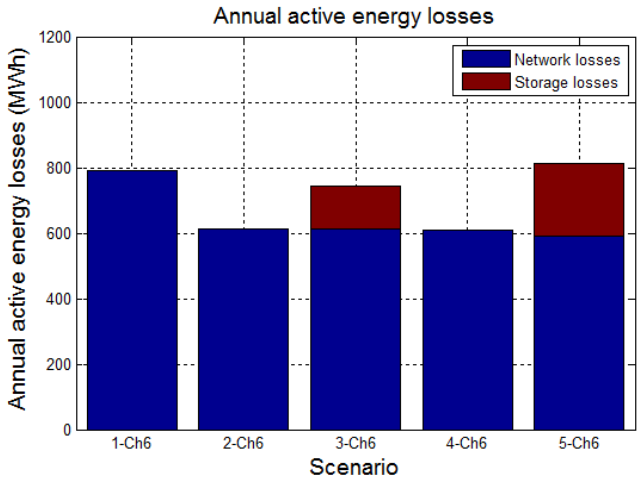

Figure 6-11: Annual active energy losses

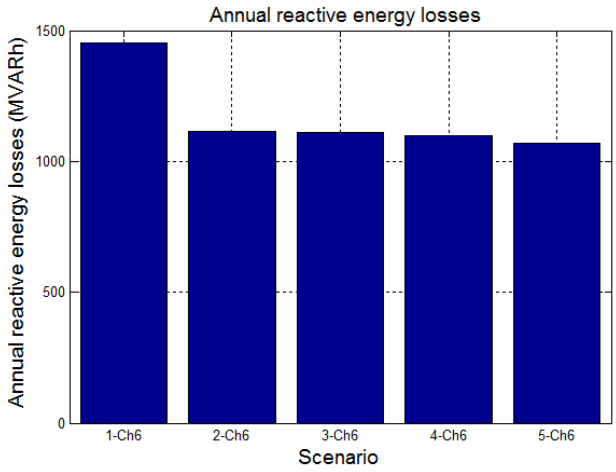

Figure 6-12: Annual reactive energy losses

However, BESSs are relatively low-efficiency devices, with the AC/AC round-trip efficiency of the most efficient storage technology limited to only 77%. As a result, BESSs encounter significant charging/discharging losses, and the overall system losses (network losses plus BESSs losses) for scenarios 3-Ch6 and 5-Ch6 are 21.4% and 33.8% greater than the corresponding values for scenarios 2-Ch6 and 4-Ch6, respectively. These values, however, are still comparable to the losses of the base-case scenario (1-Ch6).

6.6.5 Evaluating the Economic Feasibility of the Proposed BESSs

In this section, the costs and benefits associated with the installation of the proposed BESSs are compared to assess their cost-effectiveness.

`  `

6.6.5.1 Calculating the Costs Associated with the Installation of the Proposed BESSs

The proposed BESSs are associated with the following cost components:

i) Cost of storage devices: As concluded earlier in Section 6.6.1, Zn/Br batteries operating in the power-saving discharge state offer the most economical option. The annual cost of integrating Zn/Br BESSs in the test system is depicted in Tables 6-3 and 6-4.

ii) Cost of extra system losses: As shown in Section 6.6.4.7, the proposed BESSs increase the overall system losses. The annual cost of the extra losses incurred in the system is estimated using the average weighted hourly price for electricity in Ontario in 2013 (0.0265 CAD/kWh or 0.0236 $/kWh).

The different cost components associated with the installation of the proposed BESSs in scenarios 3-Ch6 and 5-Ch6 for the system under study are given in Table 6-14.

Table 6-14: Annual costs associated with the installation of the proposed BESSs ($/year)

Cost component	Scenario 3-Ch6	Scenario 5-Ch6
Storage devices	89449	167031
Extra system losses	4854	3092
Total annual cost	**94303**	**170123**

6.6.5.2 Calculating the Benefits Associated with the Installation of the Proposed BESSs

As explained in Section 6.6.4.3, with scenario 2-Ch6, 67.74% and 57.45% of 25 kVA and 50 kVA secondary distribution transformers are overloaded and require upgrading to 37.5 kVA and 75 kVA transformers, respectively, and with scenario 4-Ch6, all secondary distribution transformers must be upgraded. The installed BESSs in scenarios 3-Ch6 and 5-Ch6, on the other hand, can provide a means of eliminating this problem completely because their application ensures that the power flowing through each distribution transformer never exceeds its rated capacity. As a result, with scenarios 3-Ch6 and 5-Ch6, no transformers must be upgraded. In view of that, the benefits associated with the proposed BESSs are the cost savings achieved by avoiding distribution transformer upgrades.

Based on the analysis performed in [207], the total capital cost savings achieved by avoiding distribution transformer upgrades ($TCCS_{Trans}$) can be approximated as:

`  `

$$TCCS_{Trans} = MP_{Trans} + (LE_{Trans} \times M_{LE,Trans}) \quad (6.48)$$

where MP_{Trans} is the distribution transformer manufacturer's selling price; LE_{Trans} is the distribution transformer's fixed installation, labor, and equipment costs and $M_{LE,\ Trans}$ is the markup factor on the transformer's fixed installation, labor, and equipment costs.

The total annual cost savings ($TACS_{Trans}$) achieved by avoiding distribution transformer upgrades are computed by multiplying the total capital cost savings ($TCCS_{Trans}$) by the capital recovery factor (CRF) for a project lifetime of 40 years and at a 7.7% annual interest rate:

$$TACS_{Trans} = TCCS_{Trans} \times CRF \quad (6.49)$$

Data provided in [207] and [208] (shown in Table 6-15) are used for the calculation of the total annual cost savings achieved by avoiding distribution transformer upgrades. Results for scenarios 3-Ch6 and 5-Ch6 are depicted in Table 6-16.

Table 6-15: Cost components for secondary distribution transformers [207, 208]

Cost component	37.5 kVA transformers	75 kVA transformers
Manufacturer's selling price ($)	1703	3488
Fixed costs ($)	2001	2001
Markup factor on the fixed costs	1.52	1.52

Table 6-16: Annual cost savings associated with the installation of the proposed BESSs ($/year)

Cost savings	Scenario 3-Ch6	Scenario 5-Ch6
Avoiding distribution transformer upgrades	**22399**	**36852**

6.6.5.3 Performing a Cost/Benefit Analysis

In this step, the total annual benefits associated with the installation of the proposed BESSs are compared to the total incurred annual costs. Results are depicted in Figure 6-13.

Results reveal that the utilization of BESSs to facilitate the integration of PHEVs and PV electricity in distribution systems is not a cost-effective solution: the annual costs associated with the installation of the proposed BESSs exceed their annual benefits. This cost-ineffectiveness is attributed mainly to the high cost of available storage technologies.

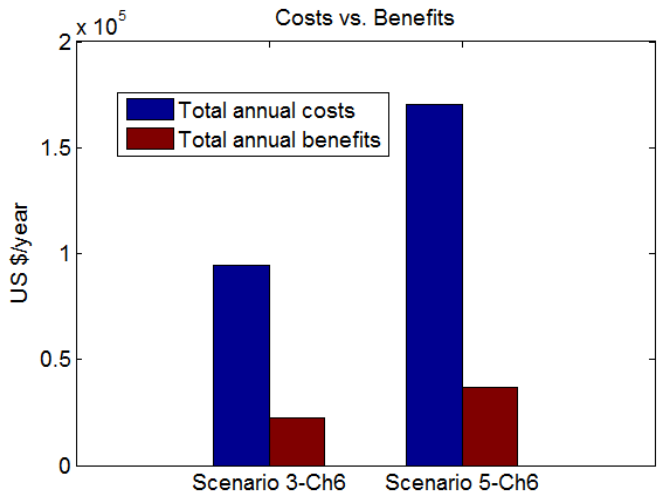

Figure 6-13: Annual costs and benefits associated with the proposed BESSs

6.6.6 Discussion of the Results

Previous results attest to the potential of using BESSs to facilitate the integration of PHEVs and PV electricity in residential distribution networks, with respect to both mitigating distribution transformer overloading during PHEV charging periods and limiting reverse power flow through the transformers during PV peak generation periods so that it is kept within permissible limits. Moreover, the stored energy levels in the BESSs are always maintained within designated limits despite the high variability in PV array output and PHEV charging demands, thus successfully satisfying all design criteria.

The proposed design methodology offers several advantages:

i) Generic: In the presented case study, the proposed design methodology was effectually used to determine the appropriate sizes and operating schedules for 78 distinct BESSs with different numbers of PHEVs and PV arrays connected to each transformer.

ii) Realistic: It takes into consideration the stochastic nature of the PV array output, existing electrical loads and PHEV charging demand.

iii) Simple: The proposed BESSs are sized during the offline planning stage. After that, during the system's online operation, only simple equations (presented in Section 6.4.4) are programmed into charging controllers, such as to produce charging/discharging decisions on the fly.

The main shortcomings of the proposed solution are summarized below:

i) Cost-ineffectiveness: BESSs are generally regarded as expensive technologies, which is quite evident in Section 6.6.5. As a result, the annual costs associated with the installation of the proposed BESSs exceed the anticipated annual benefits. However, some studies forecast that the cost of BESSs will be reduced in the near future: battery costs have already declined from the beginning of 2009 to the middle of 2012 by almost 30% [209]; thus, it is not too optimistic to predict that, by 2030, the cost of BESSs will fall to 21.8% of their 2012 values [209].

ii) Increased system losses: BESSs are relatively low-efficiency devices; thus, the overall system losses for scenarios 3-Ch6 and 5-Ch6 are 21.4% and 33.8% greater than the corresponding values for scenarios 2-Ch6 and 4-Ch6, respectively.

This last disadvantage, however, can be overcome by using DC electricity to interface PHEVs and PV arrays, hence altering the distribution system architecture from a single layer AC system into a bilayer AC-DC system. This proposal is based on the fact that both PV systems and PHEVs are inherently DC in nature: PV arrays produce DC power, and PHEV batteries are charged primarily by DC electricity. Providing a DC interface for these technologies can therefore eliminate the power conversion stage required for interfacing with the existing AC network. Eliminating the DC/AC inversion stage in PV arrays and the AC/DC rectification stage in PHEV battery chargers would increase the overall system efficiency by counting out the losses of the extra conversion stages, which could, in turn, compensate for the additional losses associated with the BESSs. This point is investigated in detail in the next chapter.

6.7 Summary and Conclusions

This chapter has presented a probabilistic sizing and scheduling methodology for BESSs to enable their use for facilitating the integration of PV arrays and PHEVs in residential distribution networks. MC simulation results demonstrated the technical feasibility of the proposed design: BESSs installed in secondary networks can mitigate distribution transformer overloading and limit the reverse flow of power through the transformers so that it is kept within permissible limits. The main shortcomings of the proposed approach are its cost-ineffectiveness and the fact that its implementation increases the overall system losses. This latter shortcoming, however, can be overcome by using DC electricity to interface PHEVs and PV arrays, thereby eliminating the power conversion stage required for PHEVs and PV arrays (which are fundamentally DC technologies) to interface with the existing AC network. This point is investigated in detail in the next chapter.

Chapter 7
Innovative Residential Distribution System Architecture for Improved Integration of PHEVs and PV Arrays

7.1 Introduction

In previous chapters, the author studied the aggregated impacts of PHEVs and PV electricity on residential distribution networks. The performed analysis showed that these two technologies have adverse impacts on secondary distribution networks in terms of secondary distribution transformer overloading and increased reverse power flow. To lessen these impacts, the author suggested using small-scale dispersed BESSs installed at secondary distribution transformers to store PV electricity generated during low demand periods, when reverse power flow is most likely to occur, and then reuse this energy to meet part of the PHEV charging demand during peak demand periods, when this demand is most likely to overload secondary distribution transformers. MC simulation results demonstrated the technical viability of the proposed solution: BESSs installed in secondary distribution networks can mitigate distribution transformer overloading and limit the reverse flow of power through the transformers so that it is kept within permissible limits. The main shortcomings of the proposed solution are its cost-ineffectiveness and the fact that its implementation increases the overall system losses.

More than 100 years after the war of the currents between Edison and Westinghouse, DC distribution of electrical power has again come to the forefront as a possible means to handle the challenges facing the power system in the smart grid era. In this chapter, the author is proposing a novel bilayer (AC-DC) residential distribution system architecture to facilitate the integration of PHEVs and PV electricity in residential distribution networks.

The remainder of the chapter is organized as follows: Section 7.2 reviews the existing literature on DC distribution systems; Section 7.3 presents the proposed bilayer system; Section 7.4 outlines the proposed operation of the bilayer system; Section 7.5 details the MC-based probabilistic benchmark used in the analysis; Section 7.6 describes the probabilistic methodology used to size and schedule the operation of different system components; Section 7.7 presents the case study used to validate the proposed design methodology; Section 7.8 presents the simulation results for a range of scenarios; and finally, Section 7.9 summarizes the conclusions.

7.2 DC Distribution in the Smart Grid

In the early days of electricity, DC electricity- which was Edison's battle horse- was used in electrical power systems. The generation, transmission and distribution of electrical power had to be at the same voltage level because there was no practical way to step up/down DC voltages. For that reason, low DC voltages in the order of 100 Vdc were used throughout the whole system to be compatible with incandescent lamps (which were the primary load at that time). In order to keep losses and voltage drops within acceptable levels, the Edison DC system needed thick copper conductors and local generators; early DC generating plants needed to be within about 1.5 miles of the furthest customer [210]. The adoption of AC generators in 1886 by George Westinghouse dramatically changed the situation and led to what is known historically as "War of the currents" that took place in the late 1880s. AC electricity won the battle as it can be stepped up/down using transformers; thus, there was no need for generating stations to be close to loads. At the beginning, the AC system was a single phase system; later on, the poly phase system was introduced by Nikola Tesla and was integrated with the Westinghouse AC system [210].

However, with the untraditional challenges facing the power system in the smart grid era, DC distribution has again come to the forefront as a possible means to address these challenges and several researchers have shown increased interest in the applicability of DC distribution systems. For example, in [211], the authors investigated the feasibility of adopting DC electricity in LV and MV distribution networks. The performed analysis showed that DC distribution system allows for a better utilization of the HV/MV transformers' capacity, allowing an increase in the supplied demand without upgrading existing transformers. Similarly, the author of [212] compared the merits of both stand-alone AC and DC distribution systems. The study concluded that for residences supplied by a PV array (or another DC generator), the total conversion efficiency within the residential DC distribution system will be greater than that for the corresponding AC system. In [213], the authors examined the feasibility of utilizing DC distribution systems in commercial applications. The authors concluded that the implementation of DC distribution systems in the commercial sector is feasible and cost-effective. An interesting paper [214] studied the possibility of using available-in-market appliances in a DC distribution environment. The rationale for the research described in the paper arises from the fact that most electronic appliances operate basically on DC power and hence contain an AC/DC rectifier in their power supply circuits. These power supply circuits can be bypassed, making it possible to operate the appliance using either AC or DC electricity without any

modification. Different appliances (compact fluorescent lamps, LED lamps, TV sets, and computers) were tested by using an AC supply as the base-case and then the test replaced the AC supply with a DC one. Experimental results concluded that most electronic appliances can be fed using either type of electricity without any modification. Moreover, it was found that the power quality in the steady state operation is improved significantly when these appliances are fed by DC electricity.

In the following sections, the author will discuss the key drivers for such an increased interest in DC distribution systems as well as their benefits, shortcomings and applications.

7.2.1 Key Drivers of DC Distribution Systems in the Smart Grid

As mentioned earlier, researchers have shown an increased interest in DC distribution systems. The following points summarize the main drivers for such an increased interest:

i) Many of the smart grid technologies are inherently DC in nature: the majority of distributed energy resources (i.e., PV arrays, fuel cells) produce DC power; PHEVs' batteries are fundamentally charged by DC electricity; local storage options are DC in nature. Thus, by implementing DC distribution systems, the DC/AC conversion stage required to interface these technologies to the existing AC network can be eliminated. Eliminating the DC/AC inversion stage in PV systems and the AC/DC rectification stage in PHEVs' battery chargers increases system efficiency by counting out the losses of this conversion stage, and improves system reliability by decreasing the number of probable failure points. Reducing the number of power conversion stages also reduces the overall harmonic distortion in the power network.

   Similarly, wind systems can be better optimized and controlled if interfaced by DC electricity [215]. Wind turbines are usually operating at variable speeds and thus producing variable frequency AC output. To interface wind systems with the AC grid, an AC/DC/AC converter is used, which is an expensive solution. A cheaper and simpler solution is to connect an AC/DC converter directly to a DC grid. This solution would also eliminate a power conversion stage, thereby increasing system efficiency and reliability.

ii) As explained earlier, most smart devices and electronic appliances operate on DC power and hence contain an AC/DC rectifier in their power supply circuits. Today's domestic power supplies (with small transformers) usually have a power conversion efficiency of only 60 to 70% [216, 217]. As a result, more than 1 trillion kWh of electricity is wasted annually in these low-efficiency power supplies [218]. The situation becomes even worse due to the no-load

magnetizing losses occurring in these power supplies when the equipment is operating in stand-by mode; IEA estimated these losses to be around 62 TWh/year in the EU in 2010 [219]. These energy losses can be eliminated by implementing DC distribution systems thus replacing many small rectifiers with a more efficient centralized rectifier that provides DC electricity directly to equipment. Such a centralized rectifier is also expected to reduce the overall harmonic distortion in distribution systems.

Similarly, lighting systems –the largest single use of electricity within buildings–, are migrating towards the solid state and LED technologies. These are basically DC-powered devices that experience substantial power losses during the AC/DC rectification stage. Implementing DC distribution would eliminate these losses and improve the performance of lighting systems.

iii) The implementation of residential DC distribution systems would furnish the infrastructure required for the DC rapid-charging of PHEVs at residences, a convenience that should help promote their public acceptance.

iv) DC electricity reduces power system losses and allows for better utilization of equipment's installed capacity. This is explained by the fact that in DC systems cables do not experience active power losses due to skin and proximity effects; moreover, DC systems are not accompanied by any reactive power losses, which results in substantial reduction in the total system losses and thus better utilization of the equipment's installed capacity. In [220], it was shown that 1.5% efficiency improvement can be achieved by utilizing DC distribution systems.

v) DC electricity is generally safer than AC electricity as it does not lead to involuntary contraction of muscles [213]; also it is not associated with any harmful electromagnetic fields.

vi) DC distribution systems offer greater voltage stability than their AC counterparts. This is explained by the fact that when a voltage sag takes place in a DC distribution network, the DC-bus voltage is not greatly affected due to the stored energy in the DC-link capacitor [221]. This increased voltage stability minimizes the damage occurring to distribution equipment and improves the low voltage ride-through capability of the distribution network [221]. Moreover, DC distribution systems have lower fault levels than their AC counterparts as they are usually interfaced through power electronic converters [221]. These power electronic converters normally do not contribute that much or that long to the short circuit duty of the network due to the small thermal time constant of the utilized power electronic switches (1-2 p.u. for less than 1 cycle).

vii) If standardized, DC systems may bring an end to the plug and socket dilemma; such a goal was described by the International Electrotechnical Commission/Standardization Management Board (IEC/SMB) [222] as "No more transformers, no more travel adapters. Futuristic…but not utopic".

All these advantages have led to an increased interest in DC distribution systems, for example:

i) In South Korea, several topology studies are currently being conducted to determine the optimal DC distribution system architecture to be implemented in the existing Korean Electric Power Corporation (KEPCO) network [221].

ii) In Finland, Suur-Savon Sähkö Ltd. and Lappeenranta University of Technology (LUT) designed and installed a 3 km experimental DC distribution feeder serving 4 households in 2010 [223].

iii) The U.S. Navy is considering DC distribution in shipboard power systems as an alternative to conventional AC systems [224]. The Navy is currently implementing a form of DC distribution systems, called the zonal DC system [225], whereby the shipboard power system is divided into zones of DC and AC loads served through DC/DC and DC/AC converters.

iv) Facebook Inc. is currently operating a DC distribution system for its main datacenter in Prineville, Oregon [226].

v) IBM, Hewlett-Packard and the other major server manufacturers agreed on 2010 to produce datacenters that can accommodate both AC and DC electricity [226]. This initiative is driven by the observation that a a DC-powered datacenter is 10% more efficient than a state-of-the-art AC datacenter and 20% more efficient than a standard AC datacenter [226].

7.2.2 Challenges Facing the Implementation of DC Distribution Systems

Despite their numerous advantages, DC distribution systems have some major shortcomings that may constraint their widespread implementation:

i) Cost: The huge investments required to replace all the AC distribution infrastructure (step up/down transformers) with its DC counterpart (AC/DC and DC/DC power electronic converters) would outweigh any anticipated financial benefits for DC distribution systems [226].

ii) Lack of experience: Little experience is currently available with regards to DC distribution systems, as nobody has worked with DC electricity in over 100 years. Moreover, DC wiring is usually more expensive than AC conventional wiring because it is non-standardized [226].

iii) Ambiguous effect on system dynamics: The performance of DC distribution systems during different system disturbances should be researched thoroughly. DC systems are fed through power electronic converters and thus they are not backed up by a quasi-infinite grid to compensate for any sudden load fluctuations, making their performance highly dependent on the dynamic response of these converters. Accordingly, new standards should be established for DC distribution systems as existing standards for DC applications (e.g., IEC 61600 [227] and IEEE Std. 946 [228]) were developed mainly for auxiliary DC systems in plants and power stations, and so use simplified models to represent different power system components, making them inadequate for thorough transient analyses.

iv) Migration to DC distribution systems would necessitate the redesign of most home appliances as the majority of electrical motors used in these appliances are of the single phase induction type. Moreover, fewer vendors for DC appliances are currently available compared to AC appliances.

These challenges made the IEC/SMB board reach the conclusion that residential DC distribution are unlikely to be "coming soon to a home near you" and that the DC revolution in the residential sector "may be put off for a number of years or even decades" [222].

7.2.3 DC Distribution System Architectures Reported in the Literature

As explained earlier, there has been an increasing amount of research on the applications of DC distribution systems in the smart grid. Accordingly, several DC distribution system architectures have been proposed in the literature. Examples of these architectures are presented below:

i) DC Architecture 1: This architecture was proposed in [229] for use in the Finnish distribution network. As shown in Figure 7-1, the AC bulk power is stepped down from 20 kVac to 1 kVac by means of a step down distribution transformer, and then an AC/DC rectifier is used to convert the 1 kVac electricity into the 1.5 kVdc that is used for the distribution of electrical power. A DC/AC inverter is installed at each customer's premises to convert the 1.5 kVdc electricity into 400 Vac. In this architecture, all primary distribution feeders and secondary distribution laterals operate at the same voltage level (1.5 kVdc). The main limitation of this architecture is that DC electricity is used only for the distribution and not for the utilization of electrical power. Accordingly, customers are supplied by AC electricity only. The blue lines in Figure 7-1 define the DC portion of the system.

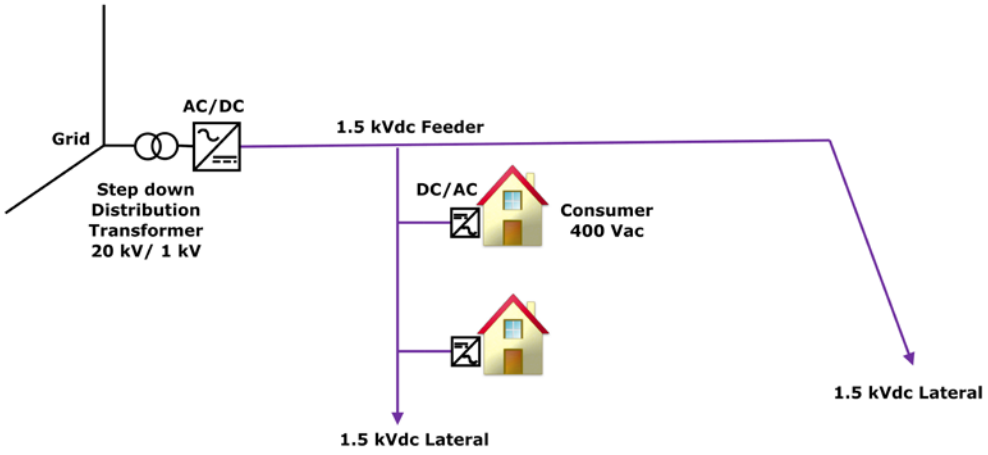

Figure 7-1: DC distribution system architecture 1

ii) DC Architecture 2: This architecture has been proposed in [221] for implementation in the KEPCO power network. As shown in Figure 7-2, AC electricity is stepped down from 22.9 kVac to 730 Vac by means of a step down distribution transformer. An AC/DC rectifier converts the 730 Vac into 1.5 kVdc electricity that is used for the primary distribution of electrical power. In this architecture, secondary step down transformers are replaced by buck DC/DC converters to step down the DC electricity from 1.5 kVdc to 400 Vdc suitable for the secondary distribution of electrical power. Each customer should have two DC/DC buck converters to step down the 400 Vdc to 200 Vdc and 12 Vdc. In this architecture, customers are supplied by DC electricity only. The blue lines in Figure 7-2 define the DC portion of the system.

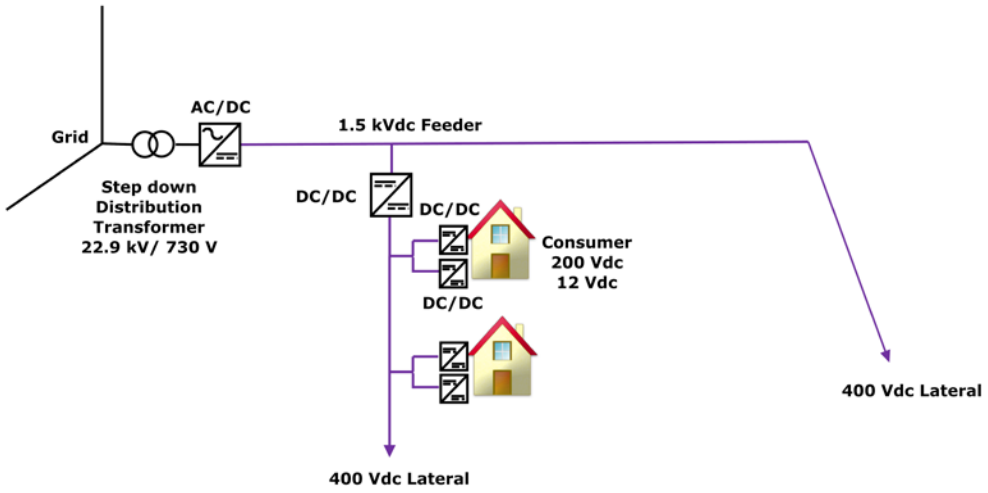

Figure 7-2: DC distribution system architecture 2

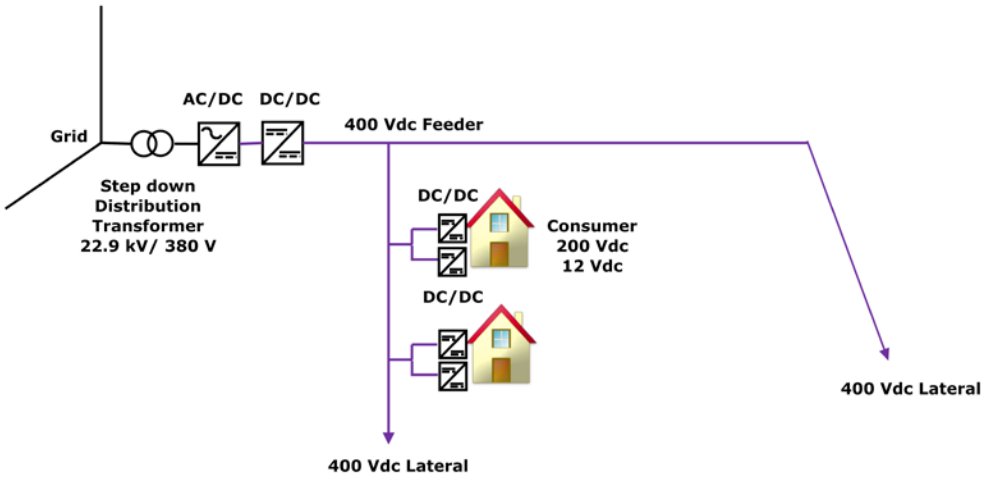

Figure 7-3: DC distribution system architecture 3

iii) DC Architecture 3: This architecture [221] is also being considered for implementation in the KEPCO power network. The main difference between this architecture and the previous one is that the distribution transformer steps down the AC electricity from 22.9 kVac to 380 Vac that is directly rectified into 400 Vdc by means of an AC/DC rectifier cascaded with a DC/DC converter. Similar to the previous architecture, each customer is equipped with two DC/DC converters to step down the 400 Vdc to 200 Vdc and 12 Vdc. Thus, customers in this architecture are also provided with DC electricity only. The blue lines in Figure 7-3 define the DC portion of the system.

iv) DC Architecture 4: This architecture (shown in Figure 7-4) is based on the zonal DC distribution system adopted by the U.S. navy in shipboard power systems [224], and its use in domestic distribution networks was suggested in [225]. In this architecture, the AC bulk power is converted into MV DC via an AC/DC rectifier placed after the substation transformer. Similar to architecture 1, the primary distribution feeders and secondary distribution laterals operate at the same voltage level. In this architecture, a DC/DC buck converter as well as a DC/AC inverter should be present at each end customer's premises to provide both LV DC and LV AC voltages, thereby eliminating the need for step down secondary distribution transformers. The literature does not provide standardized voltage levels for this architecture. The blue lines in Figure 7-4 define the DC portion of the system.

A comparison between these different architectures is presented in Table 7-1.

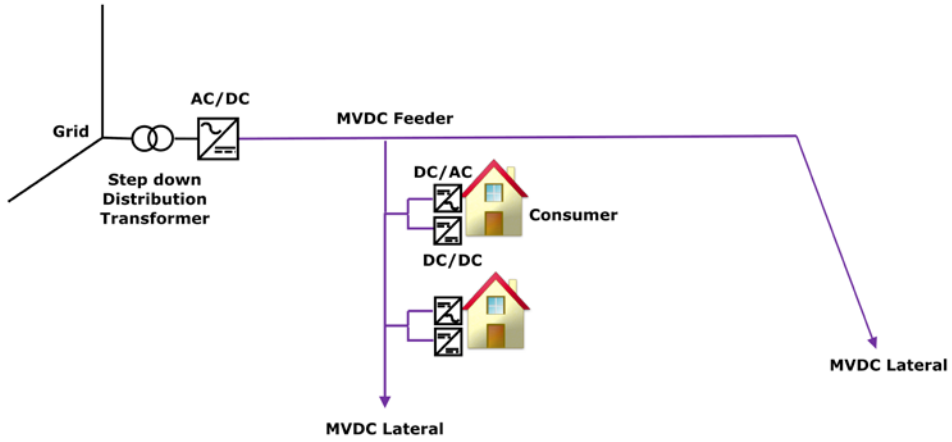

Figure 7-4: DC distribution system architecture 4

Table 7-1 Comparison of different DC distribution system architectures

	Type of supply provided to the end customers	Number of cascaded Power electronic conversion stages	Power electronic converters installed at end customer's premises	Comments
Architecture 1	AC only	2	DC/AC	DC electricity is used only for the distribution, not the utilization, of electrical power
Architecture 2	DC only	3	DC/DC DC/DC	Excessive losses due to the cascaded power electronic conversion stages
Architecture 3	DC only	3	DC/DC DC/DC	Excessive losses due to the cascaded power electronic conversion stages
Architecture 4	AC & DC	2	DC/AC DC/DC	Superficial design available in the literature

The previous architectures provide the end customers with a source of DC electricity that can be used to interface PV systems and PHEVs. Such a source of DC electricity can also be used to supply DC power directly to their electronic appliances. However, these architectures have serious drawbacks:

i) Migrating from all-AC to all-DC distribution systems is not a sufficient measure to mitigate the negative impacts of PHEVs and PV electricity on residential distribution networks. This conclusion is based on the fact that these negative impacts arise mainly from the architecture of

the distribution system itself rather than the type of electricity used (whether DC or AC). The previous DC distribution system architectures (as well as the current AC architecture) adopt the single layer architecture, with all loads and generation sources connected to the same layer. This single layer thus must meet all PHEV charging demands, resulting in substantial overloading of secondary distribution equipment during peak charging periods, and must also absorb any surplus PV generation, leading to excessive reverse power flow when PV arrays are generating their peak output. Accordingly, single layer distribution system architectures are not likely to accommodate the expected growth in PHEVs and PV electricity penetration levels, unless the distribution infrastructure undergoes massive expansion upgrades

ii) In the previous architectures, the AC distribution infrastructure (step up/down transformers) is replaced completely with its DC counterpart (AC/DC and DC/DC power electronic converters). The huge investments required to achieve such a transition would outweigh any anticipated financial benefits for DC distribution systems [226].

iii) In the previous architectures, the AC/DC rectification stage takes place at primary distribution levels, necessitating the utilization of HV power electronic switches which are much more expensive than their LV counterparts. This price gap exists because HV solid-state switches have been available only in recent years, unlike mature LV power electronic switches which have been around for the past 40 years [230]. This price gap would increase the cost of transition from all-AC to all-DC distribution systems.

iv) In the previous architectures, the distribution network would have two or more cascaded power conversion stages, which would significantly increase the cost of the DC distribution system. Moreover, in [212] it was concluded that DC distribution of electrical power would have unfavorable total conversion efficiency compared with the existing AC distribution if cascaded power electronic converters exist in the system. Accordingly, the presence of cascaded power conversion stages in the previous architectures would offset the loss savings achieved by eliminating the DC/AC inversion stage in PV systems and the AC/DC rectification stage in PHEV battery chargers

v) All household loads in architectures 2 and 3 have to be redesigned to operate on DC electricity. As explained earlier, such a shift is extremely problematic since the majority of electrical motors used in domestic appliances are of the single phase induction type.

vi) In the previous architectures, secondary distribution transformers are substituted by power electronic converters before these transformers reach the end of their useful life, which represents unjustified economic loss.

vii) Another major disadvantage of the previous architectures lies in the operational difficulties accompanying the migration from all-AC to all-DC distribution systems; all customers must be disconnected for extended periods of time while replacing secondary distribution transformers with power electronic converters.

All these disadvantages would clearly outweigh any anticipated benefits for DC distribution systems. In the next section, the author is proposing a novel bilayer architecture for distribution systems that avoids the previous disadvantages.

7.3 Proposed Bilayer System

As explained earlier, the main cause of the negative impacts of PHEVs and PV electricity on distribution networks is the architecture of the distribution system itself. Distribution systems currently adopt the single layer architecture, with all loads and generation sources connected to the same layer. This single layer thus must meet all PHEV charging demands, resulting in substantial overloading of secondary distribution equipment during peak charging periods, and must also absorb any surplus PV generation, leading to excessive reverse power flow when PV arrays are generating their peak output. Another interesting fact that was demonstrated earlier is that both PV systems and PHEVs are inherently DC in nature. Providing a DC interface for these technologies would eliminate a power conversion stage and increase the conversion efficiency.

These two factors led to the novel idea of this research which is modifying the distribution system architecture so that it becomes a bilayer system composed of the traditional AC layer for interfacing with existing system loads, plus an embedded DC layer for interfacing with DC technologies present in the distribution system and currently interfaced via power electronic converters (such as PV arrays and PHEVs). A centralized bidirectional converter links the two layers and controls the power flows between them. The architecture proposed in this work represents a reasonable compromise that enables existing networks to benefit from both AC and DC electricity, thus metaphorically enjoying the best of both worlds. However, sizing and scheduling the operation of different system components is very challenging due to the uncertainties associated with existing electrical loads, the PHEV charging demand, and the PV array output.

` `

The primary contribution of the research presented in this chapter is the design and validation of the proposed bilayer system, with consideration of the above-mentioned uncertainties. The following sections provide a description of the proposed bilayer system.

7.3.1 General Architecture of the Proposed Bilayer System

The first question associated with bilayer distribution systems is where to install the DC layer of the system. The author sought an answer by considering the analysis performed in Chapter 5 that analyzed the impact on residential distribution networks of the widespread adoption of PHEVs and PV arrays. The results obtained in Section 5.3 showed that only secondary distribution networks are affected (in terms of secondary distribution transformer overloading and excessive reverse power flows), with an insignificant impact on the primary system. No additional benefit would thus accrue from constructing a DC layer parallel to the primary system: installation should be limited to the secondary distribution network (i.e., downstream from the secondary distribution transformers).

A related question is where the two layers of the bilayer system should be interconnected. From a practical perspective, the interconnection must occur at an existing system bus. Considering that the DC layer is to be installed parallel to the secondary distribution network, two possibilities thus exist:

i) The two layers are interconnected at distribution transformer MV bus: In this case, the centralized converter must convert power from MV AC to LV DC and vice versa. Such high-voltage low-power conversion requires expensive HV switches and thus would be very costly.

ii) The two layers are interconnected at distribution transformer LV bus: In this case, the centralized converter would utilize LV power electronic switches, which are cheap and readily available. This arrangement, however, requires a storage device operating in parallel with the bidirectional converter to supply part of the demand connected to the secondary distribution transformer locally (from the LV network) in order to avoid distribution transformer overloading during PHEV peak charging periods, and also to absorb excess PV generation and prevent its escalation to the MV network when PV arrays are generating their peak output. Installing a storage device in conjunction with the bidirectional converters would provide the inherent advantage of smoothing cloud-induced fluctuations in the PV array output power [22]. This last goal, however, is outside the scope of this research and is thus excluded from this discussion.

For all these reasons, the most beneficial solution is to interconnect the two layers of the proposed bilayer system at the distribution transformer LV bus.

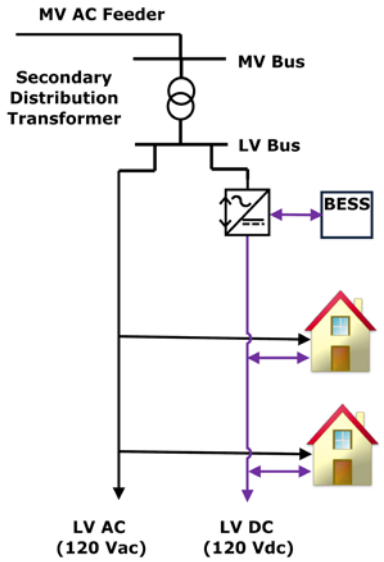

Figure 7-5: General layout of the proposed bilayer system

Previous discussion reveals that the DC layer of the bilayer system is comprised of distributed DC modules installed parallel to secondary networks. A sample bilayer module is shown in Figure 7-5.

7.3.2 DC Voltage Level

For this research, extra low voltage (ELV) 120 Vdc was selected as the operating voltage for the DC layer of the system. This selection is based on the following reasons:

i) Safety: According to IEC 60364 standards [231], low risk is associated with 120 Vdc, so the proposed bilayer system would not need protection against indirect contacts [232]. This makes the system simpler and cheaper due to the absence of grounding.

ii) Compatibility with existing circuit breakers: Interrupting DC fault currents is usually more difficult than interrupting their AC counterparts due to the absence of natural zero crossings. However, in [233] it was shown that a single breaker can be used for both LV AC and LV DC systems, but with significantly less breaking capacity in DC systems. A typical manufacturer's catalogue [234] offers circuit breakers for voltages up to 500 Vdc with rated currents up to 800 A and breaking capacities of 85 kVA. The selected voltage levels would thus be compatible with existing LV AC circuit breakers.

iii) Compatibility with existing fuses: The selected voltage level would allow existing fuses to operate normally in the DC system as it has the same root mean square value of the 120 Vac used in the AC system.

iv) Compatibility with existing household resistance equipment: The selected voltage level would allow resistance equipment (incandescent lighting and heating) to operate normally without any modifications as it has the same root mean square value of the 120 Vac used for power distribution in North America.

7.3.3 DC Layer Configuration

The literature describes two possible configurations for DC distribution system [229, 232]: unipolar and bipolar configuration. These two configurations are depicted in Figure 7-6.

Unipolar systems are inexpensive but have half the power transfer capability [229] of their bipolar counterparts. Bipolar systems, on the other hand, require additional power electronic switches and use more conductors (three conductors as opposed to two conductors in the unipolar configuration) but involve fewer voltage drops and provide greater efficiency.

In bipolar systems, customers can be connected between the positive or negative pole and the neutral, as a unipolar connection; or between the positive and negative poles and the neutral, as a bipolar connection. In the first case, there is a problem when the loads are not identical and the system falls into unbalance [232]. In [235-237], this problem was solved by adding a balancing circuit to the power electronic converter.

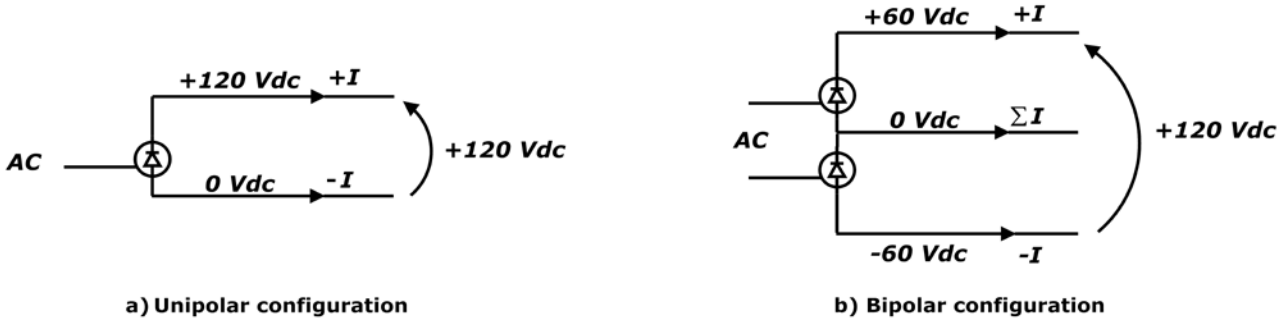

Figure 7-6: DC layer configurations

For this thesis, the author chose the bipolar configuration for the following reasons:

i) With this configuration, two voltage levels (120 Vdc and 60 Vdc) are obtained. In case the DC layer is used to supply part of the existing household loads, the 120 Vdc can be used for household resistance equipment (heating and lighting), and the 60 Vdc can be easily adapted for electronic devices (TVs, PCs, etc.).

ii) This configuration is compatible with the triplex conductors already used by North American utilities in distribution networks.

7.3.4 DC Service Drops

Because of mechanical considerations, North American utilities usually employ oversized service drops (triplex 1/0 AWG conductors). In this thesis, the author initially assumed that the conductor size of all DC service drops is the minimum allowable for their AC counterparts. The validity of this assumption will be assessed in a subsequent section.

7.3.5 Storage Technology

As explained earlier, storage technologies that are best suited for distribution system applications are long-term storage technologies such as BESSs [192, 202]. The author therefore selected BESSs for the proposed bilayer system. Similar to the previous chapter, the following variants of BESSs were considered: LA, VRLA, NA/S, Zn/Br, and VB batteries.

Power conditioning units (PCUs) for BESSs are usually composed of two stages [238]: a bidirectional AC/DC conversion stage that converts the DC power stored in the BESS into AC power suitable for the AC grid, and a bidirectional DC/DC conversion stage that converts the constant DC link voltage into variable DC voltage such as to control the charging/discharging rates. For the proposed bilayer system, only the second conversion stage is needed because the input voltage is DC in nature. Since a typical BESS AC/DC conversion stage is 95% efficient [238], its elimination increases the DC/DC round trip efficiency of BESS by a factor of 1/0.95, as shown in Table 7-2.

Table 7-2: Round trip efficiency for different BESS technologies [205]

	LA	VRLA	NA/S	Zn/Br	VB
AC/AC round trip efficiency	75%	75%	77%	70%	70%
DC/DC round trip efficiency	79%	79%	81%	79%	79%

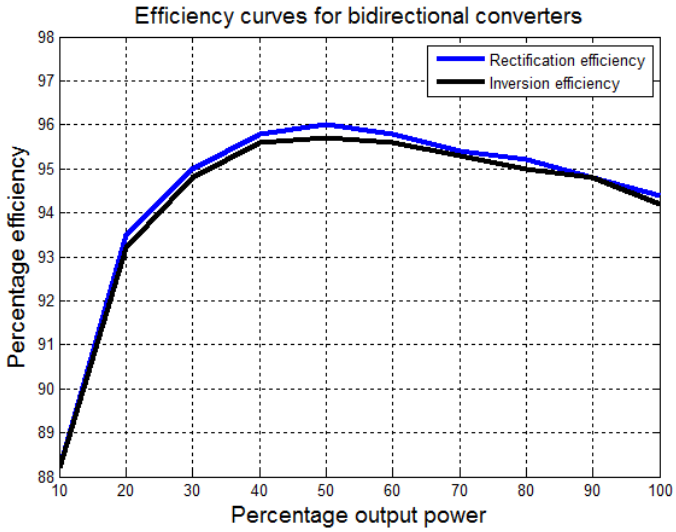

Figure 7-7: Efficiency curves for bidirectional converters

7.3.6 Availability of Bidirectional Centralized Converters

The literature describes several bidirectional converters that could be used in the proposed bilayer system [239-243]. For the application at hand, the author recommend the option presented in [243] because it features a high-efficiency, isolated bidirectional converter designed explicitly for DC power distribution systems. The efficiency curves of the selected converter are depicted in Figure 7-7.

7.3.7 Compatibility of PHEV Battery Chargers with the Proposed Bilayer System

Conventional PHEV battery chargers are usually comprised of two basic power conversion stages [244-246]: a front-end AC/DC stage that rectifies the input AC voltage, and a DC/DC stage that converts the DC bus voltage into regulated DC voltage suitable for charging batteries. This stage also provides galvanic isolation by means of a high-frequency transformer. As mentioned earlier, these battery chargers are reported to have an average efficiency of 90% [99, 163, 164].

Conventional PHEV battery chargers can be modified for use in the proposed bilayer system through the elimination of the AC/DC rectification stage. The DC/DC stage is then designed so that it boosts the 120 Vdc to the required battery bus voltage. Reference [247] features an isolated DC/DC PHEV battery charger that can be used in the proposed bilayer system. The efficiency curve of the selected charger is depicted in Figure 7-8.

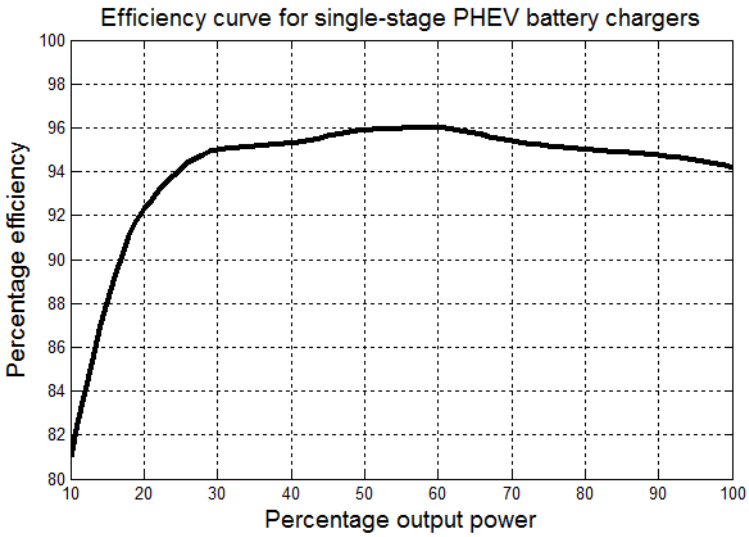

Figure 7-8: Efficiency curve for single-stage PHEV battery chargers

7.3.8 Compatibility of PV Inverters with the Proposed Bilayer System

As mentioned earlier in Section 2.2.2, most PCUs for PV systems are usually composed of two power conversion stages: a DC/DC maximum power point tracking stage with an embedded high-frequency transformer for galvanic isolation, along with a DC/AC inversion stage that performs the grid synchronization functions.

This arrangement can be modified for use in the proposed bilayer system through the elimination of the DC/AC inversion stage. PV electricity conversion losses will thus be reduced, resulting in a subsequent increase in the total energy generated by PV arrays. Reference [248] features a high efficiency DC/DC converter for PV systems that could be used in the proposed architecture. The efficiency curve of the selected single-stage PV DC/DC converter is depicted in Figure 7-9.

7.4 Proposed Operation of the Bilayer System

As explained earlier, the bilayer system should be designed in such a way as to alleviate secondary distribution transformer overloading during PHEV peak charging periods and to limit the reverse flow of power when PV arrays are generating their peak output. Important question at this point is how much power should be rectified/inverted by each converter and how much should be stored/discharged by each BESS, such as to achieve the previous goals?

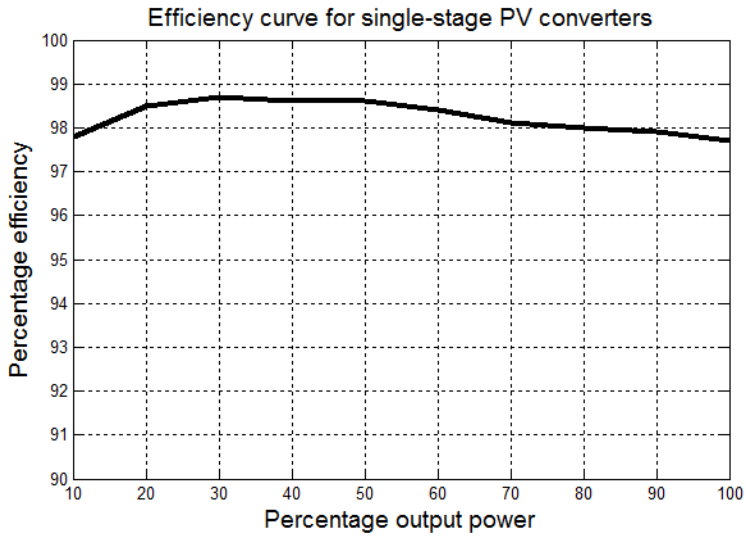

Figure 7-9: Efficiency curve for single-stage PV converters

A very important issue for consideration in the planning of bilayer system operation is that the power exchanged between the two layers via the bidirectional converter should be maximized and the power stored/discharged by the BESS should be minimized, for the following reasons:

i) According to Table 7-2, the DC/DC round trip efficiency of the most efficient storage technology is only 81%, whereas power conversion efficiency can reach up to 96% (as shown in Figure 7-7) Accordingly, the more energy stored in the BESS, the greater the system losses.

ii) Electricity usually costs less to convert than to store [137, 205, 249].

Based on these factors, the operation of each DC module can be summarized as follows:

7.4.1 Operation of the Proposed Bilayer System during the Daytime

During that time, residential PV arrays are generating their electrical output that is processed through local DC/DC power electronic converters. The DC power output of individual arrays is used for supplying any daytime PHEV charging. During that time, the bidirectional converter operates in DC/AC inversion mode, converting part of the DC power into AC electricity suitable for feeding into the AC grid (as shown in Figure 7-10).

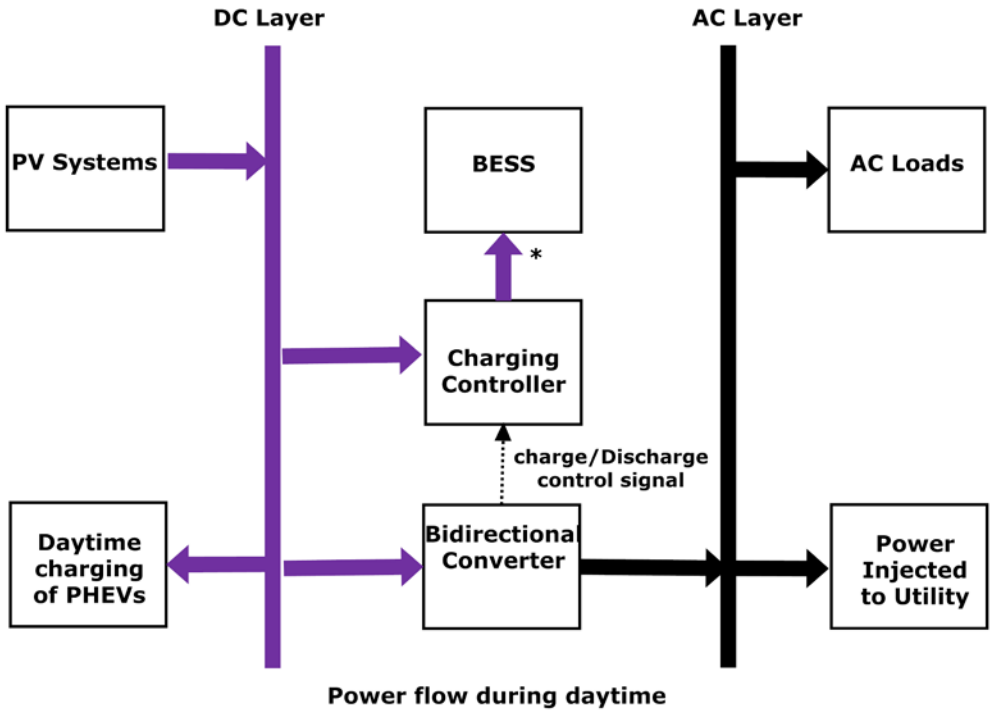

Figure 7-10: Operation of the bilayer system during the daytime

However, as shown in Figure 7-10, at noon, when PV arrays are at peak output, there will be times when inverting all available DC electricity will result in excessive reverse power flow through the distribution transformer. In such cases, the BESS operates in the charging state and stores the excess active power so that the reverse power flow through the distribution transformer is limited to a specific threshold defined based on utility regulations. As mentioned earlier, in Ontario, reverse power flow is restricted to 60% of the transformer rating. The theoretical active power stored in the BESS in this case equals:

$$P_{Ch}(i) = Max\left(-P_{DC\,bus}(i) - \frac{60\% S_{Trans\,Rated} + P_{Loads,AC}(i)}{\eta_{Inv}}, 0\right) \quad (7.1)$$

where $P_{Ch}(i)$ is the theoretical active power stored in the BESS at hour i, $S_{Trans\,Rated}$ is the transformer kVA rating, $P_{Loads,AC}(i)$ is the active power consumed by AC loads connected to the distribution

transformer LV bus at hour *i*, η_{Inv} is the converter's inversion efficiency and $P_{DC\ bus}(i)$ is the aggregated DC power at the bidirectional converter DC bus, as given by:

$$P_{DC\,bus}(i) = P_{PHEVs,DC}(i) + LOSS_{DCSD}(i) - P_{PVs,DC}(i) \tag{7.2}$$

where $P_{PHEVs,DC}(i)$ is the power consumed by all PHEVs connected to the bidirectional converter DC bus at hour *i*, $P_{PVs,DC}(i)$ is the corresponding PV power generated at hour *i* and $Loss_{DCSD}(i)$ is the power loss in the DC service drops at hour *i*.

However, the actual power that can be charged into the BESS in one hour is constrained by its power and energy ratings, as follows:

$$P_{Ch,Act}(i) = Min(P_{Ch}(i), S_{BESS\ Rated}, \frac{E_{BESS\ Rated} - E(i-1)}{\eta_{Ch}}) \tag{7.3}$$

where $P_{Ch,Act}(i)$ is the actual power charged into the BESS at hour *i*, $S_{BESS\ Rated}$ is the power rating of the BESS in kVA, $E_{BESS\ Rated}$ is the energy rating of the BESS in kWh, $E(i-1)$ is the energy stored in the BESS at hour ($i-1$) in kWh, and η_{Ch} is the BESS charging efficiency.

The charging losses ($Loss_{Ch}(i)$) in kW are given by:

$$Loss_{Ch}(i) = P_{Ch,Act}(i) \times (1 - \eta_{Ch}) \tag{7.4}$$

The stored energy level in the BESS after operating in this state for one hour ($E(i)$) is given by:

$$E(i) = E(i-1) + (P_{Ch,Act}(i) \times \eta_{Ch} \times 1h) \tag{7.5}$$

In this operating state, the input DC power inverted by the bidirectional converter ($P_{Inv}(i)$) in kW equals:

$$P_{Inv}(i) = -P_{DC\,bus}(i) - P_{Ch,Act}(i) \tag{7.6}$$

The inversion losses ($Loss_{Inv}(i)$) in kW are given by:

$$Loss_{Inv}(i) = P_{Inv}(i) \times (1 - \eta_{Inv}) \tag{7.7}$$

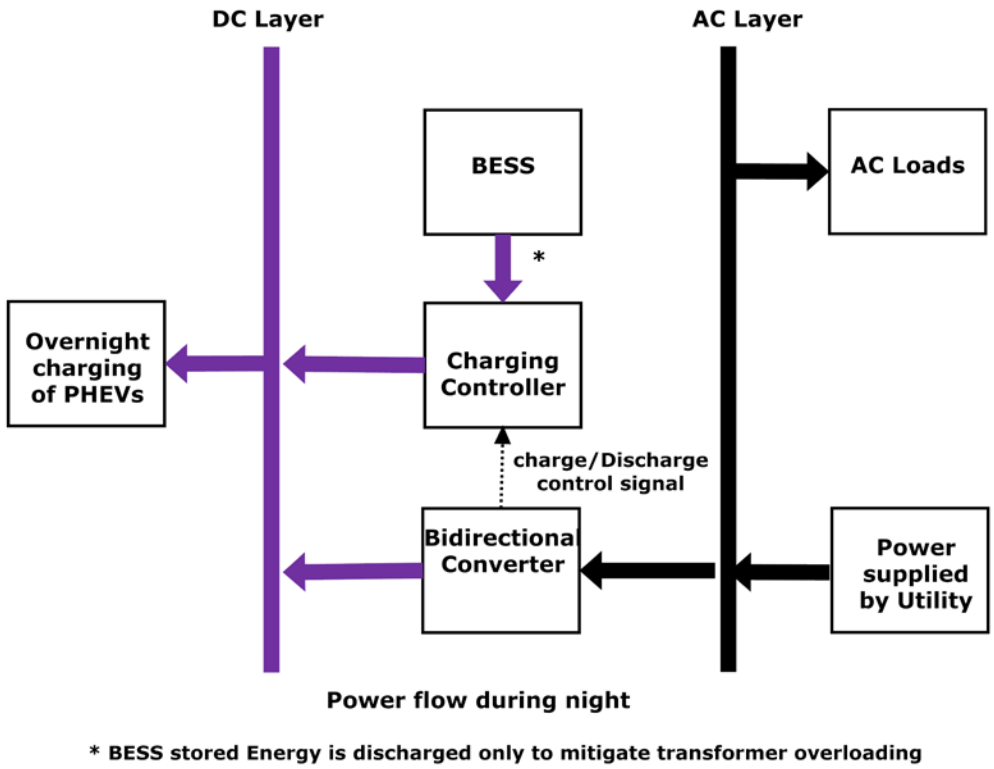

Figure 7-11: Power flow in the bilayer system during the evening and nighttime

7.4.2 Operation of the Proposed Bilayer System during the Evening and Nighttime

During that time Most PHEVs are being charged at residences, and PV systems are not generating electricity. The bidirectional converter therefore operates in rectification mode, and energy flows from the AC layer of the system into the DC module to meet PHEV charging requirements (as shown in Figure 7-11). However, as shown in Figure 7-11, there will be instances when the power that should be rectified in order to meet PHEV DC charging requirements will cause the distribution transformer to exceed its rated capacity. In such cases, the BESS operates in the discharging state and injects active power into the DC layer so as to avoid overloading the distribution transformer. The theoretical active power that should be discharged by the BESS in this case equals:

$$P_{Dis}(i) = Max\left(P_{DC\,bus}(i) - \left(\sqrt{S^2_{Trans\,Rated} - Q^2_{Loads,AC}(i)} - P_{Loads,AC}(i)\right) \times \eta_{\mathrm{Rec}}, 0\right) \qquad (7.8)$$

where $P_{Dis}(i)$ is the theoretical active power discharged by the BESS at hour *i*, $Q_{Loads,AC}(i)$ is the kVAR reactive power consumed by AC loads connected to the distribution transformer LV bus at hour *i*, and η_{Rec} is the bidirectional converter's rectification efficiency.

The actual power that can be discharged by the BESS in one hour, however, is constrained by its power rating as well as by the minimum reserve level ($E_{BESS\ Reserve}$):

$$P_{Dis,Act}(i) = Min(P_{Dis}(i), S_{BESS\ Rated} \times \eta_{Dis}, (E(i-1) - E_{BESS\ Reserve}) \times \eta_{Dis}) \tag{7.9}$$

where $P_{Dis,Act}(i)$ is the actual power discharged by the BESS at hour *i*, and η_{Dis} is the BESS discharging efficiency.

The discharging losses ($Loss_{Dis}(i)$) in kW are given by:

$$Loss_{Dis}(i) = P_{\mathrm{Dis},Act}(i) \times \frac{(1-\eta_{Dis})}{\eta_{Dis}} \tag{7.10}$$

The kWh energy level in the BESS after operating in this state for one hour ($E(i)$) equals:

$$E(i) = E(i-1) + (\frac{P_{Dis,Act}(i)}{\eta_{Dis}} \times 1h) \tag{7.11}$$

In this operating state, the input AC power being rectified by the bidirectional converter ($P_{Rec}(i)$) in kW equals:

$$\mathrm{P}_{\mathrm{Rec}}(i) = \frac{P_{DC\ bus}(i) - P_{\mathrm{Dis},Act}(i)}{\eta_{\mathrm{Rec}}} \tag{7.12}$$

The corresponding kW rectification losses ($Loss_{Rec}(i)$) equal:

$$Loss_{\mathrm{Rec}}(i) = P_{\mathrm{Rec}}(i) \times (1-\eta_{\mathrm{Rec}}) \tag{7.13}$$

However, as explained earlier, sizing and scheduling the operation of the BESS/bidirectional converter set such as to always have sufficient energy and power capacities to accommodate the surplus PV electricity (during peak production periods), and to supply the deficit in power (during peak charging period) is a challenging task due to uncertainties associated with the PV array output

existing electrical loads and the PHEV charging demand. For this chapter, the author developed a MC-based probabilistic benchmark (similar to that described in Chapters 5 and 6) for modeling these uncertainties and for use with the sizing and scheduling of different system components.

7.5 MC-Based Probabilistic Benchmark

This section describes different stages of the probabilistic benchmark used to design the proposed bilayer system.

7.5.1 Modeling Uncertainties Present in the System

The first step in implementing the proposed benchmark is the utilization of the probabilistic models previously developed in Chapter 3 to describe different uncertainties inherent in the system. To model the stochastic nature of PV array output, hourly temperature and insolation data for one year obtained from the Solar Radiation Research Laboratory were analyzed using the modeling approach described in Section 3.2. In this approach, PCA and data clustering are used to generate 19 daily output profiles that represent the stochastic nature of the variable PV supply while retaining the temporal variations within the data. The probabilities of occurrence of different output profiles are then computed and later used in the MC simulation in order to generate random PV output profiles.

To model the stochastic nature of existing residential loads, the hourly load profiles for one year given in [156] were analyzed using the load modeling approach described in Section 3.3, which represents the stochastic nature of residential loads using six daily profiles rather than 365. As explained earlier, since commercial loads are characterized by low variability in their electrical demand [171], they are represented by only one load curve, given in Figure 4-1.

To model individual driving habits that affect PHEV charging, the author employed the technique outlined in Section 3.4. Data provided by the 2009 U.S. NHTS were used for the extraction of cdfs representing daily mileage and home arrival times. These cdfs (depicted in Figures 3-16 and 3-17) are then employed in the random generation of PHEV charging profiles. To model uncertainties related to PHEV type, three types of vehicles were considered: automobiles, vans, and SUVs. As with Section 4.3.3.1, these types are assumed to have the same market share as reported in the 2009 NHTS for their gasoline counterparts. For each vehicles class, a representative PHEV was selected to exemplify the whole class.

7.5.2 Generating Random Profiles for Stochastic Electrical Quantities

As explained earlier, the MC simulation procedure starts with the generation of random profiles for the stochastic quantities in the system. The load modeling approaches explained above are first used for the generation of random loading profiles for all loads in the system (residential and commercial). The analysis continues with the generation of random output profiles for all residential PV arrays existing in the system. Since all PV arrays are located within the same residential area, they are all subject to identical environmental conditions, and are thus assigned the same daily output profile. The efficiency curves for double-stage (DC/DC-DC/AC) PV inverters (used in the traditional single layer AC system) and single-stage (DC/DC) PV converters (used in the proposed bilayer system) are depicted in Figures 3-4 and 7-9, respectively.

The final step is to use the cdfs depicted in Figures 3-16 and 3-17 to generate random PHEV charging profiles. As mentioned in Section 4.4.3, the *SOC* of the battery when each PHEV arrives home, and hence the energy required to charge its battery, depends on the random daily distance travelled. Because drivers are most likely to plug in their vehicles as soon as they arrive home, the random home arrival time is taken to be the charging start time [157, 167]. The duration required to charge the battery is dependent on the charging level. For the existing AC system, SAE J1772 standard [173] defines two residential AC charging levels for PHEVs: level-1 (1.44 kW) and level-2 (7.2 kW). The results obtained in Section 4.5 have demonstrated that level-2 chargers impact distribution networks more severely than level-1 chargers. For this work, the author therefore assumed the worst case scenario, in which all PHEVs in the AC system are charged by level-2 chargers. As mentioned earlier, double-stage battery chargers are reported to have an average efficiency of 90% [99, 163, 164]). For DC PHEV charging, the aforementioned standard defines two DC charging levels: DC level-1 chargers (16 kW to 36 kW) and DC level-2 rapid chargers (40 kW to 90 kW). Because they require special equipment and installation procedures to ensure safety, DC level-2 rapid chargers are expensive ($40,000 to $85,000) [250] and thus highly unlikely to be used for residential PHEV charging. For this research, the most basic level-1 DC chargers (16 kW) were therefore adopted. This simple arrangement, however, is capable of charging all currently commercially available PHEVs in less than 1 hour. The efficiency curve for the selected charger is depicted in Figure 7-8, as per [247].

` `

Following the procedure explained in Section 4.4.3, establishing the charging start time, the power rating of the charger, and the required charging duration enables an accurate determination of the charging profile for each PHEV present in the system.

7.5.3 Running the Load Flow Analysis

In the existing single layer AC system, all loads and generation sources are connected directly to the AC network. Thus, the three electrical quantities obtained using the previous models are aggregated for each household in order to form the inputs to the OpenDSS software used for the execution of the load flow analysis. However, this approach is unsuitable for the bilayer system because PV arrays and PHEVs are connected to the DC layer of the system, and the load flow analysis is thus executed in three stages:

i) In the first stage, MATLAB software is used to perform a DC backward-forward sweep load flow analysis for each DC module. During this stage, voltages at the bidirectional converters DC buses are assumed to be regulated at 120 Vdc. This stage calculates the losses in DC service drops, the DC voltages at different customers, and the lumped DC power at each DC converter bus.

ii) In the second stage, using the methodology described in the next section, BESS charging controllers determine the amount of DC power to be stored/discharged into/out of each BESS, and the remaining DC power is rectified/inverted into/from the AC layer of the system. By utilizing the bidirectional converter efficiency curve given in [243] and depicted in Figure 7-7, the equivalent powers for all DC modules seen at the AC side of the system can be determined.

iii) After representing the DC modules by their equivalent powers seen at the AC side of the system, the final step involves a traditional AC distribution system load flow analysis for the aggregated system using OpenDSS software.

7.5.4 Reiterating the Analysis

The above analysis is executed 365 times every year and is repeated for several thousands of years until the stopping criterion given in Eq. (4.4) is fulfilled. The resulting electrical quantities (power flows, voltages, losses, number of operations of voltage regulators, etc.) for each year are calculated and stored for future processing.

7.6 Probabilistic Sizing and Scheduling Methodology

This section describes the proposed probabilistic methodology used for sizing and scheduling the operation of different system components.

7.6.1 BESS Sizing

In this section, the author is presenting different stages of the proposed BESS sizing methodology. The proposed methodology is similar to that outlined in Section 6.4.3. A flowchart of the proposed methodology is depicted in Figure 7-12.

7.6.1.1 Determining Daily Charging/Discharging Periods

The proposed BESS sizing methodology starts with the running of the MC simulation for the test system without the inclusion of any BESSs and with the assumption that all DC power is inverted/rectified by the bidirectional converters. According to the MC simulation results, each day is divided into three periods:

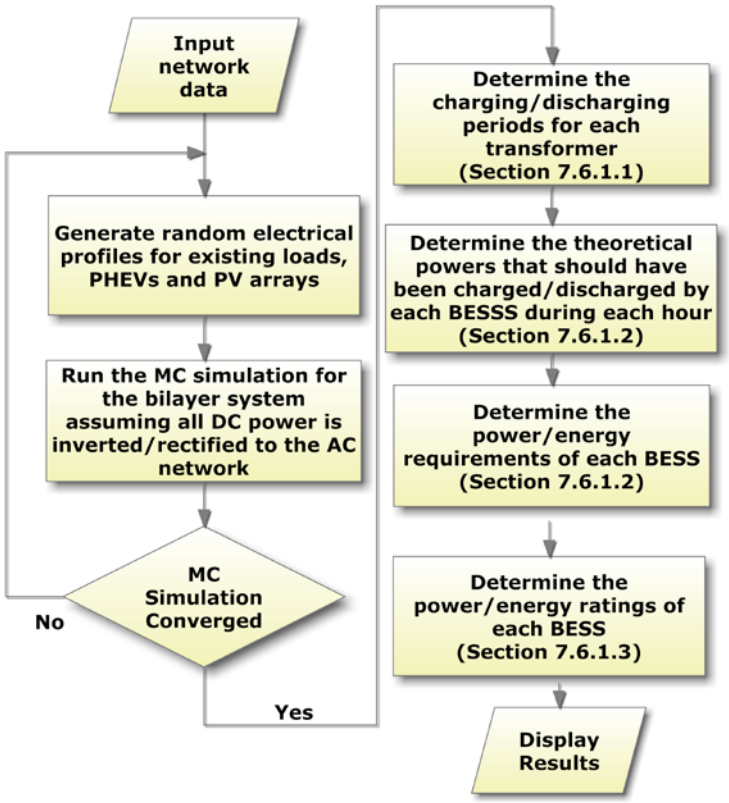

Figure 7-12: BESS probabilistic sizing methodology

` `

i) The controlled charging/discharging period: In this period (usually around late night), the distribution transformer is unlikely to be subjected to overloads or reverse power flow; the probability of either situation occurring is less than 5% (corresponding to a 95% confidence level). The BESS can thus operate in any state such as to regulate the stored energy level at a specific pre-designated level. The BESS energy level at the end of this period is denoted by E_1.

ii) The forced charging period: In this period (usually around noon), the probability of reverse power flow (due to inverted PV electricity) is greater than 5%, and the probability of overloading the distribution transformer (due to rectified PHEV charging demands) is less than 5%. The distribution transformer is thus very likely to be subjected to reverse power flow. The energy level in BESS at the end of this period is denoted by E_2.

iii) The forced discharging period: During this period (usually around evening), conditions are the opposite of those that occur during the previous period because the probability of overloading the distribution transformer is greater than 5%, and the probability of reverse power flow is less than 5%. The distribution transformer is thus very likely to be overloaded. The BESS energy level at the end of this period is denoted by E_3.

7.6.1.2 Determining Energy and Power Requirements

After these periods have been defined, equations (7.1) and (7.8) are used for the calculation of the amount of theoretical DC power that should have been charged/discharged by the BESS during each hour throughout the entire simulation period to mitigate distribution transformer overloading and limit the reverse flow of power through the transformer so that it is kept within permissible limits. During this stage, the kWh and kVA rating constraints are not taken into consideration. Once these charging/discharging powers have been determined, four important quantities are evaluated:

i) Theoretical daily charged energy (E_{Ch}): The summation of active powers charged into the BESS throughout the day.

ii) Theoretical daily discharged energy (E_{Dis}): The summation of active powers discharged by the BESS throughout the day.

iii) Theoretical hourly converter charging rating ($S_{Ch}(i)$): This quantity is calculated for the hours during which the BESS operates in the charging state. The designated charging rating for a given hour equals the active power charged into the BESS during that hour.

iv) Theoretical hourly converter discharging rating ($S_{Dis}(i)$): This quantity is calculated for the hours during which the BESS operates in the discharging state. The designated discharging rating for a given hour equals the active power discharged by the BESS during that hour.

The analysis then continues with the calculation of the cfd curves for the previous four quantities for each anticipated BESS. The developed cfds are used for the estimation of the following six quantities:

i) Maximum daily charged energy with 95% confidence ($E_{Ch}^{\max}$): This quantity is defined as the energy corresponding to 95% probability on the daily charged energy cfd curve. This definition implies that there is only a 5% probability of charging an amount of daily energy that exceeds this value, or in other words, the designated energy is the maximum daily charged energy with 95% confidence.

ii) Minimum daily charged energy with 95% confidence ($E_{Ch}^{\min}$): This quantity is the energy corresponding to 5% probability on the daily charged energy cfd curve, implying that the designated energy is the minimum daily charged energy with 95% confidence.

iii) Maximum charging kVA with 95% confidence ($S_{Ch}^{\max}$): This quantity is the kVA corresponding to 95% probability on the hourly BESS charging rating cfd curve and is used for the determination of the BESS power rating during the charging process.

iv) Maximum daily discharged energy with 95% confidence ($E_{Dis}^{\max}$): This quantity is the energy corresponding to 95% probability on the daily discharged energy cfd curve.

v) Minimum daily discharged energy with 95% confidence ($E_{Dis}^{\min}$): This quantity is the energy corresponding to a 5% probability on the daily discharged energy cfd curve, implying that the designated energy is the minimum daily discharged energy with 95% confidence.

vi) Maximum discharging kVA with 95% confidence ($S_{Dis}^{\max}$): This quantity is the kVA corresponding to 95% probability on the hourly BESS discharging rating cfd curve and is used for the determination of the BESS power rating during the discharging process.

`  `

7.6.1.3 Determining the BESS Energy and Power Ratings

The previous six quantities are then used for the estimation of the BESS energy and power ratings. To this end, the two most-extreme situations are considered:

i) The BESS is charged by $E_{Ch}^{\min}$ and discharges $E_{Dis}^{\max}$: This situation enables a determination of the energy to be charged/discharged during the controlled charging/discharging period. In this case, the BESS should have sufficient energy at the beginning of the day to allow it to discharge $E_{Dis}^{\max}$ (in the forced discharging period) after being charged only by $E_{Ch}^{\min}$ (in the forced charging period) while keeping the level of stored energy above the minimum allowable reserve level ($E_{BESS\ Reserve}$). This case necessitates that the charging/discharging process during the controlled charging/discharging period be such that the energy level at the end of this period (E_1) is at least:

$$E_1 = Max\,(E_{BESS\ \mathrm{Reserve}}, E_{BESS\ \mathrm{Reserve}} + E_{Dis}^{\max} - E_{Ch}^{\min}) \tag{7.14}$$

ii) The BESS is charged by $E_{Ch}^{\max}$ and discharges $E_{Dis}^{\min}$: This situation enables the energy rating of the BESS to be determined. In this case, the maximum energy level in the BESS occurs at the end of the forced charging period (E_2). The BESS energy rating is therefore selected so that it can be charged by $E_{Ch}^{\max}$ (in the forced charging period) without exceeding its energy rating.

This criterion is met if the BESS has an energy rating of:

$$E_{BESS\ Rated} = E_1 + E_{Ch}^{\max} \tag{7.15}$$

Substituting E_1 from Eq. (7.14) into the previous equation yields:

$$E_{BESS\ Rated} = Max\,(E_{Ch}^{\max} + E_{BESS\ \mathrm{Reserve}}, E_{Ch}^{\max} + E_{BESS\ \mathrm{Reserve}} + E_{Dis}^{\max} - E_{Ch}^{\min}) \tag{7.16}$$

The sizing methodology presented above ensures that the energy stored in the BESS throughout the day satisfies the following:

$$E_{BESS\ \mathrm{Reserve}} \le E(i) \le E_{BESS\ Rated} \tag{7.17}$$

The kVA power rating of the BESS is determined based on $S_{Ch}^{\max}$ and $S_{Dis}^{\max}$, as follows:

$$S_{BESS\,Rated} = Max(S_{Ch}^{\max}, S_{Dis}^{\max}) \tag{7.18}$$

Finally, BESSs are assumed to have power and energy ratings that are multiples of 5 kVA and 5 kWh, respectively. The ratings obtained are thus rounded to the next commercially available rating.

7.6.2 Bilayer System Scheduling

Based on the previous discussion, the operation of the bilayer system is scheduled as shown in Figure 7-13:

7.6.2.1 Forced Charging Mode

This operating mode occurs during the forced charging period when the PV power results in a reverse power flow that exceeds 60% of the transformer rating. Equations (7.1) to (7.7) describe this mode of operation.

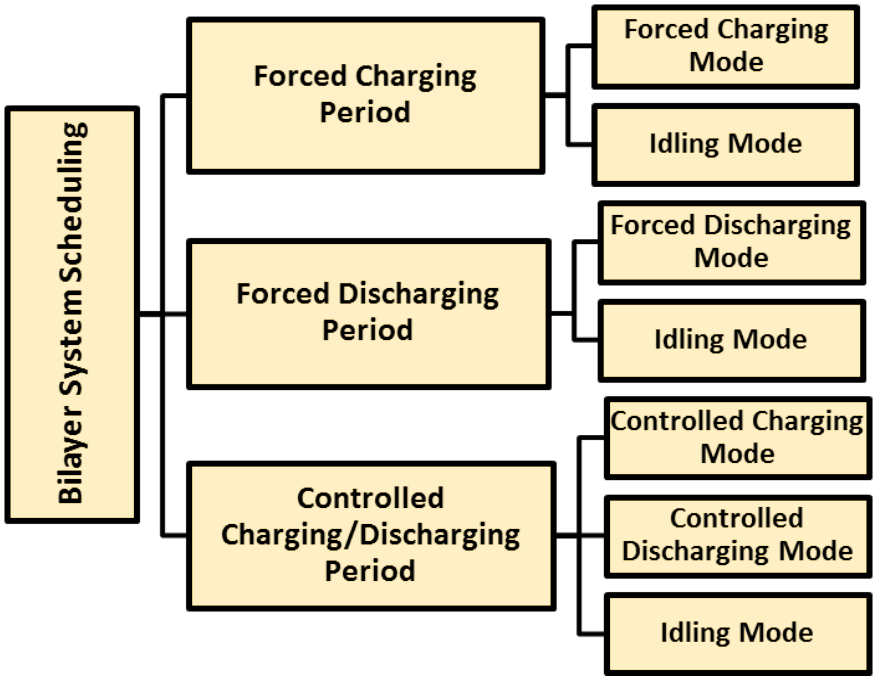

Figure 7-13: Bilayer system scheduling

`  `

7.6.2.2 Forced Discharging Mode

This operating mode occurs during the forced discharging period when the power rectified to meet PHEV DC charging requirements causes the distribution transformer to exceed its rated capacity. In this case, the BESS then limits transformer overloading by injecting active power. BESS operation in this period is expressed by equations (7.8) to (7.13).

7.6.2.3 Controlled Charging/Discharging Mode

This operating mode occurs during the controlled charging/discharging period. In this case, the energy stored in the BESS is regulated at the predetermined E_1 levels. The following two cases are considered:

i) The Energy stored in the BESS is less than E_1: In this case, the BESS operates in the controlled charging mode, storing active power until the stored energy reaches the desired E_1 level:

$$P_{Ch,Act}(i) = Min\left(\frac{E_1 - E(i)}{\eta_{Ch}}, S_{BESS\ Rated}, \sqrt{S^2_{Trans\ Rated} - Q^2_{Loads,AC}(i)} - P_{Loads,AC}(i)\right) \quad (7.19)$$

The charging losses ($Loss_{Ch}(i)$) and the kWh energy level after operation in this mode for one hour ($E(i)$) are given by equations (7.4) and (7.5), respectively. The DC power inverted by the converter and the corresponding losses are given by equations (7.6) and (7.7), respectively.

ii) Energy stored in the BESS is greater than E_1: In this case, the BESS operates in the controlled discharging mode, injecting active power until the stored energy reaches the desired E_1 level. However, the power injected by the BESS must not create a reverse power flow through the distribution transformer in excess of 60% of its rating. The active power discharged equals:

$$P_{Dis,Actual}(i) = Min\left((E(i) - E_1) \times \eta_{Dis}, S_{BESS\ Rated} \times \eta_{Dis}, P_{Loads,AC}(i) + 60\% S_{Trans\ Rated}\right) \quad (7.20)$$

The discharging losses ($Loss_{Dis}(i)$) and the kWh energy level after operating in this mode for one hour ($E(i)$) are established from (7.10) and (7.11), respectively. The DC power rectified by the bidirectional converter and the rectification losses are given by (7.12) and (7.13).

`

`

7.6.2.4 Idling Mode

If the conditions for any of the previous modes of operation have not been met, the bilayer system operates in the idling mode. In this mode, the BESS does not consume or produce any active power but incurs only idling losses ($Loss_{Idling}(i)$) corresponding to the power consumed in ancillary components and internal controls and are usually represented as a percentage of the BESS's kVA rating. For this research, these losses are taken as 1% of the BESS's kVA rating [203, 204]:

$$Loss_{Idling}(i) = 1\% \times S_{BESS\ Rated} \tag{7.21}$$

These losses are supplied by the DC layer of the system so that the level of energy stored in the BESS remains unchanged. The converter can thus operate in either rectification or inversion mode, depending on the sign of the DC power:

i) If $P_{DC\ bus} < 0$ (PV generation exceeds PHEV charging demands), the converter operates in inversion mode and the DC power input to the converter is given by:

$$P_{Inv}(i) = -P_{DC\ bus}(i) - Loss_{Idling}(i) \tag{7.22}$$

The corresponding inversion losses are given by Eq. (7.7).

ii) If $P_{DC\ bus} > 0$ (PHEV charging demands exceed PV production), the converter operates in rectification mode, and the AC power input to the converter is given by:

$$P_{\mathrm{Rec}}(i) = \frac{P_{DC\ bus}(i) + Loss_{Idling}(i)}{\eta_{\mathrm{Rec}}} \tag{7.23}$$

The corresponding rectification losses are given by Eq. (7.13).

7.6.3 Bidirectional Converter Sizing

Bidirectional converter ratings are determined using a methodology similar to that outlined in Section 7.6.1. The flowchart of the proposed methodology is depicted in Figure 7-14.

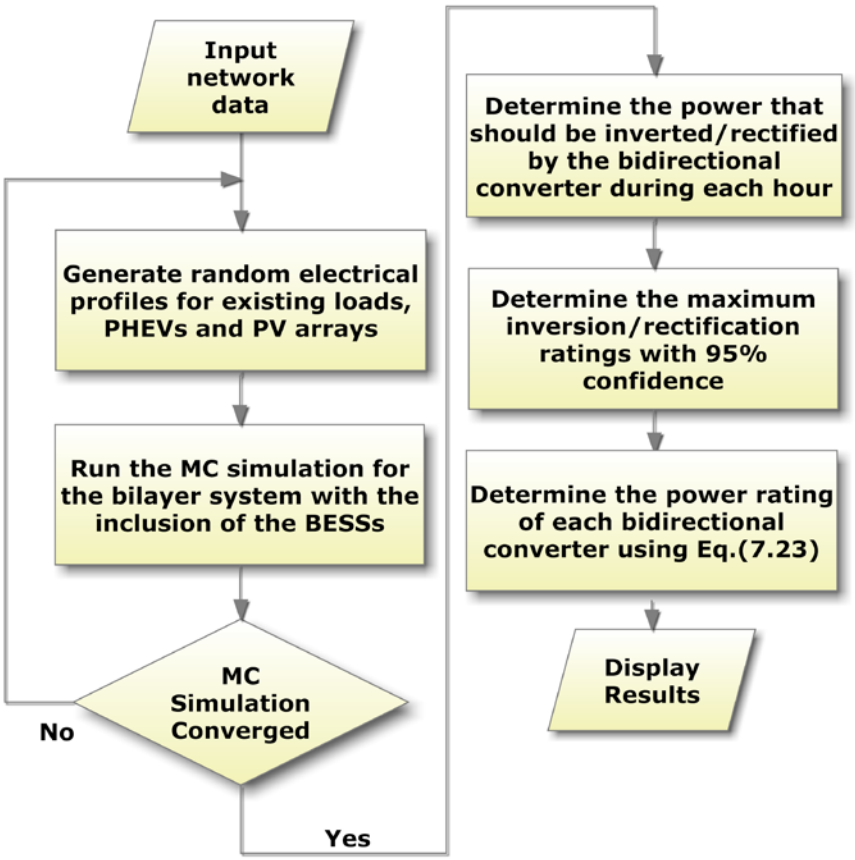

Figure 7-14: Bidirectional converter probabilistic sizing methodology

The sizing methodology starts with the running of the MC simulation for the bilayer system after the inclusion of the previously designed BESSs. After the MC simulation converges, equations (7.6), (7.12), (7.22) and (7.23) are used for calculating the theoretical powers that should be inverted/rectified by each converter during each hour throughout the entire simulation period. Once these powers levels have been determined, two quantities are evaluated for each converter:

i) Hourly converter inversion rating ($S_{Inv}(i)$): This quantity is calculated only for the hours during which the converter operates in DC/AC inversion mode. The designated inversion rating for a given hour equals the input DC power inverted by the bidirectional converter during that hour ($P_{Inv}(i)$).

ii) Hourly converter rectification rating ($S_{Rec}(i)$): This quantity is calculated for the hours during which the converter operates in AC/DC rectification mode. The designated rectification rating for

a given hour equals the input AC power rectified by the bidirectional converter during that hour ($P_{Rec}(i)$).

The analysis continues with the development of cfd curves for the previous two quantities for each converter present in the system. The resulting cfds are then employed for the estimation of the following two quantities:

i) Maximum converter inversion kVA with 95% confidence ($S_{Inv}^{\max}$): This quantity is the kVA corresponding to 95% probability on the hourly converter inversion cfd curve.

ii) Maximum converter rectification kVA with 95% confidence ($S_{Rec}^{\max}$): This quantity is the kVA corresponding to 95% probability on the hourly converter rectification cfd curve.

These quantities are used for calculating the required converter rating ($S_{Conv\ Rated}$) as follows:

$$S_{Conv\,Rated} = Max(S_{Inv}^{\max}, S_{Rec}^{\max}) \tag{7.24}$$

Similarly, bidirectional converter kVA ratings are assumed to be multiples of 5 kVA, so the ratings obtained are rounded to the next commercially available rating.

7.7 Case Study

This section outlines the case study used to evaluate the performance of the proposed bilayer system.

7.7.1 Description of the Test System

The author uses the same test system used in previous chapters. As mentioned earlier, this system is an expanded version of the IEEE 123 node test, in which each existing 22.36 kVA spot load has been expanded into a 25 kVA distribution transformer that supplies 5 households, and each 44.72 kVA spot load has been expanded into a 50 kVA distribution transformer that feeds 10 households. The system thus has a total of 625 residential customers. As explained earlier, each secondary distribution transformer should be equipped with a DC module that is connected to the transformer LV bus. Accordingly, the test system will have a total of 78 distinct DC modules. The remaining 13 spot loads are assumed to be commercial loads serving the residential area. The system was modeled using OpenDSS from the substation down to the customer meter, resulting in a system with 1684 nodes.

`  `

7.7.2 Study Assumptions and Scenarios

In this chapter, and similar to the assumptions adopted in Section 5.2.3.2, two penetration levels are assumed for PHEVs, based on the results presented in [101, 184]: short-term projection (2031 case) with 28% penetration and long-term projection (2052 case) with 52% penetration. Given that the 2009 NHTS estimates the average number of vehicles per household to be 1.9 vehicle/household, the total number of PHEVs to be considered for the short- and long-term projections is calculated to be 333 and 618, respectively. PHEVs are randomly assigned to the 625 end customers, maintaining the appropriate percentage of each vehicle type (63.08% automobiles, 10.48% vans, and 26.44% SUVs). In the case of PV arrays, it was assumed that that each household with a PHEV is equipped with a 10 kW PV array (maximum allowable size for small generation in Ontario [183]). The rationales behind these assumptions are explained in detail in Section 5.2.3.2 and 5.2.3.3. Finally, similar to the assumption adopted in Section 6.5.2, the basic reserve level ($E_{BESS\ Reserve}$) for BESSs is taken as 30% of their rated kWh [201].

The purpose of this chapter is to assess the validity of the proposed design methodology for the bilayer system and to compare its performance with that of the existing single layer AC system, under a high penetration of PHEVs and PV electricity. To achieve this goal, the author chose five study scenarios that would reflect a variety of situations suitable for both short-term (2031) and long-term (2052) projections. Details of the suggested scenarios are provided in Table 7-3.

Table 7-3: Study scenarios

	Time frame	PHEV penetration	PV arrays	Architecture
Scenario 1-Ch7	Base-case	0%	N/A	Single layer
Scenario 2-Ch7	2031	28%	10 kW/PHEV	Single layer
Scenario 3-Ch7	2031	28%	10 kW/PHEV	Bilayer
Scenario 4-Ch7	2052	52%	10 kW/PHEV	Single layer
Scenario 5-Ch7	2052	52%	10 kW/PHEV	Bilayer

The MC simulation procedure (described in Section 7.5) is executed initially for scenarios 2-Ch7 and 4-Ch7. After that, the probabilistic sizing methodology (explained in Section 7.6) is used to determine the energy and power ratings for each of the 78 BESSs and bidirectional converters present in the system in scenarios 3-Ch6 and 5-Ch6. The MC simulation is then executed again for scenarios 3-Ch7 and 5-Ch7 after the inclusion of the proposed 78 DC modules.

7.8 Results and Discussion

This section presents the results of running the MC simulation procedure for the five study scenarios.

7.8.1 Selecting the Most Economical BESS Technology

The previously explained BESS sizing methodology is used to determine the energy and power ratings for each anticipated BESS, for scenarios 3-Ch7 and 5-Ch7. Using the approach described in Section 6.6.1, the resulting ratings are then applied in the calculation of the annual cost of integrating different BESS technologies (LA, VRLA, NA/S, Zn/Br, and VB batteries) into the test system using the data provided in [205] (and shown in Table 6-2). The results are shown in Table 7-4.

Table 7-4: Annual cost of different BESS technologies ($/year)

	LA	VRLA	NA/S	Zn/Br	VB
Scenario 3-Ch7	211034	513276	4520367	**114919**	249086
Scenario 5-Ch7	477280	1253708	953155	**227109**	589275

The results reveal that Zn/Br batteries offer the most economical option, and will thus be used in the proposed design. In the subsequent sections, only Zn/Br batteries are considered in the analysis.

7.8.2 BESSs Energy and Power Ratings

Figures 7-15 and 7-16 depict the average energy and power ratings of the 78 Zn/Br BESSs installed in the bilayer system (in scenarios 3-Ch7 and 5-Ch7) as a function of the number of PHEV/PV array sets interfaced by the distribution transformer. For example, given a 25 kVA distribution transformer interfacing only one PHEV/PV array set, a BESS with energy and power ratings of approximately 20 kWh and 15 kVA, respectively, should be installed at the bidirectional converter DC bus, such as to mitigate distribution transformer overloading and limit the reverse flow of power through the transformer so that it is kept within permissible limits.

From the results, it becomes evident that due to the non-coincident nature of PHEV charging demands, the normalized BESS energy and power ratings (rating per PHEV/PV array set) decrease as the number of PHEV/PV array sets interfaced by the distribution transformer increases: for a 25 kVA distribution transformer interfacing 5 PHEV/PV array sets, the installed BESS would have average energy and power ratings of only 80 kWh and 22.5 kVA, respectively, rather than 100 kWh and 75 kVA. This corresponds to energy and power diversity factors of 1.25 and 3.33, respectively.

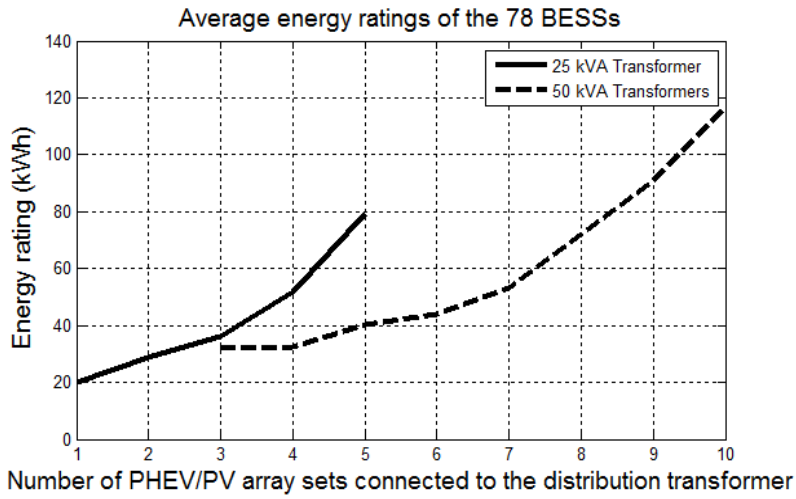

Figure 7-15: Average energy ratings of the 78 Zn/Br BESSs

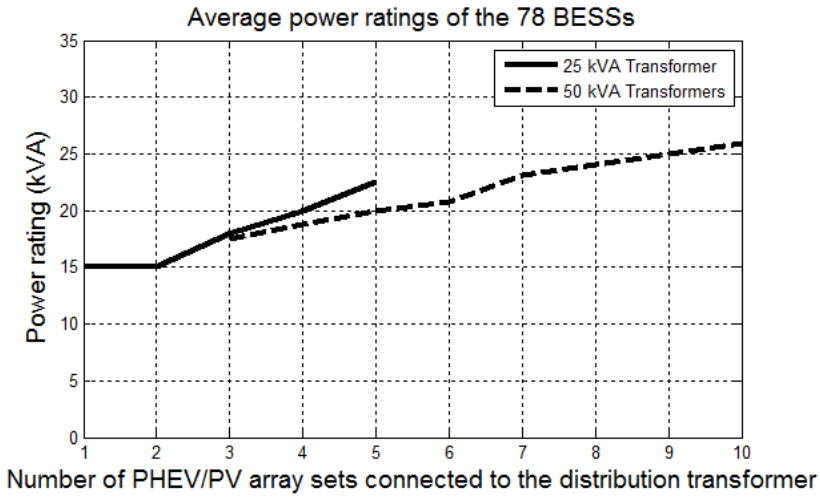

Figure 7-16: Average power ratings of the 78 Zn/Br BESSs

Tables 7-5 and 7-6 give the corresponding minimum and maximum energy/power ratings of the installed BESSs.

7.8.3 Bidirectional Converters Power Ratings

Figure 7-17 depicts the average power ratings of the 78 bidirectional converters installed in the bilayer system (in scenarios 3-Ch7 and 5-Ch7) as a function of the number of PHEV/PV array sets interfaced by the distribution transformer. For example, a 25 kVA distribution transformer interfacing only one PHEV/PV array set would have an average power rating of 10 kVA, as indicated by Figure 7-17.

Table 7-5: Minimum and maximum energy/power ratings of the BESSs (50 kVA transformers)

Number of PHEV/PV array sets	Energy Rating (kWh)		Power rating (kVA)	
	Minimum	Maximum	Minimum	Maximum
1	N/A	N/A	N/A	N/A
2	N/A	N/A	N/A	N/A
3	30	35	15	20
4	30	40	15	20
5	35	45	20	20
6	40	50	20	25
7	45	60	20	25
8	N/A	N/A	N/A	N/A
9	85	95	25	25
10	105	125	25	30

Table 7-6: Minimum and maximum energy/power ratings of the BESSs (25 kVA transformers)

Number of PHEV/PV array sets	Energy Rating (kWh)		Power rating (kVA)	
	Minimum	Maximum	Minimum	Maximum
1	20	20	15	15
2	20	35	15	15
3	30	40	15	20
4	40	65	15	25
5	70	85	20	25

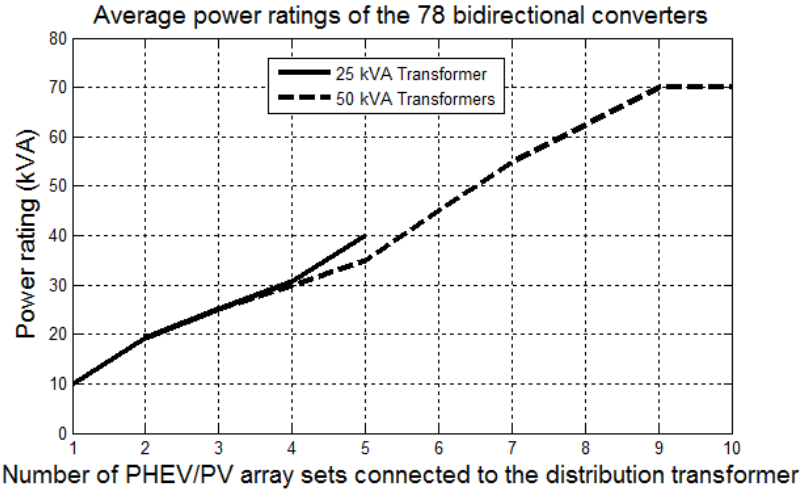

Figure 7-17: Average power ratings of the 78 bidirectional converters

` `

As with BESSs, due to the non-coincident nature of PHEV charging demands, the normalized converter rating (rating per PHEV/PV array set) decreases as the number of PHEV/PV array sets interfaced by the distribution transformer increases: for a 25 kVA distribution transformer interfacing 5 PHEV/PV array sets, the installed bidirectional converter would have an average power rating of only 40 kVA, rather than 50 kVA. This corresponds to a power diversity factor of 1.25. This high diversity will result in significant cost savings for electrical utilities, as shown in a subsequent section. Table 7-7 gives the minimum and maximum power ratings of the installed bidirectional converters.

Table 7-7: Minimum and maximum power ratings of bidirectional converters

Number of PHEV/PV array sets	50 kVA transformers		25 kVA transformers	
	Minimum	Maximum	Minimum	Maximum
1	N/A	N/A	10	10
2	N/A	N/A	15	20
3	25	25	25	25
4	30	30	30	35
5	35	35	40	40
6	45	45	N/A	N/A
7	55	55	N/A	N/A
8	N/A	N/A	N/A	N/A
9	70	70	N/A	N/A
10	70	70	N/A	N/A

7.8.4 Validation of the Bilayer System Design

This section describes the examination of the validity of the proposed design methodology for the bilayer system that was presented in Section 7.6. The validity of the design is evaluated for scenarios 3-Ch7 and 5-Ch7 with respect to the following criteria:

i) Thermal limits of DC service drops
ii) DC voltages at the end customers
iii) BESSs stored energy levels
iv) Thermal limits of the bidirectional converters

7.8.4.1 Thermal Limits of the DC Service Drops

As explained earlier, for mechanical reasons, North American utilities normally use oversized service drops. For this research, the author initially assumed that all DC service drops would have the

minimum conductor size permitted for their AC counterparts. This section describes the author's exploration of the validity of this assumption, for scenarios 3-Ch7 and 5-Ch7. The most important factor for consideration when conductors are sized for a specific application is that the current flowing in the conductors does not exceed their rated ampacity. The author verified this condition by running the MC-based probabilistic benchmark for scenarios 3-Ch7 and 5-Ch7, and then computing the frequency distribution of the currents flowing in all DC service drops during the entire simulation period. As explained earlier, these frequency distributions specify the frequency of occurrence of different ampere loadings in the DC service drops. The next step in the analysis is the development of the cfd for the resulting ampere loadings. The cfd specifies the probability that DC service drops will supply a current that is equal to or less than a specific ampere. However, in distribution planning studies, determining the probability that a component loading will exceed a specific value provides more important information. The last probability is represented by the complement of the cfd (1-cfd). For this reason, in this research, the (1-cfd) curves are used rather than the cfd curves. To simplify the analysis, these (1-cfd) curves are usually normalized with respect to the nominal ampacity of the conductor, as a representation of the percentage current loading.

Figure 7-18 shows the normalized (1-cfd) curve for the current flowing through the DC service drops in the worst case high-penetration scenario (scenario 5-Ch7). The results obtained indicate that the ampere loading in the DC service drops does not exceed 62% of their nominal ampacity, at worst. These results validate the effectiveness of the use of 1/0 AWG service drops for the DC layer of the proposed bilayer system. The previous findings also suggest that the DC layer of the system can be used for supplying additional DC loads without overloading the selected DC service drops.

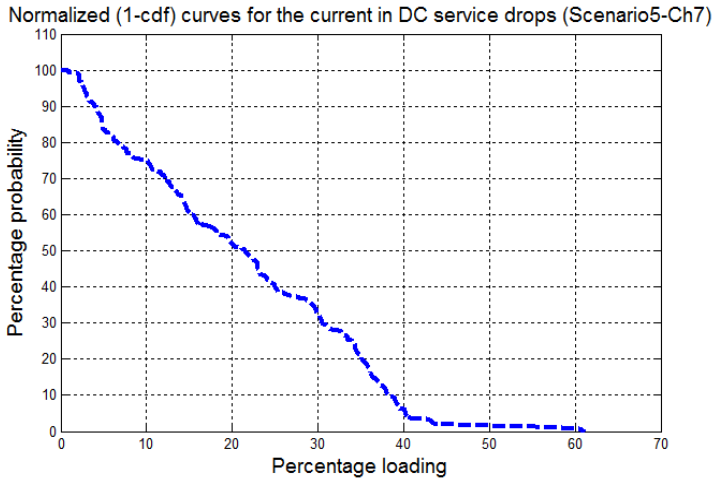

Figure 7-18: Probability of exceeding a specific loading for DC service drops (Scenario 5-Ch7)

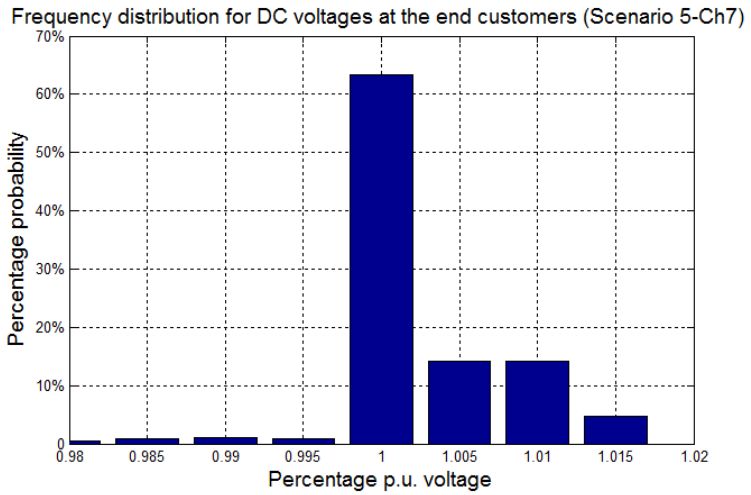

Figure 7-19: Frequency distribution for DC voltages at the end customers (Scenario 5-Ch7)

7.8.4.2 DC Voltages at the End Customers

Another important factor that should be considered in the design of the DC layer of the system is that DC voltages at the end customers must be maintained within acceptable limits. To verify this condition, the author used the three-stage load flow analysis in order to compute the resulting DC voltages at the end customers throughout the entire simulation period. Figure 7-19 shows the frequency distribution for these voltages during the worst case high-penetration scenario (scenario 5-Ch7).

The impact of using oversized DC service drops is quite significant: DC voltages at the end customers, for the worst-case high-penetration scenario (scenario 5-Ch7), will never violate the 0.98 p.u. -1.015 p.u. range, indicating excellent DC voltage profiles, and thus satisfying the design criteria.

7.8.4.3 BESS Stored Energy Levels

According to Eq. (7.17), the energy stored in all BESSs present in the system should always be maintained within $E_{BESS\ Rated}$ and $E_{BESS\ Reserve}$ (taken in this research as 30% of $E_{BESS\ Rated}$).

To verify this condition, the author used the MC simulation results for scenarios 3-Ch7 and 5-Ch7 in order to calculate the frequency distribution of the energy stored in the BESS throughout the entire simulation period. The results for the worst-case high-penetration scenario (scenario 5-Ch7) are depicted in Figure 7-20.

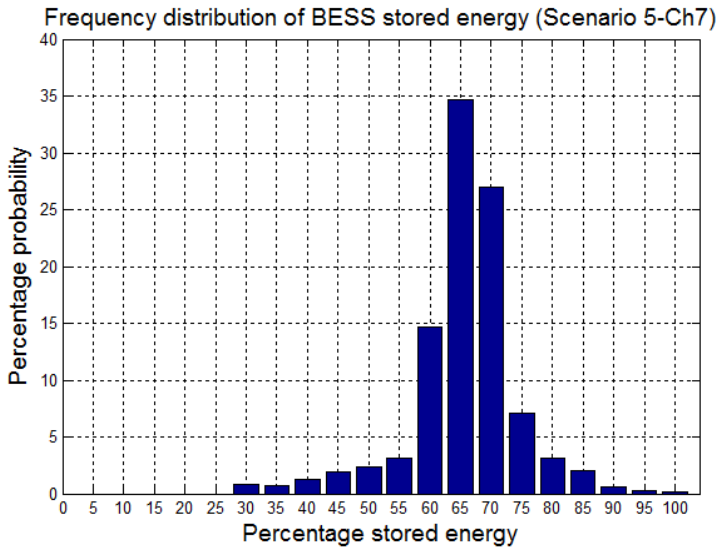

Figure 7-20: Frequency distribution for BESS stored energy (Scenario 5-Ch7)

Figure 7-20 indicates that the energy stored in the BESSs is always maintained within the designated limits (30% to 100% of the rated kWh), thus satisfying the design criteria.

These results confirm the effectiveness of the proposed BESS sizing methodology that was presented in Section 7.6.1. Similar conclusion is obtained for scenario 3-Ch7.

7.8.4.4 Thermal Limits of the Bidirectional Converters

As explained in Section 7.6.3, the power flowing through the bidirectional converters should not exceed their kVA ratings. To verify this condition, the author used the MC simulation results to calculate the probability of exceeding a specific loading percentage for all of the bidirectional converters in the system, for scenarios 3-Ch7 and 5-Ch7. The results are shown in Figure 7-21.

The results confirm the effectiveness of the bidirectional converter sizing methodology explained in Section 7.6.3. Bidirectional converters are unlikely to exceed their kVA ratings: The probability of the bidirectional converter ratings being exceeded is less than 0.04% at worst, thus satisfying the design criteria.

The results obtained in Sections 7.8.4.1-7.4.8.4 confirm the validity of the proposed design methodology for the bilayer system.

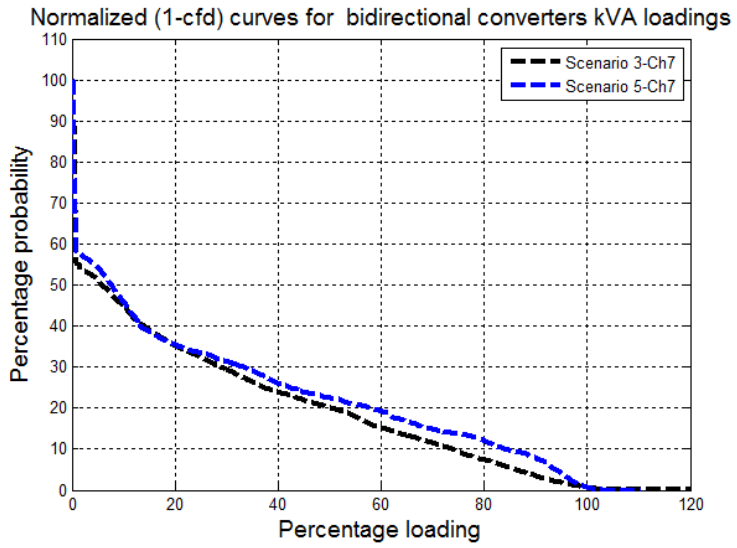

Figure 7-21: Probability of exceeding a specific loading for bidirectional converters

7.8.5 Evaluating the Performance of the Proposed Bilayer System

After the validity of the proposed design methodology for the bilayer system was confirmed, the author used the simulation results abstracted from the developed MC-based probabilistic benchmark in order to compare the performance of the proposed bilayer system (scenarios 3-Ch7 and 5-Ch7) with that of the existing single layer AC system (scenarios 1-Ch7, 2-Ch7, and 4-Ch7) for both short-term (2031) and long-term (2052) projections. The evaluation criteria are discussed in the following subsections.

7.8.5.1 Substation Average Daily Demand

The average daily demand for the distribution substation during the study scenarios is depicted in Figure 7-22. The negative values indicate the occurrence of reverse power flow.

From Figure 7-22, it can be observed that, for scenarios 2-Ch7 and 4-Ch7, PHEV charging demands increase the peak substation demand over the base-case values (scenario 1-Ch7), and shift it from morning to the early evening. PV arrays, on the other hand, produce their maximum output at noon, which, for scenario 4-Ch7, results in reverse power flow through the substation transformer at noon.

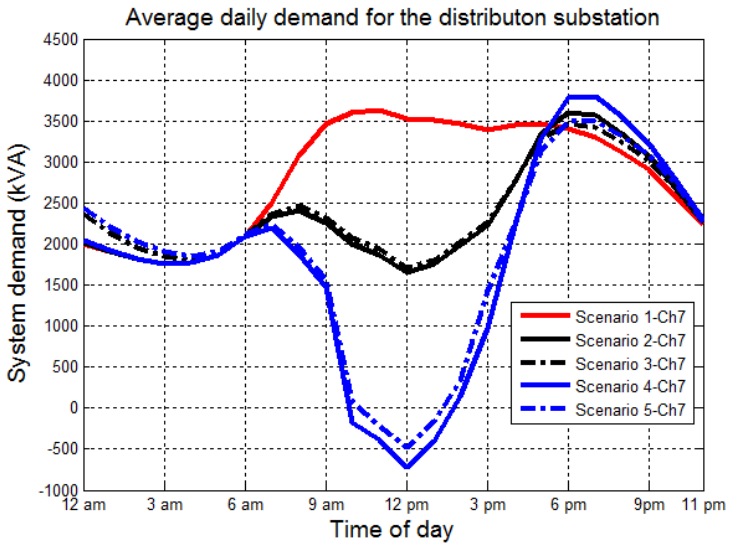

Figure 7-22: Average daily demand for the distribution substation

As indicated in Figure 7-22, the positive impact of the proposed bilayer system is significant: at noon, excess PV production is stored in BESSs to limit the reverse power flow through the secondary distribution transformers so that it remains within the acceptable 60% threshold. Accordingly, for scenario 5-Ch7, the reverse power flow apparent at the substation transformer is less than the corresponding value for scenario 4-Ch7. However, the amount of the reduction is minor because BESSs start to charge only after the reverse power flow exceeds the predetermined 60% threshold. This stored energy is then reused in order to meet a portion of the PHEV charging demand so that the distribution transformer is prevented from overloading. The peak substation demands for scenarios 3-Ch7 and 5-Ch7 are therefore less than the corresponding values for scenarios 2-Ch7 and 4-Ch7, respectively.

As stated earlier, average data does not provide an insight into the likelihood of the anticipated benefits of the proposed bilayer system. MC outputs, however, come with a probability distribution that can be used to derive valuable probabilistic indices, as explained below.

7.8.5.2 Probability of Overloading Distribution Equipment

The previously developed probabilistic benchmark is used for the computation of the frequencies of occurrence of different kVA loadings in each equipment class (primary feeder, secondary distribution transformers, single phase AC laterals, and AC service drops) during the entire simulation interval.

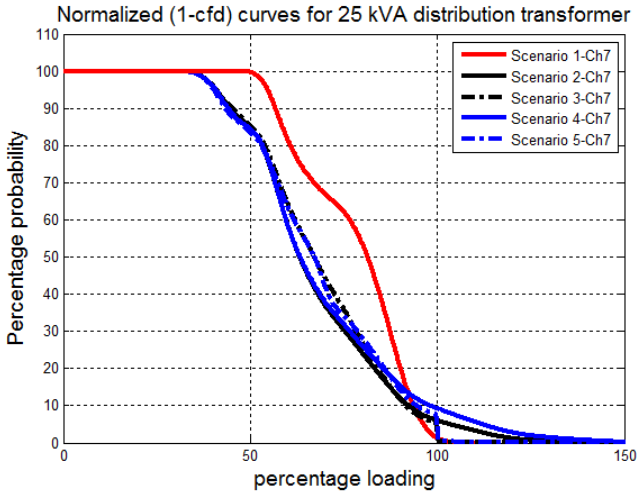

Figure 7-23: Probability of exceeding a specific percentage loading for 25 kVA transformers

The resulting frequency distributions are then utilized for the development of normalized (1-cfd) curves for each equipment class. As explained earlier, these curves denote the percentage of time this class will supply a demand that exceeds a specific loading percentage Figure 7-23 provides a sample normalized (1-cfd) curve for 25 kVA distribution transformers.

The probability of exceeding a certain class of distribution equipment rating is then determined from the corresponding normalized (1–cfd) curve as the probability corresponding to 100% loading. Table 7-8 shows the probability of exceeding the ratings for a variety of distribution equipment classes during each of the study scenarios.

Table 7-8: Probability of exceeding equipment ratings

Scenario	1-Ch7	2-Ch7	3-Ch7	4-Ch7	5-Ch7
Primary Feeder	0%	0.01%	0%	0.11%	0%
50 kVA transformers	0%	5.31%	0.11%	9.18%	0.15%
25 kVA transformers	0%	6.07%	0.12%	9.33%	0.17%
Single phase laterals	0%	0%	0%	0%	0%
Service drops	0%	0%	0%	0%	0%

Similar to the results obtained in Section 6.6.4.2, the impact of diversity revealed in Table 7-8 is quite significant: the primary feeder is unlikely to be overloaded during any of the scenarios studied, with the worst probability at only 0.11%. Table 7-8 also indicates also that, for scenarios 2-Ch7 and 4-Ch7, increased PHEV charging demands render the secondary distribution transformers susceptible to significant overloads. However, in the proposed bilayer system (scenarios 3-Ch7 and 5-Ch7),

during peak demand periods, energy stored in the BESSs is used to meet a portion of the demand locally, thus mitigating the overloading of the distribution transformers. This effect is illustrated by the bend occurring at 100% loading in the (1-cfd) curve for 25 kVA transformers that is depicted in Figure 7-23. As a result, the probability of overloading the distribution transformers is significantly reduced in scenarios 3-Ch7 and 5-Ch7: the overloading probability of 25 kVA transformers, for example, decreases from 6.07% in scenario 2-Ch7 to 0.12% in scenario 3-Ch7 and from 9.33% in scenario 4-Ch7 to 0.17% in scenario 5-Ch7. These positive results can be improved further by increasing the confidence level adopted in Section 7.6.1 during the BESS sizing process. Increasing the confidence level, however, will increase the required BESSs ratings, and hence, their overall cost.

As stated earlier, North American utilities usually oversize AC overhead laterals and service drops. As a result, their loading does not exceed 60% and 30% of their rated capacity during study scenarios 2-Ch7 and 4-Ch7, respectively. AC laterals and service drops are thus unlikely to be overloaded during any of the scenarios, and thus have not been included in the analysis.

7.8.5.3 Upgrade Requirements

The peak demand for each piece of equipment in the system (with 95% confidence) is computed for each scenario. This piece of equipment is flagged as overloaded and requiring upgrading if the peak demand calculated exceeds its rated capacity. The results are shown in Table 7-9.

Table 7-9: Percentage of equipment requiring upgrades

Scenario	1-Ch7	2-Ch7	3-Ch7	4-Ch7	5-Ch7
Primary Feeder	0%	0%	0%	0%	0%
50 kVA transformers	0%	57.45%	0%	100%	0%
25 kVA transformers	0%	67.74%	0%	100%	0%

As explained earlier, the components most influenced by increased PHEV penetration are the secondary distribution transformers. For the system under study, for scenario 2-Ch7, 57.45% and 67.74% of 50 kVA and 25 kVA secondary distribution transformers, respectively, are overloaded and require upgrading, and for scenario 4-Ch7, all secondary distribution transformers should be upgraded. The proposed bilayer system, however, can eliminate this problem completely because its implementation ensures that the power supplied by each distribution transformer never exceeds its rated capacity. As a result, with scenarios 3-Ch7 and 5-Ch7, no transformers must be upgraded and costly system upgrades are avoided.

`  `

7.8.5.4 Reverse Power Flow

Figure 7-22 signifies the weak chronological coincidence between PV array production and system peak demand. Such a chronological coincidence results in excessive reverse power flows at noon, when PV arrays are generating their peak output. This reverse power flow leads to adverse impacts on distribution networks [13, 14].

To study the impact of the proposed bilayer system on the reverse power flows, the author used the MC-based probabilistic benchmark to calculate two quantities: the probability of the occurrence of reverse power flow in distribution transformers, and the corresponding maximum magnitude for that reverse power flow as a percentage of the transformer rating (with 95% confidence), during different study scenarios. The results are shown in Tables 7-10 and 7-11, respectively.

Table 7-10: Probability of the occurrence of reverse power flow

Scenario	1-Ch7	2-Ch7	3-Ch7	4-Ch7	5-Ch7
Substation transformer	0%	0%	0%	14.88%	12.85%
50 kVA transformers	0%	5.6%	4.59%	20.49%	19.89%
25 kVA transformers	0%	6.17%	5.5%	20.59%	19.72%

Table 7-11: Peak reverse power flow as a percentage of the transformer rating

Scenario	1-Ch7	2-Ch7	3-Ch7	4-Ch7	5-Ch7
Substation transformer	0%	0%	0%	30%	18.24%
50 kVA transformers	0%	37.9%	34.4%	80.48%	59.73%
25 kVA transformers	0%	57.84%	53.01%	82.92%	59.97%

Due to the presence of commercial loads in the system, the substation transformer is not subjected to high rates of reverse power flow. However, this is not the situation for the secondary distribution transformers where higher rates of reverse power flow can occur, in scenarios 2-Ch7 and 4-Ch7. For example, in scenario 4-Ch7, the reverse power flow through the 25 kVA transformers may reach 82.92% of the transformer rating, thus violating acceptable limits.

Table 7-10 also indicates that the bilayer system has a minor impact on the probability of the occurrence of reverse power flow in the distribution transformers. This result is attributable to the fact that BESSs begin to charge only after the reverse power flow exceeds 60% of the transformer rating.

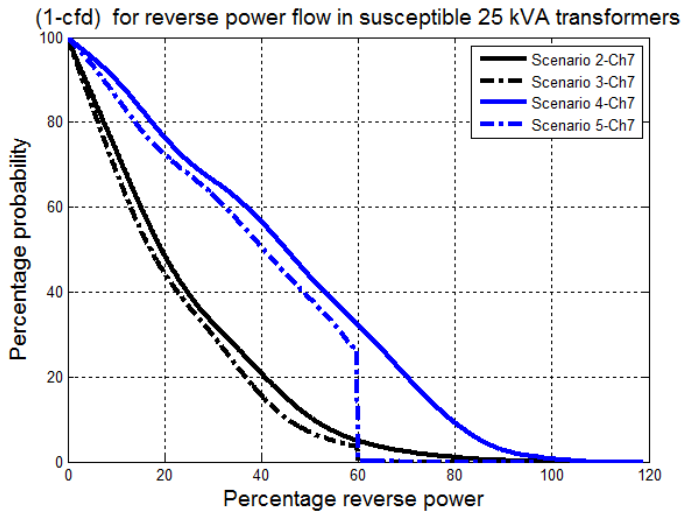

Figure 7-24: Probability of exceeding a specific reverse power flow in susceptible 25 kVA distribution transformers

However, as shown in Table 7-11, the proposed bilayer system is capable of limiting the maximum reverse power flow through the distribution transformers so that it remains within acceptable limits. For scenarios 3-Ch7 and 5-Ch7, this effect is indicated by the bend at the point corresponding to 60% reverse power in the (1-cfd) curve for the 25 kVA transformers, as shown in Figure 7-24.

7.8.5.5 AC System Voltages

The probability of violating range-A voltage limits during the five study scenarios was estimated using the probabilistic benchmark. The results are listed in Table 7-12.

Table 7-12: Probability of violating range-A voltage limits

Scenario	1-Ch7	2-Ch7	3-Ch7	4-Ch7	5-Ch7
At the end customer	0%	0%	0%	0.1%	0%
At the distribution transformers	0%	0%	0%	0.1%	0%
Along the primary feeder	0%	0%	0%	0.3%	0%

Table 7-12 reveals that, for scenario 4-Ch7, increased PV and PHEV penetration leads to an insignificant violation of range-A limits. The proposed bilayer system, however, has a positive impact on system voltages because it eliminates the probability of violating range-A voltage limits, as indicated for scenario 5-Ch7. This effect can be attributed to the fact that, in the proposed bilayer system, BESSs operate to alleviate secondary distribution transformer overloading during PHEV peak

charging periods, and to limit the reverse power flow when PV arrays are generating their peak output. The under voltages that accompany PHEV peak charging periods as well as the over voltages that occur due to excessive reverse power flows are thus considerably reduced.

7.8.5.6 Number of Voltage Regulator Operations

Table 7-13 gives the average number of annual regulator actions during the five study scenarios.

Table 7-13: Annual number of regulators actions

Scenario	1-Ch7	2-Ch7	3-Ch7	4-Ch7	5-Ch7
Regulators actions	16595	19948	17374	28755	23505

Table 7-13 indicates that, in the existing single layer AC system (scenarios 2-Ch7 and 4-Ch7), the presence of PV arrays and PHEVs increases the number of regulator actions by 20% and 73%, respectively, compared to the base-case scenario (scenario 1-Ch7). The proposed bilayer system, however, reduces the number of regulator actions for scenarios 3-Ch7 and 5-Ch7 by 12.18% and 14.72% relative to their values in scenarios 2-Ch7 and 4-Ch7, respectively.

Overall, these results, together with those presented in the previous subsection, indicate that the proposed bilayer system has a positive impact on system voltages. The net effect is a reduction in the total number of regulator actions, which increases their lifetime.

7.8.5.7 PV Array Energy Production

The average annual energy produced by PV arrays during the five study scenarios is depicted in Table 7-14.

Table 7-14: Average annual energy produced by PV arrays

Scenario	1-Ch7	2-Ch7	3-Ch7	4-Ch7	5-Ch7
PV generated energy (MWh)	0	5409	5585	10032	10358

An examination of Table 7-14 confirms that the proposed bilayer system has a positive impact on PV array productivity: the amounts of PV energy produced with scenarios 3-Ch7 and 5-Ch7 are approximately 3.25% greater than the corresponding values with scenarios 2-Ch7 and 4-Ch7, respectively. These results can be explained by the reduction in the losses achieved by the elimination of the extra DC/AC inversion stage in the PV array inverters. PV power conversion losses are thus

reduced, leading to increased PV power conversion efficiency and correspondingly greater PV array productivity.

This potential benefit is particularly important for residential PV owners, given the generous incentives offered by several government entities with the goal of facilitating the adoption of solar electricity in the residential sector. For example, For example, upon its launch in October 2009, the microFIT program (funded by the Ontario Power Authority) offered 80.2 CAD cents/kW for electricity generated by small PV generators [7], which is 5.94 times the provincial peak price for electricity. Any increase in PV array production will therefore create significant revenue for residential PV owners. Moreover, eliminating the extra rectification stage can also be expected to reduce the overall initial cost of PV systems, further expediting their widespread adoption in the residential sector.

7.8.5.8 Energy Consumed by PHEVs

The average annual energy required for charging PHEVs during the five study scenarios is itemized in Table 7-15.

Table 7-15: Average annual energy consumed by PHEVs

Scenario	1-Ch7	2-Ch7	3-Ch7	4-Ch7	5-Ch7
Energy consumed by PHEVs (MWh)	0	1022	970	1898	1801

Table 7-15 demonstrates that, for scenarios 3-Ch7 and 5-Ch7, the proposed bilayer system reduces the energy required to charge PHEVs by approximately 5.1% compared to the values for scenario 2-Ch7 and 4-Ch7, respectively. This reduction can be ascribed to the decreased losses stemming from the elimination of the extra AC/DC rectification stage in PHEV battery chargers. As explained earlier in Section 7.3.7, typical double-stage PHEV battery chargers have an efficiency rating of 90% [99, 163, 164]. Eliminating the additional conversion stage will cut charging losses and increase charger efficiency. The result will be an approximate 5.1% reduction in the total energy required for PHEV charging.

7.8.5.9 Total System Losses

The annual active and reactive energy losses in the test system for different study scenarios are given in Table 7-16, and depicted in Figures 7-25 and 7-26.

Table 7-16: Total system losses

Scenario	Active energy losses (MWh)					Reactive energy losses (MVARh)
	AC Network losses	Losses in DC service drops	BESSs losses	Converters losses	Overall system losses	
1-Ch7	791.87	0	0	0	791.87	1451.71
2-Ch7	612.99	0	0	0	612.99	1114.27
3-Ch7	610.24	57.46	181.19	216.75	1065.64	1107.63
4-Ch7	608.41	0	0	0	608.41	1100.17
5-Ch7	585.12	106.31	274.21	385.34	1350.98	1042.57

As shown in Table 7-16, the presence of PV electricity reduces the losses in the AC network significantly: the active energy losses for scenarios 2-Ch7 and 4-Ch7 are 22.59% and 23.17% less than the corresponding value for the base-case scenario (scenario 1-Ch7). This observation is explained by the fact that PV electricity supplies part of the system demand locally, which decreases the amount of energy flowing from MV to LV networks, and accordingly reduces the incurred network losses. Similar figures are obtained for the reactive energy losses (23.24% and 24.22%).

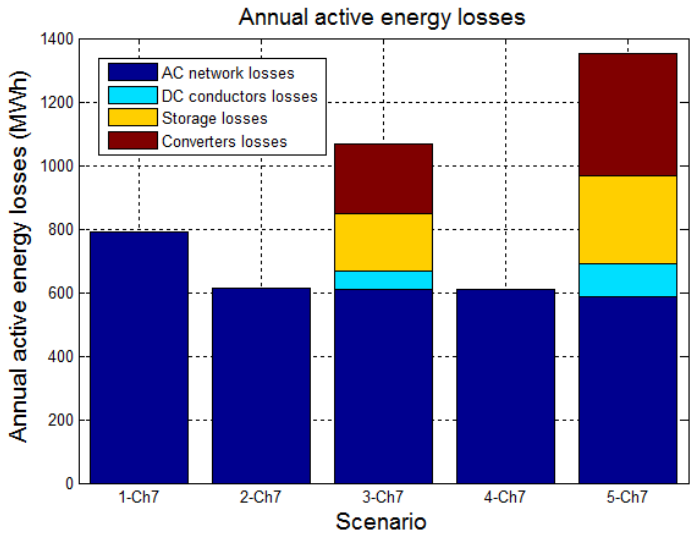

Figure 7-25: Annual active energy losses

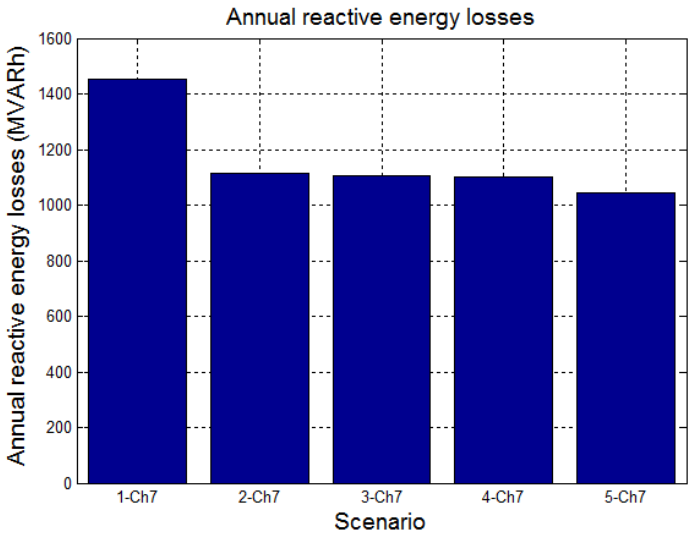

Figure 7-26: Annual reactive energy losses

Figures 7-25 and 7-26 make it evident that the proposed bilayer system has a minor positive impact on the losses in the AC network. This observation is explained by the fact that energy stored in the 78 BESSs are used to meet a portion of the system demand locally (i.e., from the LV network) during PHEV peak charging periods. As a result, the active energy losses in the AC network in scenarios 3-Ch7 and 5-Ch7 are reduced by 0.45% and 3.83% from the corresponding values in scenarios 2-Ch7 and 4-Ch7, respectively. Similar figures are obtained for the reactive energy losses (0.6% and 5.24%). This positive impact is only minor as BESSs come into play only when PHEV charging demands cause secondary distribution transformers to become overloaded.

Nevertheless, overall system active energy losses for scenarios 3-Ch7 and 5-Ch7 are 73.84% and 122.05% greater than the corresponding values for scenarios 2-Ch7 and 4-Ch7, respectively, due to the additional losses incurred in the 78 BESSs (which have a DC/DC round trip efficiency of only 79%), bidirectional converters and DC service drops.

However, a comprehensive energy loss indicator should consider the energy loss savings achieved by utilizing DC electricity to interface PHEVs and PV arrays. If these energy loss savings (228 and 423 MWh for scenarios 3-Ch7 and 5-Ch7, respectively) are taken into consideration, the effective losses in scenarios 3-Ch7 and 5-Ch7 are only 36.64% and 52.36% greater than the corresponding values for scenarios 2-Ch7 and 4-Ch7, respectively. These values are comparable to the losses obtained in the previous chapter using BESSs alone (scenarios 3-Ch6 and 5-Ch6 respectively).

` `

Moreover, these disappointing results can be improved by increasing the utilization of DC electricity in the LV system. Such a target can be achieved by using the DC layer of the proposed bilayer system to supply part of the existing household electronic loads. Most of these loads (TVs, electronic equipment, PCs, etc.) are basically powered by DC electricity and are currently interfaced to the AC network via AC/DC power electronic converters. By providing a direct DC supply to these devices, the extra AC/DC conversion stage can be eliminated. Eliminating the extra rectification stage increases system efficiency by counting out the losses of this conversion stage which could, in turn, compensate for the additional losses associated with the bilayer system. This point is analyzed in detail in a subsequent section.

7.8.6 Evaluating the Economic Feasibility of the Proposed Bilayer System

In this section, the costs and benefits associated with the implementation of the proposed bilayer system are compared to assess its cost-effectiveness.

7.8.6.1 Calculating the Costs Associated with the Implementation of the Proposed Bilayer System

The proposed bilayer system is associated with the following cost components:

i) Cost of storage devices: As concluded in Section 7.8.1, Zn/Br batteries offer the most economical option. The annual cost of integrating Zn/Br BESSs in the proposed bilayer system is depicted in Table 7-4.

ii) Cost of DC service drops: The cost of installing triplex 1/0 AWG ACSR conductors is estimated to be around 4788.52/MLF (thousand linear feet). This estimation is based on the following data [251]:

Table 7-17: Different cost components for 1/0 AWG ACSR conductors

Cost component	Cost
Material	1368.98
Foreman electrician ($50.45/hour for 10.00 hours)	504.52
Electricians ($49.02/hour for 40.00 hours)	1960.95
Equipment operators, Lights ($40.72/hour for 10.00 hours)	407.24
Line-truck, 32' reach (with 46' high aerial platform) ($54.68/hour for 10.00 hours)	546.83
Total capital cost / MLF	**4788.52**

The total capital cost for DC service drops can be calculated as:

$$TCC_{DCSD} = UC_{DCSD} \times L_{DCSD} \tag{7.25}$$

where TCC_{DCSD} is the total capital cost for the DC service drops, UC_{DCSD} is the unit cost for DC service drops (4788.52 $/MLF), and L_{DCSD} is the total length of DC service drops in MLF.

The total annual cost for DC service drops (TAC_{DCSD}) can be computed by multiplying the total capital cost (TCC_{DCSD}) by the capital recovery factor (CRF) given in Eq. (6.42) (for a project lifetime of 40 years and at a 7.7% annual interest rate):

$$TAC_{DCSD} = TCC_{DCSD} \times CRF \tag{7.26}$$

iii) Cost of bidirectional converters: The total capital cost for bidirectional converters (TCC_{Conv}) is given by:

$$TCC_{Conv} = PCSU_{Conv} \times S_{Conv\,Rated} \tag{7.27}$$

where $PCSU_{Conv}$ is the unit cost for bidirectional converters ($/kVA), given in [252] as 129 $/kVA. This value represents the cost of a commercially available line interactive UPS performing the same function of the proposed bidirectional converter.

The total annual capital cost for bidirectional converters ($TACC_{Conv}$) can be computed by multiplying the total capital cost (TCC_{Conv}) by the capital recovery factor (CRF):

$$TACC_{Conv} = TCC_{Conv} \times CRF \tag{7.28}$$

The annual maintenance and replacement cost for power electronic converters is usually taken as a percentage of the total capital cost. For this research, based on the analysis performed in [253], this percentage is taken to be 9%. Accordingly, the annual maintenance and replacement cost for bidirectional converters ($AMRC_{Conv}$) is calculated as:

$$AMRC_{Conv} = TCC_{Conv} \times 0.09 \tag{7.29}$$

` `

The total annual cost for bidirectional converters (TAC_{Conv}) is calculated as the sum of the total annual capital cost and the annual maintenance and replacement cost:

$$TAC_{Conv} = TACC_{Conv} + AMRC_{Conv} \tag{7.30}$$

iv) Cost of interfacing DC/DC converters: As explained earlier, PV arrays and PHEVs are interfaced to the DC layer of the proposed bilayer system via DC/DC converters. As with bidirectional converters, the total annual cost for DC/DC converters (TAC_{DCConv}) is the sum of the total annual capital cost ($TACC_{DCConv}$) and the annual maintenance and replacement cost ($AMRC_{DCConv}$):

$$TAC_{DCConv} = TACC_{DCConv} + AMRC_{DCConv} \tag{7.31}$$

The total annual capital cost for DC/DC converters ($TACC_{DCConv}$) is given by:

$$TACC_{DCConv} = TCC_{DCConv} \times CRF \tag{7.32}$$

where TCC_{DCConv} is the total capital cost for DC/DC converters, as given by:

$$TCC_{DCConv} = PCSU_{DCConv} \times S_{DCConv\,Rated} \tag{7.33}$$

where $PCSU_{DCConv}$ is the unit cost for DC/DC converters ($/kVA), given in [254] as 62.5 $/kVA.

As with bidirectional converters, the annual maintenance and replacement cost for DC/DC converters ($AMRC_{DCConv}$) is taken as 9% of their capital cost [253].

$$AMRC_{DCConv} = TCC_{DCConv} \times 0.09 \tag{7.34}$$

v) Cost of extra system losses: As stated earlier, the proposed bilayer system increases the overall system losses due to the additional losses incurred in the 78 BESSs (which have a DC/DC round trip efficiency of only 79%), bidirectional converters and DC service drops. The annual cost of the effective extra losses incurred in the bilayer system is estimated using the average weighted hourly price for electricity in Ontario in 2013 (0.0265 CAD/kWh or 0.0236 $/kWh).

The different cost components associated with the implementation of the proposed bilayer system in scenarios 3-Ch7 and 5-Ch7 are shown in Table 7-18.

Table 7-18: Annual costs associated with the implementation of the proposed bilayer system ($/year)

Cost component	Scenario 3-Ch7	Scenario 5-Ch7
Storage devices	114919	227109
DC service drops	7753	14417
Bidirectional converters	58406	96387
DC/DC converters	92628	171904
Extra system losses	5302	7542
Total annual cost	**279008**	**517359**

7.8.6.2 Calculating the Benefits Associated with the Implementation of the Proposed Bilayer System

The proposed bilayer system is associated with the following cost savings:

i) Cost savings due to the elimination of PV array inverters: As stated earlier, utilizing DC electricity to interface PV arrays eliminates the need for sophisticated multiple-stage PV inverters. The total capital cost savings achieved by the elimination of PV array inverters ($TCCS_{PV}$) are calculated as:

$$TCCS_{PV} = CC_{PV} \times N_{PVs} \tag{7.35}$$

where CC_{PV} is the capital cost for 10 kW PV inverters (taken as $4509 according to [255]) and N_{PVs} is the total number of PV arrays in the test system (333 and 618 in scenarios 3-Ch7 and 5-Ch7, respectively).

The total annual capital cost savings ($TACCS_{PV}$) are computed by multiplying the total capital cost savings ($TCCS_{PV}$) by the capital recovery factor (CRF):

$$TACCS_{PV} = TCCS_{PV} \times CRF \tag{7.36}$$

As with bidirectional converters, the annual maintenance and replacement cost savings ($AMRCS_{PV}$) are taken as 9% of the total capital cost savings [253].

$$AMRCS_{PV} = TCCS_{PV} \times 0.09 \tag{7.37}$$

` `

Finally, the total annual cost savings achieved by the elimination of PV array inverters ($TACS_{PV}$) are the sum of the total annual capital cost savings ($TACCS_{PV}$) and the annual maintenance and replacement cost savings ($AMRCS_{PV}$):

$$TACS_{PV} = TACCS_{PV} + AMRCS_{PV} \tag{7.38}$$

ii) Cost savings due to the elimination of PHEV battery chargers: As with PV array inverters, utilizing DC electricity to interface PHEVS eliminates the need for sophisticated multiple-stage PHEV chargers. The total capital cost savings achieved by the elimination of PHEV battery chargers ($TCCS_{PHEV}$) are calculated as:

$$TCCS_{PHEV} = PCSU_{PHEV} \times S_{PHEV} \times N_{PHEVs} \tag{7.39}$$

where $PCSU_{PHEV}$ is the unit cost for PHEV battery chargers ($/kVA), estimated from [256] to be equal to 148.5$/kVA, S_{PHEV} is the rating of PHEV battery chargers (7.2 kW), and N_{PHEVs} is the total number of PHEVs in the test system (333 and 618 in scenarios 3-Ch7 and 5-Ch7, respectively).

The total annual capital cost savings ($TACCS_{PHEV}$) are computed by multiplying the total capital cost savings ($TCCS_{PHEV}$) by the capital recovery factor (CRF):

$$TACCS_{PHEV} = TCCS_{PHEV} \times CRF \tag{7.40}$$

As in the previous sections, the annual maintenance and replacement cost savings ($AMRCS_{PHEV}$) are taken as 9% of the total capital cost savings [253]:

$$AMRCS_{PHEV} = TCCS_{PHEV} \times 0.09 \tag{7.41}$$

Finally, the total annual cost savings achieved by the elimination of PHEV battery chargers ($TACS_{PHEV}$) is the sum of the total annual capital cost savings ($TACCS_{PHEV}$) and the annual maintenance and replacement cost savings ($AMRCS_{PHEV}$):

$$TACS_{PHEV} = TACCS_{PHEV} + AMRCS_{PHEV} \tag{7.42}$$

iii) Cost savings achieved by avoiding distribution transformer upgrades: As explained earlier, the proposed bilayer system mitigates distribution transformer overloading, thus eliminating the need for transformer upgrades. The cost savings achieved by avoiding these upgrades are given in Table 6-16.

The different cost savings associated with the implementation of the proposed bilayer system in scenarios 3-Ch7 and 5-Ch7 are shown in Table 7-19.

Table 7-19: Annual cost savings associated with the implementation of the proposed bilayer system ($/year)

Cost savings	Scenario 3-Ch7	Scenario 5-Ch7
Elimination of PV array inverters	257021	476994
Elimination of PHEV battery chargers	60946	113107
Avoiding distribution transformer upgrades	22399	36852
Total annual saving	**340366**	**626953**

7.8.6.3 Performing a Cost/Benefit Analysis

In this step, the total annual benefits associated with implementing the proposed bilayer system are compared to the total incurred annual costs. Results (shown in Figure 7-27) reveal that the proposed bilayer system is cost-effective: the annual benefits associated with its implementation exceed the extra annual costs. This cost-effectiveness can be explained by the fact that in the proposed bilayer system, multiple-stage sophisticated PV array inverters (operating only during daytime and idle for the rest of the day) and PHEV battery chargers (operating only in the evening and idle for the rest of the day) are replaced by a centralized bidirectional converter, whose overall diversified rating is less than the summation of the individual ratings of the small dispersed power conversion stages. For example, given a 50 kVA distribution transformer interfacing 10 PHEV/PV array sets, the 10 PHEV battery chargers (rated at 7.2 kVA each) as well as the 10 PV array inverters (rated 10 at kVA each) are replaced by a centralized bidirectional converter with an average rating of 70 kVA, as opposed to 172 kVA of dispersed power conversion stages in the traditional single layer AC system.

As explained earlier, the main drawback of the proposed bilayer system is increased system losses. This drawback can be overcome by increasing the utilization of DC electricity in the LV network. Such a target can be achieved by using the DC layer of the proposed bilayer system to supply part of the existing household electronic loads. This proposal is explained in detail in the next section.

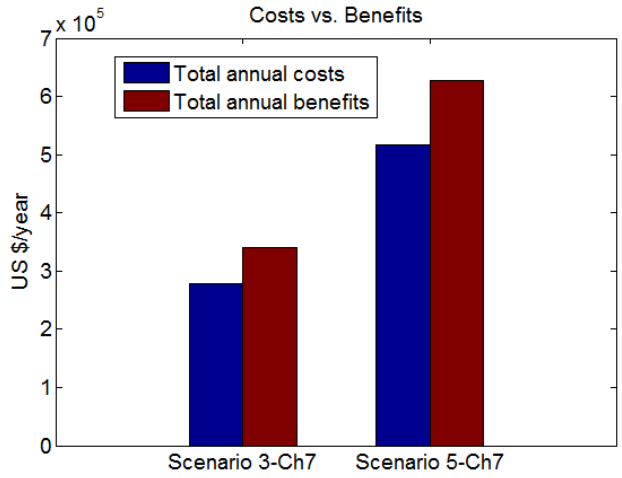

Figure 7-27: Annual costs and benefits associated with the proposed bilayer system

7.8.7 Using DC Electricity to Supply Existing Household Electronic Loads

Previous results reveal that the main technical drawback associated with the proposed bilayer system is the excessive energy losses incurred in BESSs, bidirectional converters and DC service drops. To overcome this drawback, the author proposes using the DC layer of the bilayer system to supply part of the existing household electronic loads directly with DC electricity. As explained earlier, most household electronic devices are basically powered by DC power and hence contain an AC/DC rectifier in their power supply circuits. The power supply in these devices can be bypassed, making it possible to operate the appliance directly using DC electricity. The rationale behind this proposal can be summarized in the following points:

i) A study performed by EPRI and Ecos Consulting [216, 217] revealed that most small-scale power supplies for household electronic devices have a power conversion efficiency of about 60 to 75%. Similarly, the analysis performed in [257] reported more conservative results of 30 to 60%. As a result, more than 1 trillion kWh of electricity is wasted annually due to these low-efficiency power supplies [218]. Another study [258] estimated that more than 5% of all electrical power used by a typical U.S. household is wasted due to inefficient AC to DC power conversion in small-scale electronic devices. These energy losses can be reduced by using the DC layer of the proposed bilayer system to supply existing household electronic loads directly with DC electricity. Nevertheless, in this case, there should be a DC/DC buck converter installed at each household to step down the 120/60 Vdc (provided by the proposed bilayer system) to the DC voltage levels needed by electronic devices.

ii) The advantage of the proposed idea is that DC/DC power converters have much higher conversion efficiency than their AC/DC counterparts: unidirectional DC/DC converters can easily achieve power conversion efficiency as high as 90% [259-261]. This point is explained by the fact that DC/DC converters have fewer power electronic switches than do AC/DC rectifiers.

iii) What makes the proposed idea even more appealing is that consumer electronics are the fastest growing portion of residential electricity use [258]. According to an article published in *MIT Technology Review* [262], electronic devices currently account for up to a 20% of the total household electrical consumption. However, with the anticipated migration of lighting systems towards the solid state and LED technologies, it is expected that DC-powered devices will constitute more than 50% of the total residential consumption within the next 20 years [262].

Based on the previous discussion, the efficiency of small-scale AC/DC power supplies is taken as 75% (as an optimistic assumption), whereas the efficiency of DC/DC buck converters installed at end customers' premises is taken as 90% (as a conservative assumption).

7.8.7.1 Considering the Effect of DC-Powered Household Electronic Loads in the MC Simulation

The DC power supplied to DC-powered household electronic loads in household x at hour i ($P_{Loads,DC}(i, x)$) is given by:

$$P_{Loads,DC}(i,x) = P_{Loads,AC}(i,x) \times \frac{\eta_{AC/DC}}{\eta_{DC/DC}} \times DC_{Penet} \tag{7.43}$$

where $P_{Loads,AC}(i, x)$ is the AC active power demand of household x at hour i (sampled from the selected six representative segments depicted in Figure 3-11), $\eta_{AC/DC}$ is the efficiency of small-scale AC/DC power supplies (taken as 75%), $\eta_{DC/DC}$ is the efficiency of DC/DC centralized buck converters installed at each household (taken as 90%) and DC_{Penet} is the percentage of household electronic loads supplied by DC electricity (DC loads penetration level). For this research, 26 different penetration levels for DC-powered household electronic loads are considered in the analysis (from 0% up to 25% penetration).

The energy loss savings achieved by using DC electricity in household x ($ELS(i, x)$) is given by:

$$ELS(i,x) = P_{Loads,DC}(i,x) \times \left(\frac{\eta_{DC/DC}}{\eta_{AC/DC}} - 1\right) \tag{7.44}$$

` `

The DC power delivered by the distribution transformer to supply DC-powered household electronic loads at hour *i* ($P_{Loads,DC}(i)$) is given by:

$$P_{Loads,DC}(i) = \sum_{x=1}^{N_{Household,Transformer}} P_{Loads,DC}(i,x) \tag{7.45}$$

where $N_{Households,Transformer}$ is the number of households supplied by the distribution transformer.

Accordingly, Eq. (7.2) denoting the aggregated DC demand at the bidirectional converter DC bus is modified to:

$$P_{DC\,bus}(i) = P_{PHEVs,DC}(i) + LOSS_{DCSD}(i) + P_{Loads,DC}(i) - P_{PVs,DC}(i) \tag{7.46}$$

After that, the probabilistic sizing methodology explained in Section 7.6 is used to determine the modified energy and power ratings of the 78 BESSs and bidirectional converters present in the test system after accounting for the presence of the DC-powered household electronic loads. Finally, the MC simulation procedure explained in Section 7.5 is executed again for the test system until the designated convergence criterion given in Eq. (4.4) is fulfilled. This procedure is repeated 26 different times (corresponding to the 26 penetration levels of DC-powered household electronic loads) for study scenarios 3-Ch7 and 5-Ch7. In the next section, the author uses the results of the MC-based probabilistic benchmark to analyze the impacts of the proposed idea on the overall system losses.

7.8.7.2 Impacts on System Losses

The annual active energy losses in different system components for scenarios 3-Ch7 and 5-Ch7 are depicted in Figures 7-28 and 7-29, respectively. From the figures, it is clear that using the DC layer of the proposed bilayer system to supply part of the existing household electronic loads with DC electricity decreases the losses in the AC network, BESSs and DC converters. However, this is not the case for the bidirectional converters as the losses incurred in these devices increase as the penetration level of DC-powered household electronic loads increases. This last observation is explained by the fact that increasing the penetration level of DC-powered household electronic loads increases the power requirements in the DC layer of the system. Accordingly, the amounts of power being rectified by bidirectional converters also increase. The net effect is a slight increase in the losses incurred in bidirectional converters.

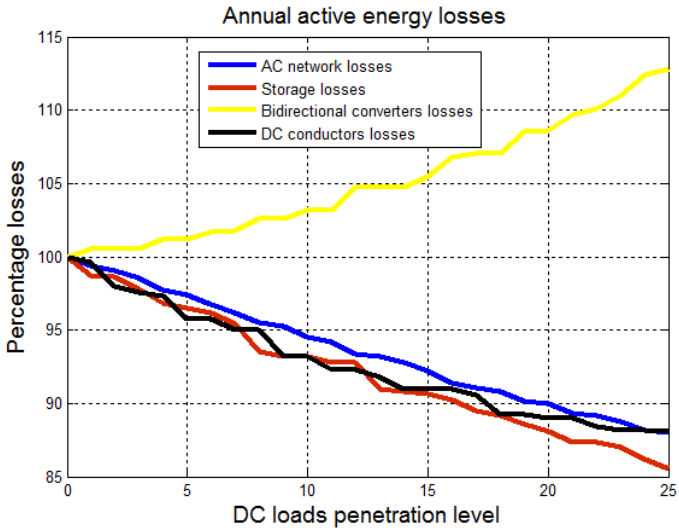

Figure 7-28: Annual active energy losses (scenario 3-Ch7)

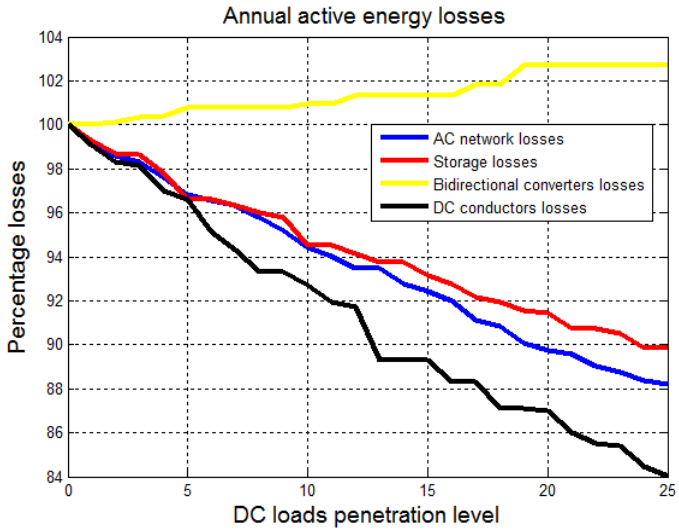

Figure 7-29: Annual active energy losses (scenario 5-Ch7)

The overall system active energy losses (losses in the AC network, BESSs, bidirectional converters and DC service drops) for scenarios 3-Ch7 and 5-Ch7 are depicted in Figure 7-30. From the figure, it is evident that using the DC layer of the proposed bilayer system to supply part of the existing household electronic loads with DC electricity has an overall positive impact on the losses in the test system: as the penetration level of DC-powered household electronic loads increases from 0% to 25%, the overall system losses in scenarios 3-Ch7 and 5-Ch7 are reduced by 7.34% and 7.59%, respectively.

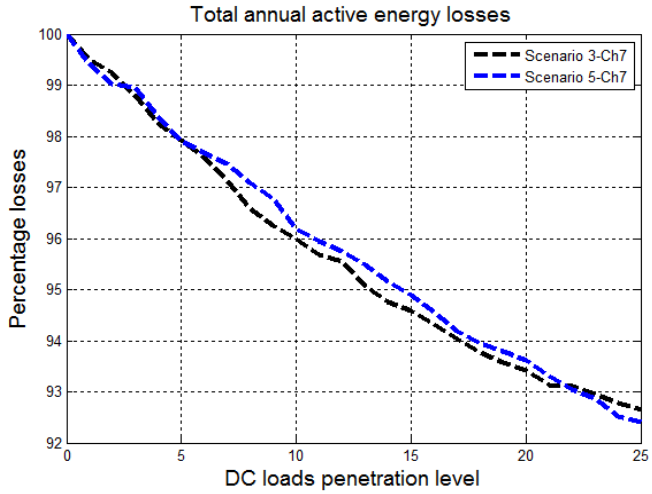

Figure 7-30: Total annual active energy losses

However, as stated earlier, a comprehensive energy loss indicator should consider the energy loss savings associated with the proposed bilayer system:

i) Energy loss savings achieved by using DC electricity to charge PHEVs;

ii) Energy loss savings achieved by using DC electricity to interface PV arrays;

iii) Energy loss savings achieved by using DC electricity to supply part of the existing household electronic loads.

These energy loss savings for scenarios 3-Ch7 and 5-Ch7 are depicted in Figures 7-31 and 7-32.

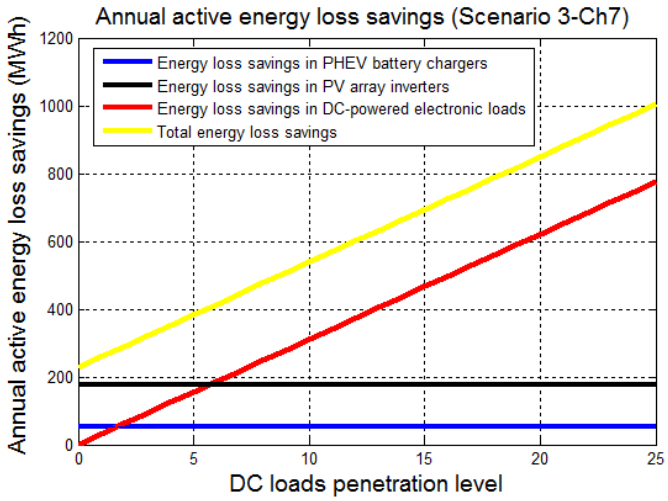

Figure 7-31: Annual active energy loss savings (Scenario 3-Ch7)

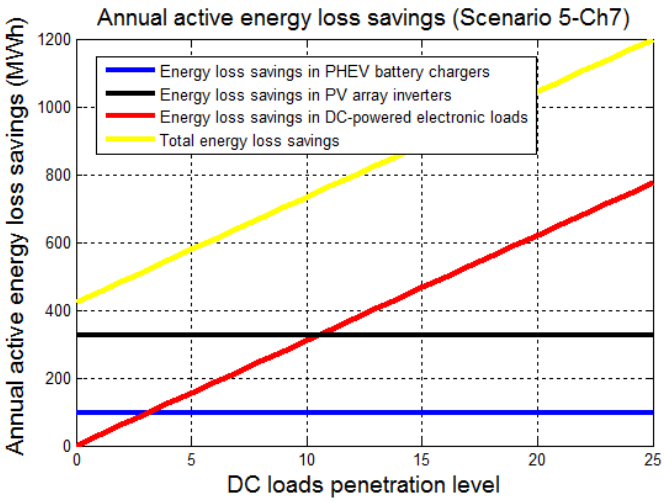

Figure 7-32: Annual active energy loss savings (Scenario 5-Ch7)

From previous figures, it is clear that the energy loss savings achieved by using DC electricity to supply part of the existing household electronic loads are highly dependent on the penetration level of DC-powered loads. Conversely, the energy loss savings achieved by using DC electricity to interface PHEV battery chargers and PV arrays are independent of the penetration level of DC-powered household electronic loads, and are constant for each study scenario.

The ratios between the previous energy loss savings and the additional losses associated with the proposed bilayer system (losses in BESSs, bidirectional converters and DC service drops) for both study scenarios are depicted in Figure 7-33.

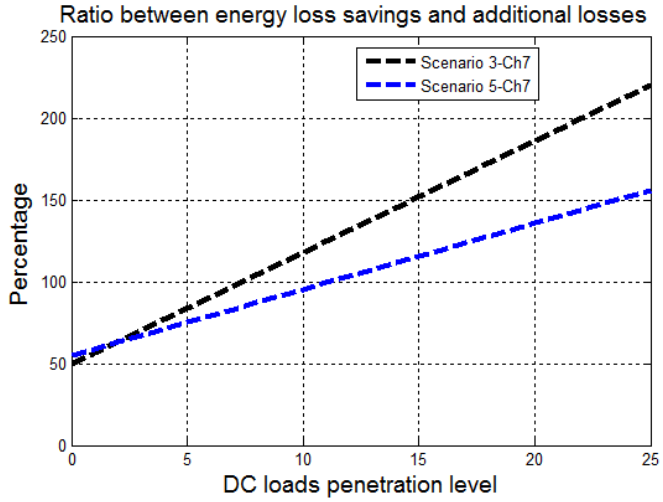

Figure 7-33: Ratio between energy loss savings and extra losses incurred in the bilayer system

From Figure 7-33, it is evident that using the DC layer of the proposed bilayer system to interface PHEV battery chargers and PV arrays is not a sufficient measure to compensate for the extra losses incurred in the BESSs, bidirectional converters and DC service drops. The energy loss savings achieved by the adoption of the previous measure can compensate for only 49.94% and 55.03% of the extra losses associated with the proposed bilayer system in scenarios 3-Ch7 and 5-Ch7, respectively. However, using the DC layer of the proposed bilayer system to supply part of the existing household electronic loads with DC electricity has a significant positive impact on the overall system losses. The last measure is able to compensate for the extra losses incurred in the bilayer system at 7.4% and 11.1% penetration levels of DC-powered household electronic loads in scenarios 3-Ch7 and 5-Ch7, respectively. Increasing the penetration level of DC-powered household electronic loads beyond these thresholds has the potential to reduce the losses incurred in the system, as shown in Figure 7-34.

Figure 7-34 reveals that the energy loss savings associated with the elimination of the extra power conversion stages in PV inverters, PHEV battery chargers and household electronic devices are quite significant. For example, if household electronic loads equivalent to 10% of the total household demand are supplied by DC electricity, the resulting energy loss savings are equivalent to 52.6% and 56.3% of the total energy losses incurred in the bilayer system (losses in the AC network, BESSs, bidirectional converters and DC service drops) in scenarios 3-Ch7 and 5-Ch7, respectively. These results suggest that the proposed bilayer system is particularly advantageous in the long-term projection, when there is a substantial penetration of DC-powered electronic loads.

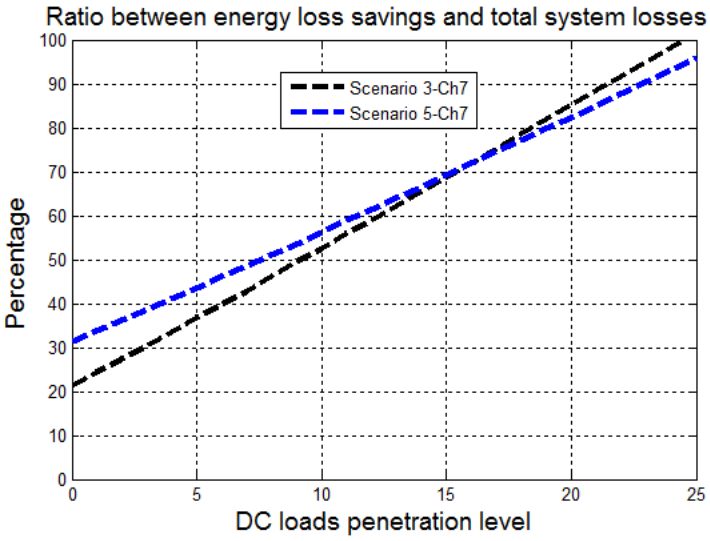

Figure 7-34: Ratio between energy loss savings and total system losses

7.8.8 Discussion of the Results

The analysis presented in this chapter indicates that the proposed bilayer system is expected to improve the performance of distribution systems that include a high penetration of PV arrays and PHEVs, in the following ways:

i) Improved integration of PHEVs: The proposed bilayer system mitigates distribution transformer overloading, thus eliminating the need for costly system upgrades in order to accommodate the expected growth in PHEVs. This advantage will give rise to significant cost savings for electric utilities. Moreover, with the proposed bilayer system, single-stage DC/DC PHEV battery chargers replace expensive, multiple-stage AC/DC- DC/DC chargers, thus reducing the initial cost of the charging equipment.

   The elimination of the AC/DC rectification stage also increases charger efficiency since the losses associated with this conversion stage are also eradicated, which in the case of the system under study, leads to an approximately 5.1% reduction in the energy required to meet PHEV charging demands.

   Another inherent advantage of the proposed bilayer system is that it offers customers the convenience of charging their PHEVs using DC rapid-chargers at their residences so that they will no longer need to pay higher rates for fast-charging electricity.

ii) Improved integration of PV electricity: The proposed bilayer system limits reverse power flow through the distribution transformers during peak generation periods so that it remains within acceptable limits. This feature eliminates a major technical drawback associated with the integration of PV electricity. Additionally, in the proposed bilayer system, single-stage DC/DC converters replace sophisticated, multiple-stage DC/DC-DC/AC PV inverters, a shift that is expected to reduce the overall initial cost of PV systems and to facilitate their widespread adoption, especially in the residential sector.

   The elimination of the DC/AC inversion stage in PV systems increases PV power conversion efficiency because the losses associated with this conversion stage are also removed, leading to an approximately 3.25% increase in PV array productivity, in the case of the system under study.

iii) Cost-effectiveness: The performed cost/benefit analysis showed that the proposed bilayer system is cost effective: the cost savings associated with the proposed bilayer system exceed its implementation costs. This cost-effectiveness can be explained by the fact that in the proposed

bilayer system, multiple-stage sophisticated PV array inverters (operating only during daytime) and PHEV battery chargers (operating only in the evening) are replaced by a centralized bidirectional converter, whose overall diversified rating is less than the summation of the individual ratings of the small dispersed power conversion stages. For example, given a 50 kVA distribution transformer interfacing 10 PHEV/PV array sets, the 10 PHEV battery chargers (rated at 7.2 kVA each) as well as the 10 PV array inverters (rated 10 at kVA each) are replaced by a centralized bidirectional converter with an average rating of 70 kVA, as opposed to 172 kVA of dispersed power conversion stages in the traditional single layer AC system.

iv) Reduced system losses: If the DC layer of the proposed bilayer system is used only to interface PHEVs and PV arrays, the energy loss savings achieved by the elimination of the extra power conversion stages in these two technologies are not enough to compensate for the additional losses incurred in the proposed bilayer system. The resulting energy loss savings can only compensate for 49.94% and 55.03% of these additional losses in scenarios 3-Ch7 and 5-Ch7, respectively. However, using the DC layer of the proposed bilayer system to supply part of the existing household electronic loads has a significant positive impact on the system losses and is able to compensate for the extra losses associated with the proposed bilayer system at 7.4% and 11.1% penetration levels of DC-powered household electronic loads in scenarios 3-Ch7 and 5-Ch7, respectively. Increasing the penetration level of DC-powered household electronic loads beyond these thresholds has the potential to reduce the losses incurred in the system significantly. For example, if household electronic loads equivalent to 10% of the total household demand are supplied by DC electricity, the resulting energy loss savings are equivalent to 52.6% and 56.3% of the total energy losses incurred in the bilayer system in scenarios 3-Ch7 and 5-Ch7, respectively. These results suggest that the proposed bilayer system is particularly advantageous in the long-term projection, when there is a substantial penetration of DC-powered household electronic loads.

v) Improved system voltages: The proposed bilayer system improves system voltages, thus reducing the number of operations of voltage regulators, and increasing their life expectancy.

7.9 Summary and Conclusions

In this chapter, an innovative bilayer architecture for residential distribution systems has been introduced. Key design and operational aspects of the proposed architecture have been presented. The

previously developed MC-based probabilistic benchmark has been used to size and schedule the operation of different system components, with consideration of the various uncertainties inherent in the system.

MC simulation results confirmed the technical merit of the proposed bilayer architecture, with respect to both increasing PV array productivity by 3.25% and decreasing the amount of energy required to meet PHEV charging demands by 5.1%. The simulation results also indicated that BESSs installed in the DC layer of the proposed system can mitigate distribution transformer overloading and limit the reverse flow of power through the transformers so that it is kept within permissible limits.

The performed cost/benefit analysis confirmed the cost-effectiveness of the proposed bilayer system for the test system under study: the cost savings associated with the bilayer system exceed its implementation costs. This cost-effectiveness is attributed to the fact that, in the proposed bilayer system, multiple-stage sophisticated PV array inverters (operating only during daytime) and PHEV battery chargers (operating only in the evening) are replaced by a centralized bidirectional converter, whose overall diversified rating is less than the summation of the individual ratings of the small dispersed power conversion stages.

The simulation results revealed that if the DC layer of the proposed bilayer system is used only to interface PHEVs and PV arrays, the energy loss savings achieved by the elimination of the extra power conversion stages in these two technologies are not enough to compensate for the additional losses associated with the proposed bilayer system. However, using the DC layer of the proposed bilayer system to supply part of the existing household electronic loads with DC electricity has a significant positive impact on the system losses and is able to compensate for the extra losses associated with the proposed bilayer system at 7.4% and 11.1% penetration levels of DC-powered household electronic loads in scenarios 3-Ch7 and 5-Ch7, respectively. Increasing the penetration level of DC-powered household electronic loads beyond these thresholds has the potential to increase the efficiency of the distribution system significantly. This last observation suggests that the proposed bilayer system is particularly advantageous in the long-term projection, when there is a substantial penetration of DC-powered household electronic loads.

Chapter 8
Summary, Contributions and Future Work

8.1 Summary

The research performed in this thesis analyzes the performance of distribution systems under a high penetration of PHEVs and PV electricity and presents new approaches to facilitate the integration of these two technologies into existing networks. The analysis starts by developing appropriate probabilistic models for different uncertainties inherent in the distribution system. Hourly insolation and temperature data provided by the Solar Radiation Research Laboratory are used to estimate PV systems DC power output. After that, the equivalent AC output power is computed using a typical inverter efficiency curve. The 24 data points representing the PV electrical output in each day are assembled in a data segment. The resulting 365 data segments representing the whole year are evaluated for similarities using PCA, and similar segments are grouped into one cluster. For each cluster, a representative segment is selected, and its probability of occurrence is computed. The same approach is repeated for the data segments containing daily loading profiles for existing electrical loads (abstracted from the IEEE RTS system). To model individuals' driving habits that impact PHEV charging, data for 1,048,576 people and 309,164 vehicles provided by the 2009 U.S. NHTS are analyzed for the extraction of cdfs representing daily mileage and home arrival times.

After that, the analysis continues by using the previously developed probabilistic models to construct a MC-based probabilistic benchmark for assessing the impacts of the uncontrolled charging of PHEVs on residential distribution networks. Simulation results showed that distribution transformer overloading is the bottleneck blocking the widespread adoption of PHEVs. The uncontrolled charging of PHEVs can be detrimental to these transformers, for which the diversity effect is not as clear as it is at primary system levels.

However, PHEVs are not the only challenge facing distribution systems in the smart grid era; integrating PV electricity in existing networks represents another major challenge. An important question that arises here is: what are the resulting aggregated impacts when the distribution system is under a high penetration of both PHEVs and PV electricity? This question is discussed in Chapter 5, where the previously developed MC-based probabilistic benchmark is expanded to assess the aggregated impacts of PHEVs and PV electricity on residential distribution systems. The performed analysis showed that PV electricity has the potential to meet a portion of PHEV charging demands

and thus reduce the loading of different distribution system equipment. This reduction leads to a decrease in the number of distribution transformers that require upgrading in the medium-term projection. However, this is not the case for the long-term projection, as PV electricity is not able to meet the much increased demand resulting from higher PHEV penetration. As a result, all secondary transformers should still be upgraded in the long-term projection whether PV arrays are present in the system or not. Another important conclusion made in this chapter is that the negative impacts of PHEVs and PV electricity on the test system under study are restricted to secondary networks only, with an insignificant impact on the primary system.

In Chapter 6, the author proposes using BESSs as a possible means of mitigating the aggregated impacts of both PV electricity and PHEVs such as to facilitate their integration into distribution networks. This objective can be achieved by storing PV electricity generated during low demand periods, when reverse power flow is most likely to occur, in small-scale dispersed BESSs located downstream of secondary distribution transformers. Then, reusing this energy to meet part of the PHEV charging demand during peak periods when this demand is most likely to overload distribution equipment. The previously developed MC-based probabilistic benchmark is used to size and schedule the operation of the proposed BESSs, with consideration of the various uncertainties inherent in the system. Simulation results demonstrated the technical feasibility of the proposed solution: BESSs installed in secondary distribution networks can mitigate distribution transformer overloading and limit the reverse flow of power through the transformers so that it is kept within permissible limits. However, the performed cost-benefit analysis for the system under study showed that the utilization of BESSs to facilitate the integration of BESSs and PV electricity in distribution networks is not cost-effective as the costs associated with the proposed BESSs exceed their anticipated benefits.

In Chapter 7, a novel bilayer architecture for residential distribution systems is proposed as a means of facilitating the integration of PHEVs and PV electricity. With the proposed architecture, the distribution system becomes a bilayer system composed of the traditional AC layer for interfacing with existing system loads, plus an embedded DC layer for interfacing with DC technologies present in the distribution system and currently interfaced via power electronic converters (such as PV arrays and PHEVs). A centralized bidirectional converter coupled with a storage device links the two layers and controls the power flow between them. After that, the MC-based probabilistic benchmark is used to size and schedule the operation of different system components, with consideration of the various uncertainties inherent in the system. Simulation results suggest that the proposed bilayer system

would facilitate the integration of PV electricity and PHEVs in the residential sector: utilizing the DC layer of the proposed system to interface PHEVs and PV arrays would significantly mitigate distribution transformer overloading and limit the reverse flow of power through the transformers so that it is kept within permissible limits. The analysis also revealed that the elimination of the extra DC/AC conversion stage, which is required for PHEVs and PV arrays to interface with the existing AC network, would increase PV array productivity and decrease the amount of energy required to meet PHEV charging demands. A cost/benefit analysis confirmed the cost-effectiveness of the bilayer system: the cost savings associated with the bilayer system exceed its implementation costs. This cost-effectiveness is attributed to the fact that, in the proposed bilayer system, multiple-stage sophisticated DC/AC PV array inverters (operating only during daytime) and AC/DC PHEV battery chargers (operating only in the evening) are replaced by a centralized bidirectional converter, whose overall diversified rating is less than the summation of the individual ratings of the small dispersed power conversion stages. Another important conclusion made in this chapter is that if the DC layer of the proposed bilayer system is used only to interface PHEVs and PV arrays, the energy loss savings achieved by the elimination of the extra power conversion stages in these two technologies for the system under study are not enough to compensate for the additional losses associated with the proposed bilayer system. However, using the DC layer of the proposed system to supply part of the existing household electronic loads with DC electricity can compensate for the extra losses associated with the proposed bilayer system and increase distribution system overall efficiency. This conclusion suggests that the technical merit of the proposed bilayer system is more evident in the long-term projection, when there is a substantial penetration of DC-powered electronic loads.

By comparing the solutions presented in Chapters 6 and 7 (Table 8-1), it becomes evident that both solutions have the potential to facilitate the integration of PHEVs and PV electricity in the residential sector, with respect to both mitigating secondary distribution transformer overloading and limiting reverse power flow through the transformers during PV peak generation periods so that it is kept within permissible limits. However, the traditional solution involving the use of small-scale dispersed BESSs (proposed in Chapter 6) is expensive and not economically feasible. The futuristic bilayer distribution system architecture (proposed in Chapter 7), on the other hand, is advantageous and cost-effective. Moreover, the proposed bilayer architecture would increase PV array productivity and decrease the amount of energy required to meet PHEV charging requirements, while at the same time offering customers the convenience of charging their PHEVs using DC rapid-chargers at their residences.

Table 8-1: Comparison between the proposed solutions

	Installing BESSs (Solution 1)	Bilayer system (Solution 2)
Mitigating distribution transformer overloading	Yes	Yes
Limiting reverse power flow through distribution transformers	Yes	Yes
Improving AC system voltages	Yes	Yes
Decreasing the number of voltage regulators actions	Yes	Yes
Increasing PV array productivity	No	Yes
Decreasing PHEV charging requirements	No	Yes
Allowing for PHEV DC rapid-charging at residences	No	Yes
Cost-effective	No	Yes

These advantages suggest that the bilayer system (proposed in Chapter 7) is the more efficient and cost-effective alternative for residential distribution systems with a high penetration level of PHEVs and PV arrays.

8.2 Contributions of the Thesis

The main contributions of this research are as follows:

i) The development of a probabilistic model to represent the uncertainties associated with the PV array output.

ii) The development of a probabilistic model to represent the uncertainties associated with existing electrical loads.

iii) Analyzing transportation data provided by the 2009 U.S. NHTS for the extraction of probability distribution functions that can be used to model individual driving habits impacting the charging process, such as home arrival times and daily distances travelled.

iv) Utilizing the previous probabilistic models for the development of a MC-based probabilistic benchmark that can be used to assess the aggregated impacts of PHEVs and PV systems on residential distribution networks, with consideration of different uncertainties in the system.

v) Developing a probabilistic sizing and scheduling methodology for BESSs to enable their use for facilitating the integration of PV arrays and PHEVs in residential distribution networks.

` `

vi) Proposing a novel bilayer architecture for distribution systems as a means of mitigating the negative impacts of PHEVs and PV electricity on residential distribution networks.

vii) Utilizing the previously developed MC-based probabilistic benchmark to size and schedule the operation of the components of the proposed bilayer system, with consideration of different uncertainties inherent in the system.

8.3 Directions for Future Work

In continuation of this research, the following topics are suggested for future analysis:

i) Studying the effect of implementing time-of-use demand response programs on PHEV charging demands.

ii) Utilizing the proposed MC-based probabilistic benchmark to develop a smart charging algorithm for PHEVs, with consideration of the various uncertainties inherent in the system.

iii) Studying the feasibility of using BESSs installed in the DC layer of the proposed bilayer system to smooth cloud-induced fluctuations in the PV array output power.

iv) Developing a comprehensive household energy consumption model to estimate the anticipated penetration of DC-powered electronic loads in the residential sector.

` `

Publications from this Research

Journal Papers:

1. M.S. ElNozahy and M.M.A.Salama, “Uncertainty-Based Design of a Bilayer Distribution System for Improved Integration of PHEVs and PV Arrays”, Accepted for publication in the IEEE Transactions on Sustainable Energy, pp. 1-16
2. M.S. ElNozahy, Tarek K. Abdel-Galil and M.M.A.Salama, “Probabilistic ESS Sizing and Scheduling for Improved Integration of PHEVs and PV Systems in Residential Distribution Systems”, Accepted for publication in Electric power Systems Research, pp. 1-12
3. M. S. ElNozahy and M. M. A. Salama, "A Comprehensive Study of the Impacts of Plug-in Hybrid Electric Vehicles on Residential Distribution Networks", IEEE Transactions on Sustainable Energy, vol.5, no.1, pp.332,342, Jan. 2014
4. M. S. ElNozahy and M. M. A. Salama, “Studying the Feasibility of Charging Plug-in Hybrid Electric Vehicles Using Photovoltaic Electricity in Residential Distribution Systems", Electric Power Systems Research, vol. 110, pp. 133-143, May 2014
5. M. S. ElNozahy and M. M. A. Salama, "Technical Impacts of Grid-Connected Photovoltaic Systems on Electrical Networks—A review", Journal of Renewable and Sustainable Energy, 5: 032702, pp. 1-12, May 2013
6. M.S. ElNozahy and M.M.A.Salama, “A Novel Load Modeling Approach for Smart Grid Applications”, International Journal of Electric power and Energy Systems, pp. 1-12 (Under Review)

Conference Papers:

7. M. S. ElNozahy, M. M. A. Salama and R. Seethapathy "A Probabilistic Load Modelling Approach using Clustering Algorithms", Power and Energy Society General Meeting, 2013 IEEE, Vancouver, pp. 1-5, 21-25 July 2013
8. M. S. ElNozahy and M. M. A. Salama, "A Probabilistic Approach for Modelling Photovoltaic Systems’ Electrical Output”, Proceedings of the 15th International Middle East Power Systems Conference, Egypt, pp.1-8, 21-25 Dec. 2012

Bibliography

[1] L. Rajamani, "The Cancun climate agreements: reading the text, subtext and tea leaves," *International and Comparative Law Quarterly*, vol. 60, pp. 499-519, 2011.

[2] M. Meinshausen, N. Meinshausen, W. Hare, S. C. B. Raper, K. Frieler, R. Knutti, *et al.*, "Greenhouse-gas emission targets for limiting global warming to 2 C," *Nature*, vol. 458, pp. 1158-1162, 2009.

[3] "World energy outlook special report 2013: Redrawing the energy climate map," International Energy Agency, 2013.

[4] "International energy outlook 2013," U.S. Department of Energy, 2013.

[5] A. Zahedi, "Maximizing solar PV energy penetration using energy storage technology," *Renewable and Sustainable Energy Reviews*, vol. 15, pp. 866-870, January 2010.

[6] W. F. Marion, C. J. Riordan, and D. S. Renné, *Shining on: A primer on solar radiation data*: National Renewable Energy Laboratory, 1992.

[7] (August 2010). *Feed-in tariff prices for renewable energy projects in Ontario: August 13, 2010*. Available: http://microfit.powerauthority.on.ca/sites/default/files/page/Price_Schedule_August_13_2010.pdf

[8] (March 2014). *Bi-weekly microFIT report: November 2013*. Available: http://microfit.powerauthority.on.ca/sites/default/files/bi-weekly_reports/mFIT%20Report%20Bi-Weekly%20Nov%201%2C2013.pdf

[9] M. Kintner-Meyer, K. Schneider, and R. Pratt, "Impacts assessment of plug-in hybrid vehicles on electric utilities and regional US power grids, Part 1: Technical analysis," Pacific Northwest National Laboratory, 2007.

[10] M. J. Scott, M. Kintner-Meyer, D. B. Elliott, and W. M. Warwick, "Impacts assessment of plug-in hybrid vehicles on electric utilities and regional US power grids: Part 2: Economic assessment," Pacific Northwest National Laboratory, 2007.

[11] J. Duncan, T. Halliburton, B. Heffernan, S. Hardie, N. Watson, and G. Coates, "Electric vehicles: Impacts on New Zealand's electricity system," New Zealand Centre for Advanced Engineering (CAENZ), 2010.

[12] V. H. M. Quezada, J. R. Abbad, and T. G. S. Roman, "Assessment of energy distribution losses for increasing penetration of distributed generation," *Power Systems, IEEE Transactions on*, vol. 21, pp. 533-540, 2006.

[13] B. Mather, "Analysis of high-penetration levels of PV into the distribution grid in california," U.S. Department of Energy, 2011.

[14] M. Thomson, "Automatic voltage control relays and embedded generation," *Power Engineering Journal*, vol. 14, pp. 71-76, 2000.

[15] "Technical interconnection requirements for distributed generation: Micro generation & small generation, 3-phase, less than 30 kW," Hydro One Networks Inc., 2010.

[16] J. Taylor, A. Maitra, M. Alexander, D. Brooks, and M. Duvall, "Evaluations of plug-in electric vehicle distribution system impacts," in *Power and Energy Society General Meeting, 2010 IEEE*, 2010, pp. 1-6.

[17] Q. Kejun, Z. Chengke, M. Allan, and Y. Yue, "Load model for prediction of electric vehicle charging demand," in *Power System Technology (POWERCON), 2010 International Conference on*, 2010, pp. 1-6.

[18] L. Kelly, A. Rowe, and P. Wild, "Analyzing the impacts of plug-in electric vehicles on distribution networks in British Columbia," in *Electrical Power & Energy Conference (EPEC), 2009 IEEE*, 2009, pp. 1-6.

[19] F. Lambert, "Secondary distribution impacts of residential electric vehicle charging," Public Interest Energy Research, California Energy Commission, 2000.

[20] G. A. Putrus, P. Suwanapingkarl, D. Johnston, E. C. Bentley, and M. Narayana, "Impact of electric vehicles on power distribution networks," in *Vehicle Power and Propulsion Conference, 2009. (VPPC '09). IEEE*, 2009, pp. 827-831.

[21] N. DeForest, J. Funk, A. Lorimer, B. Ur, I. Sidhu, P. Kaminsky, *et al.*, "Impact of widespread electric vehicle adoption on the electrical utility business–Threats and opportunities," University of California, Berkeley, 2009.
[22] J. H. R. Enslin, "Network impacts of high penetration of photovoltaic solar power systems," in *Power and Energy Society General Meeting, 2010 IEEE*, 2010, pp. 1-5.
[23] J. Enslin, "Grid impacts and solutions of renewables at high penetration levels," Quanta Technology, 2009.
[24] H. Asano, K. Yajima, and Y. Kaya, "Influence of photovoltaic power generation on required capacity for load frequency control," *Energy Conversion, IEEE Transactions on,* vol. 11, pp. 188-193, 1996.
[25] S. M. Chalmers, M. M. Hitt, J. T. Underhill, P. M. Anderson, P. L. Vogt, and R. Ingersoll, "The effect of photovoltaic power generation on utility operation," *Power Apparatus and Systems, IEEE Transactions on,* vol. PAS-104, pp. 524-530, 1985.
[26] A. F. Povlsen and A. S. Elsam, "Impacts of power penetration from photovoltaic power systems in distribution networks," International Energy Agency, 2002.
[27] M. Thomson and D. G. Infield, "Impact of widespread photovoltaics generation on distribution systems," *Renewable Power Generation, IET,* vol. 1, pp. 33-40, 2007.
[28] N. Miller and Z. Ye, "Distributed generation penetration study " National Renewable Energy Laboratory, 2003.
[29] A. Woyte, T. Vu Van, K. Purchala, R. Belmans, and J. Nijs, "Quantifying the occurrence and duration of power fluctuations introduced by photovoltaic systems," in *Power Tech Conference Proceedings, 2003 IEEE Bologna*, 2003, p. 7 pp. Vol.3.
[30] K. Myers, S. Klein, and D. Reindl, "Assessment of high penetration of photovoltaics on peak demand and annual energy use," Public Service Commission of Wisconsin, 2010.
[31] J. W. Brennan Louw, Tim Wohlgemut, "Economic impacts of solar energy in ontario," ClearSky Advisors, 2010.
[32] M. Duvall, E. Knipping, M. Alexander, L. Tonachel, and C. Clark, "Environmental assessment of plug-in hybrid electric vehicles. Volume 1: Nationwide greenhouse gas emissions," *Electric Power Research Institute, Palo Alto, CA,* vol. 1015325, 2007.
[33] J. C. Gomez and M. M. Morcos, "Impact of EV battery chargers on the power quality of distribution systems," *Power Delivery, IEEE Transactions on,* vol. 18, pp. 975-981, 2003.
[34] L. Kelly, "Probabilistic modelling of plug-in hybrid electric vehicle impacts on distribution networks in British Columbia," Master of applied science, Mechanical Engineering, University of Victoria, Victoria, British Columbia, 2009.
[35] S. Rahman and G. B. Shrestha, "An investigation into the impact of electric vehicle load on the electric utility distribution system," *Power Delivery, IEEE Transactions on,* vol. 8, pp. 591-597, 1993.
[36] S. Shafiee, M. Fotuhi-Firuzabad, and M. Rastegar, "Investigating the impacts of plug-in hybrid electric vehicles on power distribution systems," *Smart Grid, IEEE Transactions on,* vol. 4, pp. 1351-1360, 2013.
[37] A. D. Hilshey, P. D. H. Hines, P. Rezaei, and J. R. Dowds, "Estimating the impact of electric vehicle smart charging on distribution transformer aging," *Smart Grid, IEEE Transactions on,* vol. 4, pp. 905-913, 2013.
[38] H. Turker, A. Hably, and S. Bacha, "Smart charging of plug-in hybrid electric vehicles (PHEVs) on the residential electric grid regarding the voltage plan," in *Electric Vehicle Conference (IEVC), 2013 IEEE International*, 2013, pp. 1-6.
[39] "IEEE recommended practice for utility interface of photovoltaic (PV) systems," *IEEE Std 929-2000*.
[40] F. A. Farret and M. G. Simões, *Integration of alternative sources of energy*: Wiley Online Library, 2006.
[41] D. M. Chapin, C. S. Fuller, and G. L. Pearson, "A new silicon p-n Junction photocell for converting solar radiation into electrical power," *Journal of Applied Physics,* vol. 25, pp. 676-677, 1954.
[42] A. Goetzberger and V. U. Hoffmann, *Photovoltaic solar energy generation*: Springer, 2005.
[43] L. Wu, Z. Zhao, and J. Liu, "A single-stage three-phase grid-connected photovoltaic system With modified MPPT method and reactive power compensation," *Energy Conversion, IEEE Transactions on,* vol. 22, pp. 881-886, 2007.

[44] S. Ong, C. Campbell, P. Denholm, R. Margolis, and G. Heath, "Land-use requirements for solar power plants in the United States," National Renewable Energy Laboratory, 2013.
[45] P. Luukkonen, P. Bateman, J. Hiscock, Y. Poissant, D. Howard, and L. Dignard-Bailey, "National survey report of PV power applications in Canada," Canmet Energy, 2013.
[46] G. Masson, M. Latour, and D. Biancardi, "Global market outlook for photovoltaics until 2016," European Photovoltaic Industry Association, 2012.
[47] (May 2014). *German solar power output up 60 pct in 2011*. Available: http://af.reuters.com/article/commoditiesNews/idAFL6E7NT1WK20111229?sp=true.
[48] L. Solarbuzz, "German PV market 2006," Solarbuzz Inc., 2007.
[49] (October 2014). *Recent Facts about Photovoltaics in Germany*. Available: http://www.ise.fraunhofer.de/en/publications/veroeffentlichungen-pdf-dateien-en/studien-und-konzeptpapiere/recent-facts-about-photovoltaics-in-germany.pdf
[50] (May 2014). *Wichtigste änderungen und fördersätze photovoltaik*. Available: http://www.solarwirtschaft.de/fileadmin/content_files/EEG2009_Zusammenfass.pdf
[51] (September 2011). *2020 renewable transmission conceptual plan based on inputs from the RETI process*. Available: http://www.caiso.com/242a/242ae729af70.pdf.
[52] "Renewable energy country attractiveness indices," Ernst & Young, 2010.
[53] (May 2011). *India to unveil 20GW solar target under climate plan*. Available: http://www.reuters.com/article/2009/07/28/idUSDEL104230
[54] Y. Ueda, T. Oozeki, K. Kurokawa, T. Itou, K. Kitamura, Y. Miyamoto, *et al.*, "Detailed performance analysis results of grid-connected clustered PV systems in Japan–First 200 Systems Results of Demonstrative Research on Clustered PV Systems," *20th European PVSEC, Barcelona*, 2005.
[55] F. Katiraei, K. Mauch, and L. Dignard-Bailey, "Integration of photovoltaic power systems in high-penetration clusters for distribution networks and mini-grids," National Resources Canada , 2009.
[56] H. Laukamp, M. Thoma, T. Meyer, and T. Erge, "Impact of a large capacity of distributed PV production on the low voltage grid," in *19th European Photovoltaic Solar Energy Conference*, Paris, France, June 2004, pp. 7-11.
[57] S. Cobben, B. Gaiddon, and H. Laukamp, "Impact of photovoltaic generation on power quality in urban areas with high PV population," PV Upscale, 2008.
[58] J. H. R. Enslin and P. J. M. Heskes, "Harmonic interaction between a large number of distributed power inverters and the distribution network," *Power Electronics, IEEE Transactions on*, vol. 19, pp. 1586-1593, 2004.
[59] P. McNutt, J. Hambrick, and M. Keesee, "Effects of photovoltaics on distribution system voltage regulation," in *34th IEEE Photovoltaic Specialists Conference (PVSC)*, Philadelphia, PA June 2009, pp. 001914-001917.
[60] J. T. Day and W. J. Hobbs, "Reliability impact of solar electric generation upon electric utility systems," *Reliability, IEEE Transactions on*, vol. 31, pp. 304-307, 1982.
[61] W. T. Jewell, R. Ramakumar, and S. R. Hill, "A study of dispersed photovoltaic generation on the PSO system," *Energy Conversion, IEEE Transactions on*, vol. 3, pp. 473-478, 1988.
[62] (May 2014). *Integrating PV on distribution*. Available: http://www.ece.cmu.edu/~electriconf/2011/pdfs/Navigant%20-%20Integrating%20PV%20on%20Distribution%20-%20CMU%20Electricity%20Industry%20-%2003-09-2011.pdf
[63] W. T. Jewell and T. D. Unruh, "Limits on cloud-induced fluctuation in photovoltaic generation," *Energy Conversion, IEEE Transactions on*, vol. 5, pp. 8-14, 1990.
[64] L. Haifeng, J. Licheng, D. Le, and A. A. Chowdhury, "Impact of high penetration of solar photovoltaic generation on power system small signal stability," in *Power System Technology (POWERCON), 2010 International Conference on*, 2010, pp. 1-7.
[65] T. Yun Tiam and D. S. Kirschen, "Impact on the power system of a large penetration of photovoltaic generation," in *Power Engineering Society General Meeting, 2007. IEEE*, 2007, pp. 1-8.
[66] R. Shah, N. Mithulananathan, R. Bansal, K. Y. Lee, and A. Lomi, "Influence of large-scale PV on voltage stability of sub-transmission system," *International Journal on Electrical Engineering and Informatics*, vol. 4, pp. 148-161, 2012.

[67] V. Levi, M. Kay, and I. Povey, "Reverse power flow capability of tap-changers," in *Electricity Distribution, 2005. CIRED 2005. 18th International Conference and Exhibition on*, 2005, pp. 1-5.
[68] C. Whitaker, J. Newmiller, M. Ropp, and B. Norris, "Distributed photovoltaic systems design and technology requirements," Sandia laboratories 2008.
[69] W. L. Kling, A. Orths, V. Cuk, J. F. G. Cobben, R. B. Timens, B. Verhelst, *et al.*, "Power quality issues related to new means of distributed generation and loads," in *Power and Energy Society General Meeting, 2011 IEEE*, 2011, pp. 1-7.
[70] D. G. Infield, P. Onions, A. D. Simmons, and G. A. Smith, "Power quality from multiple grid-connected single-phase inverters," *Power Delivery, IEEE Transactions on*, vol. 19, pp. 1983-1989, 2004.
[71] M. Aiello, A. Cataliotti, S. Favuzza, and G. Graditi, "Theoretical and experimental comparison of total harmonic distortion factors for the evaluation of harmonic and interharmonic pollution of grid-connected photovoltaic systems," *Power Delivery, IEEE Transactions on*, vol. 21, pp. 1390-1397, 2006.
[72] W. Freitas, X. Wilsun, C. M. Affonso, and H. Zhenyu, "Comparative analysis between ROCOF and vector surge relays for distributed generation applications," *Power Delivery, IEEE Transactions on*, vol. 20, pp. 1315-1324, 2005.
[73] N. Jenkins and et al., *Embedded generation*: Institution of Engineering and Technology, 2000.
[74] W. Freitas, H. Zhenyu, and X. Wilsun, "A practical method for assessing the effectiveness of vector surge relays for distributed generation applications," *Power Delivery, IEEE Transactions on*, vol. 20, pp. 57-63, 2005.
[75] M. A. Redfern, O. Usta, and G. Fielding, "Protection against loss of utility grid supply for a dispersed storage and generation unit," *Power Delivery, IEEE Transactions on*, vol. 8, pp. 948-954, 1993.
[76] H. Kobayashi, K. Takigawa, E. Hashimoto, A. Kitamura, and H. Matsuda, "Method for preventing islanding phenomenon on utility grid with a number of small scale PV systems," in *Photovoltaic Specialists Conference, 1991., Conference Record of the Twenty Second IEEE*, 1991, pp. 695-700 vol.1.
[77] J. Sung-Il and K. Kwang-Ho, "An islanding detection method for distributed generations using voltage unbalance and total harmonic distortion of current," *Power Delivery, IEEE Transactions on*, vol. 19, pp. 745-752, 2004.
[78] S. K. Salman, D. J. King, and G. Weller, "New loss of mains detection algorithm for embedded generation using rate of change of voltage and changes in power factors," in *Developments in Power System Protection, 2001, Seventh International Conference on (IEE)*, 2001, pp. 82-85.
[79] P. Fu-Sheng and H. Shyh-Jier, "A detection algorithm for islanding-prevention of dispersed consumer-owned storage and generating units," *Energy Conversion, IEEE Transactions on*, vol. 16, pp. 346-351, 2001.
[80] P. O'Kane and B. Fox, "Loss of mains detection for embedded generation by system impedance monitoring," in *Developments in Power System Protection, Sixth International Conference on*, 1997, pp. 95-98.
[81] G. A. Smith, P. A. Onions, and D. G. Infield, "Predicting islanding operation of grid connected PV inverters," *Electric Power Applications, IEE Proceedings* -, vol. 147, pp. 1-6, 2000.
[82] H. Guo-Kiang, C. Chih-Chang, and C. Chern-Lin, "Automatic phase-shift method for islanding detection of grid-connected photovoltaic inverters," *Energy Conversion, IEEE Transactions on*, vol. 18, pp. 169-173, 2003.
[83] Y. Jun, C. Liuchen, and C. Diduch, "A new adaptive logic phase-shift algorithm for anti-islanding protections in inverter-based DG systems," in *Power Electronics Specialists Conference, 2005. (PESC '05). IEEE 36th*, 2005, pp. 2482-2486.
[84] S. Yuyama, T. Ichinose, K. Kimoto, T. Itami, T. Ambo, C. Okado, *et al.*, "A high speed frequency shift method as a protection for islanding phenomena of utility interactive PV systems," *Solar Energy Materials and Solar Cells*, vol. 35, pp. 477-486, 1994.
[85] M. E. Ropp, M. Begovic, and A. Rohatgi, "Analysis and performance assessment of the active frequency drift method of islanding prevention," *Energy Conversion, IEEE Transactions on*, vol. 14, pp. 810-816, 1999.

` `

[86] G. Hernandez-Gonzalez and R. Iravani, "Current injection for active islanding detection of electronically-interfaced distributed resources," *Power Delivery, IEEE Transactions on*, vol. 21, pp. 1698-1705, 2006.

[87] H. Karimi, A. Yazdani, and R. Iravani, "Negative-sequence current injection for fast islanding detection of a distributed resource unit," *Power Electronics, IEEE Transactions on*, vol. 23, pp. 298-307, 2008.

[88] V. Menon and M. H. Nehrir, "A hybrid islanding detection technique using voltage unbalance and frequency set point," *Power Systems, IEEE Transactions on*, vol. 22, pp. 442-448, 2007.

[89] P. Mahat, C. Zhe, and B. Bak-Jensen, "A hybrid islanding detection technique using average rate of voltage change and real power shift," in *Power & Energy Society General Meeting, 2009. IEEE*, 2009, pp. 1-1.

[90] Y. Jun, C. P. Diduch, and C. Liucheng, "Islanding detection using proportional power spectral density," *Power Delivery, IEEE Transactions on*, vol. 23, pp. 776-784, 2008.

[91] A. Ishibashi, M. Imai, K. Omata, S. Sato, T. Takagi, Y. Nakachi, *et al.*, "New type of islanding detection system for distributed generation based on voltage angle difference between utility network and distributed generation site," in *Developments in Power System Protection, 2004. Eighth IEE International Conference on*, 2004, pp. 542-545 Vol.2.

[92] C. G. Bright, "COROCOF: comparison of rate of change of frequency protection. A solution to the detection of loss of mains," in *Developments in Power System Protection, 2001, Seventh International Conference on (IEE)*, 2001, pp. 70-73.

[93] X. Wilsun, Z. Guibin, L. Chun, W. Wencong, W. Guangzhu, and J. Kliber, "A power line signaling based scheme for anti-islanding protection of distributed generators: Part I: Scheme and analysis," in *Power Engineering Society General Meeting, 2007. IEEE*, 2007, pp. 1-1.

[94] W. Wencong, J. Kliber, Z. Guibin, X. Wilsun, B. Howell, and T. Palladino, "A power line signaling based scheme for anti-islanding protection of distributed generators: Part II: Field test results," in *Power Engineering Society General Meeting, 2007. IEEE*, 2007, pp. 1-1.

[95] H. H. Zeineldin, A. Saif, M. M. Salama, and A. Zobaa, "Three-dimensional non-detection zone for assessing anti-islanding detection schemes," *Electric Power Components and Systems*, vol. 38, pp. 621-636, 2010.

[96] B. Kroposki and A. Vaughn, "DG power quality, protection, and reliability case studies report," National Renewable Energy Laboratory, 2003.

[97] G. Delille, B. François, and G. Malarange, "Dynamic frequency control support by energy storage to reduce the impact of wind and solar generation on isolated power system's inertia," *Sustainable Energy, IEEE Transactions on*, vol. 3, pp. 931-939, 2012.

[98] H. Ibrahim, A. Ilinca, and J. Perron, "Energy storage systems: Characteristics and comparisons," *Renewable and Sustainable Energy Reviews*, vol. 12, pp. 1221-1250, 2008.

[99] J. Taylor, A. Maitra, M. Alexander, D. Brooks, and M. Duvall, "Evaluation of the impact of plug-in electric vehicle loading on distribution system operations," in *Power & Energy Society General Meeting, 2009. PES '09. IEEE*, 2009, pp. 1-6.

[100] S. W. Hadley and A. A. Tsvetkova, "Potential impacts of plug-in hybrid electric vehicles on regional power generation," *The Electricity Journal*, vol. 22, pp. 56-68, 2009.

[101] W. Short and P. Denholm, "A preliminary assessment of plug-in hybrid electric vehicles on wind energy markets," National Renewable Energy Laboratory, 2006.

[102] P. Mohseni and R. G. Stevie, "Electric vehicles: Holy grail or fool's gold," in *Power & Energy Society General Meeting, 2009. IEEE*, 2009, pp. 1-5.

[103] (May 2014). *Tesla debacle highlights need for new EV battery technology*. Available: http://www.forbes.com/sites/rosskennethurken/2013/02/12/tesla-debacle-highlights-need-for-new-ev-battery-technology/

[104] K. Feeney and D. Adams, "Economic viability of electric vehicles," AECOM Australia, 2009.

[105] M. Book, M. Groll, X. Mosquet, D. Rizoulis, and G. Sticher, "The comeback of the electric car: How real, how soon, and what must happen next?," The Boston Consulting Group, 2009.

[106] M. Rowand, "The Electricity utility-business case," in *Plug-In Conference*, San Jose, CA, May 2008, pp. 1-7.

[107] P. T. Staats, W. M. Grady, A. Arapostathis, and R. S. Thallam, "A statistical method for predicting the net harmonic currents generated by a concentration of electric vehicle battery chargers," *Power Delivery, IEEE Transactions on*, vol. 12, pp. 1258-1266, 1997.
[108] C. Mersman, M. Morcos, and N. Dillman, "On the design of a novel microprocessor—Based battery charger for electric vehicles," in *Proc. Eighth Europe. Power Electron. Conf., Lausanne, Switzerland*, 1999.
[109] Y. Wang, R. O'Connell, and G. Brownfield, "The harmonic impact of electric vehicle battery chargers on residential power distribution," in *Proceedings of the American Power Conference*, 1999, pp. 692-697.
[110] V. E. Wagner, J. C. Balda, D. C. Griffith, A. McEachern, T. M. Barnes, D. P. Hartmann, *et al.*, "Effects of harmonics on equipment," *Power Delivery, IEEE Transactions on*, vol. 8, pp. 672-680, 1993.
[111] K. Clement-Nyns, E. Haesen, and J. Driesen, "The impact of charging plug-in hybrid electric vehicles on a residential distribution grid," *Power Systems, IEEE Transactions on*, vol. 25, pp. 371-380, 2010.
[112] I. Sharma, C. Canizares, and K. Bhattacharya, "Smart charging of PEVs penetrating Into residential distribution systems," *Smart Grid, IEEE Transactions on*, vol. 5, pp. 1196-1209, 2014.
[113] G. Qiuming, S. Midlam-Mohler, V. Marano, and G. Rizzoni, "Study of PEV charging on residential distribution transformer life," *Smart Grid, IEEE Transactions on*, vol. 3, pp. 404-412, 2012.
[114] C. Gellings, "Estimating the costs and benefits of the smart grid: a preliminary estimate of the investment requirements and the resultant benefits of a fully functioning smart grid," Electric Power Research Institute, 2011.
[115] W. Kramer, S. Chakraborty, B. Kroposki, and H. Thomas, "Advanced power electronic interfaces for distributed energy systems," National Renewable Energy Laboratory, 2008.
[116] (May 2014). *Chrysler to source next-gen EV batteries from A123 systems*. Available: http://www.leftlanenews.com/chrysler-to-source-electric-vehicle-batteries-from-a123-systems.html
[117] M. H. Kalos and P. A. Whitlock, *Monte Carlo methods*: Wiley-VCH, 2008.
[118] G. Fishman, *Monte Carlo: Concepts, algorithms, and applications*: Springer, 1996.
[119] W. A. Omran, M. Kazerani, and M. M. A. Salama, "A Clustering-Based Method for Quantifying the Effects of Large On-Grid PV Systems," *Power Delivery, IEEE Transactions on*, vol. 25, pp. 2617-2625, 2010.
[120] B. H. Chowdhury, "Effect of central station photovoltaic plant on power system security," in *Photovoltaic Specialists Conference, 1990., Conference Record of the Twenty First IEEE*, 1990, pp. 831-835.
[121] F. A. Viawan, F. Vuinovich, and A. Sannino, "Probabilistic approach to the design of photovoltaic distributed generation in low voltage feeder," in *Probabilistic Methods Applied to Power Systems, 2006. (PMAPS 2006). International Conference on*, 2006, pp. 1-7.
[122] I. Abouzahr and R. Ramakumar, "An approach to assess the performance of utility-interactive photovoltaic systems," *IEEE Transactions on Energy Conversion*, vol. 8, pp. 145-153, 1993.
[123] L. Shaobo, H. Minxiao, F. Ruixiang, and H. Xiaodong, "Configuration of energy storage system for distribution network with high penetration of PV," in *Renewable Power Generation (RPG 2011), IET Conference on*, 2011, pp. 1-6.
[124] R. Xu and D. C. Wunsch, *Clustering*: Wiley-IEEE Press, 2009.
[125] E. I. Ortiz-Rivera and F. Peng, "Analytical model for a photovoltaic module using the electrical characteristics provided by the manufacturer data sheet," in *Power Electronics Specialists Conference, 2005. (PESC '05). IEEE 36th*, 2005, pp. 2087-2091.
[126] H. S. Rauschenbach, *Solar cell array design handbook: The principles and technology of photovoltaic energy conversion*: Van Nostrand Reinhold Ltd., 1980.
[127] S. Liu and R. A. Dougal, "Dynamic multiphysics model for solar array," *Energy Conversion, IEEE Transactions on*, vol. 17, pp. 285-294, 2002.
[128] J. Bishop, "Computer simulation of the effects of electrical mismatches in photovoltaic cell interconnection circuits," *Solar cells*, vol. 25, pp. 73-89, 1988.
[129] M. Wolf and H. Rauschenbach, "Series resistance effects on solar cell measurements," *Advanced energy conversion*, vol. 3, pp. 455-479, 1963.

[130] D. Picault, B. Raison, S. Bacha, J. De La Casa, and J. Aguilera, "Forecasting photovoltaic array power production subject to mismatch losses," *Solar energy*, vol. 84, pp. 1301-1309, 2010.
[131] M. Veerachary, "PSIM circuit-oriented simulator model for the nonlinear photovoltaic sources," *IEEE transactions on aerospace and electronic systems*, vol. 42, pp. 735-740, 2006.
[132] W. Xiao, W. G. Dunford, and A. Capel, "A novel modeling method for photovoltaic cells," in *Power Electronics Specialists Conference, 2004. (PESC 04). 2004 IEEE 35th Annual*, 2004, pp. 1950-1956.
[133] M. Ropp, M. Begovic, and A. Rohatgi, "Determination of the curvature derating factor for the Georgia Tech Aquatic Center photovoltaic array," in *Photovoltaic Specialists Conference, 1997., Conference Record of the Twenty-Sixth IEEE*, 1997, pp. 1297-1300.
[134] J. V. Paatero and P. D. Lund, "Effects of large-scale photovoltaic power integration on electricity distribution networks," *Renewable Energy*, vol. 32, pp. 216-234, 2007.
[135] W. A. Omran, M. Kazerani, and M. M. A. Salama, "A study of the impacts of power fluctuations generated from large PV systems," in *Sustainable Alternative Energy (SAE), 2009 IEEE PES/IAS Conference on*, 2009, pp. 1-6.
[136] R. Perez, J. Doty, B. Bailey, and R. Stewart, "Experimental evaluation of a photovoltaic simulation program," *Solar energy*, vol. 52, pp. 359-365, 1994.
[137] T. Ishikawa, "Grid-connected photovoltaic power systems: survey of inverter and related protection equipments," International Energy Agency, 2002.
[138] F. Loxsom and P. Durongkaveroj, "Estimating the performance of a photovoltaic pumping system," *Solar energy*, vol. 52, pp. 215-219, 1994.
[139] L. I. Smith, "A tutorial on principal components analysis," *Cornell University, USA*, vol. 51, p. 52, 2002.
[140] S. Wold, K. Esbensen, and P. Geladi, "Principal component analysis," *Chemometrics and intelligent laboratory systems*, vol. 2, pp. 37-52, 1987.
[141] I. Jolliffe, *Principal component analysis*: Wiley Online Library, 2005.
[142] H. Abdi and L. J. Williams, "Principal component analysis," *Wiley Interdisciplinary Reviews: Computational Statistics*, vol. 2, pp. 433-459, 2010.
[143] K. Ferenc, L. Csaba, and B. Attila, "Cluster validity measurement techniques," in *5th WSEAS International Conference on Artificial Intelligence, Knowledge Engineering and Data Bases*, Madrid, Spain, 2005, pp. 388-393.
[144] J. C. Dunn, "A fuzzy relative of the ISODATA process and its use in detecting compact well-separated clusters," *Journal of Cybernetics*, vol. 3, pp. 32-57, January 1973.
[145] D. L. Davies and D. W. Bouldin, "A cluster separation measure," *Pattern Analysis and Machine Intelligence, IEEE Transactions on*, pp. 224-227, 1979.
[146] X. L. Xie and G. Beni, "A validity measure for fuzzy clustering," *Pattern Analysis and Machine Intelligence, IEEE Transactions on*, vol. 13, pp. 841-847, 1991.
[147] J. A. Hartigan, *Clustering algorithms*: John Wiley & Sons, 1975.
[148] M. B. D. Coutto Filho, A. M. Leite da Silva, V. L. Arienti, and S. M. P. Ribeiro, "Probabilistic load modelling for power system expansion planning," in *Probabilistic Methods Applied to Electric Power Systems, 1991., Third International Conference on*, 1991, pp. 203-207.
[149] N. D. Hatziargyriou, T. S. Karakatsanis, and M. Papadopoulos, "Probabilistic load flow in distribution systems containing dispersed wind power generation," *Power Systems, IEEE Transactions on*, vol. 8, pp. 159-165, 1993.
[150] S. Conti and S. Raiti, "Probabilistic load flow for distribution networks with photovoltaic generators Part 1: Theoretical concepts and models," in *Clean Electrical Power, 2007. (ICCEP '07). International Conference on*, 2007, pp. 132-136.
[151] M. Shukla and G. Radman, "Optimal power flow using probabilistic load model," in *System Theory, 2005. (SSST '05). Proceedings of the Thirty-Seventh Southeastern Symposium on*, 2005, pp. 439-442.
[152] Z. Tianshu, S. Wanxing, S. Xiaohui, M. Xiaoli, and S. Changkai, "Probabilistic modelling and simulation of stochastic load for power system studies," in *Computer Modelling and Simulation (UKSim), 2013 UKSim 15th International Conference on*, 2013, pp. 519-524.
[153] P. Chen, B. Bak-Jensen, and Z. Chen, "Probabilistic load models for simulating the impact of load management," in *Power & Energy Society General Meeting, 2009. IEEE*, 2009, pp. 1-8.

[154] S. W. Heunis and R. Herman, "A probabilistic model for residential consumer loads," *Power Systems, IEEE Transactions on*, vol. 17, pp. 621-625, 2002.
[155] C. Singh and Q. Chen, "Generation system reliability evaluation using a cluster based load model," *Power Systems, IEEE Transactions on*, vol. 4, pp. 102-107, 1989.
[156] C. Grigg, P. Wong, P. Albrecht, R. Allan, M. Bhavaraju, R. Billinton, *et al.*, "The IEEE reliability test system-1996. ," *Power Systems, IEEE Transactions on*, vol. 14, pp. 1010-1020, 1999.
[157] Z. Darabi and M. Ferdowsi, "Aggregated impact of plug-in hybrid electric vehicles on electricity demand profile," *Sustainable Energy, IEEE Transactions on*, vol. 2, pp. 501-508, 2011.
[158] (May 2014). *About NHTS transferability statistics* Available: http://www.rita.dot.gov/bts/sites/rita.dot.gov.bts/files/subject_areas/national_household_travel_survey/about
[159] C. Samaras and K. Meisterling, "Life cycle assessment of greenhouse gas emissions from plug-in hybrid vehicles: implications for policy," *Environmental science & technology*, vol. 42, pp. 3170-3176, 2008.
[160] P. Jaramillo, C. Samaras, H. Wakeley, and K. Meisterling, "Greenhouse gas implications of using coal for transportation: Life cycle assessment of coal-to-liquids, plug-in hybrids, and hydrogen pathways," *Energy Policy*, vol. 37, pp. 2689-2695, 2009.
[161] S. Shahidinejad, S. Filizadeh, and E. Bibeau, "Profile of charging load on the grid due to plug-in vehicles," *Smart Grid, IEEE Transactions on*, vol. 3, pp. 135-141, 2012.
[162] Q. Gong, S. Midlam–Mohler, V. Marano, and G. Rizzoni, "Virtual PHEV fleet study based on Monte Carlo simulation," *International Journal of Vehicle Design*, vol. 58, pp. 266-290, 2012.
[163] A. Maitra, K. S. Kook, A. Giumento, J. Taylor, D. Brooks, M. Alexander, *et al.*, "Evaluation of PEV loading characteristics on Hydro Quebec‘s distribution system operations," in *Electric Vehicle Symposium*, 2009, pp. 1-11.
[164] A. Maitra, J. Taylor, D. Brooks, M. Alexander, and M. Duvall, "Integrating plug-in-electric vehicles with the distribution system," in *Electricity Distribution - Part 1, 2009. CIRED 2009. 20th International Conference and Exhibition on*, 2009, pp. 1-5.
[165] P. Denholm and W. Short, "Evaluation of utility system impacts and benefits of optimally dispatched plug-in hybrid electric vehicles," National Renewable Energy Laboratory, 2006.
[166] L. Pieltain Fernandez, G. S. Roman, R. Cossent, C. M. Domingo, and P. Frias, "Assessment of the impact of plug-in electric vehicles on distribution networks," *Power Systems, IEEE Transactions on*, vol. 26, pp. 206-213, 2011.
[167] S. Shengnan, M. Pipattanasomporn, and S. Rahman, "Challenges of PHEV penetration to the residential distribution network," in *Power & Energy Society General Meeting, 2009. IEEE*, 2009, pp. 1-8.
[168] J. P. Lopes, F. J. Soares, P. Almeida, and M. M. da Silva, "Smart charging strategies for electric vehicles: Enhancing grid performance and maximizing the use of variable renewable energy resources," in *(EVS24) Intenational Battery, Hybrid and Fuell Cell Electric Vehicle Symposium, Stavanger, Norveška*, 2009.
[169] P. Papadopoulos, S. Skarvelis-Kazakos, I. Grau, L. M. Cipcigan, and N. Jenkins, "Predicting electric vehicle impacts on residential distribution networks with distributed generation," in *Vehicle Power and Propulsion Conference (VPPC), 2010 IEEE*, 2010, pp. 1-5.
[170] J. Wang, K. Wu, Z. Liu, F. Wang, and Y. Zhao, "Impact of plug-in hybrid electric vehicles on power distribution networks," in *Electric Utility Deregulation and Restructuring and Power Technologies (DRPT), 2011 4th International Conference on*, 2011, pp. 1618-1622.
[171] J. A. Jardini, C. M. V. Tahan, M. R. Gouvea, S. U. Ahn, and F. M. Figueiredo, "Daily load profiles for residential, commercial and industrial low voltage consumers," *Power Delivery, IEEE Transactions on*, vol. 15, pp. 375-380, 2000.
[172] (May 2011). *Japanese power system models*. Available: http://www2.iee.or.jp/ver2/pes/23-st_model/english/index.html
[173] (May 2011). *SAE charging configurations and ratings terminology*. Available: http://www.sae.org/smartgrid/chargingspeeds.pdf

[174] (May 2011). *Distribution test feeders*. Available: http://www.ewh.ieee.org/soc/pes/dsacom/testfeeders/index.html
[175] J. Bishop, "Profiles on residential power consumption," The Fire Protection Research Foundation, 2010.
[176] K. Clement, E. Haesen, and J. Driesen, "Coordinated charging of multiple plug-in hybrid electric vehicles in residential distribution grids," in *Power Systems Conference and Exposition, 2009. (PSCE '09)*. 2009, pp. 1-7.
[177] (May 2012). *The EV project*. Available: http://www.theevproject.com/cms-assets/documents/127233-901153.q2-2013-rpt.pdf
[178] (September 2011). *Electric vehicle network*. Available: http://www.vde.com/de/verband/pressecenter/pressemeldungen/fach-und-wirtschaftspresse/seiten/2010-35.aspx
[179] N. Shidore, T. Bohn, M. Duoba, H. Lohse-Busch, and P. Sharer, "PHEV all electric range and fuel economy in charge sustaining mode for low SOC operation of the JCS VL41M Li-ion battery using Battery HIL," in *23rd International Electric Vehicle Symposium (EVS23)*, Anaheim, CA, 2007.
[180] C. Camus, C. M. Silva, T. L. Farias, and J. Esteves, "Impact of plug-in hybrid electric vehicles in the Portuguese electric utility system," in *Power Engineering, Energy and Electrical Drives, 2009. (POWERENG '09). International Conference on*, 2009, pp. 285-290.
[181] S. W. Hadley, "Evaluating the impact of plug-in hybrid electric vehicles on regional electricity supplies," in *Bulk Power System Dynamics and Control - VII. Revitalizing Operational Reliability, 2007 iREP Symposium*, 2007, pp. 1-12.
[182] L. Poch, M. Mahalik, W. Jianhui, and A. Vyas, "Impacts of plug-in hybrid electric vehicles on the electric power system in the western United States," in *Power and Energy Society General Meeting, 2010 IEEE*, 2010, pp. 1-7.
[183] J. R. Aguero, P. Chongfuangprinya, S. Shengnan, X. Le, F. Jahanbakhsh, and H. L. Willis, "Integration of plug-in electric vehicles and distributed energy resources on power distribution systems," in *Electric Vehicle Conference (IEVC), 2012 IEEE International*, 2012, pp. 1-7.
[184] L. Xin, L. A. C. Lopes, and S. S. Williamson, "On the suitability of plug-in hybrid electric vehicle (PHEV) charging infrastructures based on wind and solar energy," in *Power & Energy Society General Meeting, 2009. PES '09. IEEE*, 2009, pp. 1-8.
[185] J. Widén, E. Wäckelgård, J. Paatero, and P. Lund, "Impacts of distributed photovoltaics on network voltages: Stochastic simulations of three Swedish low-voltage distribution grids," *Electric Power Systems Research*, vol. 80, pp. 1562-1571, 2010.
[186] (May 2014). *Upset by Ontario's rising hydro rates? When it is sunny you can be making money*. Available: http://www.solacity.com/pvinstall.htm#What_About_Payback,_and_Return-On-Investment
[187] (February 2015). *Incentives of a Green Home*. Available: http://www.bcrea.bc.ca/green-tool-kit-for-realtors/incentives-of-a-green-home
[188] A. Bedir, B. Ozpineci, and J. E. Christian, "The impact of plug-in hybrid electric vehicle interaction with energy storage and solar panels on the grid for a zero energy house," in *Transmission and Distribution Conference and Exposition, 2010 IEEE PES*, 2010, pp. 1-6.
[189] X. Li, L. A. C. Lopes, and S. S. Williamson, "Charging plug-in hybrid electric vehicles (PHEVs) with solar energy," in *3rd Canadian Solar Buildings Conference*, New Brunswick, Canada, February 2008, pp. 1-8.
[190] Y. Gurkaynak and A. Khaligh, "Control and power management of a grid connected residential photovoltaic system with plug-in hybrid electric vehicle (PHEV) load," in *Applied Power Electronics Conference and Exposition, 2009. APEC 2009. Twenty-Fourth Annual IEEE*, 2009, pp. 2086-2091.
[191] F. Locment, M. Sechilariu, and C. Forgez, "Electric vehicle charging system with PV Grid-connected configuration," in *Vehicle Power and Propulsion Conference (VPPC), 2010 IEEE*, 2010, pp. 1-6.
[192] Y. M. Atwa and E. F. El-Saadany, "Optimal allocation of ESS in distribution systems with a high penetration of wind energy," *Power Systems, IEEE Transactions on*, vol. 25, pp. 1815-1822, 2010.
[193] J. Tant, F. Geth, D. Six, P. Tant, and J. Driesen, "Multiobjective battery storage to improve PV integration in residential distribution grids," *Sustainable Energy, IEEE Transactions on*, vol. 4, pp. 182-191, 2013.

[194] R. Yu, J. Kleissl, and S. Martinez, "Storage size determination for grid-connected photovoltaic systems," *Sustainable Energy, IEEE Transactions on*, vol. 4, pp. 68-81, 2013.
[195] C. A. Hill, M. C. Such, C. Dongmei, J. Gonzalez, and W. M. Grady, "Battery energy storage for enabling integration of distributed solar power generation," *Smart Grid, IEEE Transactions on*, vol. 3, pp. 850-857, 2012.
[196] C. Jin, J. Tang, and P. Ghosh, "Optimizing electric vehicle charging with energy storage in the electricity market," *Smart Grid, IEEE Transactions on*, vol. 4, pp. 311-320, 2013.
[197] M. Takagi, Y. Iwafune, K. Yamaji, H. Yamamoto, K. Okano, R. Hiwatari, *et al.*, "Economic value of PV energy storage using batteries of battery-switch stations," *Sustainable Energy, IEEE Transactions on*, vol. 4, pp. 164-173, 2013.
[198] L. Tsung-Ying and C. Nanming, "Determination of optimal contract capacities and optimal sizes of battery energy storage systems for time-of-use rates industrial customers," *Energy Conversion, IEEE Transactions on*, vol. 10, pp. 562-568, 1995.
[199] C. H. Lo and M. D. Anderson, "Economic dispatch and optimal sizing of battery energy storage systems in utility load-leveling operations," *Energy Conversion, IEEE Transactions on*, vol. 14, pp. 824-829, 1999.
[200] A. Oudalov, R. Cherkaoui, and A. Beguin, "Sizing and optimal operation of battery energy storage system for peak shaving application," in *Power Tech, 2007 IEEE Lausanne*, 2007, pp. 621-625.
[201] D. K. Maly and K. S. Kwan, "Optimal battery energy storage system (BESS) charge scheduling with dynamic programming," *Science, Measurement and Technology, IEE Proceedings* -, vol. 142, pp. 453-458, 1995.
[202] M. Ross, R. Hidalgo, C. Abbey, and G. Joos, "Analysis of energy storage sizing and technologies," in *Electric Power and Energy Conference (EPEC), 2010 IEEE*, 2010, pp. 1-6.
[203] J. Taylor, J. W. Smith, and R. Dugan, "Distribution modeling requirements for integration of PV, PEV, and storage in a smart grid environment," in *Power and Energy Society General Meeting, 2011 IEEE*, 2011, pp. 1-6.
[204] (July 2012). *Reference guide: The open distribution system simulator (OpenDSS)* Available: http://svn.code.sf.net/p/electricdss/code/trunk/Distrib/Doc/OpenDSSManual.pdf
[205] P. Poonpun and W. T. Jewell, "Analysis of the cost per Kilowatt Hour to store electricity," *Energy Conversion, IEEE Transactions on*, vol. 23, pp. 529-534, 2008.
[206] "Annual energy outlook 2006 with projection to 2030," U.S. Department of Energy, 2006.
[207] (May 2014). *Markups for equipment price determination*. Available: https://www1.eere.energy.gov/buildings/appliance_standards/commercial/pdfs/dist_trans_chp_7.pdf
[208] (April 2014). *Distribution transformers: Medium and high voltage GE-PROLEC® conventional single-phase pole type distribution transformers*. Available: http://www.electricalmanuals.net/files/CATALOGS/GE/BUY-LOG/20_BL.pdf
[209] (May 2014). *Electric vehicle battery prices down 14% year on year*. Available: http://www.newenergyfinance.com/PressReleases/view/210
[210] (May 2014). *The War of the Currents: AC vs. DC Power*. Available: http://energy.gov/articles/war-currents-ac-vs-dc-power
[211] D. Nilsson and A. Sannino, "Efficiency analysis of low- and medium- voltage DC distribution systems," in *Power Engineering Society General Meeting, 2004. IEEE*, 2004, pp. 2315-2321 Vol.2.
[212] D. J. Hammerstrom, "AC versus DC distribution systems: Did we get it right?," in *Power Engineering Society General Meeting, 2007. IEEE*, 2007, pp. 1-5.
[213] A. Sannino, G. Postiglione, and M. H. J. Bollen, "Feasibility of a DC network for commercial facilities," *Industry Applications, IEEE Transactions on*, vol. 39, pp. 1499-1507, 2003.
[214] K. Techakittiroj and V. Wongpaibool, "Co-existance between AC-distribution and DC-distribution: In the view of appliances," in *Computer and Electrical Engineering, 2009. ICCEE '09. Second International Conference on*, 2009, pp. 421-425.
[215] F. Blaabjerg, C. Zhe, and S. B. Kjaer, "Power electronics as efficient interface in dispersed power generation systems," *Power Electronics, IEEE Transactions on*, vol. 19, pp. 1184-1194, 2004.

[216] (December 2012). *Continuing efforts for efficiency improvements in electronic power conversion devices*. Available: http://www.epri.com/abstracts/Pages/ProductAbstract.aspx?ProductId=000000000001024341
[217] (May 2014). *What lies within: Improving the efficiency of internal power supplies*. Available: http://www.esource.com//system/files/files/2008-08/CEC-TB-41_IntPowerSupplies.pdf
[218] (September 2011). *Energy challenge: Balancing the grid*. Available: http://www.moixatechnology.com/contents/approach/energy-challenge.php
[219] "European commission communication to the council and the European parliament on policy instruments to reduce stand-by losses of consumer electronic equipment," International Energy Agency, 1999.
[220] S. Gab-Su, B. Jongbok, C. Kyusik, B. Hyunsu, and C. Bohyung, "Modeling and analysis of DC distribution systems," in *Power Electronics and ECCE Asia (ICPE & ECCE), 2011 IEEE 8th International Conference on*, 2011, pp. 223-227.
[221] G. Byeon, H. Lee, T. Yoon, G. Jang, W. Chae, and J. Kim, "A research on the characteristics of fault current of DC distribution system and AC distribution system," in *Power Electronics and ECCE Asia (ICPE & ECCE), 2011 IEEE 8th International Conference on*, 2011, pp. 543-550.
[222] (July 2011). *LVDC: The end of the plugs and sockets dilemma?* Available: http://www.iec.ch/etech/2011/etech_0711/tech-4.htm
[223] A. Pinomaa, J. Ahola, and A. Kosonen, "Fifth WSPLC 2011 workshop on power line communications" power line communication concept for the LVDC smart grid" " Finnish National Research Program SGEM, July 2011.
[224] J. G. Ciezki and R. W. Ashton, "Selection and stability issues associated with a navy shipboard DC zonal electric distribution system," *Power Delivery, IEEE Transactions on*, vol. 15, pp. 665-669, 2000.
[225] M. E. Baran and N. R. Mahajan, "DC distribution for industrial systems: opportunities and challenges," *Industry Applications, IEEE Transactions on*, vol. 39, pp. 1596-1601, 2003.
[226] (July 2012). *Local direct current* Available: http://www.neuralenergy.info/2009/06/local-direct-current.html
[227] "Short-circuit currents in DC auxiliary installations in power plants and substations," *IEC Std 61660-1997*.
[228] "IEEE recommended practice for the design of DC auxiliary power systems for generating stations," *IEEE Std 946-1992*.
[229] T. Kaipia, P. Salonen, J. Lassila, and J. Partanen, "Possibilities of the low voltage DC distribution systems," in *Nordac, Nordic Distribution and Asset Management Conference*, 2006, pp. 1-10.
[230] (September 2011). *High voltage power electronics* Available: http://www.power.ece.mcgill.ca/ResearchInterests/HVPE.htm
[231] "Low-voltage electrical installations – Part 1: Fundamental principles, assessment of general characteristics, definitions " *IEC Std 60364-2005*
[232] T. Kaipia, P. Salonen, J. Lassila, and J. Partanen, "Application of low voltage DC-distribution system-a techno-economical study," in *Proceedings of CIRED*, 2007, pp. 21-24.
[233] K. Engelen, E. Leung Shun, P. Vermeyen, I. Pardon, R. D'Hulst, J. Driesen, *et al.*, "The feasibility of small-scale residential DC distribution systems," in *IEEE Industrial Electronics, IECON 2006 - 32nd Annual Conference on*, 2006, pp. 2618-2623.
[234] "Low-voltage moulded-case circuit-breakers," *Technical catalogue 604050/012, ABB*, 2012.
[235] J. Rekola and H. Tuusa, "Comparison of line and load converter topologies in a bipolar LVDC distribution," in *Power Electronics and Applications (EPE 2011), Proceedings of the 2011-14th European Conference on*, 2011, pp. 1-10.
[236] A. von Jouanne, S. Dai, and H. Zhang, "A simple method for balancing the DC-link voltage of three-level inverters," in *Power Electronics Specialists Conference, 2001. PESC. 2001 IEEE 32nd Annual*, 2001, pp. 1341-1345.
[237] H. Kakigano, Y. Miura, T. Ise, and R. Uchida, "DC Micro-grid for super high quality distribution: System configuration and control of distributed generations and energy storage devices," in *Power Electronics Specialists Conference, 2006. PESC'06. 37th IEEE*, 2006, pp. 1-7.

[238] L. Mears and H. Gotschall, "EPRI-DOE handbook of energy storage for transmission and distribution applications," EPRI and the U.S. Department of Energy, 2003.
[239] F. Jauch and J. Biela, "Single-phase single-stage bidirectional isolated ZVS AC-DC converter with PFC," in *Power Electronics and Motion Control Conference (EPE/PEMC), 2012 15th International*, 2012, pp. LS5d. 1-1-LS5d. 1-8.
[240] H. Qian, J.-S. Lai, J. Zhang, and W. Yu, "High-efficiency bidirectional AC-DC converter for energy storage systems," in *Energy Conversion Congress and Exposition (ECCE), 2010 IEEE*, 2010, pp. 3224-3229.
[241] H. Matsuo, M. Suetomi, S. Fujino, K. Harada, W. Lin, and Y. Sui, "A bidirectional AC-DC converter with high power efficiency and high power factor using fast FPGA digital control," in *Telecommunications Energy Conference (INTELEC), 2012 IEEE 34th International*, 2012, pp. 1-7.
[242] D. S. Oliveira, M. Batista IV, L. H. Barreto, and P. P. Praca, "A bidirectional single stage AC-DC converter with high frequency isolation feasible to DC distributed power systems," in *Industry Applications (INDUSCON), 2012 10th IEEE/IAS International Conference on*, 2012, pp. 1-7.
[243] H. S. Kim, M. H. Ryu, J. W. Baek, and J. H. Jung, "High-efficiency isolated bidirectional AC–DC onverter for a DC distribution system," *Power Electronics, IEEE Transactions on*, vol. 28, pp. 1642-1654, 2013.
[244] F. Musavi, M. Edington, W. Eberle, and W. G. Dunford, "Energy efficiency in plug-in hybrid electric vehicle chargers: Evaluation and comparison of front end AC-DC topologies," in *Energy Conversion Congress and Exposition (ECCE), 2011 IEEE*, 2011, pp. 273-280.
[245] M. Yilmaz and P. T. Krein, "Review of battery charger topologies, charging power levels, and infrastructure for plug-in electric and hybrid vehicles," *Power Electronics, IEEE Transactions on*, vol. 28, pp. 2151-2169, 2013.
[246] F. Musavi, M. Edington, W. Eberle, and W. G. Dunford, "Evaluation and efficiency comparison of front end AC-DC plug-in hybrid charger topologies," *Smart Grid, IEEE Transactions on*, vol. 3, pp. 413-421, 2012.
[247] K. Bae-Sung, K. Hee-Jun, J. Chunfeng, and H. Dong-Young, "A digital controlled DC-DC converter for electric vehicle applications," in *Electrical Machines and Systems (ICEMS), 2011 International Conference on*, 2011, pp. 1-5.
[248] L. Jong-Pil, M. Byung-Duk, K. Tae-Jin, Y. Dong-Wook, and Y. Ji-Yoon, "A novel topology for photovoltaic DC/DC full-bridge converter with flat efficiency under wide PV module voltage and load range," *Industrial Electronics, IEEE Transactions on*, vol. 55, pp. 2655-2663, 2008.
[249] M. R. Patel, *Introduction to electrical power and power electronics*: CRC Press, 2012.
[250] (February 2013). *Electric vehicle charging stations*. Available: http://www.gura.com/021113/8.ElectricVehicleChargingStations.pdf
[251] (May 2013). *Free construction cost data*. Available: http://www.allcostdata.info/detail.html/161233130/Service-drop-cable,-triplex,-1/0,-on-poles,-al,-ACSR-neutral,-600V,
[252] (May 2014). *Uniline offLine UPS: 1 KVA UPS*. Available: http://www.sulekha.com/ups/uniline-offline-ups-1kva-ups-prices-and-specifications
[253] K. Branker, M. Pathak, and J. M. Pearce, "A review of solar photovoltaic levelized cost of electricity," *Renewable and Sustainable Energy Reviews*, vol. 15, pp. 4470-4482, 2011.
[254] (June 2014). *2010 DOE vehicle technologies: Program review presentation*. Available: http://energy.gov/sites/prod/files/2014/03/f12/ape021_goodarzi_2010_p.pdf
[255] (May 2014). *Fronius IG plus 9995W grid tied inverter 10.0-1 UNI*. Available: http://www.pvpower.com/fronius-ig-plus-100-1-uni-inverter9995wgridtieddcdisconnect208240277vac60hz.aspx
[256] (July 2014). *GM Voltec™*. Available: http://www.pluginnow.com/content/gm-voltec%E2%84%A2#
[257] B. Mammano, "Improving power supply efficiency: The global perspective," Texas Instruments, 2007.
[258] (May 2014). *IEEE smart grid experts roundup: AC vs. DC power*. Available: http://smartgrid.ieee.org/questions-and-answers/902-ieee-smart-grid-experts-roundup-ac-vs-dc-power

[259] H. Yun, Z. Zhangming, and Y. Yintang, "A high efficiency PWM buck DC/DC converter high-level model and verification," in *Solid-State and Integrated-Circuit Technology, 2008. ICSICT 2008. 9th International Conference on*, 2008, pp. 2031-2034.

[260] C. Huang-Jen and L. Li-Wei, "A bidirectional DC-DC converter for fuel cell electric vehicle driving system," *Power Electronics, IEEE Transactions on*, vol. 21, pp. 950-958, 2006.

[261] I. D. Jitaru and G. Cocina, "High efficiency DC-DC converter," in *Applied Power Electronics Conference and Exposition, 1994. APEC '94. Conference Proceedings 1994., Ninth Annual*, 1994, pp. 638-644 vol.2.

[262] (May 2014). *Edison's revenge: The rise of DC power*. Available: http://www.technologyreview.com/news/427504/edisons-revenge-the-rise-of-dc-power/